THE EFFECT OF IRON-RICH PARTICLES ON THE FATE AND BIOAVAILABILITY OF PHOSPHORUS IN STREAMS

Stijn BAKEN

Supervisor:
Prof. E. Smolders

Members of the Examination Committee:
Prof. M. Hermy (chair)
Prof. R. Merckx
Prof. J. Diels
Prof. D. De Vos
Prof. P. Seuntjens
Dr. G. F. Koopmans

Dissertation presented in partial fulfilment of the requirements for the degree of PhD in Bioscience Engineering

May 2015

Doctoraatsproefschrift nr. 1270 aan de faculteit Bio-ingenieurswetenschappen van de KU Leuven

Acknowledgements

Als beginnende doctoraatsonderzoeker denk je wel eens: "*Ik ga een doctoraat maken.*" Op het eerste zicht lijkt er weinig mis met die bewering, hoewel je onderweg soms twijfelt of je dat doctoraat ooit wel gaat maken. Pas aan het einde van de rit besef je dat jij het niet zelf was die dat doctoraat heeft gemaakt, maar dat het eerder tot stand kwam dankzij grote en kleine bijdragen van anderen. Tot dat besef kan je enkel komen door het proces zelf te ondergaan, het staat in geen enkel boek of artikel. Zelfs doorgaans betrouwbare bronnen [1] suggereren dat een doctoraat vooral je eigen werk is (Figuur 23bis). Wijlen meneer Van Dale (1828–1872) heeft veel betekend voor het Nederlands, maar ik denk niet dat hij een doctoraat had—anders had hij wel beter geweten.

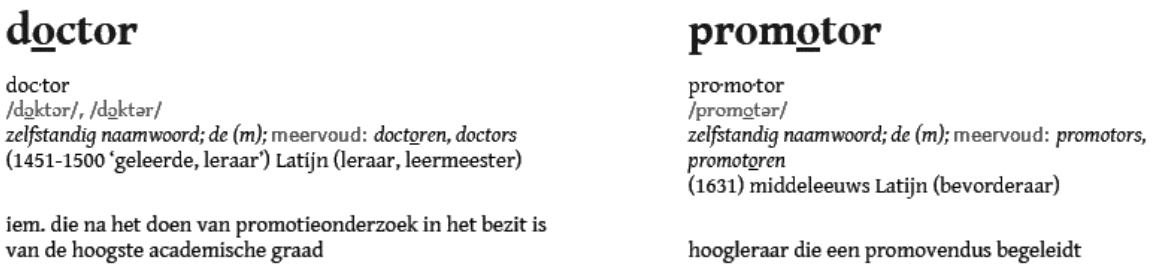

Figuur 23bis: De betekenis van de worden *doctor* en *promotor*, volgens referentie [1].

In de eerste plaats dank je een doctoraat aan je promotor. Ook hier houdt Van Dale het redelijk droog en zal ik dus uit eigen ervaring moeten spreken. Erik, ik denk niet dat ik een betere promotor had kunnen treffen. Dank voor je advies en je kritische blik; je was ondanks een volle agenda steeds beschikbaar voor overleg. Maar vooral dank voor het grote vertrouwen en de vrijheid die je mij gaf. Ik heb me altijd gewaardeerd gevoeld; dat was voor mij het belangrijkste om elke dag met plezier te gaan werken. Dank aan de voorzitter en de leden van de examencommissie, zowel voor het beoordelen van mijn werk als voor de fijne samenwerking en de discussies gedurende de afgelopen jaren.

Dank aan alle mensen met wie ik heb mogen samenwerken, of die mij op eender welke manier geholpen hebben. Om er maar enkele te noemen: de mensen van het Waterbouwkundig Laboratorium (Jan, Elin en anderen), van de VITO (Piet, Nele, Danny), van Wageningen UR (Gerwin, Inge, Peter, Rob), van het ILVO (Thijs, Fien) en van de KU Leuven (Roel, Jan, Dirk, Niels, Stefaan, Dries,...). Thanks to the people at

KTH, SLU, and MAX-lab for the fruitful collaboration (Jon Petter, Carin, Ingmar, Stefan, and others). Vind je je naam toevallig niet terug in dit lijstje, weet dan dat mijn dank er niet minder om is... Tot slot, dank aan het FWO en aan het Waterbouwkundig Laboratorium voor de centjes en voor het vertrouwen in mij als onderzoeker.

Ik had het geluk om slimme en gemotiveerde thesisstudenten onder mijn hoede te krijgen. Sophie, Emmanuel, Mieke, Claudia, Kris: dank voor jullie inzet, voor jullie aandeel in het labo- en veldwerk en voor de uitgebreide discussies. Het feit dat jullie nu allemaal ook een doctoraat (zouden willen) maken, is één van de grootste complimenten die ik voor mijn werk kreeg. Een ander deel van het labo- en veldwerk mocht ik doorschuiven naar het technisch personeel: Karla, Frans, Valentijn, Peter, Kristin. In het bijzonder de laatste twee hebben letterlijk honderden uren geïnvesteerd in metingen en veldwerk, waarvan de resultaten hier worden gepresenteerd. Alle administratie werd vlekkeloos, én met een luide giechel, verzorgd door Karlien. Dankjewel!

Dank aan mijn bureaugenoten (Bart, Maarten, Dr. Phil, Gabriel, Tovo en Christoff) en aan alle andere collega's die de afgelopen 5 jaar mijn leven op het labo gekleurd hebben. De samenwerking was altijd fijn, met vele helpende handen bij grote experimenten en met vruchtbare discussies. Maar ik onthoud toch vooral de koffiepauzes, de fratsen en de band na de uren. Een saaie vrijdagavond is dankzij jullie nooit een optie geweest, om nog maar te zwijgen van de weekendjes in Ravels. Bij welke job ga ik ooit nog zo'n sfeer vinden?

Mijn vrienden en huisgenoten zorgden de afgelopen jaren voor de nodige aanmoedigingen en babbels als de frustratiemeter eventjes in het rood ging. Bedankt voor de reisjes en uitstapjes, de bezoekjes aan Luik, de fiets- en wandeltochten, de avondjes op café, de actieve en passieve voetbalmatchen en de oeverloze discussies over relevante, minder relevante en volstrekt irrelevante onderwerpen.

Dank aan mijn familie voor de warme thuis waar ik altijd op kan rekenen, voor de steun, en om mij de mogelijkheid te geven te studeren.

En Xanne, dankjewel om mijn leven kleur te geven, voor je zotte ideeën en je brede lach, en gewoon voor wie je bent.

Als beginnende doctoraatsonderzoeker denk je wel eens: "*Ik ga iets nieuws ontdekken.*" Wanneer je dan helemaal aan het einde van de rit een dankwoord schrijft en op zoek gaat

naar wat leuke vakliteratuur uit de oude doos, word je stevig met de neus op de feiten gedrukt. Je botst op een document waaruit blijkt dat een deel van je bevindingen een slordige 170 jaar geleden al gekend waren [2] (Figuur 39). De terugblik is de makkelijkste en meest confronterende wetenschap...

Le peroxyde de fer contenu dans des terrains peu cohérents, et dans des roches pyroxéniques ou amphiboliques amenées à l'état terreux, est dissous par les eaux sous l'influence de certains produits de la pourriture des végétaux.

Partout où l'eau, ayant dissous de l'oxyde de fer, coule lentement au contact de l'air, elle abandonne une boue gélatineuse d'un brun noirâtre, formée de protoxyde et de peroxyde de fer, d'acide carbonique, d'acide crénique et d'eau. L'acide carbonique se dégage à mesure que le protoxyde de fer passe à l'état de peroxyde.

Le dépôt formé par chaque source est entraîné, lors des hautes eaux, vers un ruisseau ou vers une rivière qui le laisse déposer dans les points où son cours est ralenti. Au bout d'un certain temps, ce dépôt devient un gîte exploitable.

La composition chimique du dépôt des marais est analogue à celle du dépôt des sources, sauf l'acide phosphorique, qui est un peu plus abondant dans le premier.

Figuur 39: De vorming, de samenstelling en het lot van ijzeroxides in natuurlijke waters, zoals beschreven in 1845 (extract uit referentie [2]).

Summary

Phosphorus (P) is a limiting nutrient in many aquatic ecosystems. In agriculture, P is present in fertilizer and in animal manure. Widespread and intensive use of fertilizer and animal manure cause diffuse P emissions to the environment, leading to eutrophication of water bodies and impaired water quality. The fate of P in natural waters is strongly linked to that of iron (Fe) bearing particles, to which P can bind. Streams contain heterogeneous associations between iron and natural organic matter (NOM) which range in size from a few nanometers to more than 100 micrometer. The iron in such particles can be present under a variety of forms, ranging from small mononuclear Fe(III)–NOM complexes to large mineral Fe(III) oxyhydroxide particles with surface adsorbed NOM. Phosphorus, in the form of the phosphate anion, can bind efficiently to the surface of Fe oxyhydroxide particles. It is poorly understood how P binding to Fe-rich particles in streams is related to their size and structure, and how, in turn, the size and structure of the particles is related to their formation and to the chemistry of the streams which carry them. In addition, it is unclear how binding to such particles affects fate and environmental effects of P. The objectives of this study were 1) to determine the structure, size, and composition of natural Fe-rich particles in streams; 2) to measure P binding by such particles, and to relate this to the properties of the particles and to the properties of the streams which carry them; and 3) to determine how binding to Fe-rich particles affects the fate and bioavailability of P in natural waters.

The structure, size, and composition of Fe-rich particles in streams was measured by field-flow fractionation and membrane filtration. Soft water streams draining acidic peatland contain small (<40 nm) associations of nanoparticulate Fe oxyhydroxides and humic substances. These particles bind P, but the larger particles contain more P than the smaller ones. This is likely due to competition by humic substances for binding on the surface of Fe oxyhydroxides: large particles are less covered by humic substances and may, therefore, bind P more strongly. In moderately hard to very hard water streams, the Fe oxyhydroxide particles are larger (>40 nm) than those in the soft waters. The P in such streams is bound to ferrihydrite colloids (40–1200 nm) and to associations between Fe and clay minerals (50–150 nm). It is concluded that P may be bound to a variety of Fe

oxyhydroxide containing colloids. The results support the view that primary oxyhydroxide nanoparticles form increasingly larger aggregates with increasing water hardness, increasing pH, and increasing Fe:NOM ratio.

The effect of colloidal Fe oxyhydroxides on P bioavailability was determined in a model system with the freshwater green alga *Raphidocelis subcapitata*. Synthetic iron-organic matter colloids reduce the P uptake flux by algal cells compared to colloid-free test media. However, the P uptake flux from colloid containing solutions equals that from colloid-free ones if only the free orthophosphate concentrations are considered. This demonstrates that the colloidal P does not contribute to the P uptake flux, and hence that it is not readily bioavailable. The P added to post-synthesis ferrihydrite is bound less efficiently, and its bioavailability is higher, than if the P is present during ferrihydrite formation.

The formation and the fate of Fe-rich suspended particles were monitored in catchments which receive large Fe(II) inputs. Four Belgian lowland catchments fed by Fe-rich groundwater were sampled: the Kleine Nete catchment and three tributaries to the Demer. The groundwater contains, on average, 20 mg Fe L^{-1} and 0.4 mg P L^{-1}. As this groundwater surfaces, the soluble Fe(II) is oxidized to Fe(III) which readily forms particles (termed "authigenic"). The P is concomitantly removed from solution due to binding by the fresh Fe(III) minerals. The oxidation reaction proceeds as the groundwater surfaces and flows through the catchment into increasingly larger streams. The Fe(II) oxidation and the formation of authigenic particles is slower in winter than in summer, due to shorter travel times, lower pH, and lower temperature in winter. The authigenic particles are between 1 and 20 µm and consist of almost pure, poorly crystalline Fe oxyhydroxides similar to ferrihydrite. The mineralogy and composition of these particles change as they are transported into increasingly larger streams: the authigenic particles become larger in size due to aggregation, they become structurally more condense due to ageing reactions, and they are increasingly diluted by mixing with material from a different source. The removal of P from solution is much faster than that of Fe: it is already complete in the smallest headwater streams. The average P concentration in streams (42 µg L^{-1}) is one order of magnitude below that in groundwater (393 µg L^{-1}). The local environmental P limit for freshwater (140 µg L^{-1}) is between both values. Naturally occurring Fe in groundwater therefore alleviates the environmental risk of P in the receiving streams.

The formation of Fe-rich authigenic particles was monitored on the trajectory of draining groundwater: from the subsurface through Fe-rich sediments and into small drainage ditches of the Kleine Nete catchment. In the sediment, reductive dissolution of P-bearing Fe oxyhydroxides causes solubilization of Fe and P. Conversely, in the ditchwater, oxidative precipitation causes sequestration of Fe and P. Because the Fe is present in large excess, the removal of P is faster than that of Fe: ferric phosphate or P-saturated Fe oxyhydroxides are initially formed until P is nearly depleted. This yields a natural and highly efficient sink for P. In Fe-rich systems, the fate of P at the sediment-water interface is determined by reduction and oxidation of Fe.

Taken together, this study shows that P in streams may be bound to iron oxyhydroxide containing particles. These particles range in size between 1 nm and 100 µm. Small particles (1–40 nm) dominate in soft waters with low Fe:NOM ratio, whereas large particles (>40 nm) dominate in harder waters and at higher Fe:NOM ratio. In waters with low molar Fe:P ratio ("low Fe–high P waters"), the particles are saturated with P, and they contain Fe:P ratios around two. Conversely, in waters with high molar Fe:P ratio ("high Fe–low P waters"), most P is bound by Fe-rich particles. The strength of P binding also depends on the mechanism of particle formation: it is highest if the P is present during Fe(II) oxidation, due to coprecipitation with Fe oxyhydroxides. In contrast, it is lower if the P binds to existing Fe oxyhydroxides. The binding of P by Fe-rich particles reduces its bioavailability. In summary, the fate and effect of P in freshwater is intimately linked to the biogeochemical cycle of Fe and NOM.

Summary in layman's terms

The widespread use of phosphate, for example as a fertilizer in agriculture, has increased the phosphate concentrations in groundwater and surface water. Elevated phosphate concentrations in water bodies increase the risk for algal blooms and reduce the overall water quality. In regions with intensive animal husbandry, phosphate is one of the main threats to surface water quality.

Phosphate in natural water is present as dissolved ionic phosphate, as organic phosphate compounds, or as phosphate bound to iron-rich particles (suspended sediments and colloids). This study was devoted to the composition of these particles, and to their effect on transport and bioavailability of phosphate.

This work shows that iron-rich particles strongly affect the transport and environmental effects of phosphate in streams. The iron-rich particles are highly diverse and mostly consist of natural organic matter and iron oxyhydroxides. They range in size between a few nanometers and 100 micrometer. Particles smaller than 40 nanometer dominate in soft waters, whereas larger particles mostly occur in harder waters and in waters with relatively high iron and low organic matter concentrations. In waters with comparably high iron and low phosphate concentrations, most of the phosphate in the water column is bound to iron-rich particles. Conversely, in waters with comparably low iron and high phosphate concentrations, the particles are saturated with phosphate.

Iron plays a key role in phosphate transport in lowlands, where streams are mainly fed by groundwater. An extreme example is the catchment of the Kleine Nete, Belgium, where the groundwater is rich in iron. In the absence of oxygen, the iron is soluble and mobile in the groundwater. When the groundwater seeps into the streams, iron-rich particles are formed due to contact with atmospheric oxygen. These particles bind phosphate very effectively and remove it from the water column. As a result, phosphate concentrations in the streams are, on average, tenfold below those in the groundwater. The particle-bound phosphate is less available to algae than dissolved phosphate. In summary, iron-rich particles reduce the environmental risk associated with phosphate in streams.

Samenvatting

Fosfor (P) is een limiterend nutriënt in veel aquatische ecosystemen. In de landbouw wordt fosfaat als meststof gebruikt en is fosfor aanwezig in dierlijke mest. Dit veroorzaakt diffuse emissies naar het milieu, hetgeen resulteert in eutrofiëring van waterlichamen en een verminderde waterkwaliteit. Het lot van fosfor in natuurlijke waters is sterk verbonden met dat van ijzerrijke deeltjes. Veel waterlopen bevatten heterogene associaties van ijzer (Fe) en natuurlijke organische stof (OS) die in grootte variëren van enkele nanometers tot meer dan 100 micrometer. Het ijzer in deze associaties kan onder verschillende vormen voorkomen: van kleine mononucleaire ijzer(III)complexen met OS, tot minerale ijzer(III)oxyhydroxide deeltjes met geadsorbeerde OS. De oxyhydroxide deeltjes kunnen fosfor sterk binden aan hun oppervlak. Men weet echter niet goed hoe de bindingssterkte van fosfor aan ijzerrijke deeltjes afhangt van hun grootte en structuur, en hoe de grootte en structuur op hun beurt afhangen van de chemie van het omringende water. Bovendien is het niet duidelijk hoe zulke deeltjes het lot en de milieu-effecten van fosfor beïnvloeden. De doelstellingen van dit werk waren 1) de structuur, grootte en samenstelling van natuurlijke ijzerrijke deeltjes in waterlopen te bepalen; 2) de fosforbinding door natuurlijke ijzerrijke deeltjes te meten, en dit in verband te brengen met de deeltjeseigenschappen en met de eigenschappen van de waterloop; 3) te bepalen hoe ijzerrijke deeltjes het lot en de biobeschikbaarheid van fosfor in waterlopen beïnvloeden.

De structuur, grootte en samenstelling van ijzerrijke deeltjes in waterlopen werd bepaald door middel van *field-flow* fractionatie en membraanfiltratie. Waterlopen in een veengebied met zacht water bevatten voornamelijk kleine (<40 nm) associaties van ijzeroxyhydroxide-nanodeeltjes en humusbestanddelen. De grootteverdeling van fosfor lijkt op die van ijzer, maar naarmate de deeltjes groter worden, bevatten ze relatief meer fosfor. Dit komt wellicht door competitie tussen humusbestanddelen en fosfaat voor binding aan het oppervlak van ijzeroxyhydroxides. Grote deeltjes zijn minder bedekt door humusbestanddelen en kunnen daardoor fosfor sterker binden. In waterlopen met matig hard tot zeer hard water werden grotere (>40 nm) ijzeroxyhydroxidedeeltjes aangetroffen dan in waterlopen met zacht water. Het fosfor was gebonden aan ferrihydriet colloïden

(40–1200 nm) of aan ijzer-kleiassociaties (50–150 nm). Samengevat kan fosfor gebonden zijn aan zeer diverse, ijzeroxyhydroxide bevattende colloïden. Deze colloïden bestaan wellicht uit kleine, primaire oxyhydroxide-nanodeeltjes, die steeds grotere aggregaten vormen naarmate de waterhardheid, de pH en de Fe:OS-verhouding stijgen.

Het effect van colloïdale ijzeroxyhydroxides op de biobeschikbaarheid van fosfor werd nagegaan in een modelsysteem met de zoetwateralg *Raphidocelis subcapitata*. Synthetische Fe-OS-colloïden verminderen de fosforopname door algen in vergelijking met testoplossingen zonder colloïden. Als echter enkel het vrij ionisch orthofosfaat wordt beschouwd, is de fosforopname uit testoplossingen met of zonder colloïden identiek. Dit toont aan dat het colloïdaal fosfor op korte termijn niet biobeschikbaar is. Wanneer fosfor tijdens de vorming van ferrihydrietcolloïden aanwezig is, is de binding sterker en de biobeschikbaarheid lager, dan wanneer het fosfor achteraf wordt toegevoegd aan reeds gevormde colloïden.

De vorming en het lot van ijzerrijke deeltjes werd gemonitord in stroombekkens die grote hoeveelheden ijzer ontvangen via het grondwater. Vier Belgische, door grondwater gevoede laaglandbekkens werden bestudeerd: het stroombekken van de Kleine Nete en drie zijrivieren van de Demer. Het grondwater in deze stroombekkens bevat gemiddeld 20 mg Fe L^{-1} en 0.4 mg P L^{-1}. Wanneer dit grondwater aan de oppervlakte komt, oxideert het goed oplosbare ijzer(II) tot het slecht oplosbare ijzer(III) dat neerslaat als “autigene” (*in situ* gevormde) deeltjes. Deze oxidatiereactie vindt plaats terwijl het water door het stroombekken in steeds grotere waterlopen vloeit. De oxidatie van ijzer(II) en de vorming van autigene deeltjes gebeurt trager in de winter dan in de zomer door een lagere temperatuur, lagere pH en kortere verblijftijd in de winter. De autigene deeltjes zijn tussen 1 en 20 µm groot en bestaan uit een vrijwel puur ijzeroxyhydroxide dat sterk lijkt op ferrihydriet. De mineralogie en samenstelling van de deeltjes verandert terwijl ze naar steeds grotere waterlopen worden getransporteerd: de autigene deeltjes worden groter door aggregatie, ze worden structureel meer condens door verouderingsreacties, en ze worden verdund door menging met deeltjes van een andere oorsprong. De verwijdering van fosfor is veel sneller dan de verwijdering van ijzer, en is al vrijwel voltooid in de kleinste bovenlopen. De gemiddelde fosforconcentratie in waterlopen (42 µg L^{-1}) is een orde van grootte lager dan die in grondwater (393 µg L^{-1}). De milieunorm voor fosfor in waterlopen is 140 µg L^{-1}. Dit toont aan dat natuurlijk voorkomend ijzer in grondwater het milieurisico van fosfor in de ontvangende waterlopen vermindert.

De vorming van ijzerrijke deeltjes werd bestudeerd langs het traject van drainerend grondwater in het bekken van de Kleine Nete, d.w.z. vanuit de ondergrond door ijzerrijk sediment naar open drainagegrachten. In het sediment worden fosfor en ijzer gemobiliseerd door reductive oplossing van fosforhoudende ijzeroxyhydroxides. In de drainagegracht worden fosfor en ijzer daarentegen geïmmobiliseerd. Omdat ijzer in overmaat aanwezig is, wordt fosfor sneller geïmmobiliseerd dan ijzer: ijzerfosfaten of fosforverzadigde ijzeroxyhydroxides worden initieel gevormd totdat het fosfor bijna volledig is vastgelegd. Dit leidt tot een natuurlijke en zeer efficiënte verwijdering van fosfor. In ijzerrijke systemen wordt het lot van fosfor aan de grens tussen sediment en oppervlaktewater bepaald door reductie en oxidatie van ijzer.

Samenvattend toont deze studie aan dat fosfor in waterlopen gebonden wordt door ijzeroxyhydroxide bevattende deeltjes. Deze deeltjes variëren enorm in grootte (tussen 1 nm en 100 µm). Kleine deeltjes (1–40 nm) domineren in zacht water met lage Fe:OS-verhouding, terwijl grotere deeltjes (>40 nm) domineren in harder water en bij hoge Fe:OS-verhouding. In waters met een lage molaire Fe:P ratio (“laag ijzer, hoog fosfor” waters) zijn de deeltjes verzadigd met fosfor: ze bevatten een molaire Fe:P ratio van ongeveer twee. In waters met een hoge molaire Fe:P ratio (“hoog ijzer, laag fosfor” waters) daarentegen wordt het merendeel van het fosfor gebonden door de ijzerrijke deeltjes. De sterkte van fosforbinding door dergelijke deeltjes hangt tevens af van het vormingsmechanisme. De binding is sterker als het fosfor aanwezig is tijdens de vorming van de deeltjes door oxidatie van ijzer(II), maar minder sterk bij binding op reeds bestaande ijzerdeeltjes. De biobeschikbaarheid van fosfor verlaagt door de binding aan ijzerrijke deeltjes. Het lot en het effect van fosfor in waterlopen is sterk gerelateerd aan de biogeochemische cycli van ijzer en natuurlijke organische stof.

Vulgariserende samenvatting

Het overmatig gebruik van fosfaten, bijvoorbeeld als meststof in de landbouw, heeft geleid tot verhoogde fosfaatconcentraties in het grond- en oppervlaktewater. Dit veroorzaakt op zijn beurt de kans op algenbloei en verlaagt de algemene waterkwaliteit. In gebieden met intensieve veehouderij, zoals Vlaanderen, is de fosfaatbelasting van het oppervlaktewater één van de belangrijkste bedreigingen voor de waterkwaliteit.

Fosfaat in water kan aanwezig zijn als het opgelost (vrij) fosfaatanion, als organische fosfaatverbindingen of als fosfaat gebonden aan anorganische deeltjes (gesuspendeerde partikels en colloïden). Dit onderzoek handelt over de samenstelling van die deeltjes en hun invloed op het transport en op de biologische beschikbaarheid van fosfaat.

Dit werk toont aan dat ijzerrijke deeltjes het transport en de schadelijke effecten van fosfaat in waterlopen sterk beïnvloeden. De ijzerrijke deeltjes zijn zeer divers en bestaan voornamelijk uit natuurlijke organische stof en oxyhydroxides van ijzer. Ze variëren in grootte tussen enkele nanometer en 100 micrometer. Deeltjes kleiner dan 40 nm komen eerder voor in zacht water, terwijl grotere deeltjes eerder voorkomen in hard water en in water met relatief veel ijzer en weinig organische stof. In water dat relatief veel ijzer en weinig fosfaat bevat, is het merendeel van het fosfaat in de waterkolom gebonden door ijzerrijke deeltjes. In water met relatief veel fosfaat en weinig ijzer daarentegen zijn de deeltjes verzadigd met fosfaat.

Het ijzer speelt een sleutelrol bij het transport van fosfaat in vlakke gebieden, waar de waterlopen voornamelijk door grondwater gevoed worden. Een extreem voorbeeld is het bekken van de Kleine Nete, waar het grondwater zeer rijk is aan ijzer. In het grondwater is het ijzer, in afwezigheid van zuurstof, goed oplosbaar. Wanneer het grondwater opkwelt in de waterlopen, komt het in contact met zuurstof. Dit leidt tot de vorming van ijzerrijke deeltjes die het fosfaat vastleggen en verwijderen uit de waterkolom. Hierdoor zijn de concentraties fosfaat in de waterlopen gemiddeld tienmaal lager dan die in het grondwater. Het fosfaat dat gebonden aan ijzerrijke deeltjes, is bovendien minder beschikbaar voor algen dan opgelost fosfaat. IJzerrijke deeltjes verminderen dus het milieurisico van fosfaat in het oppervlaktewater.

List of abbreviations

AF4	asymmetric flow field-flow fractionation
Al	aluminum
As	arsenic
BEC	background equivalent concentration
C	carbon
Ca	calcium
DET	diffusive equilibration in thin films
DL	detection limit
DO	dissolved oxygen
DOC	dissolved organic carbon
DPS	degree of phosphorus saturation
EC	electrical conductivity
EXAFS	extended X-ray absorption fine structure
Fe	iron
Fe(II)	ferrous iron
Fe(III)	ferric iron
HFO	hydrous ferric oxide
IC	inorganic carbon
ICP-MS	inductively coupled plasma-mass spectrometry
kDa	kilodalton
LCF	linear combination fitting
LOQ	limit of quantification
NOM	natural organic matter
OC	organic carbon
P	phosphorus
Si	silicon
SRNOM	Suwannee River natural organic matter
temp	temperature
WT	wavelet transform

Table of contents

Chapter 1 Interactions between iron and phosphorus in the environment

The biogeochemistry of iron

Iron (Fe) is a transition metal, has atomic number 26 and atomic weight 55.85 g mol^{-1}, and is the fourth most abundant chemical element in the Earth's crust. Iron ore, which consists of iron oxide minerals, has been widely mined and processed to metallic iron or steel since the iron age. During the year 2013, approximately 2 800 million metric tons of iron ore were extracted from the earth's surface, equivalent to 107 kg per ha of land surface on earth. In soils, Fe is present in large concentrations, e.g. the median Fe content in agricultural topsoils in Europe is 17 000 mg Fe kg^{-1} [3]. The high soil Fe concentrations are in marked contrast with the low Fe concentrations in streams. The median Fe concentration in filtered European stream water is only 0.07 mg Fe L^{-1} [4], which highlights the general insolubility of Fe in the environment.

Iron is an essential micronutrient for all forms of life. In plants, for example, Fe is a constituent of heme and Fe-S proteins, and has functions in key metabolic processes, such as photosynthesis. The Fe is taken up and translocated by active transporters, and intracellular Fe homeostasis is maintained by storage and release from cellular compartments such as vacuoles and plastids [5]. Despite its high concentrations in soils, Fe is a major limiting nutrient for plant growth in calcareous soils, due to its limited solubility and bioavailability at high pH [6,7]. In contrast, Fe toxicity to plants may also occur and can be found in plants grown in submerged soils (e.g. rice) and in wetland vegetation. This is related to the reduction and solubilization of Fe in anoxic environments [8]. In the open ocean (pH 8.5), Fe is the key limiting nutrient for primary production by phytoplankton [9]. Iron fertilization of the ocean has therefore been used as a means to boost ocean productivity and carbon sequestration, although this practice is controversial due to its unknown side-effects on pelagic ecosystems [10,11]. In freshwater environments, Fe deficiency has been observed in cyanobacteria, which have a relatively high Fe requirement [12]. However, the effects of Fe on nutrient bioavailability and

ecosystem functioning is mostly through its strong interaction with phosphorus (P), which in many freshwater systems is the most limiting nutrient for primary production [13].

In the environment, the dominant oxidation states of Fe are +II and +III. In reduced environments, such as waterlogged soils or sediments, the Fe concentrations in the pore water can exceed 100 mg L^{-1}. Under such conditions, the highly soluble Fe(II) is present as the Fe^{2+} ion which may be adsorbed on clay surfaces [14] or complexed by organic matter [15]. It may also form minerals, such as siderite, $FeCO_3$, or vivianite, $Fe_3(PO_4)_2$. Under strongly reducing conditions, the Fe(II) may be bound in sulfide minerals, such as pyrite, FeS_2. Iron(II) may also occur in silicate minerals, such as olivine, the mica biotite, and the clay mineral illite. However, in many moderately reduced environments, a large fraction of the Fe(II) commonly occurs as free ionic Fe^{2+}, and it is therefore generally considered highly mobile in anoxic soils and sediments [16].

In oxic environments, Fe(III) is the dominant oxidation state. In oxic streams and in the pore waters of well aerated soils, the Fe concentrations rarely exceed 1 mg L^{-1}. The Fe^{3+} cation is readily hydrolyzed and polymerized, thereby forming a variety of oxyhydroxide minerals. The hydrous ferric oxide (HFO) is a highly amorphous polymeric Fe oxyhydroxide phase which readily forms [17]. This reaction may be simplified as [18]

$$Fe^{3+} + 3H_2O \rightarrow Fe(OH)_3 + 3H^+ \qquad \textit{(Equation 1.1)}$$

The solubility of hydrous ferric oxide is very low: $K_S = 10^{2.5}$–$10^{5.0}$ M^{-2}. Therefore, the activity of free Fe^{3+} ions is commonly very low in natural waters, and it strongly depends on pH (e.g. 10^{-12} M at pH 5 and 10^{-18} M at pH 7). Crystallization of the HFO may yield a wide range of Fe oxyhydroxides of varying crystallinity. The Fe oxyhydroxides include, in order of increasing crystallinity and decreasing solubility, ferrihydrite (crystal structure $Fe_{10}O_{14}(OH)_2$ [19]), goethite (α-FeOOH), and hematite (α-Fe_2O_3), which commonly occur in soils throughout the world [20] (Figure 1.1). The Fe in these minerals is surrounded by either 4 or 6 oxygen atoms in tetrahedral or octahedral coordination.

In reduced soils and sediments, net reduction of Fe(III) to Fe(II) often occurs by reductive dissolution: reduction of Fe oxyhydroxides produces soluble Fe^{2+} ions. This reaction may proceed either biotically or abiotically [21,22]. In oxic systems, the reverse reaction (oxidative precipitation) dominates: oxidation of Fe(II) and the subsequent formation of Fe oxyhydroxides. The Fe may be oxidized abiotically, but microbially mediated Fe(II) oxidation may outpace the chemical oxidation reaction under acidic conditions [23] or at

low dissolved oxygen concentrations [24,25]. The coupling of reductive dissolution and oxidative precipitation may lead to Fe cycling, which has been observed in a variety of environments including sediments, groundwater seeps, and lakes [26–28]. Redox cycling of Fe in aquatic media is mediated by reactions involving H_2O_2 and $OH^\bullet$ radicals, such as the Fenton reaction [29]:

$$Fe(II) + H_2O_2 \rightarrow Fe(III) + OH^- + OH^\bullet \qquad \textit{(Equation 1.2)}$$

Organic acids, humic substances, and UV light may affect the production or removal of H_2O_2 and $OH^\bullet$ radicals, and may therefore mediate the Fe(II)–Fe(III) equilibrium in natural waters [29,30].

Streams generally contain low "dissolved" (<0.45 µm) concentrations of Fe, *i.e.* in the order of 0.01–1 mg Fe L^{-1} [4]. Reduced Fe(II) may exist as free Fe^{2+} ions, or it may be loosely bound to natural organic matter (NOM) [15]. However, the Fe speciation in oxic streams is usually dominated by Fe(III). The Fe(III) may be bound to NOM as mononuclear Fe complexes, *i.e.* single Fe^{3+} ions chelated by a fulvic or humic acid (Figure 1.2). At low Fe:NOM ratio, mononuclear Fe–NOM complexes are formed, and complexation by NOM suppresses Fe oxyhydroxide formation [31]. The Fe^{3+} complexation capacity of NOM depends on pH, on competition by other cations such as Ca and Al, and on NOM quality [32–34]. If the Fe concentration exceeds the complexation capacity of NOM, the Fe is hydrolyzed, polymerized, and oxyhydroxides are formed. A generic prediction of Fe binding to NOM in streams is shown in Figure 1.3. At low pH, more Fe is bound as mononuclear complexes than at high pH: the activity of the free Fe^{3+} cation in equilibrium with a Fe oxyhydroxide phase decreases strongly with increasing pH. Figure 1.3 shows that the concentration of mononuclear Fe–NOM complexes typically is about an order of magnitude lower than the total "dissolved" (<0.45 µm) Fe in pH-neutral streams, suggesting that the Fe oxyhydroxides dominate the Fe speciation. These Fe oxyhydroxides may either be fully amorphous HFO, or they may crystallize to some extent, e.g. as in ferrihydrite (Figure 1.2). Both forms of Fe oxyhydroxides may be embedded in a NOM matrix, or NOM may be adsorbed at their surface [31,35–39] (Figure 1.4). The size of these associations likely depends on particle aggregation, which is a function of the zeta potential of the particles, of the ionic strength, and of cations capable of bridging, such as Ca. Primary ferrihydrite particles are <10 nm in size [19], but ferrihydrite in natural waters spans a wide size range, ranging up to the micrometer

scale [40]. Taken together, the Fe(III) in natural waters is present under highly diverse forms, ranging from mononuclear Fe complexes at low Fe:NOM ratio to Fe minerals with adsorbed NOM at high Fe:NOM ratios.

The formation of Fe-rich particles and the export of Fe from catchments has been addressed by a number of studies. At the oxic-anoxic boundary in lakes, *in situ* oxidation of Fe(II) produces Fe oxyhydroxides, which have been identified as ferrihydrite and lepidocrocite [26,41–43]. Such may also occur in catchments fed by reduced groundwater [44]. In the pore waters of anoxic soils and sediments, Fe(II) concentrations exceeding 10^{-3} M are common [45,46], but even under oxic conditions, an appreciable part of the Fe may be present as reduced Fe(II) [47]. In a boreal catchment, it was shown that Fe export occurs as Fe(III)–NOM associations [48]. On a larger scale, Fe export from Northern European catchments is related to that of organic matter [49,50]. Taken together, the above studies indicate that in temperate and boreal catchments, where redox gradients are prominent, Fe export is mostly related to Fe(II) solubilization and Fe–NOM associations. It remains unclear how the Fe(III)–NOM associations are formed, e.g. by oxidation of previously solubilized Fe(II), by binding and complexation of Fe(III), or by solubilization of existing Fe oxyhydroxide particles.

The Fe in natural waters may affect the fate of various nutrients and toxicants. The Fe^{3+} may compete for complexation on NOM with cationic trace metals, such as Cu^{2+}, Cd^{2+}, and Zn^{2+} [34]. Conversely, particles rich in Fe oxyhydroxides may strongly bind oxyanions, such as phosphate ($H_2PO_4^-$ and its conjugated bases, further denoted as PO_4) and arsenate ($H_2AsO_4^-$ and its conjugated bases, further denoted AsO_4), and cationic trace metals, such as lead (Pb^{2+}) [51]. This may increase the mobility, but decrease the bioavailability of these elements in the water column. Field-flow fractionation studies have shown that natural nanoparticles (1–100 nm) in streams are a mixture of organic C-dominated and Fe-dominated entities [52–56]. The organic C-dominated particles are mostly small (<3 nm) and consist of humic substances. They may carry cationic trace elements, such as Ni and Cu. The Fe-rich nanoparticles are larger (>4 nm), consist of Fe oxyhydroxide–NOM associations, and carry e.g. P, Pb, V, and Mn. Large particles rich in (>0.45 µm) are mobilized during rainstorm events and may carry e.g. As, V, Pb, and Cr [57,58]. Clearly, the environmental fate of Fe affects that of many other elements.

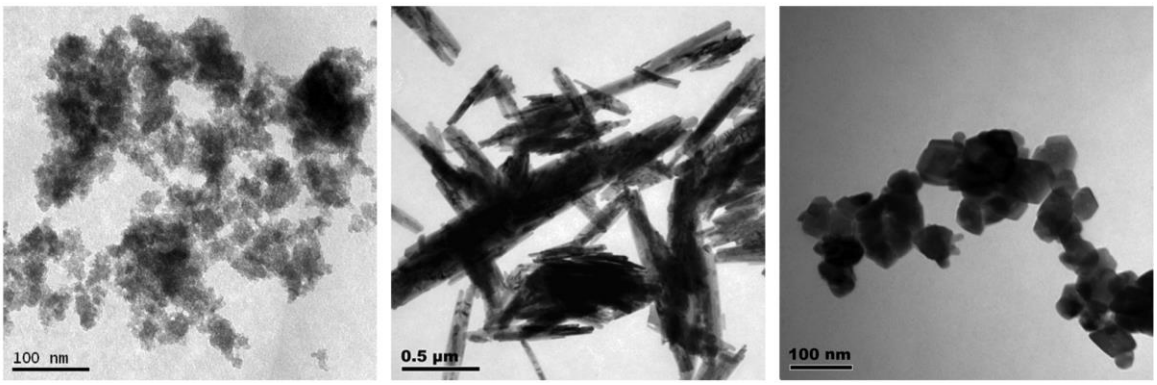

Figure 1.1: Transmission electron microscopy images of common Fe oxyhydroxides in the environment, from Wang et al. (ref. [59]). **Left**, ferrihydrite; **Middle**, goethite; **Right**, hematite

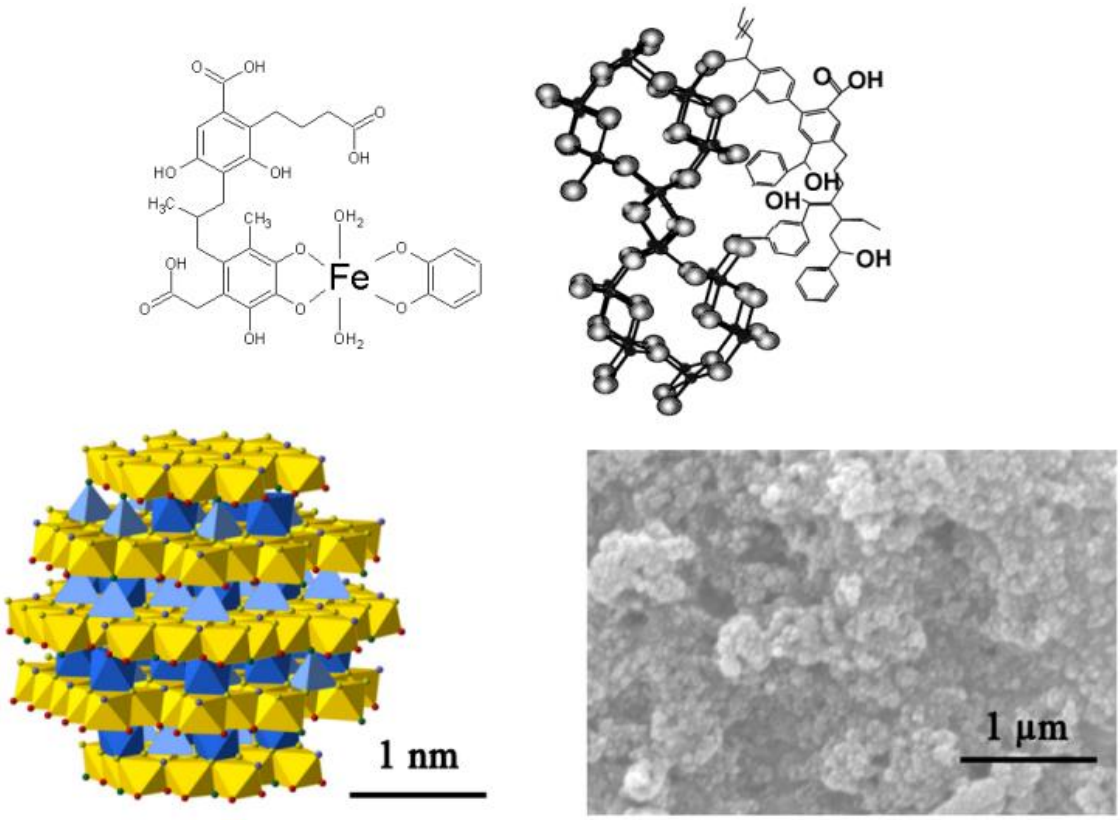

Figure 1.2: Fe species in natural waters. **Top left**, a mononuclear complex of Fe(III) with the catechol groups of a fulvic acid. **Top right**, a hypothetical amorphous polymer of hydrolyzed Fe with a surface adsorbed fulvic acid, modified from ref. [60] (black dots: Fe, gray spheres: O). **Bottom left**, a hypothetical surface depleted primary ferrihydrite particle of 2.5 nm, from ref. [61] (yellow: octahedral Fe; blue: tetrahedral Fe; colored dots: O in different configurations). **Bottom right**, scanning electron microscopy image of freeze-dried natural ferrihydrite colloids.

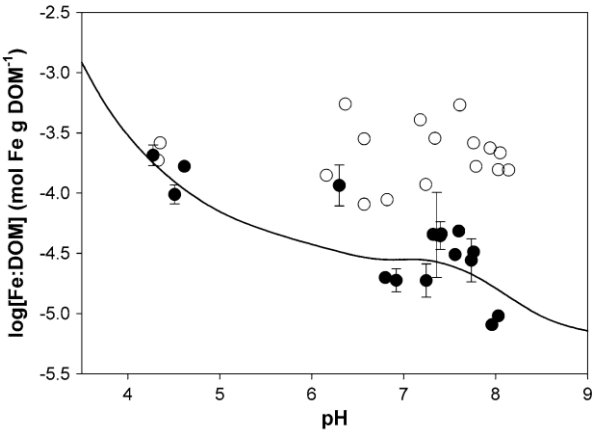

Figure 1.3: The chemical speciation of Fe(III) in filtered freshwater samples. The amount of mononuclear Fe(III) complexed by organic matter decreases with increasing pH (full circles: observations in dialysis experiments; full line: generic model prediction). The remainder of the Fe(III) is present as colloidal Fe oxyhydroxides (empty circles). Note the logarithmic concentration scale. Reproduced from Lofts et al. [18]

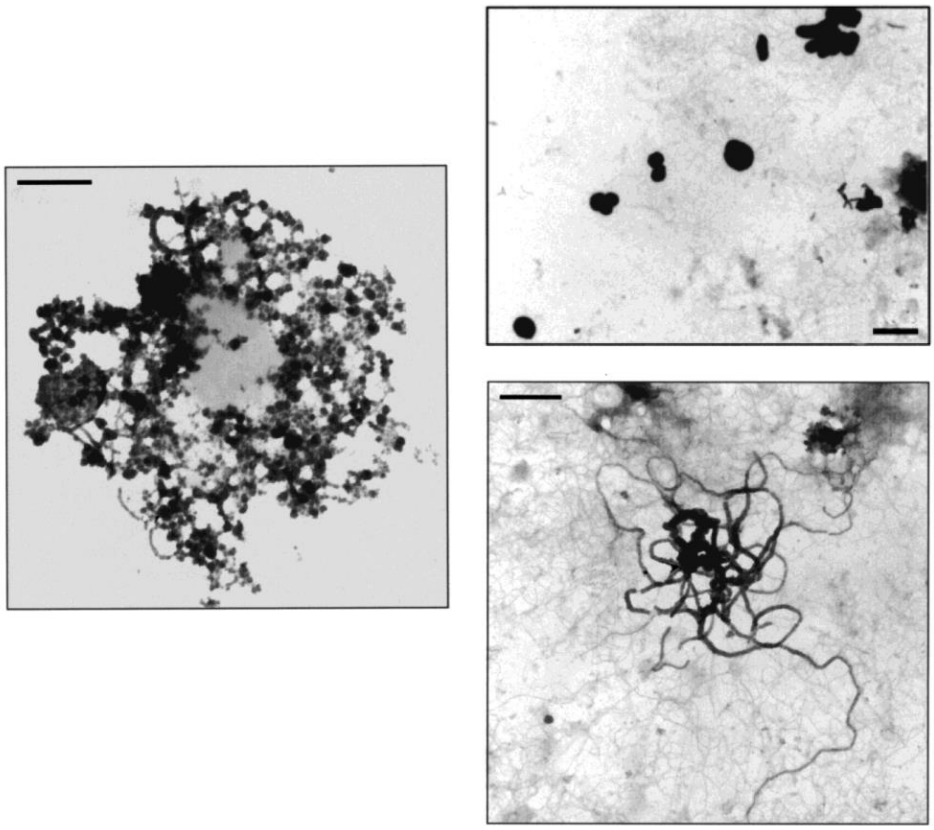

Figure 1.4: Transmission electron microscope images illustrating the diversity of natural iron–organic matter associations in lakes and streams (scale bars: 500 nm), reproduced from Perret et al. [39]. **Left**: nanosized Fe-rich granules (10–50 nm) embedded in organic matter. **Top right**: single Fe-rich globules. **Bottom right**: Fe-rich material covers organic fibrils.

The sources and environmental effects of phosphorus

Phosphorus (P) has recently received renewed interest as a non-renewable natural resource [62]. The sustainable use, recycling, and environmental impact of P have been key policy issues over the past few years, and will likely continue to do so in the near future [63]. The excessive P concentrations in freshwater is a main topic on the Flemish environmental agenda for the coming decade (M. Boucneau, Flemish Environment Agency VMM, personal communication). The environmental effects of P are mostly related to its status as the limiting nutrient for primary production in many aquatic ecosystems. Excessive P emissions to the environment have caused widespread cultural eutrophication of lakes and streams throughout the world [13]. Eutrophication of water bodies is undesired, because it leads to reduced biodiversity, anoxia, odor, fish kills, toxin production, and an overall reduced desirability.

The P in water bodies may originate from point sources, such as municipal or industrial wastewater discharge, or from nonpoint sources, most notably agriculture. In many catchments, nonpoint agricultural sources are the key contributors to nutrient fluxes into surface water [64,65]. Overland flow and soil erosion are the principal pathways of P export from most catchments [65]. Such losses are related to erosion of P-bearing soil particles during storm events, mostly in fine-textured soils [66]. Conversely, in noncalcareous, well-drained lowlands with shallow groundwater tables, P export predominantly occurs via leaching to the groundwater [67]. It is unclear to what extent today's P loads of water bodies in agricultural areas are attributable to present day farming. In the decades following World War II, fertilizer application to agricultural land was practically unrestricted. This has resulted in agricultural P application rates far in excess of crop demands. The nutrient imbalance has been exacerbated by intensive animal husbandry: the application of animal slurries to agricultural land has locally created even larger P surpluses. Since P is strongly bound to soil particles, such as oxyhydroxides of Fe, Al, and Mn, the excess P has accumulated in surface and subsurface reservoirs, such as soils, groundwater, riparian soils, and sediments of rivers, lakes, and wetlands. These pools of 'legacy P' slowly leak P, causing a continued P delivery to surface water [68–70]. Leaking legacy P has caused the failure of catchment management plans to attain the desired water quality improvements, because efforts to reduce direct nutrient losses from agriculture are masked by an increased release of P from legacy pools [71]. In Western Europe, approximately 755 kg of

legacy P per ha cropland has accumulated between 1965 and 2007 due to excessive application of fertilizer and animal manure [72]. Present P application rates are better balanced to crop P removal, but environmental managers still must deal with this legacy.

The fate and environmental effects of P in natural waters depend on its chemical speciation. Common P species in soils and streams include inorganic P compounds, organic P compounds, and particle bound P. Orthophosphate (PO_4), *i.e.* phosphate in its simplest, free ionic form, is the main inorganic form of P, but condensed phosphates may occur. The organic P compounds are a highly diverse group; examples of organic P compounds occurring in natural waters include phytic acid, adenosine triphosphate (ATP), and ribonucleic acid (RNA) [73]. The contribution of organic P compounds to the concentrations of "dissolved" (<0.45 µm) P in surface water is typically low but not negligible; average contributions of 12% [74] and 20% [75] have been reported. The particle bound P has been identified as heterogeneous associations between P, Fe, organic matter, and clay minerals [76–80]. In freshwater systems, free orthophosphate is presumably the only P species which is taken up by algal cells. Organic P compounds are not directly available but need hydrolysis prior to uptake by algal cells [81]. This hydrolysis may be catalyzed by enzymes; algae may produce extracellular phosphatase enzymes in order to increase the bioavailability of organic P. Particle bound P may become partly available to biota after desorption [74,82,83]. The bioavailability of P bound to Fe and Al oxyhydroxide colloids has not yet been addressed. For practical purposes, the bioavailable P is often measured by colorimetric methods and reported as soluble reactive phosphorus (SRP) or dissolved reactive phosphorus (DRP), an approach followed in water quality monitoring programs worldwide. These colorimetric assays generally exclude most organic P compounds, but include part of the particle bound P [84].

Interactions between iron and phosphorus in soils and natural waters

In the environment, P strongly interacts with Fe due to its high affinity for Fe oxyhydroxides. Therefore, the fate of P is governed by that of Fe in many environmental systems. In soils, the Fe may be present as nanoparticulate Fe oxyhydroxide–organic matter associations, Fe in clay minerals, and Fe oxyhydroxides associated with clay minerals [85]. Oxyhydroxides of Fe and Al are the main sorbent for P in many soils. In

European soils, aqua regia extractable concentrations of Al and Fe are similar in molar terms (median 0.3 mol Fe kg^{-1} and 0.4 mol Al kg^{-1}) [3]. However, since Al is not redox active and does not dissolve upon waterlogging, the mobility of P between soil and water in temperate areas with alternating redox conditions is more dependent on Fe than on Al. Phosphate binds to ferrihydrite as a binuclear bidentate complex, and the binding consists of several kinetic stages (Figure 1.5) [86]. Fixation or ageing of P in soils has been widely observed [87] and is commonly attributed to slow diffusion of P into micropores [88]. This process, and the ubiquitous presence of Fe oxyhydroxides, makes P deficiency a key yield limiting factor in weathered soils. Conversely, in excessively fertilized soils, P losses from soils are a major concern, and Fe plays a key role in mediating such P losses. In soils prone to erosion, Fe oxyhydroxides may carry P in eroded soil particles [58] and affect the fate of P in the receiving streams [89]. In soils where P leaching occurs, the molar P:(Fe+Al) ratio in a 0.2 M oxalate soil extract, which targets poorly crystalline Fe and Al oxyhydroxides, is commonly used in order to estimate the risk of P leaching from such soils [90,91]. This approach predicts that if the molar P:(Fe+Al) ratio in the oxalate extract exceeds 0.125, then the soil solution P concentration in a noncalcareous sandy soil may exceed the threshold for P leaching of 0.1 mg P L^{-1} which is supposed to be the limit for eutrophication of natural waters [90]. In soil solutions, P-bearing colloids consisting of Al–NOM or Fe–NOM associations have been identified, and they may contribute to leaching losses of P [79,92,93]. Iron-coated sands have successfully been used as a liner in drainage pipes in order to remove P from agricultural drainage water [94].

In natural waters, P may be bound to Fe–organic matter associations. Such associations may be as small as a few nanometers [53,95–97]. In one study, clay particles have been identified as the key vectors of colloidal P in drainage waters [78]. Natural colloids containing Fe and organic matter may bind P at molar Fe:P ratios down to 2 [98,99]. The *in vitro* oxidation of Fe(II) in the presence of P confirms the extremely high capacity of oxidizing Fe to sequester P in aqueous systems [17,100–102]. Colloids, *i.e.* particles in the size range between 1 and 1000 nm, are of specific interest with respect to P binding due to their dynamic nature and their high specific surface area [103]. Colloidal P may contribute significantly to the "dissolved" (<0.45 µm) P load of streams [104,105] and may play a key role in P transport in catchments [106]. The binding of P to colloids may be governed by the colloidal pumping hypothesis: a combination of relatively fast adsorption of P to colloids, and slow aggregation kinetics of colloids to larger sizes [106–108]. Ultimately, as colloids are

transported downstream, they aggregate to larger sizes due to the increased salinity, settle to the bottom sediments, and are buried. This process is responsible for the large-scale removal of iron-rich particles and associated phosphorus from the water column in estuaries [109,110].

The fate of P in submerged soils and sediments depends on the coupled cycling of Fe, S, and organic C. In submerged soils and sediments, P may be associated with Fe oxyhydroxides [111,112]. In one study, ferric phosphate was identified as the key binding phase for P in streambed sediments [113]. Reductive dissolution of Fe, fuelled by readily degradable organic C, may release P to the solution [114]. This may not necessarily cause an increased eutrophication risk: if Fe(II) and P coexist in solution, oxygenation will promote binding of P by freshly formed Fe oxyhydroxides [115]. However, under strongly reducing conditions, Fe may be immobilized as iron sulfides, thereby promoting P release since the Fe can no longer act as a sorbent for P [89,113]. In some studies, no P release after reductive dissolution of Fe oxyhydroxides has been observed. This may be due to incomplete reductive dissolution, and the released P is bound to residual Fe and Al oxyhydroxides or to other phases [116,117]. Alternatively, at high Fe^{2+} concentrations, the P may be bound in ferrous phosphate minerals, such as vivianite, $Fe_3(PO_4)_2$ [45,46,118].

Presently, the structural properties of Fe–organic matter associations from a variety of natural waters (composition, size, and chemical structure) have been relatively well documented [31,40,95,119]. However, it is unclear how these structural properties depend on the chemical properties (water hardness, pH, total concentrations of Fe and organic matter, organic matter quality) and on the physical properties (land use, catchment geomorphology and hydrology) of the streams which carry them. In addition, it is poorly known how the functional properties of these particles, most notably the strength of P binding, relate to their structural properties and to the mechanism of their formation. Furthermore, the bioavailability of P bound to Fe-rich colloids has rarely been documented, even though this P fraction is included in the colorimetric assays which are commonly used to quantify the bioavailable P in environmental monitoring programs. This study therefore attempts to unravel how P binding to Fe-rich particles in natural waters is a function of particle properties and environmental factors.

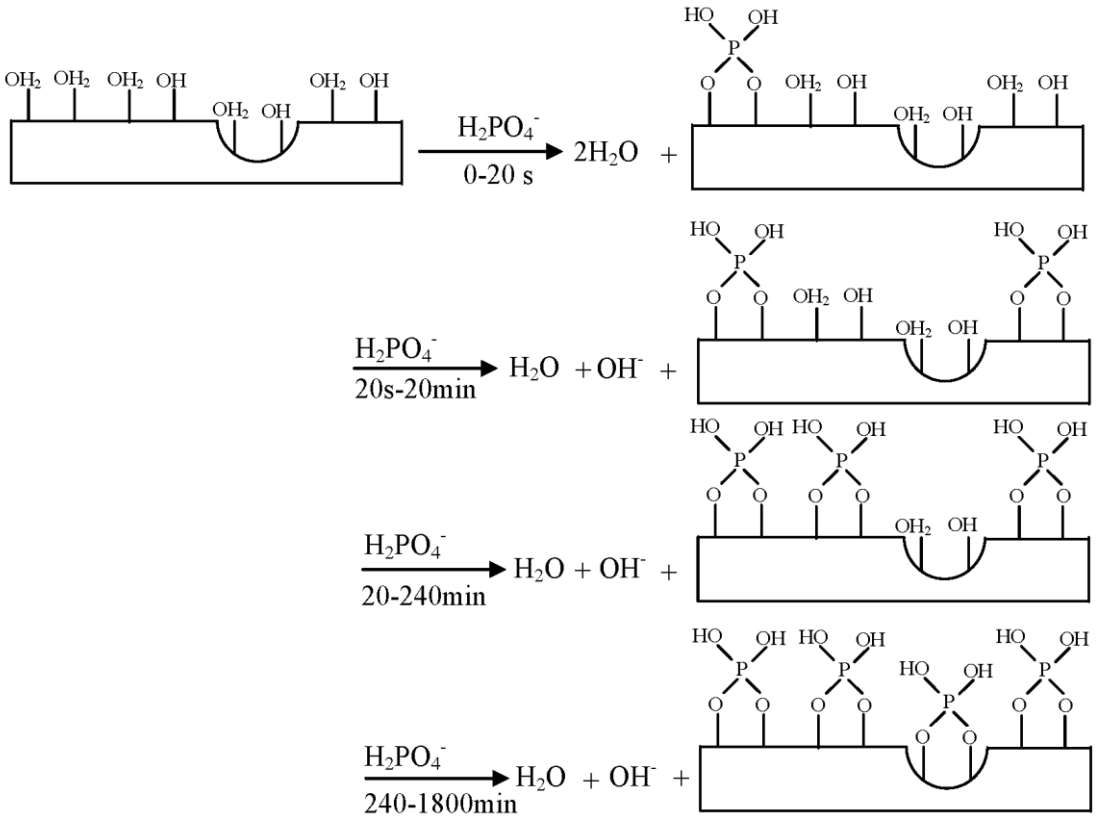

Figure 1.5: Mechanism of phosphate binding to synthetic ferrihydrite, reproduced from Wang et al. (ref. [86]). Phosphate is bound as a binuclear bidentate complex in three stages. Phosphate exchanges very quickly with two $Fe–OH_2^{+1/2}$ sites, releasing water (top). Subsequently, phosphate exchanges with a $Fe–OH_2^{+1/2}$ and a $Fe–OH^{-1/2}$ site, releasing water and OH^- (middle). Diffusion of phosphate into micropores and binding to micropore sites is the slowest process (bottom).

Objectives, hypothesis, and outline of this dissertation

The overall goal of this study was to unravel how phosphorus binding to iron-rich particles in natural waters is a function of particle characteristics and environmental factors. More specifically, the objectives were:

1. To determine the structure, size, and composition of natural iron-rich particles in streams;
2. To determine phosphorus binding by natural iron-rich particles, and to relate this to the particle properties (structure, size, composition) and to the properties of the streams which carry them (total concentrations of iron, phosphorus, and organic matter, water hardness, pH, discharge, and catchment geomorphology);
3. To determine how binding to iron-rich particles affects the fate and bioavailability of phosphorus in natural waters.

The Fe, P, and natural organic matter (NOM) form complex associations in particles. We speculated that the Fe:NOM ratio and the Fe:P ratio in particles determine the binding and fate of P (Figure 1.6). It was hypothesized that small Fe-bearing colloids prevail in soft water (<0.6 mM) and at low Fe:NOM ratio, since these factors limit particle aggregation. Furthermore, it was anticipated that the phosphate binding strength to Fe-rich particles increases with increasing Fe:NOM ratio, due to reduced competition between phosphate and NOM for sorption on a Fe oxyhydroxide phase [120–122]. In "high Fe–low P waters" where Fe is present in excess, the P is likely strongly bound by Fe-rich particles. Conversely, in "low Fe–high P waters", the Fe-rich particles become saturated with P, likely at molar ratios of around 1–2 mol Fe (mol P)$^{-1}$ as shown by a number of previous studies [17,90,98,113,123]. A survey on these hypotheses requires sampling in contrasting environments to identify the variable Fe:NOM ratios.

The above objectives and hypotheses were addressed by combining experimental work, observational field studies, and surveys in catchments. The outline of this dissertation is shown in Figure 1.7. The first part (chapters 2 and 3) addresses the role of Fe-rich colloids, *i.e.* particles <1000 nm. In chapter 2, colloids in natural waters are characterized in terms of their size and composition by field-flow fractionation and classical membrane filtration. The association of phosphorus with the various types of colloids is determined. In chapter 3, the binding of phosphorus to synthetic iron–natural organic matter

associations is addressed, and the bioavailability of particle-bound phosphorus to unicellular algae is quantified.

The second part (chapters 4, 5, and 6) focuses on the formation and fate of large Fe-rich particles (>0.45 µm), *i.e.* the fraction often operationally defined as "particulate". Such particles are produced extensively in lowland catchments fed by Fe-rich groundwater. Iron-rich particles produced *in vitro* after oxygenation of natural groundwater samples are characterized in terms of their composition, structure, and size. Their characteristics are compared to those of suspended particles in streams which are fed by such groundwater (chapter 4). In a field study, the iron and phosphorus concentrations in groundwater are determined along the trajectory of groundwater as it seeps into open drainage ditches, and the processes governing the dynamics of iron and phosphorus are inferred (chapter 5). Finally, the oxidation rate of iron, and the concomitant sequestration of phosphorus and arsenic, a toxicant of environmental concern which occurs as an oxyanion similar to phosphate, are quantified at the catchment scale. The evolution of water chemistry is traced as the groundwater surfaces and flows through the catchment into increasingly larger streams (chapter 6).

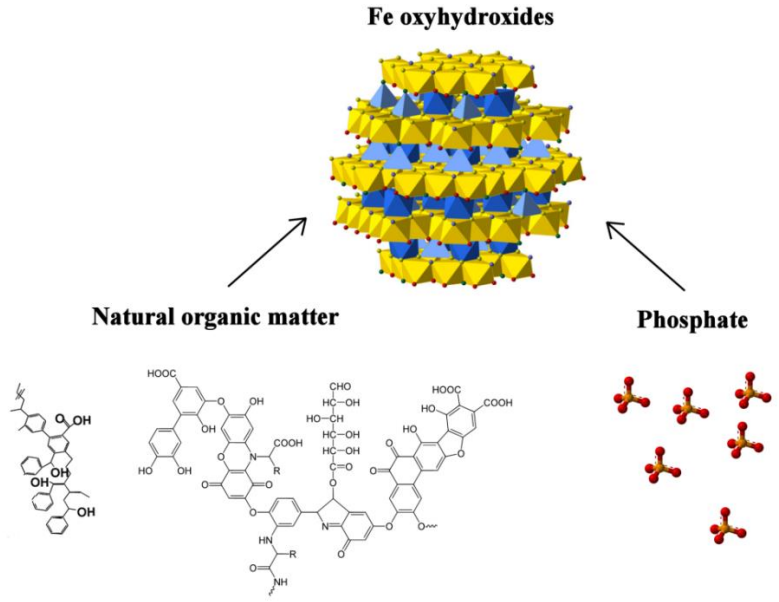

Figure 1.6: Central hypothesis of this dissertation. The Fe, NOM, and phosphate in natural waters form particles. The binding of phosphate to such particles depends on the Fe:NOM ratio, since the NOM and phosphate compete for binding on Fe oxyhydroxide surfaces. It also depends on the Fe:P ratio: at low Fe:P ratio, the Fe oxyhydroxides may become saturated with P. The size of the primary ferrihydrite particle (top) is around 2.5 nm [61], that of humic substances is commonly between 1 and 3 nm [124], and that of the phosphate anion is around 0.5 nm [125].

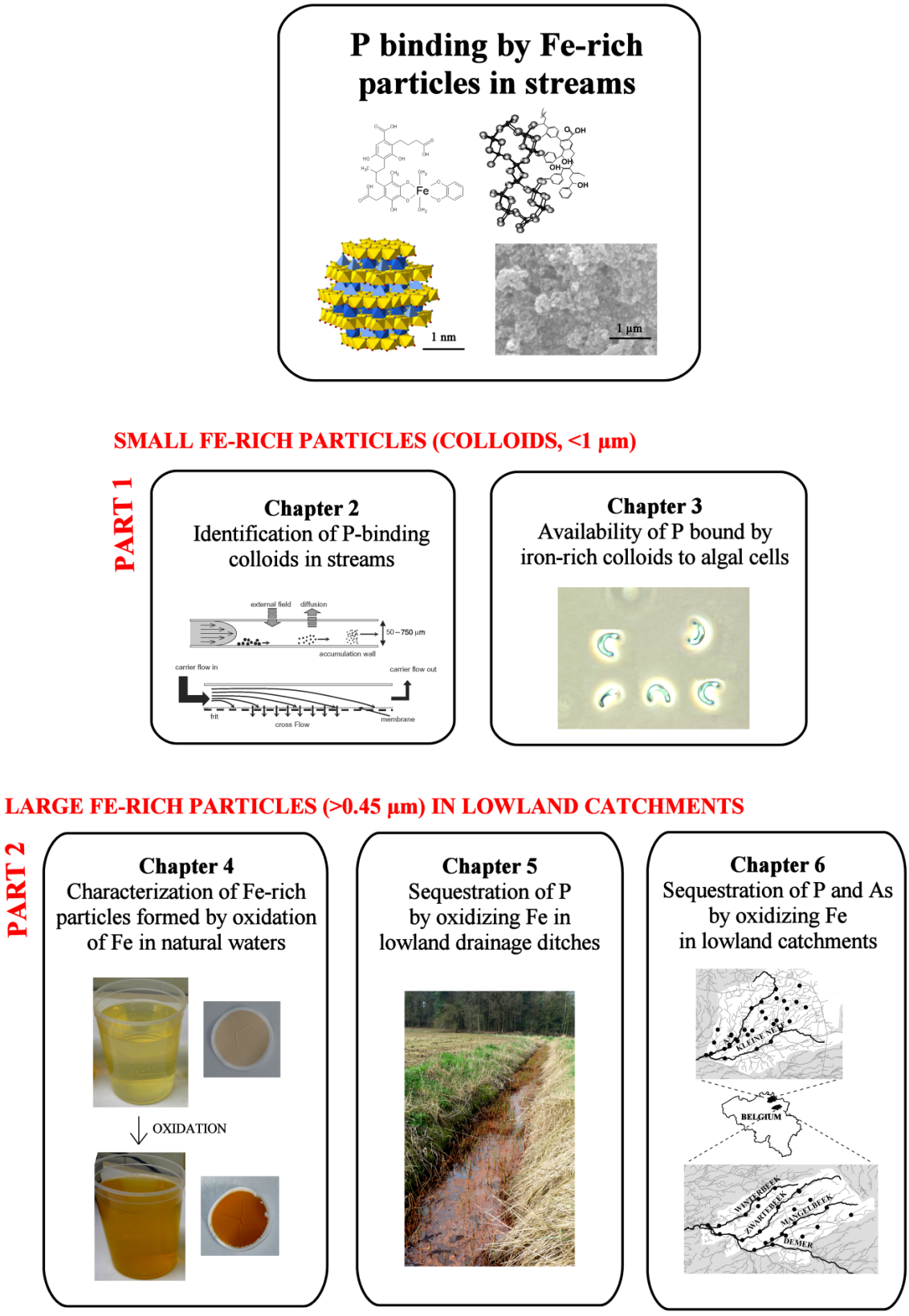

Figure 1.7: Outline of this dissertation.

Terminology of particles

No universally accepted vocabulary exists as it comes down to describing particles in natural systems [103]. The same term may have different meanings depending on the context (exact or operationally defined). This may lead to semantic confusion. Therefore, the terminology used in this dissertation is clarified here.

This dissertation uses the word *particle* to refer to any entity in natural waters which is not in *true solution* or *truly dissolved*. In order to define the true solution, Stumm and Morgan have proposed the chemical potential as a criterion: only those species or entities for which a chemical potential can be defined are considered in true solution, e.g. free metal ions, oxyanions, simple neutral molecules [126]. This criterion is not perfect, especially in the case of humic substances. One may be able to define a chemical potential for a fulvic acid molecule dissolved in water, but not if that fulvic acid forms an association with an inorganic Fe-rich phase (Figure 1.2, top right). Therefore, for practical purposes, humic substances are in this work also considered particles.

Colloids are particles below 1 µm in size. The rationale behind this cutoff is that particles roughly below this limit do not settle at any appreciable rate in natural waters, and their movement is more determined by Brownian motion than by settling [103]. *Nanoparticles* are particles below 100 nm in size. Therefore,

$$\text{nanoparticles} \subset \text{colloids} \subset \text{particles} \leftrightarrow \text{true solution}.$$

In an operationally defined context, *particles* or *particulate* is used for the >0.45 µm fraction, usually separated by membrane filtration. *Dissolved* is often used for the <0.45 µm fraction, even though this fraction is not free from particles. If these words are used in an operationally defined context in this dissertation, they are surrounded by quotation marks (“particulate”, “dissolved”), or the size range (>0.45 µm or <0.45 µm) is mentioned immediately afterwards. In chapter 2, a few additional operationally defined terms are used (Table 2.4).

Chapter 2 Identification of phosphorus bearing colloids in streamwater

Summary

Phosphorus (P) bound to colloidal matter may represent an important fraction of the P load in streams, but the composition of these heterogeneous colloids remains poorly characterized. In this study, the main colloidal vectors and their association with P in six Belgian streamwater samples were determined by field-flow fractionation ("nanoparticles", size range 1 kDa–150 nm) and by membrane filtration ("coarse colloids", size range 100–1200 nm). In soft water streams (Ca + Mg < 0.2 mM) draining upland peat, Fe–humic substances associations were identified as the main nanoparticulate vectors, with a peak between 3 and 6 nm and a long tail extending to sizes of up to 150 nm. Speciation calculations suggest that most of this Fe was present as nanoparticulate Fe oxyhydroxides. The size distribution of nanoparticulate P resembles that of Fe, but the Fe:P ratio decreases with increasing particle size. Conversely, the Fe:NOM ratio increases with increasing particle size, suggesting competition between P and NOM for binding on Fe oxyhydroxides. In two harder waters (Ca + Mg > 1 mM), P was mostly associated with colloidal ferrihydrite (40–1200 nm) and with nanoparticulate associations between Fe oxyhydroxides and clay minerals (50–150 nm). In one additional stream draining calcareous loess, the main P-bearing nanoparticles could not be identified. Overall, Fe oxyhydroxide colloids are the primary vectors of colloidal P. In waters with high Fe:P ratio, most of the P is bound by colloids. Conversely, at low total Fe:P ratio of the water, the colloids are saturated with P and most of the P is present in the <1 kDa fraction, likely as free ionic orthophosphate.

Introduction

Phosphorus in natural waters may be associated with Fe-rich colloidal material [76,97,127]. Such colloids have been identified as Fe oxyhydroxides, e.g. ferrihydrite [18,40]. Binding of P by such colloids can be highly effective: colloidal Fe-rich material may bind P at molar Fe:P ratios down to 2 [98,99]. The P-bearing colloids may additionally contain various other constituents, including organic C, Al, Ca, and Si. The dynamics and fate of colloidal P are likely governed by two processes: binding of P to Fe-rich particles, and aggregation of these particles to form larger entities [99,128]. Most fractionation studies on natural colloids use discrete size classes, or at best continuous size-distributions over a limited size range. The cut-offs are often based on nominal values, and are expressed either as hydrodynamic diameters or as molar masses which are not readily converted. For example, P associations with Fe-rich colloids have been identified in the 10–50 kDa size range, *i.e.* a few nanometers [97,127], as well as between 50 and 1000 nm [76]. The analysis of the continuous size distribution of P across a large size range would enhance our understanding of the binding of P by particles in natural waters.

Asymmetric flow field-flow fractionation (AF4) is a powerful tool for continuous size-separation and characterization of environmental nanoparticles, *i.e.* particles approximately between 1 and 100 nm [129,130]. The concepts of AF4 are explained in Box 2.1. In streamwater, AF4 studies have shown two principal types of colloidal material: organic carbon-rich colloids and Fe-rich colloids [95]. The carbon-rich colloids have mostly been identified as humic substances, ranging in size between approximately 0.5 and 5 nm. The Fe-rich colloids are generally assumed to consist mostly of Fe oxyhydroxides, and range widely in size (4–40 nm) [54,55,131]. These organic and Fe oxyhydroxide colloids may carry a wide range of other elements, which may be bound by surface complexation or coprecipitation. The associations of many trace metals and rare earth elements with natural nanoparticles have been relatively well studied by AF4 [54,55,95,131], but the association of P with nanosized material is poorly documented. This is likely due to the insufficiently low detection limits of P by ICP-MS [96]. The limited number of available AF4 studies on this topic have shown contrasting properties of colloidal P. In one study, clay particles were identified as the key vectors of colloidal P in drainage waters [78]. Others suggest that nanoparticulate P is predominantly associated with Fe-rich nanoparticles [53,95,96], but these data are based on samples from only six different

freshwater streams. As far as we are aware, no studies have characterized the colloidal P across the entire size spectrum between nanosized colloids and their aggregates exceeding 1 µm.

The goal of this work was to identify and characterize the associations between P and colloidal material in streams across a broad size range (1–1200 nm). Large colloids in streamwater were separated using membrane filtration, whereas nanoparticulate fraction was separated and characterized using AF4 coupled to UV and ICP-MS detection. Six water samples were collected from contrasting environments: soft waters draining upland peat with potentially small Fe–organic matter associations, a stream draining Fe-rich groundwater with potentially large ferrihydrite colloids, and two streams draining a calcareous area in which clay minerals may host the P-bearing colloids.

Materials and methods

Sampling

Six Belgian streams draining catchments of contrasting size, geology and hydrology were selected (Table 2.1). The Schwarzbach, Roer, and Helle streams drain the Hautes Fagnes, an upland peat area in eastern Belgium [132]. The Kleine Nete catchment is situated in a lowland area with sandy marine deposits; its streams are mainly fed by iron-rich groundwater [133]. The upper part of the Meuse catchment is dominated by calcareous sedimentary rocks, whereas the Belgian part of the Meuse drains the Ardennes massif mostly consisting of sedimentary and metamorphic (slate) rocks [134]. The Dijle catchment drains the undulating plateau of the Belgian loam belt, which is dominated by Luvisols developed on calcareous loess [135]. Both Maas and Dijle receive inputs from overland flow, and may therefore contain eroded colloids. The streams were sampled on January 14, 2014 after a dry spell of at least 3 days. The pH and electrical conductivity (EC) were measured in the field. The streamwater samples were immediately filtered in the field using membrane filters with nominal pore sizes of 1.2, 0.45, and 0.1 µm (1.2 and 0.45 µm: Chromafil Xtra PET 120/25 and 45/25 filters, diameter 25 mm, polyester membrane; 0.1 µm: Pall Acrodisc Supor filters, diameter 32 mm, hydrophylic polyethersulfone membrane). The concentrations of major and trace elements (ICP-MS), Fe(II) (ferrozine method [136]), Fe(III) (total Fe minus Fe(II)), organic and inorganic carbon (catalytic combustion and infrared detection), and major anions (anion chromatography)

were determined in the different filtrates. The UV-absorbance at 254 nm was determined spectrophotometrically and was corrected for interference by Fe(III) [137]. Corrections of the absorbance due to nitrate did not change the values by more than 1% and was not included [138]. The specific UV absorbance (SUVA), which is an indicator of humic substances and NOM aromaticity [138], was calculated as the UV absorbance per unit DOC. The term 'coarse colloids' will be used in this study to indicate the size fraction isolated by membrane filtration, *i.e.* nominally 100–1200 nm.

Field-flow fractionation

The nanoparticles in filtered streamwater samples (0.45 µm, Atlas Filtri AC-BX filter cartridge) were characterized by AF4 (AF2000, Postnova Analytics) on January 29–31, 2014 at Wageningen University, the Netherlands. The concepts of field-flow fractionation are explained in Box 2.1; the theory behind it and its application to environmental samples have been rigorously discussed elsewhere [139–143]. The AF4 setup used in this study has been described in previous studies [78,85,144]. The fractionation protocol was similar to previous work [144]; details are shown in Table 2.2. The injected sample volume was 2 mL (Kleine Nete and Helle samples) or 10 mL (Meuse, Dijle, Roer, and Schwarzbach samples). The elution lasted for 2400 s. The cross flow rate was relatively high (3 mL min^{-1}) during the first 900 s of the elution protocol in order to separate the smallest particles with high resolution. The cross flow rate then decreased within 120 s to 0.2 mL min^{-1} and remained at that value during the final 1380 s of the elution protocol in order to separate the large nanoparticles. This protocol allowed us to separate the smallest nanoparticles (up to 17 nm) with high resolution, while still including large nanoparticles (up to 150 nm) in the measurement. The AF4 system was thoroughly rinsed between each injection. After elution of a sample, the cross flow was switched off, and the channel was rinsed for 300 s. The purge valve was opened, and the channel was flushed at 4 mL min^{-1} for at least 300 s. Subsequently, a short version of the normal elution protocol was run, which used the same settings and flow rates but shorter times for each step. It consisted of 120 s focusing, 120 s elution at high cross flow (3 mL min^{-1}), 6 s transition time during which the cross flow decreased linearly, 120 s elution at low cross flow (0.2 mL min^{-1}), 180 s elution at zero cross flow, and at least 300 s of flushing with the purge valve open. The rinsing procedure included abrupt pressure changes, since previous experience with

the AF4 device had shown that material adhering to the AF4 membrane is mostly released after such pressure changes.

Size calibration showed that particles between 1 kDa and 17 nm were detected during the first part of the elution, whereas particles between 17 and 150 nm are eluted during the second part (Figure 2.2). Four proteins with hydrodynamic diameters between 3.3 and 17 nm (ribonuclease A, ovalbumin, aldolase, and thyroglobulin)[145] were well separated within the first part of the elution. This calibration yielded a linear relationship between retention time and size ($R^2 = 0.93$). The agreement between this calibration line and AF4 theory[141] (only 14% difference in slope) is excellent. The second part of the elution protocol was calibrated with polystyrene spheres (Postnova Analytics) of 20, 46, and 102 nm. In order to disperse the polystyrene particles, sodium dodecyl sulfate (0.1%) was added to the carrier. The relationship between retention time and size was linear ($R^2 = 0.997$). AF4 theory could not be applied to this second part of the elution because of the varying cross flow. For the purpose of this study, the particles detected by AF4 (1 kDa–150 nm) are referred to as "nanoparticles". The actual size of natural nanoparticles may differ somewhat from the value obtained by using the above calibration, e.g. due to nonspherical particles or nonideal behavior of the particles [146].

The AF4 was coupled online to a UV-detector and to a high-resolution ICP-MS (Element 2, Thermo Scientific). The UV signal at 254 nm was used as a proxy for aromatic organic matter [138]. It was corrected for the known contribution of Fe(III) to the UV-absorbance using a previously established correction equation [137]. The ICP-MS monitored the concentrations of selected elements at intervals of 7.4 s. The ICP-MS was calibrated by off-line aspiration of calibration standards at the beginning and at the end of each day. The calibration slopes measured at the end of a measurement day did not differ by more than 10% from those at the beginning, showing that signal drift in the ICP-MS was minimal. The median UV and ICP-MS signals recorded during focusing were considered as the baseline. For each measurement, the signals recorded during elution were converted to net signals by subtraction of the baseline. The ICP-MS signals were then converted to element concentrations at the AF4 outlet using the calibration slopes. Fractograms were constructed by plotting element concentrations versus retention time.

The background equivalent concentration (BEC) and detection limit (DL) of each element were determined from the baseline signal, *i.e.* the ICP-MS signal during sample injection.

The BEC was calculated as the median baseline signal, converted to an element concentration using the corresponding ICP-MS calibration slope. The detection limit (DL) was calculated as three times the standard deviation of the baseline signal, also converted to an element concentration. The average BEC and DL across all injections are reported (Table 2.3). In addition, two blank fractionations were performed, in which the ICP-MS signal was measured during elution of a blank sample (injection of 2 mL carrier solution). This allows to quantify the contributions of contamination due to the equipment, sample carry-over, and pressure-induced baseline drift during elution [96]. Blank fractionation 1 was performed following the normal rinsing procedure. Blank fractionation 2 was performed following minimal rinsing of the AF4 channel (flushing with purge valve open for 60 s instead of at least 300 s) and is considered to represent an upper limit to the signals picked up during the elution step. The signals recorded during both blank fractionations were converted to element concentrations using the ICP-MS calibration slopes. The 95th percentile (P_{95}) concentrations and the total amount of each element detected after blank fractionation are reported (Table 2.3). An element in a sample was considered quantifiable if the P_{95} of the concentration profile is at least 4 times larger than the P_{95} of the concentration profile of each blank fractionation. The rationale behind comparing P_{95} concentrations is to avoid erroneous interpretation of peaks as nanoparticulate material. Concentration profiles for which this condition is not met, are not shown or discussed. In addition, the total eluted amount of an element in a sample was compared to the total eluted amount of this element in both blank fractionations. The limit of quantification (LOQ) of each element was determined as 4 times the total eluted amount of this element in the blank fractionations. The rationale behind this comparison is to limit the uncertainty associated with the determination of total nanoparticulate concentrations of elements. For elements which do not fulfil this condition in a particular sample, the total nanoparticulate concentrations are reported as "<LOQ".

Box 2.1: Asymmetric flow field-flow fractionation (AF4)

Field-flow fractionation (FFF) is a flow-assisted hydrodynamic separation technique for particles in the nanometer size range [140]. FFF is performed in a flow channel, through which the particles are carried by a carrier solution. Due to interaction with an external field, the particles are retarded relative to the carrier liquid; the retention time of a particle in the channel depends on its properties. In asymmetric flow FFF (AF4), the driving force for particle separation is provided by a perpendicular (cross) flow field. The asymmetric flow channel consists of an impermeable top wall and a permeable accumulation wall, a membrane with pore size typically in the kDa range. The carrier can be a dilute solution similar to the natural medium of the particles. This is a clear advantage over the traditional size exclusion chromatography, which requires a carrier with high ionic strength.

In the flow channel, the particles form clouds. The average vertical position of a particle cloud in the channel is determined by 1) the cross flow field, which drags particles against the accumulation wall, and 2) back-diffusion away from the accumulation wall (Figure 2.1). The average cloud thickness, *l*, is determined by the Boltzmann constant *k*, the temperature *T*, and the force *F* exerted on the particles by the external field:

$$l = \frac{kT}{F} \qquad (Equation\ 2.1)$$

F is determined by the cross flow velocity v_c and the friction coefficient *f*, which is related to the diffusion coefficient *D* and the hydrodynamic diameter d_H through the Stokes-Einstein equation,

$$F = f \cdot v_c = \frac{kT}{D} \cdot v_c = 3\pi\eta d_H \cdot v_c \qquad (Equation\ 2.2)$$

where η is the viscosity of the carrier liquid. Therefore, the smallest particles are the farthest from the accumulation wall due to their high *D*. Due to the parabolic flow velocity profile of the carrier liquid in the channel, particle clouds far from the accumulation wall move faster through the channel than particle clouds closer to the accumulation wall. Therefore, the smallest particles are eluted first. It can be shown that, under the conditions typically used for fractionation of environmental nanoparticles, the relationship between d_H and retention time is linear [139].

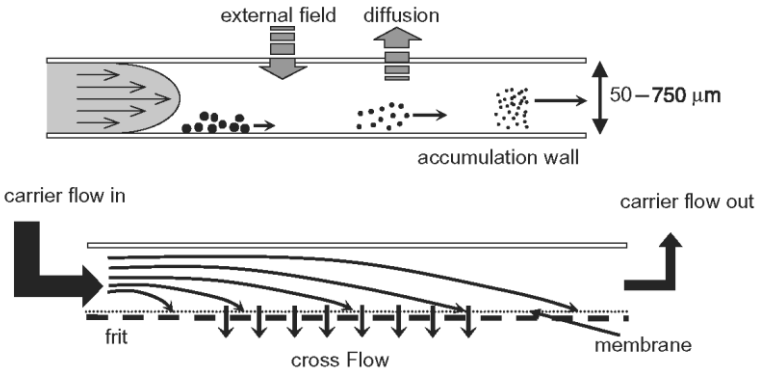

Figure 2.1: Schematic view of the flow channel in asymmetric flow field-flow fractionation (AF4), adapted from Von der Kammer et al. (ref. [140]).

Table 2.1: Characteristics of the streams and catchments sampled in this study. Sampling occurred on January 14, 2014 after a dry spell of 3 days (rainfall < 2 mm).

stream	sampling location	coordinates	stream order°	typical discharge (P_{10}–P_{90})	discharge on sampling date	catchment area*	catchment geomorphology*	dominant land use*	ref. for catchment description
				$m^3\ s^{-1}$	$m^3\ s^{-1}$	km^2			
Schwarzbach	Küchelscheid	N 50°31'16" E 6°12'20"	2	nm	<1	10	upland peat	forest	[132]
Roer	Küchelscheid	N 50°31'15" E 6°12'22"	3	0.5–9.0	3.5	50	upland peat	forest	[132]
Helle	Eupen	N 50°37'17" E 6°2'21"	3	nm	nm	72	upland peat	forest	[132]
Kleine Nete	Grobbendonk	N 51°11'39" E 4°45'15"	5	2.1–11.3	7.3	320	lowland catchment fed by iron-rich groundwater	agriculture	[133]
Maas	Wandre	N 50°51'42" E 4°40'51"	7	26–518	377	20 000	calcareous sedimentary rock; mountain range of sedimentary and metamorphic rock	agriculture; urban	[134]
Dijle	Heverlee	N 50°40'55" E 5°38'45"	4	3.3–8.6	4.8	760	incised calcareous loess plateau	agriculture	[135]

° The concept of stream orders is explained in Box 6.1.
P_{10}: 10^{th} percentile; P_{90}: 90^{th} percentile
* upstream of sampling location
nm: not measured

Table 2.2: Details of the AF4 setup and the analytical parameters used during fractionation. The protocol was based on that from a previous study [144]; adaptations are shown in bold.

AF4	AF2000, Postnova Analytics
Membrane	Polyethylenesulfone, 1 kDa
Spacer thickness	350 µm
Injection volume	**2 mL or 10 mL***
Injection flow rate	0.3 mL min^{-1}
Focusing time	**1260 (2 mL injections) or 3360 s (10 mL injections)**
Elution time	**2400 s**
Cross flow rate	
during focusing	3 mL min^{-1}
during elution, 0–900 s	3 mL min^{-1}
during elution, 900–1020 s	linearly decreasing from 3 to 0.2 mL min^{-1}
during elution, 1020–2400 s	0.2 mL min^{-1}
Detector flow rate	0.5 mL min^{-1}
Slot pump flow rate	**0 mL min^{-1}**
Carrier	3 mM $NaHCO_3$, pH 8.3

UV-DAD (diode array detector)	PN3241, Postnova Analytics
Monitored wavelength	254 nm
Time per reading	0.64 s

High resolution ICP-MS	Element 2, Thermo Scientific
Monitored elements	**^{27}Al ^{28}Si ^{31}P ^{43}Ca ^{51}V ^{52}Cr ^{56}Fe ^{60}Ni ^{63}Cu ^{75}As ^{98}Mo ^{114}Cd ^{118}Sn ^{208}Pb**
Time per reading	**7.4 s**
Operation mode	Medium resolution

* the 10-mL injections were performed by 5 sequential injections of 2 mL at 10-minute intervals during focusing.

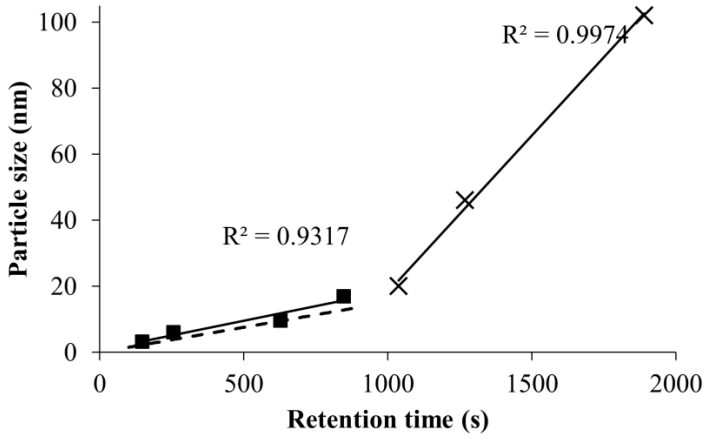

Figure 2.2: Size calibration of AF4. Proteins with known hydrodynamic diameter (3–17 nm; squares) eluted during the first part of the elution protocol at high cross flow. The regression line (full line; slope: 0.017 nm s^{-1}) almost coincides with predictions based on AF4 theory [143] (dashed line). Polystyrene particles (20–102 nm; crosses) eluted during the second part at low cross flow (slope: 0.095 nm s^{-1}).

Table 2.3: Detection of selected elements measured by ICP-MS following field-flow fractionation. The background equivalent concentrations (BEC) and detection limits (DL) are derived from baseline measurements. The background signal picked up during elution was quantified in two blank fractionations; the 95th percentile (P_{95}) concentrations and the total detected amount of each element are reported.

			Blank fractionation 1		**Blank fractionation 2**	
	BEC	**DL**	**P_{95}**	**total**	**P_{95}**	**total**
	nM	***nM***	***nM***	***nmol***	***nM***	***nmol***
P	3.5	2.8	5	0.03	8	0.10
Fe	4.7	3.2	2	0.01	12	0.12
Al	5.6	6.4	6	0.05	9	0.1
Si	400	115	173	1.6	130	1.1
Ca	600	165	146	<1	111	<1

* Blank fractionation 1 was performed following the normal rinsing procedure. Blank fractionation 2 was performed following minimal rinsing

Results and discussion

The terminology of different size fractions used in this study is repeated for clarity in Table 2.4. The general characteristics and composition of streamwater samples is shown in Table 2.5. The concentrations of selected elements in different size classes (Table 2.6), and the size distribution of selected elements within the nanoparticulate fraction (Table 2.7 and Figure 2.3) are shown. The fractograms (Figure 2.3) exhibit a step in the region where the cross flow changed. At high cross flow (retention times <900 s), one minute corresponds to a particle interval of around 1 nm, whereas at low cross flow (retention times >1020 s), one minute corresponds to a particle interval of 5.4 nm. Because the detector flow rate remains constant, particles at the AF4 outlet are more concentrated under low cross flow conditions. The change from high to low cross flow therefore results in a 5.4-fold increase in element concentrations and UV-absorbance. This step, which is a consequence of the fractionation protocol used, should not be interpreted as a distinct peak but rather as the continuation of the signal under decreasing cross flow.

The concentrations of nanoparticulate Fe (1 kDa–150 nm) recovered after field-flow fractionation are between 19 and 72% of the Fe concentrations measured after membrane filtration with nominal pore size 100 nm. This difference may be caused by small (<1 kDa) Fe–fulvic acid complexes which may pass the AF4 membrane[124], or by large Fe-rich colloids which did not elute before the fractionation was terminated. Alternatively, and perhaps most importantly, part of the nanoparticulate material may be lost by adsorption to the AF4 membrane. Low recoveries have been observed in many field-flow fractionation studies, even for elements such as Fe and Cu which commonly have very low free ion concentrations [56,85,96,147,148]. For this reason, the concentrations reported in Table 2.6 may be an underestimation of the true concentrations in the fraction between 1 kDa and 150 nm.

The six sampled waters can broadly be subdivided into two categories based on water hardness: the three upland peat streams are soft waters (Schwarzbach, Roer, Helle: Ca + Mg < 0.2 mM), whereas the other streams are harder waters (Kleine Nete, Maas, Dijle: Ca + Mg > 1 mM). This coincides with two classes of the size of the colloids. The colloids in the soft waters are dominated by small nanoparticles in the size range between 1 and 40 nm (Tables 2.6 and 2.7). These samples have generally similar characteristics:

slightly acidic pH, low electrical conductivity, low concentrations of major cations and anions, aromatic NOM typical for upland peats (as evidenced by the high SUVA), and low P concentrations (<0.7 µM). In contrast, the colloidal fraction in the streams with harder water is dominated by large nanoparticles and colloids between 40 and 1200 nm.

Colloidal vectors

The colloids in the three upland peat streams are similar, and the Fe and Al distribution suggests that they mostly consist of small nanoparticles between 1 and 40 nm (Tables 2.6 and 2.7). Coarse colloids are a minor fraction: no more than 15% of the colloidal Fe and Al is between 100 and 1200 nm in size. In the nanoparticulate fraction, Fe, Al, Ca, and humic substances (as evidenced by the UV absorbance) are identified as the main constituents (Figure 2.3). Si was not detected in these nanoparticles (concentrations at the AF4 outlet below 150 nM). Fe is the main constituent of the Schwarzbach and Roer nanoparticles, whereas in the Helle, nanoparticulate Al concentrations are above those of Fe. The size distributions of Fe, Al, and humic substances are characterized by a main peak around 2–6 nm and are skewed towards larger particle sizes with a long tail extending to particle sizes of up to 150 nm. The step around 20 nm is due to the changing cross flow and must be interpreted as the continuation of this tail. Interestingly, the main UV peak maximum (2–3 nm) occurs at lower sizes than the maxima of the main Fe and Al peaks (3–6 nm). The difference in peak maxima is not due to the time delay between the UV detector and the ICP-MS: the first peak of Cu, which strongly binds humic substances, exactly matches that of the UV signal. This has also been observed in previous studies, albeit less clearly [53–55], and it suggests that complexes of Fe and Al with humic substances are not the dominant Fe and Al forms present in this size range. Likely, most of the Fe and Al in the peaks with maxima between 3 and 6 nm consists of small Fe and Al oxyhydroxide particles. This is underpinned by speciation calculations with WHAM7.0 [149], which show that 77–90% of the Fe(III) in these samples (and 93% of the Al in the Helle) is present as colloidal hydrous ferric oxide, the remainder of the Fe and Al being present as complexes with humic substances [34]. Ferrihydrite, a common Fe oxyhydroxide in colloidal material from natural waters [40], occurs as nanosized primary particles in the 2–10 nm range [61,150]. Likely, the main Fe peak in these samples (3–6 nm) consists of small primary ferrihydrite-like particles, while the tail of the size distribution towards large particle sizes (up to 150 nm) may reflect aggregates of such primary

particles. This view is in agreement with an earlier field-flow fractionation study [151]. In the Roer, the Fe and Al signals exhibit a small secondary peak at around 80 nm, which likely consists of such aggregates.

The nanosized Fe and Al oxides likely have adsorbed humic substances at their surfaces which may prevent further aggregation. In nanoparticles from the Roer, and to a lesser extent also in those from the Schwarzbach, the main UV peak at 2.5 nm is followed by a secondary peak at 5 nm, which coincides with the major Fe peak. This may be due to adsorbed humic substances at the surface of nanosized Fe and Al oxides. However, interpretation of the UV signal may be tricky: Fe(III) also absorbs light at 254 nm. We corrected the UV measurements for the presence of Fe [137], but this correction may not be perfect. The Ca in these nanoparticles may be complexed by humic substances, or it may be coprecipitated with Fe oxides [17]. The Ca signal after field-flow fractionation is in all samples very noisy (Figure 2.3 shows Ca as moving average for clarity) and in the range of the background signal, and therefore it must be interpreted with caution. In summary, the main colloidal vectors in these samples are likely associations between humic substances and Fe oxyhydroxide particles.

Contrary to the samples from upland peat streams, the colloids in the Kleine Nete, Maas, and Dijle samples are mostly in the size range between 40 and 1200 nm as shown by the Fe and Al fractograms and filter fractions (Figure 2.3, Tables 2.6 and 2.7). The Kleine Nete has at least 10-fold larger colloidal Fe concentrations than the Maas and Dijle. In the Kleine Nete, Fe is the key constituent across the 40–1200 nm size range. The concentrations of Al are comparably low, and no nanoparticulate Si or Ca was detected. The UV signal exhibits a sharp peak with maximum around 2.5 nm, which likely consists of humic substances, and a broad peak between 40 and 150 nm which is difficult to interpret because of the high Fe concentration in these nanoparticles (the correction due to UV-absorption by Fe was 60–70% [137]). Fe-rich particles in the Kleine Nete have been identified in the 4–72 µm size range (10^{th}–90^{th} percentile) and mainly consist of ferrihydrite (Chapter 4). The colloidal Fe in this stream is part of a larger and continuous size distribution of Fe in particles, and the colloidal Fe is likely also present as ferrihydrite.

The nanoparticles in the Maas exhibit narrow peaks of Ca and UV with maxima around 2–3 nm, and a small Fe peak in the same size range. This hints at Ca and Fe complexed

by humic substances. The 40–150 nm size range is dominated by large peaks of Al, Fe, and Si with very similar concentration profiles. The molar ratio of Si:Al is 1.3 across the whole 40–150 nm size range, and 1.5 near the peak maximum. The quantification of Si concentrations is subject to some uncertainty: the Si signal in blank fractionations was relatively high (up to 150 nM) and was accounted for by subtraction. The Al and Si peaks are indicative of aluminosilicate minerals. Since previous studies have identified clay minerals in natural water samples in this size range by field-flow fractionation [52,78,152], we assume here that these particles consist of clay minerals. The Fe is present in this size range at concentrations similar to those of Al and Si. The Fe is likely associated with the clay minerals, e.g. by isomorphic substitution in the mineral lattice or as Fe oxyhydroxide at the surface of the clay [153–155]. The coarse colloids (100–1200 nm) contain Fe and Al in approximately equal molar ratios. No Si was detected in this fraction, but detection of low colloidal Si concentrations by membrane filtration is difficult since a large fraction of the Si occurs as free H_4SiO_4 monomers in natural waters [156]. Therefore, based on these data, it cannot be determined whether clay minerals are also present in the 100–1200 nm fraction.

The smallest nanoparticles in the Dijle (peak maximum at 2–3 nm) exhibit similar features as in the Maas, *i.e.* a sharp peak in UV and Ca concentration, and a small peak of Fe, suggesting Ca and Fe are complexed by humic substances. The large nanoparticles (40–150 nm) mainly consist of Fe, with smaller amounts of Al and possibly also humic substances. No nanoparticulate Si or Ca was detected in this fraction, *i.e.* their concentrations at the AF4 outlet were below approximately 150 nM. In the fraction between 100 and 1200 nm, only Fe was detected. The speciation of Fe in the 40–1200 nm fraction is unclear. It may be present as oxyhydroxide particles, but its presence in clays cannot be excluded since Si bearing colloids may be present at concentrations below the detection limit.

Table 2.4: Nomenclature of operationally defined particle fractions used in this study.

name	**size range**	**remarks**
colloids	1 kDa–1200 nm	
coarse colloids	100–1200 nm	the fraction separated by membrane filtration
nanoparticles	1 kDa–150 nm	the fraction separated by field-flow fractionation
→ large nanoparticles	40–150 nm	
→ small nanoparticles	1 kDa–40 nm	

Table 2.5: Characteristics and composition of filtered (<0.45 µm) streamwater samples.

	pH	**EC**	**Mg**	**Ca**	**Si**	**OC**	**UV_{254}**	**SUVA**	**Fe**	**Fe(II)**	**Al**	**P**	**Mn**	**Cu**	**Zn**	**Pb**	**IC**	**Cl**	**SO_4**	**NO_3**
		µS cm^{-1}	mg L^{-1}	mg L^{-1}	mg L^{-1}	mg L^{-1}	cm^{-1}	L $(g \cdot cm)^{-1}$	µg L^{-1}	µg L^{-1}	µg L^{-1}	µg L^{-1}	µg L^{-1}	µg L^{-1}	µg L^{-1}	µg L^{-1}	mg L^{-1}	mg L^{-1}	mg L^{-1}	mg L^{-1}
Schwarzbach	6.3	36	0.9	2	1.7	7.1	0.231	33	308	128	153	3	58	0.5	28	0.50	1	3	5	2
Roer	6.8	67	1.5	4	1.7	5.4	0.197	36	276	99	76	6	38	0.5	13	0.29	2	8	6	4
Helle	6.9	93	1.8	5	2.3	6.4	0.163	25	155	56	294	21	71	1.6	72	0.48	2	10	11	4
Kleine Nete	7.2	565	6.1	34	4.2	8.9	0.218	25	904	137	31	53	133	1.1	20	0.14	16	65	90	8
Maas	7.9	323	4.8	42	2.6	4.5	0.087	19	40	22	22	56	13	0.9	8	0.08	26	17	21	15
Dijle	7.9	866	12.0	104	6.8	4.6	0.083	18	43	9	5	114	112	0.5	4	0.11	59	66	61	31

EC: electrical conductivity OC: organic carbon UV_{254}: UV-absorption at 254 nm
SUVA: specific UV-absorption IC: inorganic carbon

Table 2.6: The concentration of Fe, Al, P, and organic C in different size fractions of streamwater samples. The <1200 nm, <450 nm, and <100 nm size fractions were isolated by membrane filtration; the 1 kDa–150 nm size fraction was isolated by field-flow fractionation.

	size fraction	**Fe**	**Fe(II)**	**Al**	**P**	**OC**
		µM	***µM***	***µM***	***µM***	***µM***
Schwarzbach	*<1200 nm*	5.7	2.3	5.8	0.1	561
	<450 nm	5.5	2.3	5.7	0.1	588
	<100 nm	5.2	1.9	5.6	0.1	573
	1 kDa–150 nm	1.4		0.2	0.04	
Roer	*<1200 nm*	5.2	1.7	2.9	0.2	461
	<450 nm	4.9	1.8	2.8	0.2	453
	<100 nm	4.5	1.5	2.7	0.2	486
	1 kDa–150 nm	3.1		0.5	0.1	
Helle	*<1200 nm*	2.9	1.1	11.4	0.7	548
	<450 nm	2.8	1.0	10.9	0.7	536
	<100 nm	2.5	0.9	10.1	0.6	534
	1 kDa–150 nm	0.5		0.8	<0.2	
Kleine Nete	*<1200 nm*	24.1	2.9	1.4	2.1	758
	<450 nm	16.2	2.5	1.2	1.7	741
	<100 nm	5.8	0.9	0.5	0.7	842
	1 kDa–150 nm	4.2		0.2	0.4	
Maas	*<1200 nm*	0.89	0.44	1.0	1.9	354
	<450 nm	0.72	0.40	0.8	1.8	380
	<100 nm	0.43	0.31	0.6	1.8	378
	1 kDa–150 nm	0.24		0.2	0.1	
Dijle	*<1200 nm*	1.72	0.40	0.3	4.0	412
	<450 nm	0.77	0.17	0.2	3.7	377
	<100 nm	0.28	0.12	0.4	3.4	411
	1 kDa–150 nm	0.06		<0.04	0.1	

OC: organic carbon; empty fields: not measured.

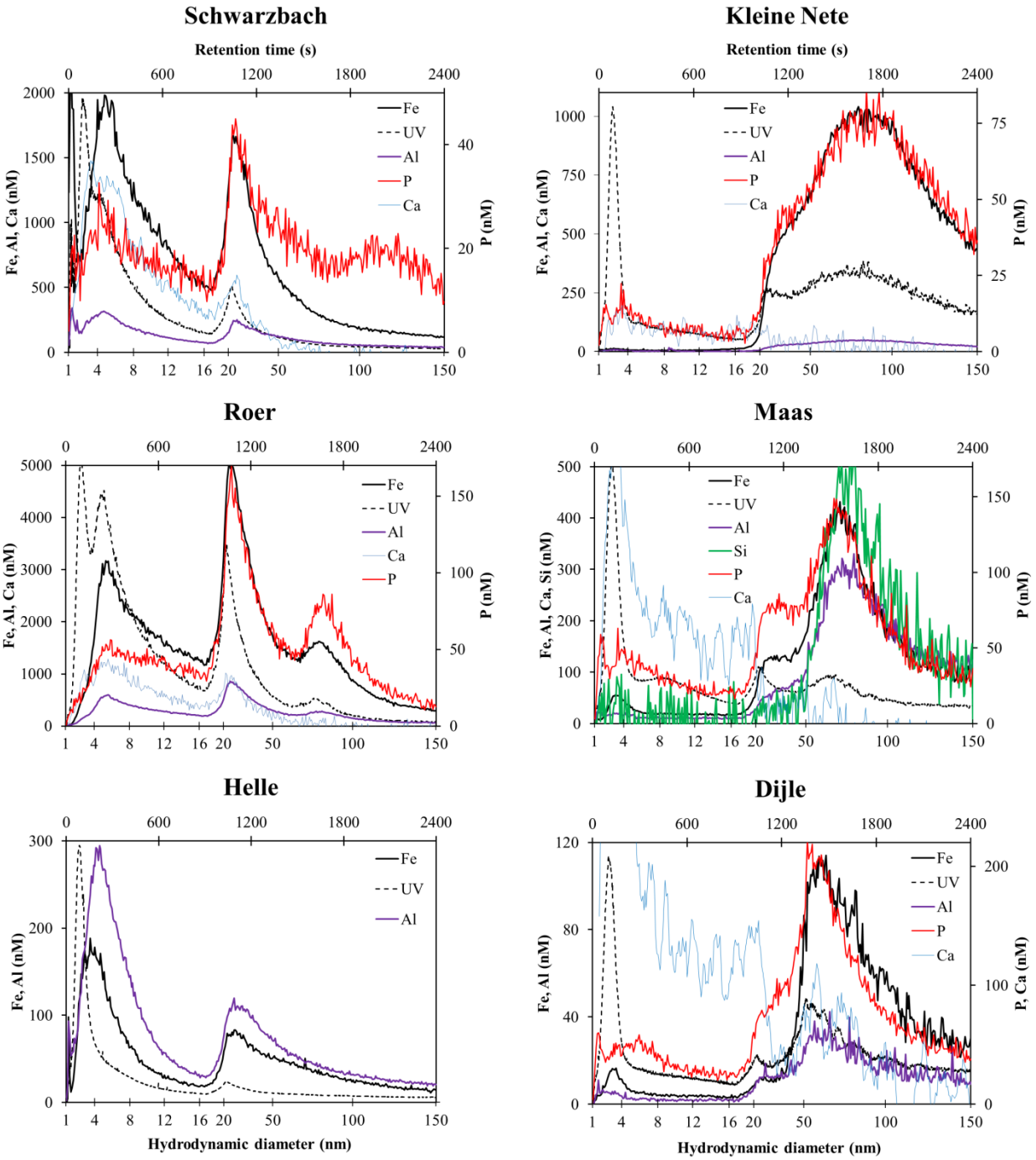

Figure 2.3: Fractograms of selected elements (in nM) and the UV absorbance (arbitrary units) after field-flow fractionation of natural nanoparticles from streamwater. The data are plotted versus retention time (s, top axis) and hydrodynamic diameter (nm, bottom axis). The step around 20 nm (1000 s) is caused by the decrease in cross flow rate and the corresponding change in scale of the hydrodynamic diameter axis. **Left**: soft water samples (hardness <0.6 mM); **Right**: moderately hard to very hard water samples (hardness >0.6 mM).

Table 2.7: Size distribution of selected elements and of the UV signal at 254 nm in nanoparticles as determined by field-flow fractionation (in %).

	size fraction	Fe	Al	P	UV_{254}
Schwarzbach	*1 kDa–40 nm*	81	72	54	90
	40–150 nm	19	28	46	10
Roer	*1 kDa–40 nm*	68	68	56	88
	40–150 nm	32	32	44	12
Helle	*1 kDa–40 nm*	70	74		84
	40–150 nm	30	26		16
Kleine Nete	*1 kDa–40 nm*	10	16	19	39
	40–150 nm	90	84	81	61
Maas	*1 kDa–40 nm*	17	11	35	66
	40–150 nm	83	89	65	34
Dijle	*1 kDa–40 nm*	11		32	47
	40–150 nm	89		68	53

UV_{254}: UV signal at 254 nm; empty fields: below LOQ or not measured.

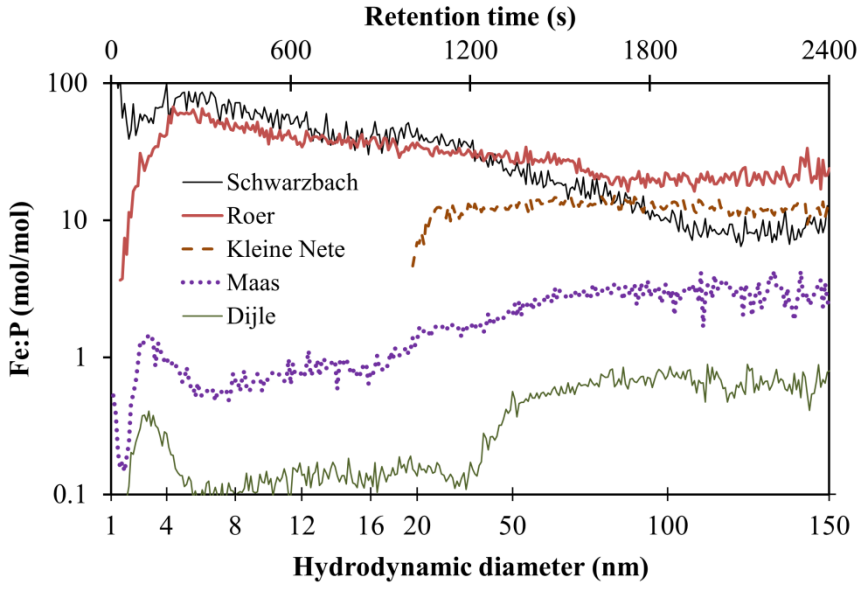

Figure 2.4: Molar Fe:P ratios in nanoparticles from streamwater.

The association of P with Fe-rich colloids

The three upland peat streams (Schwarzbach, Roer, Helle) contain low P concentrations (<0.7 µM). Little or no P is present in the 100–1200 nm size fraction. In the Roer and Schwarzbach, part of the P was present as nanoparticles (Table 2.6). In the Roer, the nanoparticulate P concentrations were well detectable, whereas in the Schwarzbach, they were near the LOQ. In the Helle, no nanoparticulate P could be detected, but this is likely because the injected sample volume was only 2 mL, compared to 10 mL for the Roer and Schwarzbach. The size distribution of nanoparticulate P in these samples consists of a maximum at around 5 nm and a long, slowly decreasing tail which spans the entire size range up to 150 nm. The step around 20 nm is due to the changing cross flow and must be interpreted as the continuation of this tail. In addition, a small peak at large particle sizes is present in both samples, between approximately 90 and 130 nm in the Schwarzbach and between 70 and 100 nm in the Roer. The overall size distribution of P is similar to that of Fe. Likely, in these samples, the Fe oxyhydroxide–humic substances associations are the key vectors of nanoparticulate P. Part of the P in in these oligotrophic, low-P systems may be present as organic P compounds, but most organic P compounds are small (<3 nm) [157] and may not be withheld by the AF4 membrane (nominal pore size 1 kDa). The association of P with Fe and Al bearing nanoparticles of similar size in streams has been documented by previous field-flow fractionation studies [95,96]. A notable difference between the size distributions of Fe and P is that the tail decreases faster for Fe than for P. This results in decreasing Fe:P ratios with increasing particle size: from around 75 to 9 mol Fe (mol P)$^{-1}$ in the Schwarzbach, and from 60 to 20 mol Fe (mol P)$^{-1}$ in the Roer (Figure 2.4). A similar trend is observed for vanadium (V), an element which commonly occurs as the vanadate (VO_4) oxyanion and which is commonly associated with Fe oxyhydroxides in natural waters [158] (data not shown). Hence, P and V are preferentially bound to large nanoparticles, which appears contradictory to their smaller specific surface area. It is speculated that this may be an effect of competition between P and humic substances at the surface of Fe oxyhydroxide nanoparticles. Figure 2.3 shows that the larger nanoparticles have higher Fe:UV ratios (UV signal corrected for Fe), suggesting they contain less humic substances. Previous studies have already shown that humic substances can reduce P binding at oxyhydroxides surfaces in soils through competition effects [121]. It is well established that organic C affects the crystallinity and properties of Fe oxyhydroxides [159,160]. In addition, it has been shown that the binding of

oxyanions by organic matter-Fe oxide associations is affected by the Fe:organic C ratio [161,162]. However, the proposed mechanism for more efficient P binding to large nanoparticles is speculative and needs experimental validation. Part of the humic substances in the smallest nanoparticles is likely not associated to Fe-rich nanoparticles, and therefore the exact Fe:organic C ratio in the Fe-rich nanoparticles remains unknown. In summary, associations between Fe oxyhydroxides and humic substances are likely the key vectors of nanoparticulate P in these samples, and the largest nanoparticles bind comparably more P per unit Fe than the smaller nanoparticles.

In the Kleine Nete, more than 80% of the P is bound to colloids (Table 2.6). In the nanoparticulate fraction, the size distribution of P almost exactly matches that of Fe (Figure 2.3). The Fe:P ratio in small nanoparticles could not be quantified, but in the 40–150 nm size fraction, it is relatively constant at around 13 mol Fe (mol P)$^{-1}$ (Figure 2.4) which is equal to the Fe:P ratio in the 100–1200 nm fraction. This strongly suggests that the composition of the 40–1200 nm size fraction is highly uniform and consists of P bound to Fe oxyhydroxide aggregates. Binding of oxyanions to Fe oxides may occur according to two mechanisms: post-synthesis adsorption or coprecipitation with oxidizing Fe [163]. Studies in the Kleine Nete catchment (Chapters 5 and 6) suggest that coprecipitation may be the key mechanism of P binding to Fe oxyhydroxides in this catchment, because P and reduced Fe(II) both originate from groundwater and simultaneously enter oxic environments.

In the Maas and the Dijle, only a small fraction of the P is recovered in the colloids of the 1 kDa–1200 nm size range (around 10% in the Dijle and 17% in the Maas, Table 2.6). These low fractions are in contrast with the higher fractions in the three other waters (>40%), which suggests the P is mostly present as free ionic orthophosphate or as small (<1 kDa) organic P molecules. In both samples, the size distribution of nanoparticulate P exhibits a small peak with a maximum around a few nanometers and a large tail, and a large peak between 50 and 100 nm. In the latter region, the size distribution of P matches that of Fe fairly well (Figure 2.3). In the Maas, the Fe:P ratio in this size range is between 2 and 3 mol Fe (mol P)$^{-1}$ (Figure 2.4). Colloidal and nanoparticulate Fe oxyhydroxides containing such high P concentrations have previously been identified in this size range [98,99]. It is therefore likely that in the Maas, the nanoparticulate P is mostly bound to Fe oxyhydroxide–clay associations, but this fraction is small compared to the free orthophosphate. In the Dijle, the Fe:P ratio in large nanoparticles (40–150 nm) is around

0.75 mol Fe (mol P)$^{-1}$. These particles cannot consist of P bound to Fe oxyhydroxides or of ferric phosphates, which have Fe:P ratios down to approximately 1 mol Fe (mol P)$^{-1}$ [17]. The P was not bound as nanosized Ca phosphates either, given the low Ca concentrations in this fraction (Figure 2.3). It remains unclear to what vector the nanoparticulate P is bound. In the coarse colloids (100–1200 nm), the Fe:P ratio is 2.3. Therefore, in this size fraction, the P may be bound to Fe-rich colloids. However, this is somewhat speculative since the P vector in the nanoparticulate fraction cannot be Fe oxyhydroxides alone. Therefore, the identity of the P-bearing colloids in the Dijle remains largely unknown. The high Fe:P ratios in nanoparticles and colloids from the Maas and Dijle compared to other streams (Figure 2.4) is readily explained by the Fe:P ratio in the 1.2 µm-filtrates (<0.5 for the Maas and Dijle versus >10 for the Roer, Schwarzbach, and Kleine Nete). High nanoparticulate Fe:P ratios are observed in streams with high total Fe:P ratios, but streams with low Fe:P ratios have Fe-rich nanoparticles which are saturated with P.

Conclusions

Taken together, this study identified Fe oxyhydroxide colloids as primary vectors of colloidal P. In soft, acidic, and humic-rich waters, small Fe-rich nanoparticles (1–40 nm) dominate. These nanoparticles mostly consist of Fe oxyhydroxides with small amounts of mononuclear Fe–NOM complexes. These waters have a high Fe:P ratio, and the P is preferentially bound to large particles. The reverse trend is observed for NOM, suggesting NOM to outcompete phosphate at low Fe:NOM ratio. In contrast, larger Fe-rich particles (40–1200 nm) dominate in harder, more alkaline waters. These consist of Fe oxyhydroxides which may be associated with clay minerals. At high total Fe:P ratio, as in the Kleine Nete, Fe oxyhydroxide colloids bind most of the P in the water. At low total Fe:P ratio, as in the Maas and Dijle, the Fe oxyhydroxide colloids are saturated with P.

The colloids reflect the geomorphological properties of the catchments they originate from. Streams draining acidic upland peat receive soil percolate rich in humic substances, resulting in small humic-rich nanoparticles. The Fe–NOM colloids may be formed as water percolates through the soil [164], or they may be formed by in-stream oxidation of Fe(II) [15]. The Kleine Nete is fed by Fe-rich groundwater which is oxidized in-stream [165], resulting in high Fe concentrations, large particles, a high Fe:P ratio in the particles, and low free ionic orthophosphate concentrations. The Maas contains clay minerals, which

are likely weathering products of the Ardennes mountain range it drains. We expected to find clay minerals in the Dijle because it drains a calcareous loess area where clays (e.g. illite) likely occur. Possibly they were present at concentrations below the detection limit. Alternatively, the clay may have been present as larger aggregates due to the very hard water. The Maas and Dijle do not receive high Fe inputs, and therefore the Fe-rich nanoparticles in these streams are saturated with P. Most of the P in these streams is smaller than 1 kDa and likely occurs as free ionic orthophosphate.

Chapter 3 The bioavailability of phosphorus bound to iron-organic matter colloids

This chapter is adapted from Baken et al., *Water Res.* **59** 198–206 (ref. [166]).

Summary

The bioavailability of phosphorus (P) in natural waters strongly depends on its speciation. In this study, the effect of iron-organic matter colloids on sorption and bioavailability of P was determined. The freshwater green alga *Raphidocelis subcapitata* was exposed to media spiked with radiolabelled $^{33}PO_4$, and the uptake of ^{33}P was monitored for 1 hour. The media contained various concentrations of synthetic iron-organic matter colloids with a size between 10 kDa and 0.45 µm. EXAFS spectroscopy showed that these colloids predominantly consisted of ferrihydrite with small amounts of organically complexed Fe. In colloid-free treatments, the P uptake flux by the algae obeyed Michaelis-Menten kinetics. In the presence of iron-organic matter colloids at 9 or 90 µM Fe, corresponding to molar Fe:P ratios between 6 and 47 mol Fe (mol P)$^{-1}$, the truly dissolved P (<10 kDa) was between 4 and 60% of the total P. These colloids reduced the P uptake flux by algal cells compared to colloid-free treatments at the same total P concentration. However, the P uptake flux from colloid containing solutions equalled that from colloid-free ones when expressed as truly dissolved P. This demonstrates that colloidal P did not contribute to the P uptake flux. It is concluded that, on the short term, phosphate adsorbed to ferrihydrite colloids is not available to algal cells.

Introduction

Phosphorus is a limiting nutrient in many aquatic ecosystems, and eutrophication of such systems has often been linked to excessive P inputs [13]. The bioavailability of P depends on the P speciation. In natural water samples, the bioavailability of P to algae may be measured in various ways, and an operationally defined distinction is made between the immediate and the potential bioavailability [167]. The immediate or direct P bioavailability is measured by short-term (minutes-hours) experiments, which allow the detection of P influx by means of radioactive tracers. This P fraction is useful for better understanding P dynamics in aquatic systems, especially if the focus is on the "dissolved" (<0.45 µm) P fraction. In contrast, long-term (days-weeks) experiments in P-limited solutions measure the algal growth response (as biomass yield or cell numbers) and determine the potential or ultimate bioavailability. The potentially available P fraction comprises both the directly available P and the P that can ultimately be transformed into available forms by biotic or abiotic hydrolysis [167].

Both the immediate and the potential P bioavailability strongly depend on P speciation. The potential P bioavailability in natural waters may range from 0 to 100% of the total P, depending on the source and, hence, on P speciation [168]. Free orthophosphate is immediately available, but organic and colloidal P compounds may contribute in varying degrees to the immediate or potential P bioavailability. The bioavailability of organic P is relatively well documented: the immediate bioavailability of most model organic P compounds (e.g. nucleotides, phosphate esters) is below 20%, whereas their potential bioavailability varies widely between 2 and 72%, depending on the compound [169–171]. Less attention has so far been paid to the bioavailability of colloidal P. Colloidal P might, for instance, be desorbed from the colloid surface and thereby contribute to the P bioavailability. Alternatively, diffusion limited conditions may occur if the P uptake rate exceeds the diffusion flux. If desorption of colloidal P is quick and takes place in an unstirred depletion layer adjacent to the cell, colloidal P might enhance the P uptake flux. Such has previously been observed for P uptake by *Brassica napus* roots [172]. Previous studies on the algal bioavailability of colloidal P have yielded variable and contrasting results [173–175] which emphasizes the need for further exploring the colloidal P fraction. Moreover, to our knowledge, the immediate bioavailability of P in a well-defined model system has never been related to measurements of free P.

This study was set up to measure the immediate (short-term) bioavailability of colloidal orthophosphate to freshwater green algae in a model system. A washed P-starved culture of the freshwater green alga *Raphidocelis subcapitata* was exposed to media containing orthophosphate as the only P-source and either or not containing synthetic iron-organic matter colloids. The P uptake flux, measured using a $^{33}PO_4$ radiotracer, was used as a proxy for the immediate P bioavailability. It was hypothesized that iron-organic matter colloids reduce the free P concentration, and thereby also the P bioavailability.

Materials and methods

Test organism and culture conditions

The freshwater green alga *Raphidocelis subcapitata*, formerly known as *Pseudokirchneriella subcapitata* or as *Selenastrum capricornutum*, was selected as the test species. This member of the Chlorophyceae class occurs in nutrient-rich freshwaters [176] and has been used extensively in toxicity testing. It has also been used for bioassays for P in freshwaters [74,177,178]. A pure culture of *Raphidocelis subcapitata* was obtained from the Culture Collection of Algae and Protozoa (CCAP 278/4, Oban, U.K.). A subculture was initiated in a cellulose-stoppered Erlenmeyer flask containing sterile culture medium with adequate P supply (a modified WC medium; Table 3.1) which was inoculated with between 2 x 10^3 and 5 x 10^3 cells mL^{-1}. The culture was kept at ambient temperature on a negatoscope with continuous illumination from the bottom by cool white lamps (Master TL-E Circular Super 80 32W/840, Philips). The culture was replaced every 1–2 weeks by initiating a new subculture. A sample of the culture was regularly checked by microscopy and no contamination by bacteria or other micro-organisms was observed. The cell density was monitored by particle counting (HIAC Royco 9705). The exponential growth rate between day 1 and day 4 ranged between 1.0 and 1.1 day^{-1}.

Algae for the P uptake experiments were harvested under sterile conditions from cultures grown for 6–10 days (cell density between 1 x 10^6 and 4 x 10^6 cells mL^{-1}). The algae were centrifuged (15 min, 6000 *g*), washed with ultrapure water, and the algal pellet was transferred to a sterile P-free medium (Table 3.1). The cell density at this stage was around 1 x 10^6 cells mL^{-1}. After installation on the negatoscope, the algae were starved for P for 7–12 days, during which the cell density increased to approximately 3 x 10^6 cells mL^{-1}. On the day of the uptake experiment, the P-starved algae were isolated

and washed in a similar way as described above. The algal pellet was then suspended in an aliquot of water at a cell density of approximately 1 x 10^7 cells mL^{-1} for use in the P uptake experiments. The internal P concentration of the algae in this suspension was between 0.4 and 0.6% P on a dry-weight basis, compared to around 2% P for cultures grown under adequate P supply. This shows that the culture was indeed P-starved.

Table 3.1: Composition of the culture medium, the P-free medium, and the test medium (before addition of P and Fe) used in the P uptake experiments.

	Culture medium	**P-free medium**	**Test medium**	
$CaCl_2 \cdot 2H_2O$	0.25	0.25	0.005	mM
$MgSO_4 \cdot 7H_2O$	0.15	0.15	0.003	mM
$NaHCO_3$	0.15	0.15	0.15	mM
$NaNO_3$	1.0	1.0	1.0	mM
$K_2HPO_4 \cdot 3H_2O$	0.050	x	x	mM
KNO_3	x	0.10	0.10	mM
SRNOM	x	x	10	mg L^{-1}
HEPES buffer	2.0	2.0	2.0	mM
pH	7.5	7.5	7.5	
ionic strength	3.6	3.6	2.3	mM
$Na_2H_2EDTA + FeCl_3 \cdot 6H_2O$	12	12	x	µM
$CuSO_4 \cdot 5H_2O$	0.040	0.040	x	µM
$ZnSO_4 \cdot 7H_2O$	0.077	0.077	x	µM
$CoCl_2 \cdot 6H_2O$	0.042	0.042	x	µM
$MnCl_2 \cdot 4H_2O$	0.89	0.89	x	µM
$Na_2MoO_4 \cdot 2H_2O$	0.025	0.025	x	µM
H_3BO_3	16	16	x	µM

x: not present
SRNOM: Suwannee River natural organic matter

Test media and treatments

All test media had a uniform background composition (Table 3.1). Compared to the culture medium, the test media contained less Ca and Mg, no P, no trace metals, and they additionally contained Suwannee River natural organic matter (SRNOM). The Ca and Mg concentrations were reduced in order to avoid aggregation and precipitation of the iron-organic matter colloids. Preliminary experiments showed that the Fe-SRNOM colloids readily flocculated and settled if Ca and Mg concentrations are as in the culture medium.

The test media of different treatments had varying Fe and P concentrations. The colloid-free treatments did not contain Fe colloids and had free orthophosphate as the only P source. The P was added to the test media 24 hours before the start of the experiment as pre-mixed aliquots of $^{31}PO_4$ (from an orthophosphate standard solution, KH_2PO_4 in H_2O, with a certified PO_4 concentration of 1000 mg L^{-1}, Merck Millipore) and radiolabelled $^{33}PO_4$ (from $H_3{}^{33}PO_4$ in H_2O, Perkin Elmer). The colloid-containing treatments were prepared by addition of 9 or 90 µM Fe(II) L^{-1} (as dissolved $FeSO_4 \cdot 7H_2O$) to the test media 48 hours before the start of the experiment. The Fe concentration of 9 µM is within the range commonly encountered in filtered streamwater samples, albeit towards the high end (10^{th}–90^{th} percentile of European streams: 0.14–13 µM Fe) [4], whereas the 90 µM was included because it was anticipated that the effects on P binding would be more easily detected. Oxidation of Fe(II) to Fe(III) occurred within a few hours at pH 7.5 [179]. This yielded Fe oxyhydroxides which were in the colloidal size range due to the stabilization by SRNOM. After 24 hours of oxidation, the test media were filtered in order to remove any "particulate" iron (>0.45 µm, Chromafil PET-45/25 membrane filters), and the pH was checked and adapted to 7.5. The colloid containing treatments were further subdivided. In the P adsorption treatments, P was added 24 hours before the start of the experiment, *i.e.* after the synthesis of the iron-organic matter colloids, and therefore the binding of P occurred mainly at the surface of the colloids. In the P coprecipitation treatments, P was added just before the addition of the Fe(II), and therefore P binding also occurred by coprecipitation. The $^{33}PO_4$ was always added simultaneously with the $^{31}PO_4$, and therefore ^{33}P was a perfect tracer for orthophosphate. The activity of ^{33}P in all treatments was approximately 4.5 nCi mL^{-1} (167 Bq mL^{-1}).

The total initial P and Fe concentrations in the test media were measured by ICP-MS (Agilent 7700x, LOQ: 0.08 µM P). The "truly dissolved" or "free" P, *i.e.* the P that was

not colloidal, was determined after centrifugal ultrafiltration of the test media (Vivaspin 6 centrifugal concentrator with 10 kDa PES membrane, Sartorius Stedim) and measurement of the ^{33}P activity in the ultrafiltrate by liquid scintillation counting (Tri-Carb 2800TR, Perkin Elmer). Centrifugal ultrafiltration has previously successfully been used for the separation of colloidal from truly dissolved species in environmental samples [180]. Preliminary experiments showed that orthophosphate was not retained by the 10 kDa membrane: the recovery of ^{33}P in the ultrafiltrate of colloid-free test media and of ultrapure water spiked with $^{33}PO_4$ was >95%. Distribution coefficients (K_D) of P were calculated as the colloidal P concentration (expressed per kg Fe since the exact mass of the colloids is unknown) divided by the free P concentration.

Speciation of the colloidal Fe

Two samples of the synthetic colloids used in the uptake experiment were prepared for measurement of the size distribution and EXAFS (Extended X-ray Absorption Fine Structure) spectroscopy. These samples contained the same background composition as the test media and contained nominal Fe additions of 90 µM Fe (corresponding to 9000 µmol Fe (g SRNOM)$^{-1}$; sample A) and 9 µM Fe (corresponding to 900 µmol Fe (g SRNOM)$^{-1}$; sample B). They did not contain P. The size distribution of Fe was measured by ICP-MS after 24 hours of oxidation and after filtration of the test media over 0.45 µm membrane filters (Chromafil PET-45/25), 0.1 µm membrane filters (Acrodisc filters with Supor membrane, Pall Life Sciences), and 10 kDa ultrafiltration concentrators (Vivaspin 6). The Fe(II) concentration in these samples was measured with the ferrozine method [136].

Freeze-dried subsamples of the colloidal samples A and B were measured by Fe-edge (7112 eV) EXAFS spectroscopy at the wiggler beamline I811, MAX-lab, Lund, Sweden. The concepts of EXAFS spectroscopy are explained in Box 4.1 (Chapter 4), and the measurements were performed under the same conditions as described in Chapter 4. Standard spectra of 2-line ferrihydrite and Fe complexed by SRNOM (90 µmol Fe (g SRNOM)$^{-1}$) were also measured, and standard spectra of goethite, lepidocrocite, and the Fe(III)–trisoxalate complex were obtained from earlier studies [40,181,182]. The EXAFS spectra were analyzed by wavelet transforms (WT), linear combination fitting (LCF), and conventional EXAFS modelling. The WT of EXAFS spectra can be used to qualitatively discriminate between the nature of the backscattering

atoms. Heavy backscattering atoms (such as Fe) cause oscillations at high *k* values, whereas lighter backscattering atoms cause oscillations at lower *k* values. We use the WT method in order to detect the presence of Fe backscattering atoms in the second and third coordination shells, which causes a pronounced maximum in the WT plot at around $k = 7$ Å^{-1} and R = 3 Å [183]. Plots of the WT modulus were calculated using the method developed by Funke et al. [184] (parameters: $\eta = 8$, $\sigma = 1$) which is implemented in the Igor Pro script. Linear combination fitting (LCF) was applied to the k^3-weighted EXAFS spectra using a least-squares algorithm. The sum of the contributions of all standards was constrained to equal 1. In order to address the uncertainty associated with LCF due to noise at high k-values, the higher limit of the *k*-range was varied between 8.5 Å^{-1} and 12.0 Å^{-1}. For the conventional EXAFS modelling, the model described in Chapter 4 was used. The model included single scattering Fe–O and multiple scattering Fe–O–O interactions in the first coordination shell, a single scattering Fe–Fe2 interaction in the second coordination shell, and a single scattering Fe–Fe3 interaction in the third coordination shell. This model contained a total of 14 parameters, 7 of which were fixed or constrained (Table 3.3).

Uptake experiment

The short-term P uptake experiment was conducted as described previously [185]. One single culture of *R. subcapitata* was used with an internal P concentration of 0.4%. The experiment was carried out in triplicate in acid washed 100-mL beakers, each containing 15 mL of test medium. The beakers were placed on the negatoscope under ambient conditions. Aliquots of the washed P-starved algae culture were added to the test media to yield a final cell density of 5×10^5 cells mL^{-1}. The addition of the algae marked the start of the experiment.

Approximately 5, 30, and 60 minutes after the addition of the algae, 1-mL samples were transferred into Eppendorf tubes and immediately centrifuged (15 min, 6000 *g*) in order to separate the algae from the test medium. The supernatant was removed, the remaining pellet was suspended in 1 mL of ultrapure water, and the ^{33}P activity in both fractions was measured by liquid scintillation counting (Tri-carb 2800TR, Perkin Elmer) after the addition of 2 mL scintillation cocktail (Ultima Gold, Perkin Elmer). The recovery of ^{33}P in the pellet and in the supernatant was always between 96 and 103% of the total ^{33}P in the test medium. The algal pellet was not washed because earlier experiments using

various washing media showed that no extracellular phosphate could be removed [185]. Preliminary tests also showed that, under the conditions of this experiment (*i.e.* low concentrations of divalent cations in the test media), very little adsorption of colloids onto the surface of algal cells or precipitation of colloids during the centrifugation step occurred: the loss of Fe from the supernatant after centrifugation was on average 3% (and never more than 7%) compared to the Fe initially present. It could therefore be assumed that all ^{33}P recovered in the pellet was internalized by the algae.

Calculations

The internalized P concentration (P_{int}, in µM) was calculated as the total initial P concentration in the medium, multiplied by the fraction of the ^{33}P recovered in the algal pellet. For each treatment, a linear regression model was fitted to plots of the internalized P concentration versus time (t, in s) using a least-squares algorithm (n = 9). The slope of this linear model (S, in µM s^{-1}) represents the P uptake rate by the algae. It was converted to a P uptake flux, expressed per unit cell surface (F_P , in pmol P cm^{-2} s^{-1}), using

$$F_P = \frac{S}{A \cdot C} \cdot 1000 = \frac{dP_{int}}{dt} \cdot \frac{1}{A \cdot C} \cdot 1000 \qquad (Equation\ 3.1)$$

where A is the average surface area of *R. subcapitata* cells ($67 \cdot 10^{-8}$ cm^2 cell^{-1}, ref. [186]), and C is the cell density of *R. subcapitata* in the experiment which equaled $5 \cdot 10^5$ cells mL^{-1}. The P uptake flux, F_P, is in this experiment used as a measure of the immediate P bioavailability.

The P uptake flux in colloid-free treatments were related to the orthophosphate concentration in the test medium by fitting them to a Michaelis-Menten type equation,

$$F_P = F_{MAX} \frac{[PO_4]}{K_M + [PO_4]} \qquad (Equation\ 3.2)$$

with F_{MAX} the P uptake flux at saturation (in pmol P cm^{-2} s^{-1}), K_M the half-saturation constant (in µM), and [PO$_4$] the orthophosphate concentration in the test medium (in µM) measured as P concentration by ICP-MS. Parameter optimization, calculation of interpolated values, and their estimated standard errors and 95% confidence limits were performed using a nonlinear least squares algorithm (the NLIN procedure) in SAS 9.3.

Results and Discussion

Speciation of the colloidal Fe

The majority of the Fe added to the test media was recovered in the fraction between 0.1 µm and 10 kDa (Table 3.2). The latter roughly corresponds to a hydrodynamic diameter between 2 and 3 nm [145]. This confirms that the Fe was predominantly present in the colloidal fraction. The Fe in the colloidal fraction was partly (8–23%) still present as reduced Fe(II) bound to the iron-organic matter colloids. The near absence of truly dissolved Fe(II), *i.e.* Fe(II) in the <10 kDa fraction, indicates that the oxidation process was completed after 24 hours as expected from earlier studies [179]. Preliminary experiments revealed that, in the absence of SRNOM, the Fe readily flocculated and settled, which suggests that the SRNOM stabilized the colloids. This is in agreement with earlier studies which have shown that colloidal Fe strongly interacts with and may be stabilized by natural organic matter [15,38].

The EXAFS spectrum of the colloidal sample A (9000 µmol Fe (g SRNOM)$^{-1}$) strongly resembles that of ferrihydrite, whereas that of the colloidal sample B (900 µmol Fe (g SRNOM)$^{-1}$) shows resemblance to both the ferrihydrite and the Fe–SRNOM complex (Figure 3.1). The wavelet transform plots of both colloidal samples confirm the presence of Fe–Fe interactions as evidenced by the pronounced maximum around k = 7 Å^{-1} and R = 2.8 Å (Figure 3.2). Such Fe–Fe interactions are absent from the wavelet transform plots of the Fe–SRNOM complex standard, confirming that the Fe in this standard was indeed present as organic complexes and that it was not hydrolyzed. The linear combination fitting results confirm that ferrihydrite was the predominant constituent of both colloidal samples. Depending on the *k*-range used, the colloidal sample A was fitted as 83–87% ferrihydrite, 7–9% lepidocrocite, 2–8% Fe–SRNOM complex, and <3% of goethite and Fe–oxalate complex. The colloidal sample B was fitted as 63–83% ferrihydrite, 7–33% Fe–SRNOM complex, and <3% of the other standards. Especially for sample B, the fitted fraction of Fe–SRNOM strongly depended on the *k*-range used and increased as the higher limit of the *k*-range increased. This reflects the uncertainty associated with the LCF method. The EXAFS spectra of the iron-organic matter colloids and that of ferrihydrite were well fitted by the proposed model with Fe–O interactions in the first coordination shell around 1.98 Å and with Fe–Fe interactions in the second and third coordination shells around 3.05 and 3.43 Å (Table 3.2). The former

distance refers to edge-sharing Fe octahedra, whereas the latter refers to corner-sharing octahedra [187]. The fits are shown in Figure 3.1; note that in EXAFS spectroscopy, peaks in Fourier transformed spectra appear at slightly lower R than the true interatomic distance, because the interaction between the photoelectron and the coulomb potentials of the scattering atoms causes a phase shift in the oscillations of the EXAFS spectrum. The inclusion of a triangular multiple scattering path (Fe–O–O) significantly improved the model fits as evidenced by a lower chi-squared statistic. The Fe–Fe interactions in sample A were more pronounced than those in sample B, as reflected by the higher coordination numbers. Even though the LCF analysis suggested the presence of Fe-organic complexes, no Fe–C interactions could be refined in either colloidal sample. Since C is a much lighter element than Fe, Fe–C interactions are easily overshadowed by Fe–Fe interactions [40].

The EXAFS spectra and the refined Fe–Fe distances in our samples agree well with naturally occurring ferrihydrite [188] and with previous studies on Fe and SRNOM [31]. Upon oxidation of Fe(II) in circumneutral waters, the expected reaction product may be a hydrous ferric oxide with few corner-sharing Fe–Fe linkages, 2-line ferrihydrite, or lepidocrocite, depending on the Si concentrations [17,100]. The Si concentrations in the test media (around 7 µM Si L^{-1}) are in the range where ferrihydrite formation can be expected. It is concluded that the colloids predominantly consisted of ferrihydrite with small amounts of lepidocrocite (sample A) and Fe–NOM complexes.

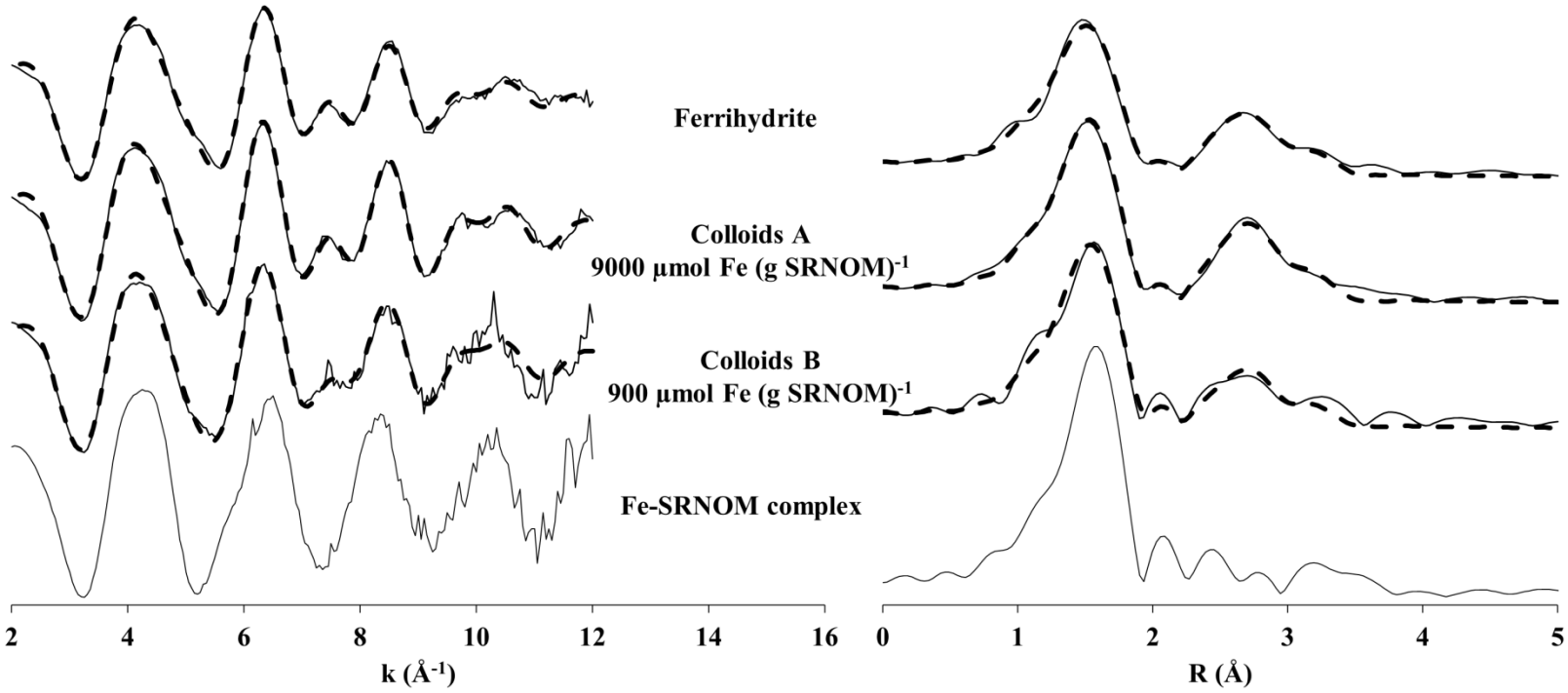

Figure 3.1: k^3-weighted Fe EXAFS spectra (**left**) and their Fourier transforms (**right**) of ferrihydrite, synthetic iron-organic matter colloids, and Fe complexed by Suwannee River natural organic matter. Full lines are observed data; dashed lines are model fits.

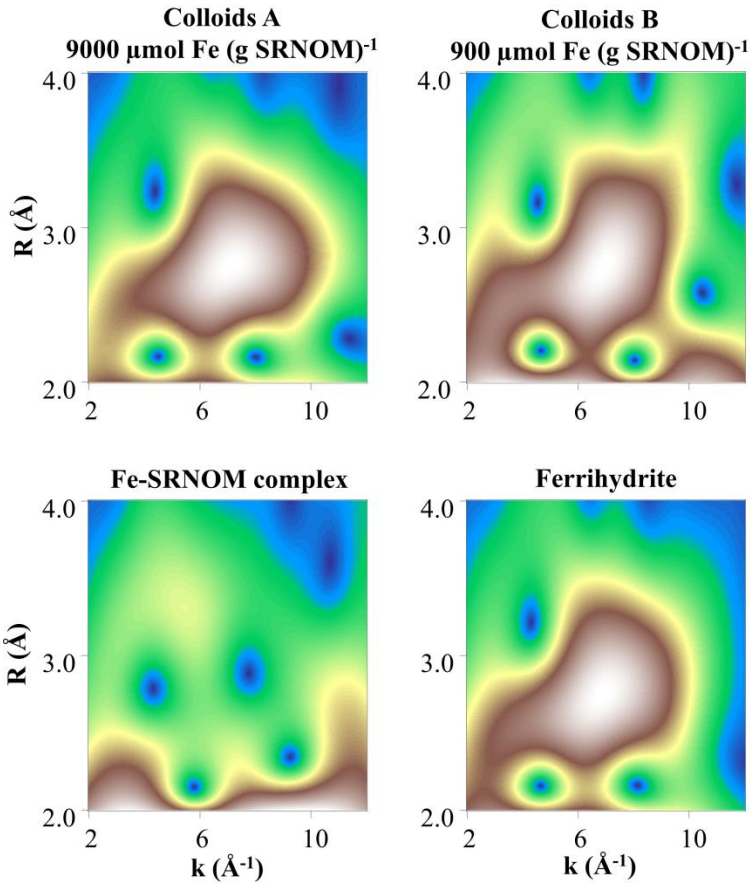

Figure 3.2: Wavelet transform modulus of the EXAFS spectra of Fe–natural organic matter colloids (top) and reference compounds (bottom). The maximum around k = 7 Å^{-1} and R = 2.8 Å refers to Fe–Fe interactions. White: high magnitude; blue: low magnitude.

Table 3.2: Speciation and size distribution of Fe in the synthetic colloids (all data in µM Fe).

Sample	**Unfiltered**		**<0.45 µm**		**<0.1 µm**		**<10 kDa**	
(nominal Fe concentration)	**Fe**	**Fe(II)**	**Fe**	**Fe(II)**	**Fe**	**Fe(II)**	**Fe**	**Fe(II)**
Colloids A 9000 µmol Fe (g SRNOM)$^{-1}$	86.3	7.3	84.3	7.3	72.5	6.1	0.7	0.4
Colloids B 900 µmol Fe (g SRNOM)$^{-1}$	8.8	2.3	8.6	2.1	7.9	1.8	1.1	0.4

Table 3.3: Optimal parameter values and uncertainties for the R-space fits of EXAFS spectra of synthetic iron-organic matter colloids and ferrihydrite.

sample	Red χ^2	S_0^2 (1)	E_0 (eV)	Fe–O (2)		Fe–Fe2 (3)		Fe–Fe3 (3)		Fe–O–O (4)
				R (Å)	σ^2 (Å^2)	N	R (Å)	N	R (Å)	R (Å)
Ferrihydrite	469	0.78*	0.34 ± 0.51	1.98 ± 0.01	0.0112 ± 0.0004	2.7 ± 0.4	3.05 ± 0.01	1.5 ± 0.4	3.44 ± 0.02	3.38 ± 0.01*
Colloids A: 9000 µmol Fe (g SRNOM)$^{-1}$	365	0.78*	0.63 ± 0.51	1.98 ± 0.01	0.0089 ± 0.0004	3.6 ± 0.5	3.06 ± 0.01	1.8 ± 0.4	3.43 ± 0.02	3.38 ± 0.01*
Colloids B: 900 µmol Fe (g SRNOM)$^{-1}$	117	0.78*	1.33 ± 0.54	1.99 ± 0.01	0.0090 ± 0.0005	2.5 ± 0.7	3.07 ± 0.02	1.4 ± 0.6	3.4 ± 0.03	3.40 ± 0.01*

Red χ^2: reduced chi-square statistic

S_0^2: passive amplitude reduction factor

E_0: edge energy

R: half path length

σ^2: Debye-Waller factor or bond distance distribution

N: degeneracy

*: constrained parameter

(1) S_0^2 was set to 0.78 which was obtained from a first-shell fit of ferrihydrite between R = 1.0 and 2.0 Å and with N set to 6.

(2) N of the Fe–O path was set to 6.

(3) σ^2 of the Fe–Fe paths was set to 0.014 for the Fe–Fe2 path and to 0.009 for the Fe–Fe3 path. These values were derived from a fit of ferrihydrite between R = 2.0 and 4.0 Å while keeping the first shell parameters fixed.

(4) For the Fe–O–O multiple scattering path, N was set to 24, R was constrained to equal 1.707 times that of the Fe–O path, and σ^2 was constrained to equal that of the Fe–O path.

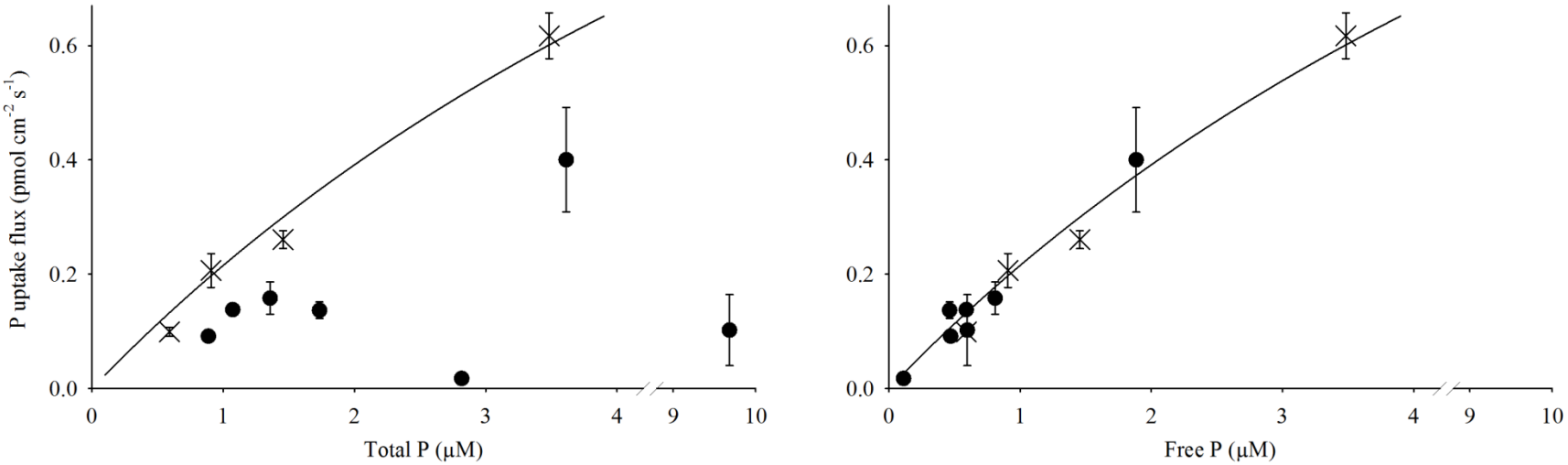

Figure 3.3: Phophorus uptake flux in colloid-free (crosses) and colloid-containing (closed circles) treatments plotted versus total (**left**) and free (<10 kDa; **right**) P concentrations. The full line is the Michaelis-Menten equation fitted to the colloid-free treatments. Error bars represent 95% confidence limits.

Table 3.4: Flux of P uptake by *R. subcapitata* at different P concentrations and with or without iron-organic matter colloids. In colloid-free treatments, the total P equalled the free P concentration, which is operationally defined as <10 kDa. In P adsorption treatments, P was added after the oxidation of ferrous iron and the formation of the colloids. In P coprecipitation treatments, P was added before the addition of ferrous iron. The distribution coefficient K_D is defined as the colloidal P concentration (expressed per unit Fe) divided by the free P concentration.

Treatment	**Treatment type**	**Fe**	**Total P**	**Fe:P**	**Free P (<10 kDa)**		**K_D**	**Uptake flux (pmol P cm^{-2} s^{-1}) ± 95% confidence limits**		
		µM	*µM*	*mol:mol*	*µM*	*%*	*10^6 L (kg Fe)$^{-1}$*	observed	predicted from total P	predicted from free P
1	colloid-free	0.5	0.6		0.6	100	x	0.10 ± 0.01	0.13 ± 0.03	
2	colloid-free	0.5	0.9		0.9	100	x	0.21 ± 0.03	0.20 ± 0.04	
3	colloid-free	0.5	1.5		1.5	100	x	0.26 ± 0.02	0.30 ± 0.06	
4	colloid-free	0.5	3.5		3.5	100	x	0.62 ± 0.04	0.60 ± 0.09	
5	colloid-free	0.5	5.9		5.9	100	x	0.78 ± 0.07	0.85 ± 0.09	
6	colloid-free	0.5	9.6		9.6	100	x	1.22 ± 0.11	1.12 ± 0.09	
7	colloid-free	0.5	26.3		26.3	100	x	1.58 ± 0.31	1.61 ± 0.16	
8	P adsorption	80.4	1.7	47	0.5	27	0.6	0.14 ± 0.01	0.35 ± 0.07	0.11 ± 0.02
9	P adsorption	84.9	3.6	24	1.9	52	0.2	0.40 ± 0.09	0.62 ± 0.09	0.37 ± 0.07
10	P coprecipitation	7.9	0.9	9	0.5	53	2.0	0.09 ± 0.01	0.19 ± 0.04	0.11 ± 0.02
11	P coprecipitation	7.5	1.1	7	0.6	55	1.9	0.14 ± 0.01	0.23 ± 0.05	0.13 ± 0.03
12	P coprecipitation	8.1	1.4	6	0.8	60	1.5	0.16 ± 0.03	0.28 ± 0.06	0.18 ± 0.04
13	P coprecipitation	81.8	2.8	29	0.1	4	5.3	0.02 ± 0.01	0.51 ± 0.08	0.03 ± 0.01
14	P coprecipitation	84.5	9.7	9	0.6	6	3.2	0.10 ± 0.06	1.12 ± 0.09	0.13 ± 0.03

Phosphate binding to colloidal ferrihydrite

Orthophosphate was quickly and efficiently bound to the iron-organic matter colloids, as evidenced by the high K_D values between $2 \cdot 10^5$ and $5 \cdot 10^6$ L (kg Fe)$^{-1}$ (Table 3.4). The colloids contained between 0.01 and 0.1 mol P (mol Fe)$^{-1}$. The free (truly dissolved, *i.e.* <10 kDa) P concentration was between 4 and 60%. In the adsorption treatments, to which the P was added after the formation of the iron-organic matter colloids, the P had roughly 10-fold lower K_D values than in similar coprecipitation treatments, in which P was present during the formation of the colloids. This is in good agreement with Mayer & Jarrell [100]: P binding to Si-containing Fe hydroxides is stronger if the P is present during their formation. Voegelin et al. [17,123] showed that, upon oxidation of Fe(II) at pH 7 in the presence of phosphate, a Fe–phosphate phase is formed as long as free ionic phosphate is present. Therefore, the P binding in the coprecipitation treatments likely occurred through coprecipitation of Fe and P. Other earlier work on environmental samples has also demonstrated high P binding to freshly formed Fe(III) colloids and precipitates [98,99].

P uptake flux by algal cells

In all treatments, the increase in internalised ^{33}P fraction with time was linear between 5 and 60 minutes after the start of the experiment. The slope of the linear regression was converted to the P uptake flux (Table 3.4). The P uptake flux of treatments 13 and 14 had relatively wide confidence limits compared to the other treatments, which was due to the low internalised ^{33}P activity in these treatments. The concept of a constant P uptake flux is based on the assumptions of a one-step internalisation and a constant external P concentration. It may not accurately reflect the actual uptake process [189], but has proven satisfactory for algal P uptake in a wide range of studies. The 60-minute interval was selected based on preliminary tests, which showed that the ^{33}P internalisation levelled off after 120 minutes. At high external P concentrations, internal feedback mechanisms may cause a reduced P uptake flux [185]. Conversely, in the treatments with low (<2 µM) free P concentrations, the deviation from linearity was likely due to the decrease in solution P concentration, which was up to 70% after 120 minutes. The uptake of P was not limited by diffusion of P towards the cell surface. The maximum diffusion flux to a spherical cell in an unstirred solution was estimated assuming a cell radius of R = 5 µm, a bulk P concentration of C = 0.5 µM, a cell surface P concentration of zero, and a diffusivity of P in water of $D = 10^{-5}$ cm^2 s^{-1} [190]. The predicted maximum diffusion flux to the surface of

the sphere is $D \cdot C \cdot R^{-1}$ = 10 pmol cm^{-2} s^{-1}, which exceeds the fluxes observed in our experiment by more than an order of magnitude. Even though the assumption of spherical cells is flawed for *R. subcapitata*, it is unlikely that P uptake by starved *R. subcapitata* cells was diffusion limited.

In the colloid-free treatments, *i.e.* with free orthophosphate as the only P source, the P uptake flux obeyed Michaelis-Menten kinetics (all data in Table 3.4, data at low P concentrations plotted in Figure 3.3). The Michaelis-Menten parameters and their estimated standard errors were: $K_M = 9.1 \pm 1.4$ µM and $F_{MAX} = 2.2 \pm 0.2$ pmol cm^{-2} s^{-1}. The F_{MAX} is in the range of values previously encountered for Chlorophyceae, whereas the K_M is slightly above that range [81].

In the colloid-containing treatments, the observed P uptake flux was lower than that in colloid-free treatments with similar total P concentrations (Figure 3.3). However, if plotted against free P concentrations, the colloid-containing treatments coincide with the Michaelis-Menten curve. In other words, the P uptake flux in a medium containing colloids equalled that in a hypothetical colloid-free medium with the same free P concentration. The Michaelis-Menten equation fitted to the colloid-free treatments was used to predict the P uptake flux in colloid-containing treatments. Two types of predictions were made: one using the total P concentration, and another using the free P concentration (Table 3.4). The predictions based on the total P concentrations exceed the observed values by factors between 1.5 and 30. The predictions based on the free P concentrations are between 0.8 and 1.5 times the observed values (average 1.1, standard error 0.1). The above shows that the colloidal P did not contribute to the P uptake flux and was therefore not immediately available under the conditions of this experiment.

Our findings are in line with earlier work on algal growth response which indicated no or limited long-term (ultimate) algal availability of P adsorbed to synthetic Fe colloids [175]. However, that study used very large colloid concentrations, and a quantitative analysis was hampered by a lack of separating the free P fraction from the colloidal P. We did not observe diffusion limited uptake, which is in contrast with earlier work on P uptake by plant roots [172]. This difference is not explained by size effects: the radius of root hairs is typically a few µm [191], *i.e.* in the same range as the size of *R. subcapitata* cells. Part of the difference may be due to the fact that the algal cells are distributed uniformly in the test media, whereas root hairs are not, which may cause local P depletion in the vicinity of the

roots. However, the difference is most likely explained by different free P concentrations (0.01–0.02 µM in the plant uptake experiment versus 0.1–2 µM in this study), which cause a larger diffusive flux towards the cell surface.

The orthophosphate concentrations in European streams commonly range between 0.1 and 4.2 µM (P_{10}-P_{90}) with a median value of 0.8 µM [192]. The P concentrations used in this study are highly representative of those typically encountered in streams. Therefore, the results of this study, which showed that P uptake was not diffusion limited, may be of great relevance for algal uptake of P in streamwater. Since the P bound to inorganic colloids is included in colorimetric P assays, these results cast doubt on the validity of such assays as a measure of the directly bioavailable P fraction in natural waters. However, some uncertainties remain. This experiment used only one specific set of conditions (ionic strength, pH, Fe concentration, NOM concentration and quality). In natural waters, these conditions range widely, which may affect P binding and release by Fe-rich colloids. Diffusion limited P uptake by biota may occur in streams with very low free P concentrations. Moreover, *R. subcapitata* has a relatively low P uptake rate [81], and colloidal P may be more available to other biological species with high P uptake rates. Under such conditions, colloidal P may still contribute to the P uptake flux by desorption of P from colloidal surfaces in the diffusion layer. Furthermore, it is unclear whether colloidal P may to some extent be available on the longer term. These issues warrant further studies on the bioavailability of the colloidal P fraction.

Conclusions

This study shows that the P bound to synthetic Fe–organic matter colloids is not directly available to algae. Since this P fraction is commonly included in colorimetric P assays, these findings cast doubt on the validity of such assays as a measure of the bioavailable P fraction, an approach commonly used in water quality monitoring programs. Further research should determine whether these findings can be extended to natural colloids, and whether the P bound to such colloids may partially become available on the long term.

Chapter 4 Oxidation of iron in natural waters produces authigenic particles

This chapter is adapted from Baken et al., *Appl. Geochem.* **39** 59–68 (ref. [133]).

Summary

When Fe(II)-bearing groundwater surfaces in streams, authigenic Fe-rich particles are produced by oxidation. Such freshly precipitated Fe minerals may be transported as suspended sediment and have a profound impact on the fate of trace metals and nutrients in rivers. The objective of this study was to monitor changes in mineralogy and composition of authigenic material from its source to increasingly larger streams. Groundwater, streamwater, and suspended sediment in streams of different order were sampled in the Kleine Nete catchment (Belgium), a lowland with Fe-rich groundwater. Fresh authigenic material (>0.45 µm) was produced by oxidizing filtered (<0.45 µm) groundwater and streamwater. This material contained, on average, 44% Fe, and smaller concentrations of C, P, and Ca. EXAFS spectroscopy showed that the Fe was present as poorly crystalline Fe oxyhydroxide with a structure similar to that of ferrihydrite. The Fe concentration in the suspended sediment samples decreased to 36–40% (stream order 2), and further to 18–26% (stream order 4 and 5). Conversely, the concentrations of organic C, Ca, Si, and trace metals increased with increasing stream order, suggesting mixing of authigenic material with suspended sediment from a different source. The Fe speciation in the suspended sediment was similar to that in fresh authigenic material, but more Fe–Fe interactions were observed, *i.e.* it was increasingly hydrolyzed, suggesting ageing reactions. The suspended sediment in the streams of order 4 and 5 is estimated to contain between 31% and 59% of authigenic material. The authigenic material is an important sink for P in these streams which may alleviate the eutrophication risk in this catchment.

Introduction

As Fe(II)-rich groundwater surfaces and becomes oxic, it may locally cause extensive production of Fe oxyhydroxides. The presence of this material is witnessed by reddish brown sediment at locations where groundwater seepage occurs. This Fe-rich material is termed authigenic, because it is generated in the water itself, as opposed to "allochthonous" material (e.g. eroded soil particles) which has a different origin. The structure, size, and morphology of aquatic Fe minerals depend on the pH, the natural organic matter (NOM) concentration and properties, the presence of micro-organisms, and the concentration of inorganic ligands [39,101]. Iron-rich authigenic material has been identified as ferrihydrite or lepidocrocite [193] and may contain quantitatively important concentrations (above 1 wt %) of other elements such as organic C, Ca, and P [98,99]. These elements are either coprecipitated or adsorbed at the surface of Fe oxyhydroxides. The authigenic Fe-rich material may strongly influence the fate and bioavailability of elements that have a high affinity for Fe oxyhydroxides and that typically occur at low concentrations, such as P, As, Ni, Pb, and V [51,158,194]. Especially the effect of Fe-rich authigenic material on P, which may be coprecipitated at molar ratios down to Fe:P = 2 or even lower [99,113], is expected to have large implications for many freshwater systems: reducing P concentrations has often been shown successful in counteracting eutrophication [13].

As Fe-rich authigenic material is generated in the aquatic environment, it becomes part of the sediment. It is mixed with allochthonous material, i.e. particles that have a different origin. The sediment material is then subjected to processes of aggregation, settling, and resuspension. It may be transported downstream as suspended sediment, especially at high discharge after storm events [44]. It may settle again in rivers further downstream or ultimately in estuaries, where most of the suspended Fe-rich material is expected to aggregate and settle due to the increased salinity [109]. In some cases, authigenic material may represent a significant fraction of the total suspended sediment load, and increase the need for dredging in navigable waterways. Knowledge on the fate of authigenic material is, therefore, of interest to waterway managers and contributes to a better understanding of sediment transport in rivers. Vanlierde et al. [44] studied the transport of authigenic material in the Kleine Nete catchment, a catchment with a flat topography, acid sandy soils, and Fe-rich groundwater. They estimated its annual export at between 58 and 96%

of the total suspended sediment export. This estimation was based on a sediment transport model calibrated to total suspended solids, including effects of settling, burial, consolidation, and resuspension of the sediment. However, they only briefly discussed the formation and geochemistry of Fe-rich authigenic material, and the study lacked samples of authigenic material.

The goal of the present study was, therefore, to determine the characteristics and composition of authigenic Fe-rich material. In particular, this study was set up to identify changes in mineralogy and elemental composition of suspended authigenic material as it is transported from groundwater to small brooks and, ultimately, to the major rivers. We used EXAFS (Extended X-ray Absorption Fine Structure) spectroscopy to characterize the coordination environment of Fe. The formation of authigenic Fe-rich material was simulated by allowing Fe(II)-bearing groundwater to oxidize. The produced authigenic material was compared with samples of suspended sediment from streams of increasing order. The working hypothesis is that the Fe(II) in streams is oxidized to Fe(III), and that the resulting authigenic material is increasingly diluted by mixing with allochthonous material and by adsorption reactions.

Materials and methods

The study area: lowland catchments fed by iron-rich groundwater

Two study sites in northeastern Belgium with a similar setting were selected for studying authigenic Fe-rich sediment formation (this chapter) and its implications for P and As binding (Chapters 5 and 6): the Kleine Nete catchment upstream of the town of Grobbendonk, and three major tributaries to the Demer river (Figure 4.1). The Kleine Nete catchment is located in the Belgian Campine region and drains a mostly agricultural lowland area of approximately 800 km^2, of which 590 km^2 are upstream of Grobbendonk. The studied part of the Demer catchment is mostly located in the Belgian sandy loam belt and includes its three main northern tributaries Mangelbeek, Zwartebeek, and Winterbeek, each of which drain an area of approximately 100 km^2. The topography of both study areas is flat, with the exception of a few limonite ridges which separate the three tributaries to the Demer. Common soil types in both study areas include Podzols, Plaggic Anthrosols (organic matter accumulation in the topsoil), and soils with fluvic or gleyic properties in the valleys [195].

The lithology of both study areas is similar and consists of Miocene and Pliocene sands (up to 150 m thick), deposited on top of an impermeable Oligocene clay (Boom clay), and overlain by a thin layer of Pleistocene deposits (Figure 4.2). Two groundwater systems are present in the study area: the upper Central Campine system is separated from the underlying Brulandkrijt system by the Boom clay aquitard [196,197] (Figure 4.3). Therefore, the Central Campine system is the only unconfined (phreatic) groundwater system which discharges into the streams of the study area [198]. The groundwater flow direction in this system is varied. Its recharge is mostly by percolation of rainwater (240–360 mm yr^{-1}) [197]. Within the Central Campine system, the Diestiaan aquifer likely contributes most to stream flow, due to its thickness and high permeability [44]. The Diestiaan aquifer consists of glauconitic sands which supply large amounts of Fe(II) to the groundwater [199]. The Fe concentrations in groundwater typically range between 1 and 100 mg L^{-1}. The land use in the area is characterized by intensive agriculture and animal husbandry, which cause diffuse emissions of P to the environment. After decades of excessive manure application, many soils are P-saturated [200]. The P losses mainly occur through leaching to the groundwater, owing to the well-drained sandy soils and the flat topography. The P concentrations in phreatic groundwater in the area commonly range between 0.02 and 2 mg L^{-1}.

The streams in the study area are predominantly fed by groundwater. Figure 4.4 shows the modelled year-averaged groundwater discharge and recharge in the study area. Discharge mostly occurs along the streams, highlighting that the streams in the study areas mostly gain groundwater. Separation of the baseflow contribution from the total hydrograph (Figure 4.5) shows that 10-year averaged baseflow contributions to stream flow in the study area range between 71 and 83%. Other studies have estimated the groundwater contribution to the total discharge of the Kleine Nete at between 62 and 87% [44,201,202]. The phreatic groundwater table is generally shallow and fluctuates seasonally. The groundwater may either seep directly into the streams, or it may be evacuated by drainage systems which are abundantly present in cropland throughout the area. As the Fe-rich groundwater surfaces and become oxic, large amounts of authigenic Fe-rich material are produced. The authigenic material produced in ditches or streams becomes part of the suspended sediment and is subjected to processes such as resuspension, downstream transport, settling, and burial. The Fe-rich material may also accumulate in topsoils: bog iron ore occurs in the study area and has been mined for its

iron [203]. For a more detailed discussion on the geography, hydrogeology, hydrology, and the water balances of the area, the reader is referred to other work [44,196–198,201,204]. In summary, the conditions in these catchments promote the formation and transport of large amounts of authigenic Fe-rich material.

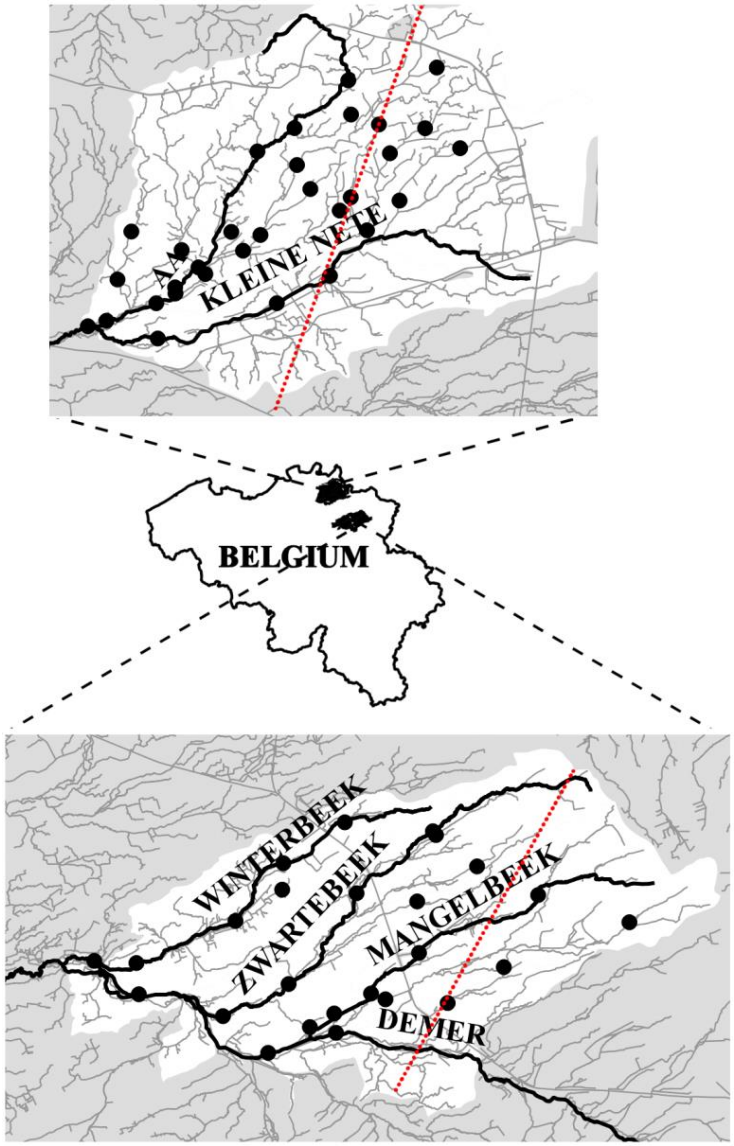

Figure 4.1: Map of Belgium with the study areas indicated: the Kleine Nete catchment upstream of the town of Grobbendonk (top) and the three northern tributaries to the Demer river. The major streams (black lines), minor streams (grey lines), and the sampling locations for the catchment-scale study (Chapter 6; black dots) are indicated. The dotted lines indicate the location of the hydrogeological cross sections (Figure 4.3).

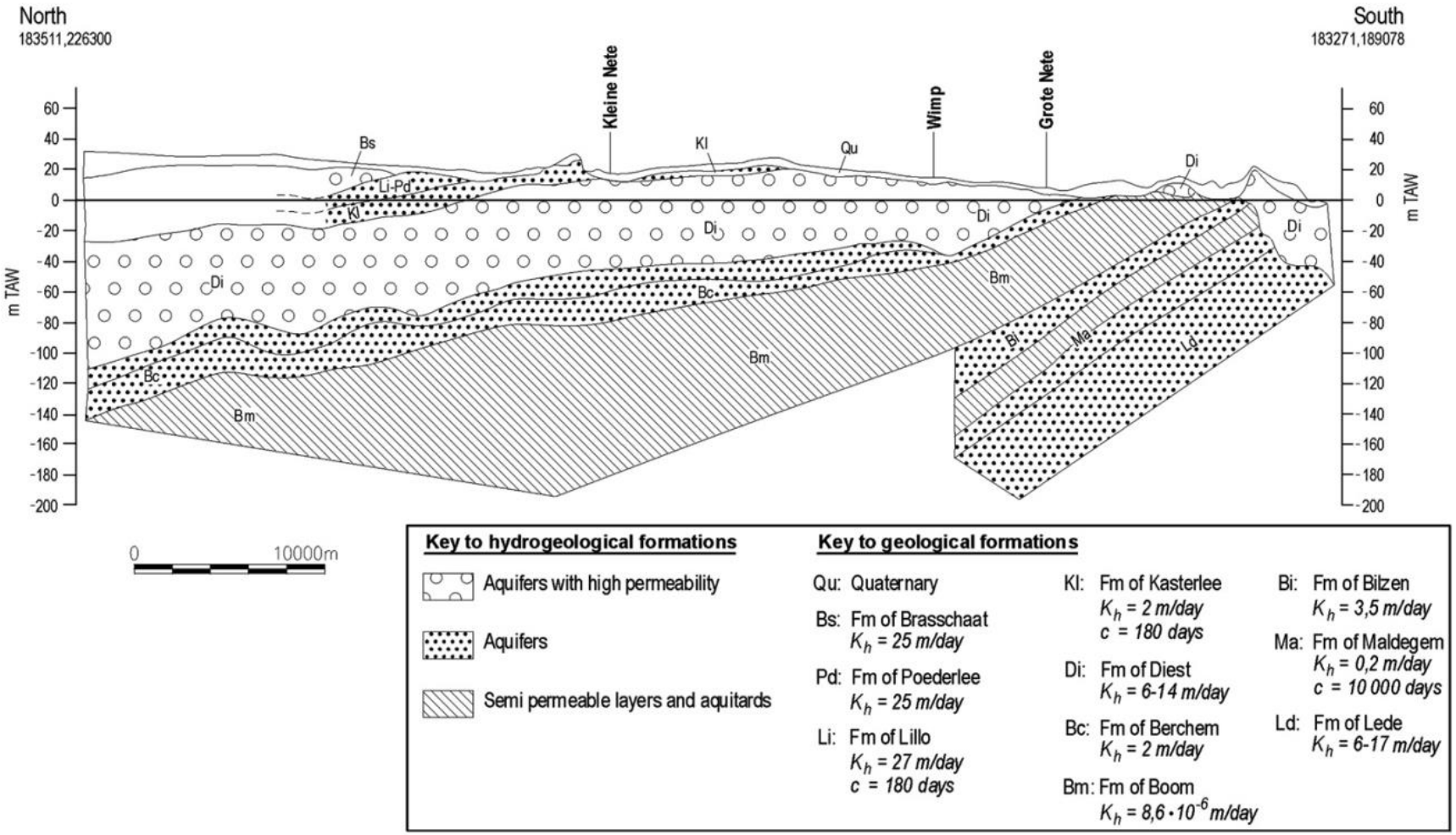

Figure 4.2: Geological cross-section of the Kleine Nete catchment along a N-S line (from Vanlierde et al. [44])

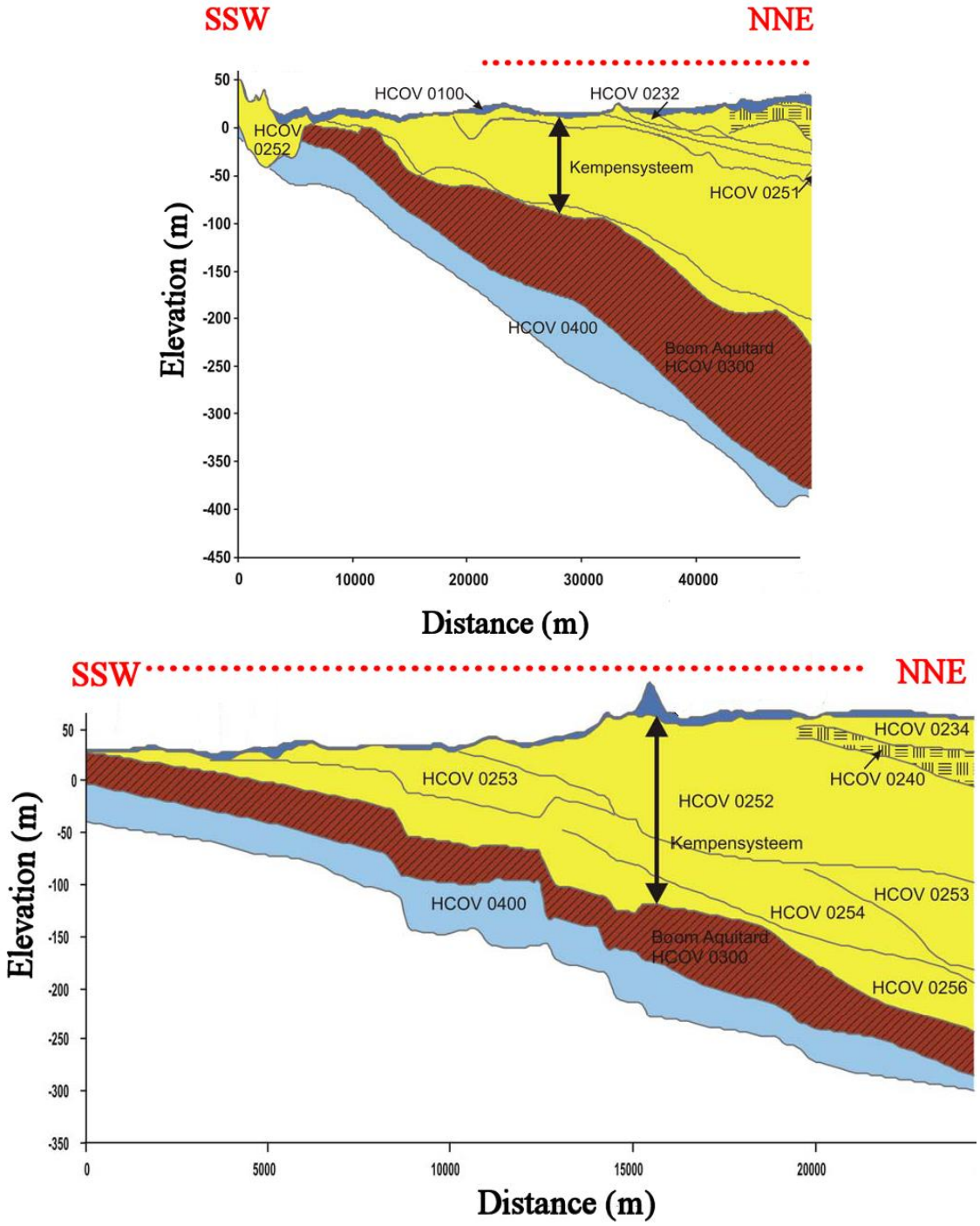

Figure 4.3: Hydrogeological profile along SSW-NNE sections across the Kleine Nete catchment (top) and the northern part of the Demer catchment (bottom), adapted from ref. [196]. The dotted lines indicate the location of each section as shown in Figure 4.1. The Central Campine groundwater system (yellow) is the only phreatic groundwater body in the study area; it is separated from the Brulandkrijt (blue; only top layer shown) groundwater system by the Boom clay aquitard (brown).

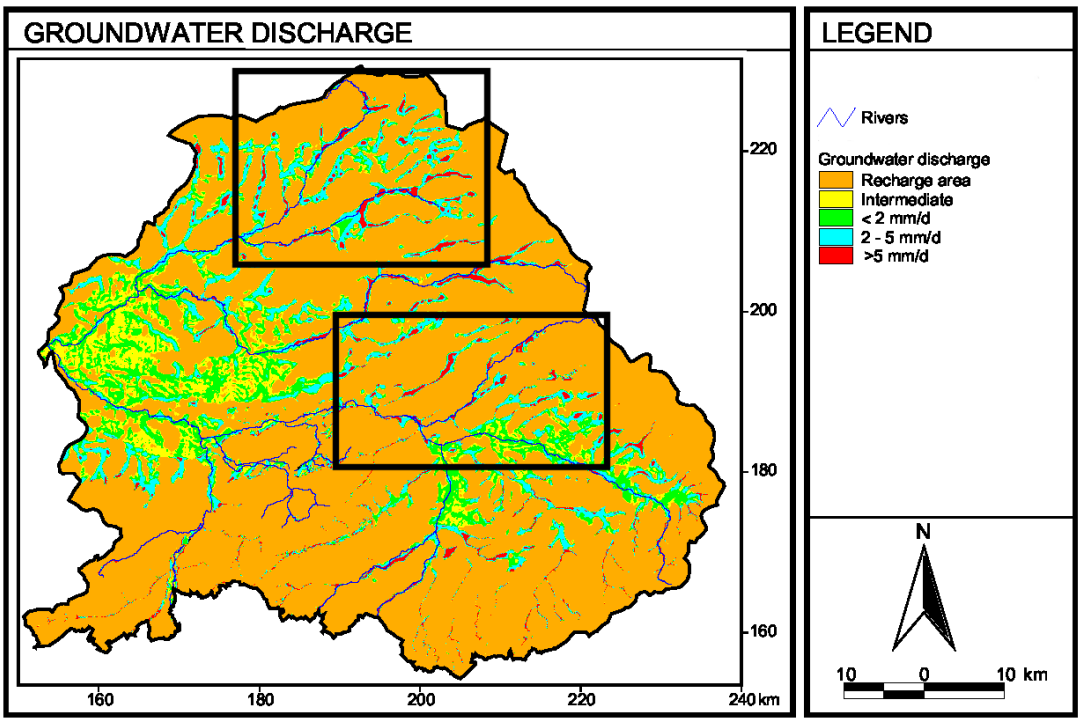

Figure 4.4: Groundwater discharge and recharge in the study area, adapted from ref. [201]. The black rectangles indicate the study area and agree with the maps in Figure 4.1. Along most stretches of the streams of the studied catchments, groundwater is discharged into the streams.

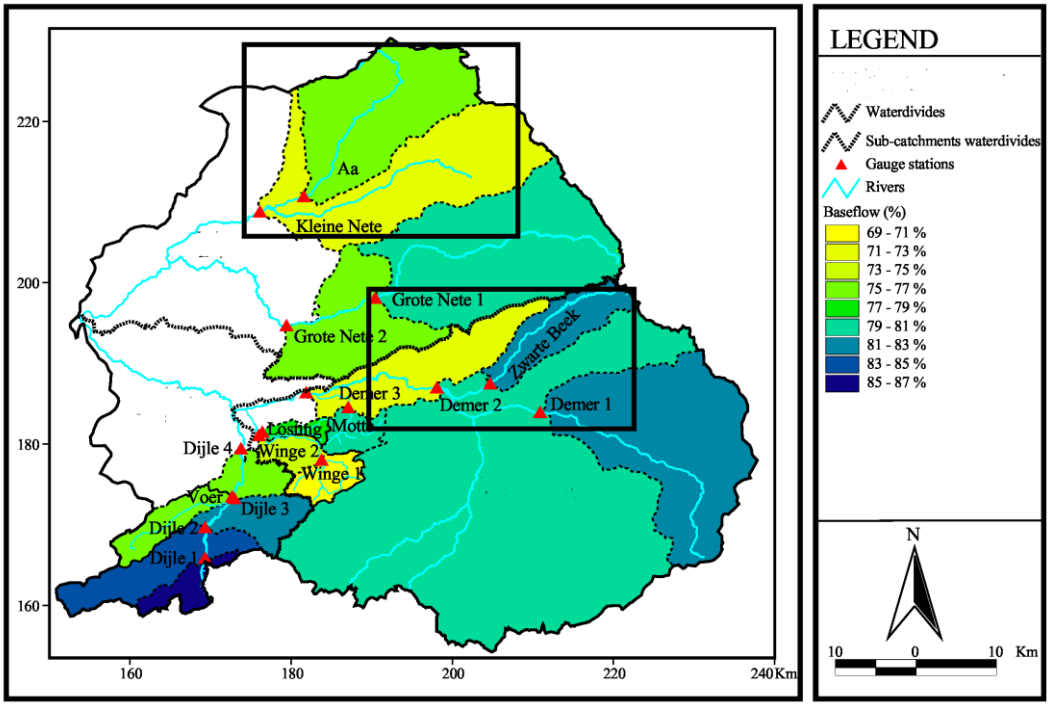

Figure 4.5: Baseflow contribution to stream flow (10-year average), calculated from the total hydrograph by numerical discharge separation (adapted from ref. [201]).

Sampling

Three sampling locations in the Kleine Nete catchment were selected: the Slootbeek (stream order 2, a small brook with deep-red bottom sediment), the Aa (stream order 4, a major tributary to the Kleine Nete), and the Kleine Nete (stream order 5). The meaning of the stream order is explained in Box 6.1 (Chapter 6). For this study, no locations in the Demer catchment were sampled. Samples of groundwater, streamwater, and suspended sediment were collected on four occasions between October 2011 and June 2012 (samplings S1–S4; Table 4.1). Between 25 and 50 L of groundwater was sampled at approximately 5 m from the watercourse using a peristaltic pump and a fully screened temporary well installed with Geoprobe®. The direct-push approach of the Geoprobe® ensures minimal disturbance, and groundwater could be sampled shortly after the installation of the well. The sampling depth was between 2.8 and 3.8 m below the ground level and depended on local hydrogeology, *i.e.*, the feasibility to pump at an appreciable rate without entry of air bubbles. The groundwater was discarded during the first 5 minutes and was then collected in plastic vessels that were continuously flushed with N_2 in order to minimize oxygen entry. The collection of groundwater generally took between 1 and 3 hours. Approximately 50 L of streamwater was sampled with a bucket. Subsamples of groundwater and streamwater were filtered in the field (nitrocellulose membrane filters, 0.45 µm pore size, 25 mm diameter, Whatman) and immediately acidified to pH 2 with HCl in order to stabilize the Fe redox speciation. The pH, dissolved O_2 concentration, redox potential, and electrical conductivity were measured in the field.

Table 4.1: Sampling locations and sampling dates

Location	Sampling date	Code
Kleine Nete	18/10/2011	S1
N 51°11’35” E4°45’26”	17/01/2012	S2
	03/04/2012	S3
	19/06/2012	S4
Confluence of Slootbeek and Aa	20/10/2011	S1
N51°12’40” E4°50’10”	10/01/2012	S2
	19/03/2012	S3
	11/06/2012	S4

The suspended sediment of the Kleine Nete and Aa was isolated with a field centrifuge (Emmie, Alfa Laval). This device allows the collection of sufficient suspended material from rivers even if suspended sediment concentrations are low. Streamwater is continuously pumped by an immersion pump into the rotating centrifuge where most of the particles are collected at the walls and the clear water exits through the center. The pump inlet was positioned at about 0.7 m above the bed and 0.5 m below the water surface. As the inlet area of the pump is relatively large, it is assumed that little or no particle segregation occurred near the inlet. Collection of sufficient suspended sediment took between 1 and 3 hours. The use of the field centrifuge was not necessary in the Slootbeek due to the high suspended sediment concentration. The suspended material was collected by sampling the water with a bucket and by centrifugation upon return to the lab.

Upon return to the lab, all samples were stored at 4°C prior to further processing. The suspended sediment samples were freeze-dried and also stored at 4°C. The composition of 0.45 µm filtered water samples was measured by the ferrozine method (Fe(II)) [136], ICP-OES (Fe and other elements), catalytic combustion (DOC), and anion chromatography. The composition of suspended sediment samples was determined by oxidative digestion (C and N), by ICP-OES after digestion in boiling *aqua regia*, and by Energy Dispersive X-ray Fluorescence (ED-XRF).

Oxidation experiments

The oxidation of Fe(II) and the production of authigenic material in natural water samples were mimicked in oxidation experiments. Groundwater, streamwater, mixed groundwater and streamwater (mixing ratio 1:1), and streamwater with added Fe(II) were allowed to oxidize under controlled conditions. The oxidation experiments were set up within 20 hours after sampling. During this storage period, some oxidative losses of Fe occurred. Immediately before the start of the experiment, subsamples of groundwater and streamwater (between 10 and 30 L) were prefiltered using two successive filters: a 5 µm polypropylene filter (Macrowind, Van Borselen filters, Zoetermeer, the Netherlands) and a 0.45 µm polypropylene-borosilicate filter (AC BX, Atlas Filtri, Limena, Italy). The prefiltration allowed oxygen entry into the groundwater samples which explains why, at the start of the experiment, even the treatments with only groundwater contained dissolved oxygen concentrations above 6 mg L^{-1} in all but one instances. Shortly after the

prefiltration, oxidation experiments were set up in transparent plastic pots, each containing a total volume of 800 mL. At least two replicates were prepared for each treatment. The treatments spiked with Fe(II) were prepared by adding an aliquot of a freshly prepared 10 g Fe(II) L^{-1} solution ($FeSO_4 \cdot 7H_2O$ dissolved in 10^{-5} M HCl) which yielded final Fe(II) concentrations between 5 and 50 mg L^{-1}. This increased the ionic strength of such treatments by between 0.36 and 3.6 mM. All treatments were homogenized and incubated at 15°C in darkness. They were neither stirred nor aerated during the course of the experiment.

The pH, the dissolved oxygen (DO) concentration, the composition of the "dissolved" (<0.45 µm) fraction, and the concentration and composition of authigenic material were monitored until the oxidation of Fe(II) was nearly complete, which lasted between 8 hours and 3 days after the start of the experiment. During the course of the experiment, the DO concentration did not vary more than 0.8 mg L^{-1} in individual treatments, and the pH did not vary more than 0.1 units, except for some treatments with only streamwater. The "dissolved" (<0.45 µm) fraction was sampled in duplicate (nitrocellulose membrane filters, 25 mm diameter, Whatman), and the concentrations of Fe(II) (ferrozine method), Fe and other elements (ICP-OES), and DOC (catalytic combustion) were measured. The Fe(III) was calculated as the difference between Fe (measured by ICP-OES) and Fe(II). After homogenization of the experimental solutions, the authigenic material was isolated in duplicate on pre-weighed nitrocellulose membrane filters (0.45 µm pore size, 47 mm diameter, Whatman) under vacuum. The filters were subsequently dried (105°C), weighed, and the composition of the authigenic material was determined by ICP-OES after digestion in boiling *aqua regia*.

EXAFS spectroscopy

The iron speciation in two authigenic samples and in three suspended sediment samples was determined by EXAFS spectroscopy. The concepts of EXAFS spectroscopy are explained in Box 4.1; the theory behind it has been discussed extensively elsewhere [205,206]. The three suspended sediment samples were collected in the Kleine Nete, Aa, and Slootbeek. The two samples of authigenic material were collected after 48 hours of oxidation of a groundwater sample and a groundwater-streamwater mix. The samples were isolated on a membrane filter, the filters were freeze dried, and the authigenic material was collected with a spatula. Iron K-edge (7112 eV) EXAFS spectra

were recorded at the wiggler beamline I811 at MAX-lab, Lund, Sweden. All EXAFS samples were mounted in aluminum holders and fixed with Kapton tape. The spectrum of a metallic iron foil was used for energy calibration. Because of a defective I_2 detector, the foil was run after every other sample. The storage ring was operated at 1.5 GeV (maximum ring current 230 mA). Beamline I811 was equipped with a Si[111] double crystal monochromator. Higher-order harmonics were reduced by detuning the second monochromator crystal to reflect approximately 40% of the maximum intensity at the end of the scans. The I_0 and I_1 detectors were 300 mm-long ion chambers (FMB-Oxford). The fluorescence detector was a passivated implanted planar silicon (PIPS) detector. More details on beamline I811 are provided by Carlson et al. [207]. The scans were recorded at ambient temperature in fluorescence mode with a Mn filter between the sample and the detector. For each sample, between 10 and 15 scans were recorded. No gradual changes were observed in subsequent scans, indicating that the sample was well preserved throughout the measurement.

Data processing and modelling was performed using the Athena and Artemis programs, respectively, which are both included in the IFEFFIT program suite [208]. In Athena, all scans of a sample were aligned which caused an energy shift of at most 0.05 eV. The scans were averaged and deglitched. The energy of the resulting spectrum was calibrated using the spectra of metallic Fe foil which were recorded after every other sample. A value of 7112 eV was assigned to the first inflection point of the Fe foil spectrum. The pre-edge region was fitted with a linear function which was subtracted from the data. The background was removed with the Autobk algorithm which is included in Athena using a *k*-weight of 2 and a rbkg parameter of 1. In order to optimize the background removal, a first-shell fit of the EXAFS spectrum was set as standard for background subtraction. The resulting spectrum was exported to Artemis for modelling. It was Fourier-transformed using a Hanning window between 2 and 12.5 $Å^{-1}$. The EXAFS model (described in the next paragraph) was fitted to the real part of the Fourier transform between 1 and 4 Å, and fits were optimized across *k*-weights of 1, 2, and 3. According to the Nyquist theorem ($N_{max} = 2\,\Delta k\,\Delta R\,\pi^{-1}$, with Δk the *k*-range of the EXAFS spectrum and ΔR the R-range considered), the amount of independent points in each spectrum was 20.

Because all EXAFS spectra resembled that of ferrihydrite, an atomic structure was assumed with Fe in a octahedral configuration to six O atoms at distances close to 2.00 Å, and with two Fe–Fe distances in the second and third coordination shells at approximately

3.03 and 3.43 Å. The former Fe–Fe distance refers to edge-sharing Fe octahedra, whereas the latter is attributed to double corner-sharing Fe octahedra [209] (Figure 4.6). Based on this atomic structure, a model for the EXAFS signal was deduced which included single scattering Fe–O and triangular Fe–O–O multiple scattering paths in the first coordination shell, a Fe–Fe2 single scattering path (for edge-sharing octahedra) in the second shell, and a Fe–Fe3 single scattering path (for corner-sharing octahedra) in the third shell. All scattering paths were calculated from the atomic structure of 2-line ferrihydrite [19] using the Atoms and FEFF codes, which are incorporated in Artemis. Each scattering path contributed significantly to the final fit. In order to reduce the number of fitting parameters, the following constraints were adopted in the EXAFS model based on the assumed atomic structure and on previous research. The degeneracy of the Fe–O single scattering path was set to 6, and that of the triangular multiple scattering Fe–O–O path to 24. The scattering distance of the Fe–O–O path was constrained to be 1.707 times that of the Fe–O path, and the Debye-Waller factor (or bond-distance distribution parameter, σ^2) of the Fe–O–O path was set equal to that of the Fe–O path [210]. The Debye-Waller factors of the Fe–Fe2 and Fe–Fe3 paths were set to 0.0089 and 0.0046 $Å^2$, respectively, which were obtained by fitting the spectrum of 2-line ferrihydrite using the model described here. After the EXAFS experiment, it was noted that self-absorption had occurred due to a high Fe concentration in the sample [205]: if the passive amplitude reduction factor (S_0^2) was fixed at a generally accepted value of 0.72 [40], first-shell fits of our samples yielded very poor fits if the coordination number of Fe–O interactions was fixed to 6, and yielded unrealistically low Fe–O coordination numbers (around 3) if this parameter was not fixed. This adverse phenomenon, which is normally avoided by dilution of the sample in BH_3, was accounted for in the modelling by fitting the amplitude reduction factor. This causes an additional fitting parameter compared to common EXAFS fitting practices. In summary, the EXAFS model had a total of 8 independent fitting parameters: the amplitude reduction factor, the edge energy, the Debye-Waller factor of the Fe–O path, the coordination numbers of the two Fe–Fe paths, and the scattering distances of all three single scattering paths. The number of fitting parameters was, therefore, less than half of the number of independent points in each spectrum.

As an alternative to the shell-by-shell fit of the EXAFS spectra, linear combination fitting (LCF) was performed on k^3-weighted EXAFS spectra in the range $k = 2.5–12$ $Å^{-1}$. Synthetically produced 2-line ferrihydrite, goethite, lepidocrocite, and Fe(III) complexed

by Suwannee River Natural Organic Matter (SRNOM) were selected as standard compounds. The Fe–SRNOM standard was prepared as follows: 50 µg Fe(II) L^{-1} (as $FeSO_4 \cdot 7H_2O$) in aqueous solution was oxidized for 24 hours at pH 7.2 in the presence 10 mg SRNOM L^{-1} and 0.2 mM $NaHCO_3^-$, and the resulting solution was frozen in liquid nitrogen and freeze dried. The iron (hydr)oxides were recorded in transmission mode at MAX-lab [182], whereas the spectrum of the Fe–SRNOM complex was recorded in fluorescence mode. The optimal fits were calculated using a least squares algorithm. The calculated contributions of each standard spectrum were scaled after fitting so that the sum of all contributions equaled 1 in order to account for the self-absorption which occurred in the samples but not in the standards. The self-absorption possibly affected the LCF results to some extent.

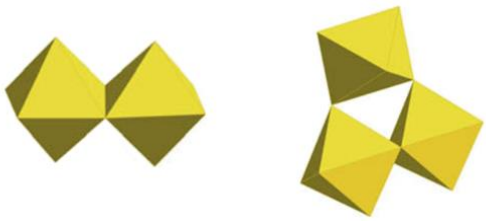

Figure 4.6: Schematic representation of typical Fe coordination structures in Fe oxyhydroxides (from ref. [209]). The Fe occurs as FeO_6 octahedra. An octahedron may share two O atoms (*i.e.* an edge, **left**) with the adjacent octahedron; the distance between the Fe atoms is then around 3.03 Å. Alternatively, an octahedron may share one O atom (*i.e.* a corner, **right**) with two adjacent octahedra; the distance between the Fe atoms is then around 3.43 Å.

Box 4.1: EXAFS spectroscopy

X-ray absorption spectroscopy (XAS) exploits the fact that the core electrons of each chemical element are characterized by a set of binding energies. If the energy of an incident X-ray is just below the binding energy of a core electron (the 'pre-edge' region), no absorption occurs. In contrast, if the X-ray energy is at or above this binding energy (the 'edge'), the absorption suddenly increases (Figure 4.7). Because the edge energies are element specific, XAS can probe a selected element present at low concentration in a heterogeneous matrix.

Extended X-ray Absorption Fine Structure (EXAFS) spectroscopy, a subtechnique of XAS, uses the oscillating part of the X-ray absorption spectrum. An incident X-ray with sufficient energy excites a core electron to a continuum state, *i.e.* it produces a photoelectron. The energy of the photoelectron wave is equal to the excess energy (incident X-ray energy minus electron binding energy). This wave is backscattered by the surrounding atoms. The wavelength of the photoelectron wave is in the same range as typical interatomic distances. If both waves are in phase, they produce a maximum in the EXAFS spectrum, whereas they produce a minimum if they are out of phase. Therefore, the oscillations in the EXAFS spectrum reveal information on the coordination environment of the selected element, such as the identity and number of neighboring atoms and the interatomic distances.

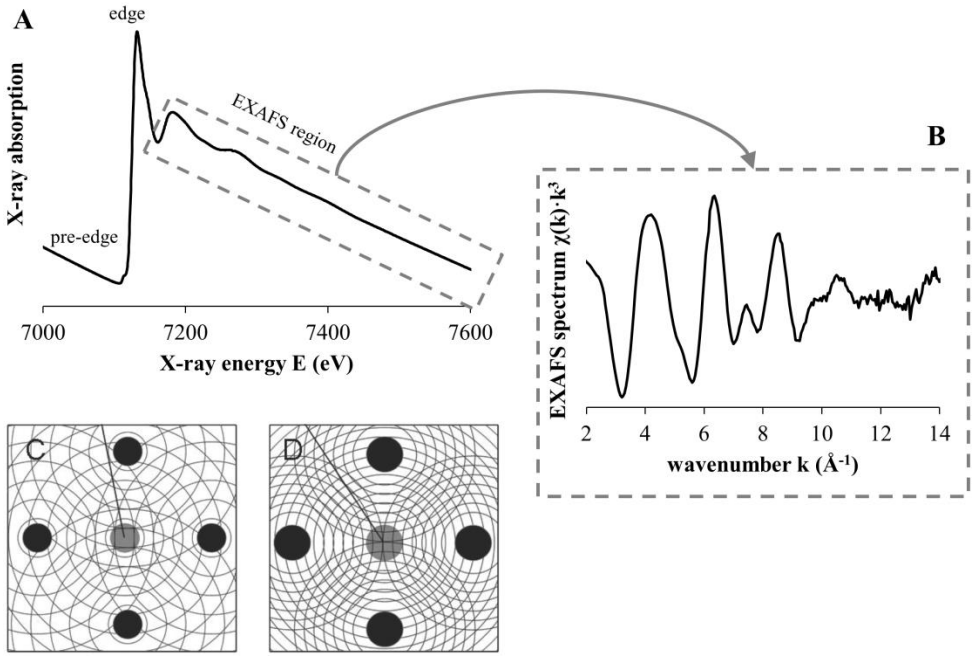

Figure 4.7: A: X-ray absorption spectrum of ferrihydrite. B: the corresponding EXAFS spectrum. C and D: photoelectron wave emitted by the central atom, and backscattered wave by the neighboring atoms (adapted from ref. [205]). In C, both waves are out of phase, producing a minimum in the EXAFS spectrum. In D, they are in phase, yielding a maximum.

Results and discussion

The composition and characteristics of water samples are reported in Table 4.2. The streams and groundwater had a pH between 6.3 and 7.2 and were moderately hard to hard. The streamwater was oxic, whereas the groundwater was generally anoxic. The latter is witnessed by the low DO concentration and redox potential as well as by the low NO_3^- and Fe(III) concentrations. Intensive agriculture in the Kleine Nete catchment may promote these reduction processes by inputs of NOM as electron donor. The Fe concentrations in groundwater varied widely depending on the sampling location. This is discussed in greater detail in Chapter 6. The P concentrations in groundwater were up to 3 mg L^{-1} and were more than an order of magnitude larger than those in streamwater (<0.1 mg L^{-1}). This is attributed to coprecipitation with or adsorption on authigenic Fe-rich material. Apart from the concentrations of Fe, NO_3^-, and P, the composition of filtered groundwater and streamwater was quite similar, which reflects that the Kleine Nete catchment is predominantly fed by groundwater. As such groundwater surfaces, Fe and P are precipitated, whereas other elements are more conservative. The seasonal variability in groundwater and streamwater composition was relatively low, except again for the Fe and P concentrations. The Fe and Fe(II) concentrations in streams were higher in winter than in summer. This is due to faster oxidation of Fe(II) and removal of Fe from the "dissolved" fraction in summer. This process is discussed in detail in Chapter 6.

Oxidation experiments

The oxidation experiments simulated the oxidation of Fe(II) and the formation of authigenic material under conditions representative for those in the streams of the Kleine Nete catchment. The pH was between 6.4 and 7.2 in all treatments. The DO concentrations in all but one of the treatments were between 6 and 10 mg L^{-1}, indicating oxic conditions throughout the experiment. In the treatments with only streamwater, little or no changes in the "dissolved" (<0.45 µm) concentrations of Fe or other elements were observed during the course of the experiment. In the other treatments, the Fe(II) concentrations decreased over time (Table 4.3). In all but one of the oxidation experiments, the final Fe(II) concentrations were below 10% of the initial concentrations. The decrease of Fe(II) was generally accompanied with a decrease in DOC and P, which most likely coprecipitated with Fe. The observed pseudo-first-order oxidation rate of Fe(II) was calculated from the decrease in Fe(II) concentrations over time. The observed

rates ranged between 0.01 and 2 h^{-1}. A relatively simple model using the pH, DO concentration, and temperature as inputs [179] was generally able to predict the Fe(II) oxidation rates within a factor two (Figure 4.8; more details about this model in Chapter 6). More elaborate models for the oxidation rate of Fe(II), which include the effect of various inorganic anions and DOM, have been developed [211,212], but these complex models were beyond the scope of this work.

Most of the Fe(II) lost from the "dissolved" fraction (<0.45 µm) was recovered as Fe(III) in the "particulate" fraction (>0.45 µm, Table 4.3). The recovery of Fe was good with losses below 15%, except in some experiments where adsorption of authigenic material to the recipient walls occurred. The Fe content of the authigenic material produced after oxidation was 44 ± 6% (average ± standard deviation), which is only slightly lower than the theoretically expected Fe content of hydrous ferric oxide if a stoichiometry of $Fe(OH)_3$ is assumed (52%). The difference may be explained by increased hydration and by the presence of other elements which are either adsorbed or coprecipitated, such as Ca, P, C, and Si. The freshly formed precipitates contained around 1% of Ca and P. The concentration of P in the freshly formed precipitates decreased as a function of oxidation time. This indicates that P was coprecipitated in the precipitates that were formed first, an interpretation in line with Voegelin et al. [17] and with the observed losses of P during storage of groundwater samples. The C concentration was measured in one sample of authigenic material and was 5.4%. Given the overall decrease in DOC concentrations during the oxidation experiment, it is likely that C was present in all samples of authigenic material. Si may also have been coprecipitated in authigenic material. Streams in the Kleine Nete catchment generally contain around 5 mg Si L^{-1}, but Si concentrations have not been measured in the authigenic material. In summary, the oxidation experiments show that, upon oxidation, Fe(II) in groundwater causes the production of authigenic particles, which contains on average 44% Fe and smaller amounts of C, Ca, and P, and possibly also Si.

Composition and characteristics of suspended sediment

All suspended sediment samples had a reddish brown color typical for Fe oxides and hydroxides. The composition and particle size of suspended sediment samples (Table 4.4) was surprisingly constant between samples collected at different times throughout the year. The suspended sediment in the Slootbeek (stream order 2) almost exclusively

consisted of Fe (36–40%), C (9.1–9.7%), and the associated O and H atoms. Its Fe content was close to the average 44% Fe that was found in authigenic material, whereas the C content was considerably higher. The mean particle size of the suspended sediment from the Slootbeek was about 3-fold larger than that of authigenic material, which may be a result of particle aggregation: the authigenic material was collected after 48 hours of oxidation, whereas the suspended sediment in the Slootbeek was likely older. The Fe speciation in the Slootbeek and in authigenic material was very similar (EXAFS experiment). These similarities, together with the fact that the Slootbeek drains an area where groundwater seepage occurs, strongly suggest that the suspended sediment in the Slootbeek almost exclusively consisted of authigenic material.

The suspended sediment samples collected in the Aa (stream order 4) and in the Kleine Nete (stream order 5) had a markedly similar composition. Compared to the suspended sediment in the Slootbeek (stream order 2), these samples contained less Fe (18–26%) and P (0.8–1.4%), more other elements such as C (14–17%) and Si (5–11%), and their mean particle diameter was about 50% larger. The molar Fe:P ratios in all suspended sediment samples and in groundwater were roughly within the same range, which shows that the fate and behavior of P is linked to that of Fe in the Kleine Nete catchment. The increased concentrations of elements such as C, Si, Ca, S, and trace metals reflect the increased contribution of additional sources of suspended sediment in the major rivers: the contribution of allochthonous material, and the adsorption of dissolved constituents, such as phosphate or NOM, to the authigenic material.

The average composition of authigenic material was elucidated in the oxidation experiments, but it was difficult to determine the composition of the other end-members based on suspended sediment samples from only 3 locations. Therefore, it was also difficult to estimate the authigenic contribution in the suspended sediment samples. One possibility is to assume that the speciation of allochthonous Fe differs from that of authigenic Fe, e.g. due to glauconite contributions. Since the EXAFS experiment showed that the Fe speciation in the suspended samples is very well conserved as authigenic material is transported to streams of increasing order, the majority of the Fe in the suspended sediment must then be of authigenic origin. At the upper limit, all Fe in the suspended sediment is authigenic. Using the results from the oxidation experiments, *i.e.* that authigenic material contains on average 44% Fe, it then follows that the authigenic contribution to the suspended sediment samples from the Aa and Kleine Nete was at most

between 41 and 59%. Another possibility to estimate the authigenic contribution is to use the Fe content of the riverbank material near the sampling locations (6.6 ± 0.8%; average ± standard error; $n = 4$) as a proxy for the Fe content of allochthonous material. It can then be estimated that the suspended sediment samples from the Aa and Kleine Nete contained between 31 and 52% authigenic material. These rough estimates (31–59%) are lower than those of Vanlierde et al. [44] who estimated the authigenic contribution to the total suspended sediment load between 58 and 96%. Even though our estimates are somewhat speculative, our study and earlier work show the quantitative importance of authigenic material in the Kleine Nete catchment. An extensive sampling of suspended sediment together with principal component analysis (PCA) and isotopic fractionation studies might better reveal the composition of the end-members and would allow for a more exact estimate of the authigenic contribution to the total suspended sediment load.

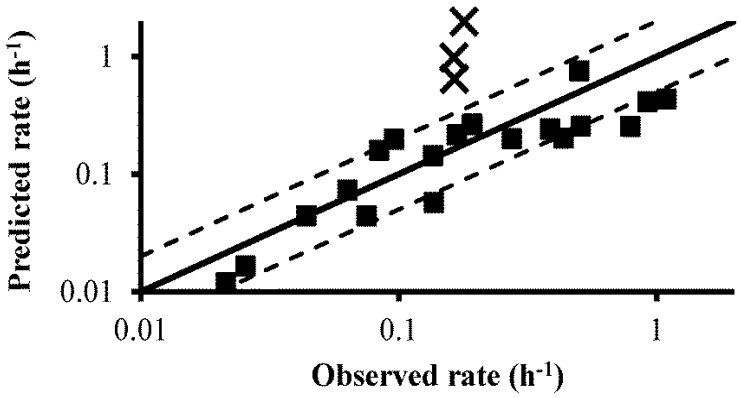

Figure 4.8: Predicted and observed oxidation rate of Fe(II) in groundwater samples, groundwater-streamwater mixtures, and streamwater samples with added Fe(II). Predictions were based on a first-order rate law for the chemical oxidation of Fe(II) (Equation 6.2). The observed oxidation rate was generally within a factor of two (dashed lines) of the predictions, except for three observations (crosses). The full line is the 1:1 line.

Table 4.2: Characteristics and composition of filtered (0.45 µm) streamwater and groundwater samples.

	Sampling	pH	EC	DO	ORP	Fe(II)	Fe	Ca	P	OC	IC	Cl^-	SO_4^{2-}	NO_3^-	SS	Q
			µS cm^{-1}	*mg L^{-1}*	*mV*	*mg L^{-1}*	*mg L^{-1}*	*mg L^{-1}*	*mg L^{-1}*	*mg L^{-1}*	*mg L^{-1}*	*mg L^{-1}*	*mg L^{-1}*	*mg L^{-1}*	*mg L^{-1}*	*m^3 s^{-1}*
Slootbeek	S1	6.7	314	5.7	282	nm	0.04	26.3	nm	3.3	13.4	nm	nm	nm	5.7	nm
streamwater	S2	6.4	369	5.5	179	9.56	9.82	38.3	0.07	7.2	16.3	30	54	2.6	20.2	nm
(stream order 2)	S4	6.7	300	5.8	278	0.55	0.72	41.8	0.02	13.4	19.0	33	51	2.0	41.8	nm
Aa	S1	7.2	546	8.1	321	nm	0.12	42.0	nm	8.2	26.7	70	46	13.6	6.3	3.6
streamwater	S2	6.8	400	7.4	184	0.52	1.21	40.4	0.08	14.3	20.3	35	48	9.7	21.1	4.5
(stream order 4)	S3	7.2	nm	6.8	309	0.35	0.41	47.9	0.02	10.3	25.8	51	56	8.6	nm	2.1
	S4	7.1	391	6.7	257	0.07	1.06	47.8	0.09	12.8	24.0	46	57	8.2	9.5	nm
Aa	S1	6.8	692	0.3	103	nm	nm	49.3	nm	7.1	35.8	78	26	<0.1		
groundwater	S2	6.3	751	0.4	124	58.0	53.8	78.7	2.18	16.8	26.5	92	51	0.6		
	S3	6.5	nm	0.5	129	28.1	28.0	42.2	3.00	11.8	23.5	73	36	<0.1		
	S4	6.4	593	0.3	112	36.7	33.2	61.4	3.07	16.1	21.8	93	83	0.4		
Kleine Nete	S1	7.0	531	9.2	385	nm	0.17	35.7	nm	7.4	16.5	57	95	5.9	9.5	4.4
streamwater	S2	7.0	487	11.1	334	0.09	0.96	35.1	0.09	9.7	14.1	62	118	7.9	29.6	0.7
(stream order 5)	S3	7.1	376	11.8	408	0.17	0.25	35.1	0.03	7.3	14.6	45	55	6.8	8.1	3.4
	S4	7.0	595	7.2	440	0.09	0.80	34.2	0.07	10.6	15.1	93	129	8.2	4.2	1.1
Kleine Nete	S1	6.8	649	0.3	101	nm	nm	29.7	nm	6.1	17.2	80	100	0.3		
groundwater	S2	6.8	581	0.5	115	14.9	15.2	34.9	0.61	14.5	23.9	68	86	0.2		
	S3	6.7	569	2.4	200	3.81	3.47	34.5	0.12	8.0	15.5	75	106	<0.1		
	S4	6.9	655	0.4	191	9.24	8.86	33.8	0.64	10.6	24.6	97	124	0.4		

nm: not measured; EC: electric conductivity; DO: dissolved oxygen; ORP: oxido-reduction potential; OC: organic carbon; IC: inorganic carbon
SS: suspended sediment; Q: discharge

Table 4.3: The evolution of the total concentrations of particulate (>0.45 µm) material, and of element concentrations in the particulate (>0.45 µm) and "dissolved" (<0.45 µm) fractions during selected oxidation experiments. The samples were collected during sampling S2; **top**: sampling location Kleine Nete; **bottom**: sampling location Aa. Treatments: A: groundwater; B: streamwater; C: 1:1 mix of groundwater and streamwater; D: streamwater spiked with Fe(II). The total Fe (final column) is the sum of "particulate" and "dissolved" Fe, and ideally should remain constant throughout each experiment.

Treatment	Oxidation time (h)	"Particulate" (>0.45 µm)						"Dissolved" (<0.45 µm)					Total
		Total	Fe	Fe	Ca	P	C	Fe(II)	Fe(III)	Ca	P	DOC	Fe
		mg L^{-1}	*mg L^{-1}*	*%*	*%*	*%*	*%*	*mg L^{-1}*	*mg L^{-1}*	*mg L^{-1}*	*mg L^{-1}*	*mg L^{-1}*	*mg L^{-1}*
A	0	8.6	2.90	34	3.5	10.4		53.10	<0.01	76.4	0.89	13.7	56.00
	30	67.0	24.21	36	1.2	1.6		23.70	<0.01	76.7	<0.01	10.9	47.91
	48*	81.5	30.43	37	1.1	1.4	5.4	16.51	<0.01	77.0	<0.01	12.0	46.94
B	0	2.2	0.61	28				0.37	0.73	41.8	0.06	13.0	1.71
	30	3.7	0.71	19				0.31	0.65	41.3	0.06	12.9	1.66
C	0	5.4	1.76	33	3.0	9.0		26.74	0.37	59.1	0.48	13.4	28.86
	30	55.4	20.90	38	1.2	1.2		2.86	<0.01	59.1	<0.01	10.0	23.76
	48*	58.5	21.61	37	1.0	1.1		0.68	0.33	59.0	<0.01	10.2	22.62
D	0	2.2	0.61	28				10.37	0.73	41.8	0.06	13.0	11.71
	30	23.7	8.01	34				0.49	2.92	41.2	0.02	11.6	11.43
A	0	7.2	3.05	42	1.1	2.5		5.90	1.53	35.7	0.13	11.7	10.48
	5	14.4	5.56	39	0.9	2.0		3.48	1.76	35.5	0.11		10.80
	24	14.4	7.25	50	0.9	1.6		0.72	2.82	35.2	0.10		10.79
	55	18.5	8.06	44	0.9	1.3		0.50	3.33	35.1	0.11		11.89
B	0	2.5	0.86	35				0.08	0.70	34.7	0.04	9.3	1.65
	9	2.7	0.74	27				0.08	0.70	35.2	0.04		1.52
	55	2.1	1.03	50				0.10	0.67	34.7	0.04		1.80
C	0	4.8	2.00	40	1.0	2.3		2.99	1.12	35.2	0.09	10.5	6.07
	2	6.5	2.80	43	0.4	2.1							
	5	7.8	3.42	44	0.8	1.7		1.59	2.21	35.1	0.10	10.1	7.22
	7	8.7	3.60	41	0.4	1.6							
	9	10.2	3.77	37	0.1	1.5		0.79	2.45	35.1	0.09	9.8	7.01
	24		3.71					0.32	2.36	34.7	0.08	9.3	6.40
	55	10.0	4.91	49	1.1	1.7		0.30	2.09	34.8	0.07	9.4	7.29
D	0	2.5	0.86	35				10.08	0.70	34.7	0.04	9.3	11.65
	5	11.9	5.23	44				2.80	3.32	34.9	0.01		11.35
	9	16.4	6.98	43				0.85	2.76	34.5	<0.01		10.59
	24	17.2	9.47	55				0.07	0.85	34.5	<0.01		10.39
	55	18.9	10.20	54				0.03	0.21	34.7	0.01		10.44

* Sample used in EXAFS analysis

Table 4.4: Composition and particle size distribution of authigenic material (selected samples) and of suspended sediment from streams of increasing order. For suspended sediment, averages ± standard deviation of samples isolated at four moments throughout the year are shown.

	sample	**C**	**Fe**	**Si**	**P**	**Al**	**Ca**	**S**	**P_{10}**	**P_{50}**	**P_{90}**
		%	***%***	***%***	***%***	***%***	***%***	***g kg^{-1}***	***µm***	***µm***	***µm***
AUTHIGENIC	oxidized groundwater	5.4	37.3	nm	1.4	<0.5	1.08	nm	1.0	4.1	18.2
MATERIAL	oxidized groundwater + streamwater (mixing ratio 1:1)	nm	36.9	nm	1.1	<0.5	0.99	nm	0.3	2.9	21.3
SUSPENDED	Slootbeek (stream order 2)	9.4±0.3	37.1±2.6	2.9±0.2	2.0±0.4	0.3±0.1	0.9±0.02	2.6±0.5	2.7±0.6	10.9±0.4	43.4±3.1
SEDIMENT	Aa (stream order 4)	16.4±1.4	20.0±2.4	7.4±3.4	1.2±0.2	1.3±0.5	1.8±0.1	5.8±0.2	4.4±0.5	18.8±1.6	85.7±13.5
	Kleine Nete (stream order 5)	15.1±1.0	24.1±1.3	5.6±0.4	1.1±0.2	1.2±0.3	1.5±0.2	6.7±1.7	4.2±0.3	16.4±1.5	72.4±13.6

nm: not measured

P_x: x^{th} percentile of the volume-weighted particle size distribution expressed as the particle diameter

EXAFS spectroscopy

The measured and fitted k^3-weighted EXAFS spectra (Figure 4.9), the magnitude of the Fourier transformed spectra (Figure 4.10), and the fitted EXAFS parameters (Table 4.5) are reported. The analysis of the pre-edge region of the spectra [213] showed that the Fe is predominantly present as Fe(III). The EXAFS spectra of suspended sediment and of authigenic material were very similar, and they all resembled that of the ferrihydrite standard. They also resembled the spectrum of a biogenic iron mineral (collected at a hydrothermal vent) very closely [209]. The spectra clearly differed from that of the goethite and lepidocrocite standards, for example by the features at around 5 and 7.5 $Å^{-1}$. They also differed from that of a Fe–SRNOM complex, although these differences are less clear. The presence of Fe in the form of reduced Fe-S minerals or glauconite must have been limited given the low concentrations of S, Na, K, Mg, and Al (each <1%), and therefore these minerals were not included as standards.

All spectra, including that of ferrihydrite, were successfully fitted by the proposed model with two Fe–Fe interactions. The large uncertainties associated with the fit of ferrihydrite are due to the fact that the Debye-Waller factors were fitted, whereas they were fixed while fitting the samples. Various models containing Fe–C interactions were also proposed, but none of them could fit the spectra well. The most notable difference between the samples and ferrihydrite is in the Fourier transformed EXAFS spectra in the region just above 3 Å (Figure 4.10). Deconvolution analysis showed that the feature of ferrihydrite in this region, which is less pronounced in the samples, is reflected in the fits by a higher contribution of corner sharing Fe: the coordination number of Fe–Fe3 was 0.9 for ferrihydrite versus 0.3–0.7 for the samples (Table 4.5). Note that in EXAFS spectroscopy, peaks in Fourier transformed spectra appear at slightly lower R than the true interatomic distance, because the interaction between the photoelectron and the coulomb potentials of the scattering atoms causes a phase shift in the oscillations of the EXAFS spectrum. The great overall similarity between all sample spectra shows that the Fe speciation in authigenic material was very similar to that in suspended sediment. This suggests that the Fe in suspended sediment indeed predominantly originates from oxidizing groundwater. Subtle differences exist between the samples: the suspended sediment samples isolated in the field had higher Fe–Fe2 and Fe–Fe3 coordination numbers than the authigenic material, *i.e.* the authigenic material is less hydrolyzed compared to downstream samples. This different degree of hydrolysis may reflect ageing effects: the

authigenic material was very fresh (48 hours old), whereas the suspended sediment samples likely were somewhat older. The results of the LCF analysis are generally in line with these findings. The LCF analysis predicts that ferrihydrite (67–82%) is the dominant species, with smaller contributions of Fe–SRNOM complexes (8–26%) and of lepidocrocite (4–15%). Our findings are in line with earlier work which showed that the oxidation of Fe(II) predominantly yields ferrihydrite in the presence of around 5 mg Si L^{-1}, a concentration typical of waters from the Kleine Nete catchment [17,43]. The EXAFS experiment shows that the Fe in authigenic material is predominantly present as poorly crystalline oxyhydroxides such as ferrihydrite, and that the Fe speciation is well conserved as the material is transported downstream to streams of increasing order.

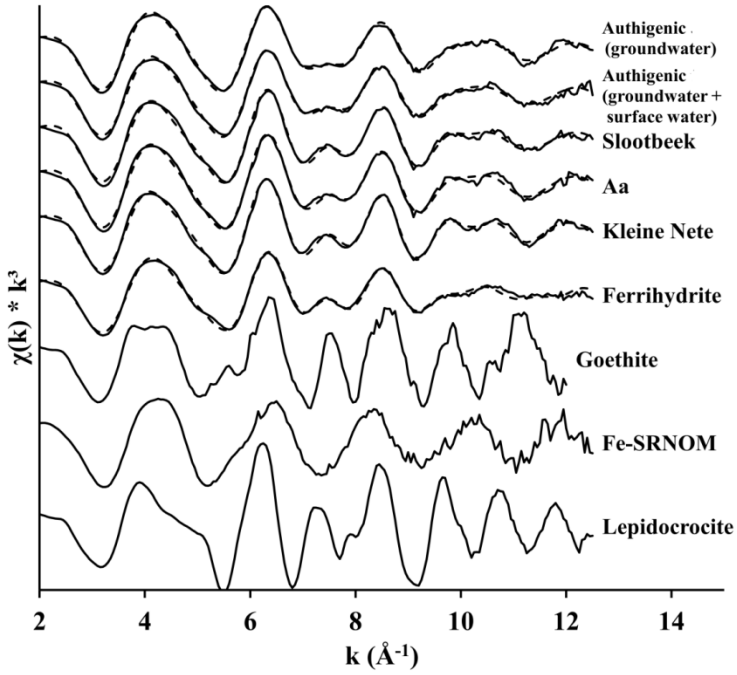

Figure 4.9: Measured (full lines) and fitted (dashed lines) k^3-weighted Fe EXAFS spectra of authigenic material and of suspended sediment from rivers of increasing order. All spectra were divided by their fitted amplitude reduction factors for easier visual comparison.

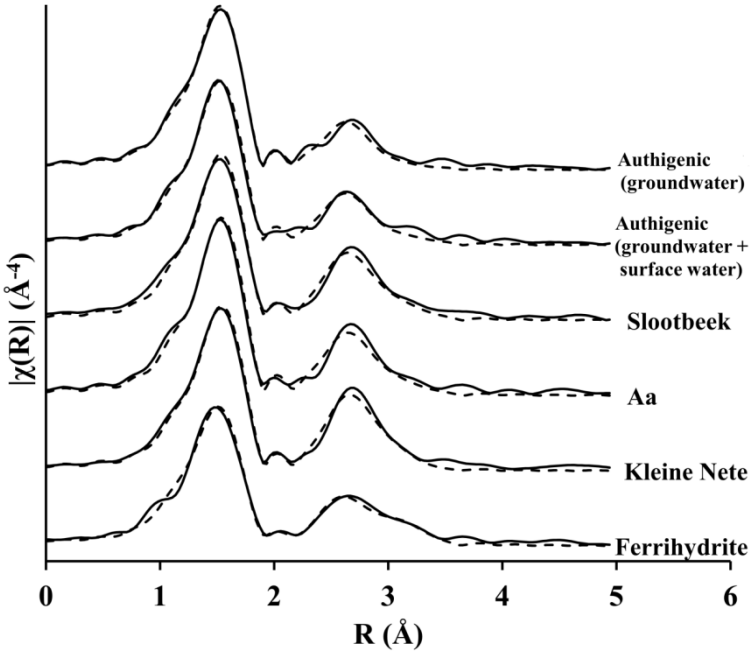

Figure 4.10: Magnitude of measured (full lines) and fitted (dashed lines) Fourier transformed k^3-weighted Fe EXAFS spectra of authigenic material and of suspended sediment from rivers of increasing order. All spectra were divided by their fitted amplitude reduction factors for easier visual comparison.

Table 4.5: Fitted parameters and uncertainties for the EXAFS spectra of 48-hour old authigenic material, suspended sediment samples, and ferrihydrite.

sample	Red χ^2	E_0 (eV)	S_0^2	Fe–O			Fe–Fe2			Fe–Fe3			Fe–O–O^
				N	R (Å)	σ^2 (Å^2)	N	R (Å)	σ^2 (Å^2)	N	R (Å)	σ^2 (Å^2)	R (Å)
Oxidized groundwater	1196	–0.32	0.45	6*	1.97 ±0.01	0.0077 ±0.0011	1.6 ±0.4	3.04 ±0.02	0.0089*	0.3 ±0.3	3.44 ±0.07	0.0046*	3.37
Oxidized groundwater + streamwater	1343	0.01	0.29	6*	1.98 ±0.01	0.0079 ±0.0013	1.8 ±0.5	3.04 ±0.02	0.0089*	0.4 ±0.4	3.45 ±0.06	0.0046*	3.37
Slootbeek *(stream order 2)*	963	0.72	0.29	6*	1.98 ±0.01	0.0077 ±0.0015	2.5 ±0.6	3.04 ±0.02	0.0089*	0.7 ±0.5	3.44 ±0.05	0.0046*	3.38
Aa *(stream order 4)*	866	0.67	0.39	6*	1.98 ±0.01	0.0071 ±0.014	2.2 ±0.6	3.05 ±0.02	0.0089*	0.6 ±0.5	3.43 ±0.05	0.0046*	3.38
Kleine Nete *(stream order 5)*	808	0.80	0.36	6*	1.99 ±0.01	0.0078 ±0.0012	2.8 ±0.5	3.05 0.01	0.0089*	0.7 ±0.4	3.43 ±0.04	0.0046*	3.39
Ferrihydrite	1043	–0.20	0.72	6*	1.97 ±0.01	0.0099 ±0.0015	1.6 ±1.2	3.02 ±0.03	0.0089	0.9 ±0.9	3.45 ±0.03	0.0046	3.37

Red χ^2: reduced chi-square statistic; E_0: edge energy; S_0^2: passive amplitude reduction factor; * parameter fixed during fitting
N: coordination number; R: interatomic distance; σ^2: Debye-Waller factor or bond distance distribution

^ For the triangular Fe–O–O multiple scattering path, N was fixed at 24, R was constrained to be 1.707 times that of the Fe–O path, and σ^2 was constrained to equal that of the Fe–O path.

Conclusions

The surfacing of Fe-rich groundwater in the Kleine Nete catchment removes Fe(II) together with DOC and P from the "dissolved" (<0.45 µm) fraction. The Fe(III) is precipitated as authigenic material, which contains 44 ± 6% Fe (average ± standard deviation) and smaller quantities of adsorbed or coprecipitated elements such as C, P, Ca, and possibly also Si. The Fe was in the form of poorly crystalline Fe oxyhydroxides with a structure similar to ferrihydrite. The mean particle size of 48-hour old authigenic material was between 3 and 4 µm. Phosphorus was very efficiently bound to authigenic material, as evidenced by the strong decrease in "dissolved" P concentrations in oxidizing groundwater.

The authigenic material becomes part of the suspended sediment and is transported to streams of increasing order. The suspended sediment in a small brook draining a groundwater seepage area almost exclusively consisted of authigenic material. Further downstream, the authigenic material is increasingly diluted by allochthonous material, and possibly also by increased adsorption of dissolved constituents onto authigenic material. This results in decreasing Fe (18–26%) and P concentrations, and increasing concentrations of other elements such as C, Si, Ca, Al, and trace metals. Apart from the changing composition, the downstream transport was also accompanied by an increase in mean particle size and in hydrolysis of Fe. These effects are likely the result of particle aggregation and of ageing of the authigenic material. The contribution of authigenic material to the suspended sediment samples from the streams of order 4 and 5 was estimated at between 31 and 59%.

Chapter 5 Phosphorus sequestration by oxidizing iron in drainage ditches

This chapter is adapted from Baken et al., *Water Res.* **2015** *71* 160–170 (ref. [214]).

Summary

Redox reactions involving iron (Fe) strongly affect the mobility of phosphorus (P) and its migration from agricultural land to freshwater. We studied the transfer of P from groundwater to open drainage ditches in the Kleine Nete catchment where, due to Fe(II) rich groundwater, the sediments of these ditches contain accumulated Fe oxyhydroxides. The average P concentrations in the groundwater feeding two out of three studied drainage ditches exceeded environmental limits for freshwaters by factors 11 and 16, but after passing through the Fe-rich sediments, the P concentrations in the ditch water were below these limits. The Fe concentrations in the sediment pore water, measured by diffusive equilibration in thin films (DET), ranged between 10 and 200 mg L^{-1} and exceeded those in the inflowing groundwater by approximately one order of magnitude. The P concentrations only marginally increased between groundwater and sediment pore water. In the poorly mixed ditchwater, the "dissolved" (<0.45 µm) Fe concentrations decreased towards the water surface due to oxidative precipitation of fresh Fe oxyhydroxides. The P concentrations decreased more sharply than those of Fe. The dynamics of Fe and P are governed by reduction reactions in the sediment and by oxidation reactions in the ditchwater. In the sediment, reductive dissolution of P-containing Fe oxyhydroxides causes solubilization of Fe and P, but P may be buffered by adsorption on residual Fe oxyhydroxides. Conversely, in the ditchwater, oxidative precipitation causes more efficient immobilization of P than of Fe: the Fe is present in excess, and ferric phosphate or P-saturated Fe oxyhydroxides are first formed until P in solution is nearly depleted. The combination of these processes yields a natural and highly efficient sink for P. It is concluded that, in Fe-rich systems, the fate of P at the sediment-water interface is determined by reduction and oxidation of Fe.

Introduction

Excessive fertilization of agricultural land has resulted in large losses of phosphorus (P) from soils to the aquatic environment. This has caused cultural eutrophication of lakes, streams, and estuaries in many developed countries worldwide [13,215,216]. Losses of P from agricultural land may occur either by soil erosion and overland flow or by leaching, *i.e.* vertical transport through the soil profile. In well-drained soils with low P sorption capacity, P losses predominantly occur through leaching [217]. Such percolates may cause P-enrichment of shallow groundwater and may ultimately reach the aquatic environment via the groundwater flow. The lowland areas of Belgium and the Netherlands have acid sandy soils with a long history of excessive fertilizer application. These soils are P-saturated and exhibit large leaching losses to shallow groundwater [90,200]. In such soils, it is difficult to balance agronomic needs (optimal crop production) and environmental concerns (limited P leaching) [218].

The transport of P from percolate or groundwater through drains to the aquatic environment is often assumed to be conservative, *i.e.* it is not much affected by chemical processes [219,220]. However, as P-enriched groundwater surfaces, it seeps through micro-oxic and highly redox-active environments, such as the linings of drainage tubes or the sediments of streams and ditches. In such environments, P may undergo complex chemical interactions with several redox-active elements, most notably with Fe. As Fe oxyhydroxides are submerged and become anoxic, they may undergo reductive dissolution, which is often microbially mediated [221]. Conversely, in oxic or micro-oxic environments, the reduced and highly mobile Fe(II) may be re-oxidized either chemically [179] or biotically [222]. The oxidized Fe(III) readily precipitates as authigenic Fe oxyhydroxides, such as ferrihydrite or lepidocrocite [41,133,223].

Several studies have already addressed the interactions between Fe and P at the interface between anoxic and oxic environments. Reductive dissolution of Fe oxyhydroxides generally releases associated P [116], and the release of P from reconstructed wetlands is of environmental concern [114,224]. However, in some cases, the release of P from anoxic sediments is limited, possibly due to formation of vivianite [46,225]. The subsequent oxidation of Fe(II) produces Fe oxyhydroxides which combine a high specific surface area with a high affinity for oxyanions [51]. They may bind P by adsorption or coprecipitation and are very efficient sinks for P. The formation of various ferric

phosphate minerals with low molar Fe:P ratios, in some cases even down to unity, have been reported in synthetic solutions [17,100,226], stream sediments [113], and lakes [98,99].

The coupling of reductive dissolution and oxidation of Fe may lead to intense Fe cycling, which has been observed in a variety of environments including sediments, groundwater seeps, and lakes [26–28,115]. Diffusive techniques, such as Diffusive Gradients in Thin films (DGT) or Diffusive Equilibration in Thin films (DET), are highly suited for probing the chemical composition of such environments. Some recent methodological studies have already simultaneously determined spatially resolved Fe and P concentrations using diffusive techniques [227], and a study by Xu et al. [228] showed a strong relationship between Fe and P concentrations in the pore waters of an incubated sediment. However, few studies have examined Fe–P interactions in systems with combined reduction and oxidation reactions. Based on column experiments, Kjaergaard et al. [229] speculate that if P and Fe(II) are concomitantly released from submerged soils, the export of P may be attenuated by the downstream re-oxidation of Fe(II) and subsequent binding of P. Zak and Gelbrecht [230] and Zak et al. [114] showed that even if high P concentrations are measured in the pore waters of reconstructed wetlands, the risk of P export is limited if molar Fe:P ratios in soils and pore waters do not fall below a critical value of 10 mol Fe (mol P)$^{-1}$. Other studies on lake sediment have suggested similar critical values [231,232]. Clearly, immobilization of P by oxidation of Fe is a key process limiting P export from selected environments.

This study was set up in order to identify the processes which govern the dynamics of Fe and P at the anoxic–oxic boundary. More specifically, we set out to determine how chemical Fe–P interactions in the sediment of drainage ditches can reduce the "dissolved" (<0.45 µm) P concentrations from far above to well below environmental limits. The transport of P from Fe(II)-bearing groundwater to open drainage ditches was monitored in an agricultural area where P losses predominantly occur through leaching [200,217]. Vertical concentration profiles of P and Fe at the sediment-water interface of open drainage ditches were measured at 1 cm resolution using the DET (diffusive equilibrium in thin films) technique. Our approach relied on field measurements, since laboratory studies of redox-sensitive systems are inherently prone to artefacts [233]. We hypothesize that P export from drainage ditches is reduced by binding on freshly produced Fe oxyhydroxides, and that P is scavenged in the oxic zone as long as the Fe:P ratio in the source (groundwater or sediment) exceeds a threshold value.

Materials and methods

Study sites

The setting, geology, and hydrogeology of the Kleine Nete catchment is described in Chapter 4. Two lowland agricultural sites adjacent to streams of the Kleine Nete catchment were selected for this study (Figure 5.1). At both sites, agricultural fields are drained by open ditches. At the bottom of the ditches, a reddish brown precipitate occurs, suggesting enrichment of Fe. Since the groundwater table fluctuates seasonally, the ditches generally drain groundwater from October to April, whereas in summer, the groundwater table is usually just below the bottom of the ditches. The top sediment layer is, therefore, oxic during the summer months but submerged and likely more reduced during the winter. Site 1, located in the municipality of Retie, has two similar open drainage ditches (labelled ditch 1 and ditch 2) adjacent to the same agricultural field. They receive no inputs from tributary ditches or pipes until their outlet into the nearby stream. The ditches are between 0.7 and 1 m wide, 200 m in length, and the sediment surface is around 70 cm below the soil surface. The field was used for growing fodder maize during the summer of 2013. Before that, the field had been permanent grassland for at least 5 years and received annual organic manure inputs corresponding to at most 35 kg P ha^{-1}. According to the Belgian soil map, the soils consist of (very) wet and strongly gleyic sandy loam with a reduction horizon at 100–120 cm below the soil surface (WRB classification: Fluvic Gleyic Umbrisol [195]). The groundwater table at this site fluctuates seasonally between 5 and 70 cm below the soil surface. Site 2, located in the municipality of Vorselaar, consists of an area of fallow fields drained by a network of ditches. One ditch of this network was selected for this study and was labelled ditch 3. These ditches are smaller than at site 1: approximately 30 cm wide and 20 cm deep. According to the Belgian soil map, the soils consist of wet and strongly gleyic sandy loam with a reduction horizon between 100 and 120 cm depth and with a thick humic accumulation in the topsoil (WRB classification: Fluvic Gleyic Umbrisol [195]). The adjacent fields had been permanent grassland for at least two years, and they receive organic manure inputs similar to those at site 1. The groundwater table fluctuates seasonally between 10 and 40 cm below the soil surface.

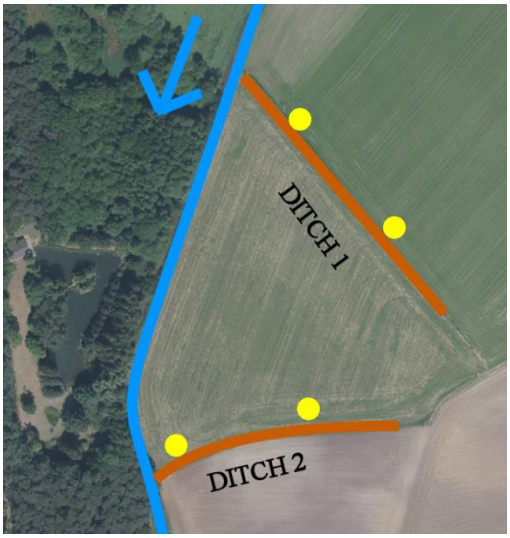

Site 1 (Retie)

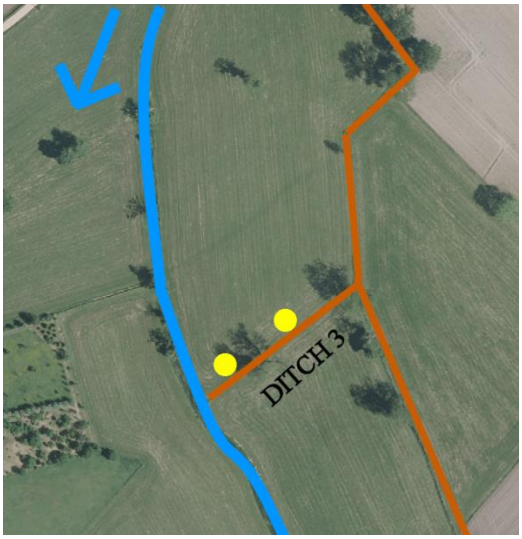

Site 2 (Vorselaar)

Ditch 2

Ditch 3

Figure 5.1: Bird's-eye views and pictures of the sampling sites. The ditches are indicated in reddish brown, the groundwater monitoring wells in yellow, and the streams and their flow direction in blue.

Sampling of sediment, groundwater, and ditchwater

At two locations next to each drainage ditch, two groundwater monitoring wells (filtered between 1 and 2 m depth) were installed at close distance (<5 m) to the ditch. Automatic hydraulic head loggers (Mini-divers, Schlumberger Water Services) were installed which measured the height of the water table every 15 minutes. Near the outlet of ditch 1, a V-notch was installed, and the discharge of the ditch into the adjacent river was monitored between December 2013 and February 2014. In August 2013, when the drainage ditches were dry, the sediment of each ditch and the underlying parent material was sampled down to 60–90 cm below the sediment surface with a gouge auger. The sediment cores were subdivided into 10 cm-sections, air-dried, and the concentrations of oxalate extractable elements (P_{ox}, Fe_{ox}, Al_{ox}, Mn_{ox}) were determined according to Schwertmann [234]. This procedure is generally used in order to quantify the poorly crystalline oxyhydroxides of Fe, Al, and Mn, and the associated P. The P sorption capacity (PSC) and the degree of P saturation (DPS) of each section were calculated as:

$$PSC = 0.5 \cdot (Fe_{ox} + Al_{ox}) \qquad (Equation\ 5.1)$$

$$DPS = \frac{P_{ox}}{PSC} \qquad (Equation\ 5.2)$$

with Fe_{ox}, Al_{ox} and P_{ox} in molar units [90,200].

The groundwater and ditchwater were sampled on 6 occasions between September 2013 and February 2014 in each ditch. The groundwater was sampled with a peristaltic pump after first discarding at least three well volumes. The ditchwater was sampled at two locations in each ditch with a syringe and was withdrawn either 1 or 10 cm below the water surface. The pH, water temperature, and O_2 concentration were measured in the field (CellOx 325 and SenTix 21 electrodes, WTW, Germany). Groundwater and ditchwater samples were membrane filtered in the field (Acrodisc syringe filters with Supor 0.45 µm membrane), and subsamples were immediately acidified (HCl, final concentration 0.01 M). The dissolved organic carbon (DOC), Fe(II), and total element concentrations were determined in the acidified subsamples. The DOC was measured as the non-purgeable organic carbon on an elemental analyzer (AnalytikJena, Multi N/C 2100), the Fe(II) was determined colorimetrically using the ferrozine method [136], and total element concentrations (including P and Fe) were measured with ICP-MS (Agilent 7700x). The soluble reactive P (SRP) was determined in selected samples by the

molybdenum blue method [235]. The concentrations of anions (Cl, SO_4, and NO_3) were determined in the non-acidified subsamples of selected samples with anion chromatography (Dionex ICS-2000 with AS18 column), and dissolved inorganic carbon (DIC) was determined with an elemental analyzer (AnalytikJena, Multi N/C 2100). All constituents were determined after membrane filtration (0.45 µm) and are referred to as "dissolved".

Concentration profiles of Fe and P by diffusive equilibration

The diffusive equilibration in thin films (DET) technique was used to collect vertically resolved profiles (resolution 1 cm) of the Fe and P concentrations in the sediment pore water and in the overlying layers of water in the drainage ditches [236,237]. The diffusive gel is in contact with the sampled water through a 0.45 µm membrane filter, and after diffusive equilibration, the composition of the water in the DET gel is equal to that of the sediment pore water. DET probes with a window of 1.8 x 15 cm were assembled and deoxygenated [238], and the probes were inserted into the sediment for 24 hours. Upon retrieval, the probes were immediately immersed in 0.01 M NaOH in order to immobilize Fe and P. Upon return to the lab, the probes were disassembled, the diffusive gels were sliced in sections of 10 mm, immersed in 1 M HCl, and the Fe and P concentrations were measured by ICP-MS. The detection limits in sediment pore waters sampled by this method were 0.1 mg L^{-1} for P and 0.03 mg L^{-1} for Fe.

We anticipated that the precipitation of Fe oxyhydroxides, caused by immersion in NaOH, also causes immobilization of P as long as sufficiently large amounts of Fe are present to bind the P. This was verified in synthetic solutions containing 10 mg L^{-1} Fe(II) (as $FeSO_4 \cdot 7H_2O$) and varying concentrations of P (from a stock solution of 1000 mg L^{-1} PO_4 as KH_2PO_4, Merck Millipore) buffered at pH 4 by 0.01 M acetic acid. The low pH was adopted in order to avoid oxidation of Fe(II) to Fe(III) under ambient conditions. Four gel slices were inserted into each solution and were deployed for 24 hours. Immediately after retrieval from the solution, the Fe and P in the gel slices were immobilized by immersion in 0.01 M NaOH. Thereafter, the gels were re-eluted by immersing them in 1 M HCl for 24 hours. The concentrations of Fe and P in the synthetic solutions and in the gel eluates were measured with ICP-MS.

Results

Sediment cores

The cores of the ditch sediment and the underlying parent material exhibited markedly similar characteristics in all three studied ditches. The top 1 cm of the sediment layer consisted mostly of finely textured, reddish brown material. Based on the soil color, a reduction horizon was observed between 30 and 50 cm below the surface of the ditch sediment. Above the reduction horizon, black and reddish brown colors dominated, which are indicative of accumulations of organic matter and Fe oxyhydroxides. Below the reduction horizon, the soil was permanently reduced and consisted of pale, greenish grey sands. The oxic layer was relatively deep, because the sediment cores were taken in summer when the groundwater levels were at their lowest. It is expected that the oxic layer is less deep in winter, when the ditches evacuate groundwater.

Oxalate extractions (Figure 5.2) showed that the top sediment layer was highly enriched in poorly crystalline Fe oxyhydroxides: the concentration of oxalate extractable Fe was up to 11% on a dry weight basis. The oxalate extractable concentrations of Fe and P in the top layers exceeded those in the deeper layers by one or two orders of magnitude. In contrast, the Fe:P ratio did not differ more than by a factor or 4, and the vertical distribution patterns of Fe and P were markedly similar. The concentrations of oxalate extractable Al and Mn did not follow the vertical distribution of Fe, and molar concentrations of Al and Mn were much lower than those of Fe in the top sediment layer (data not shown). This shows that P was strongly associated with poorly crystalline Fe oxyhydroxides, but less so with oxyhydroxides of Al and Mn. The DPS in the top sediment layers of the studied ditches was between 13 and 31%. Acid sandy soils are considered P-saturated and pose a risk for leaching of P if they have a DPS in excess of 25% [90]. Even though the applicability of this criterion has never been validated for drainage ditch sediments, it appears at first glance that the drainage ditches may have limited ability to retain inputs of groundwater-borne P.

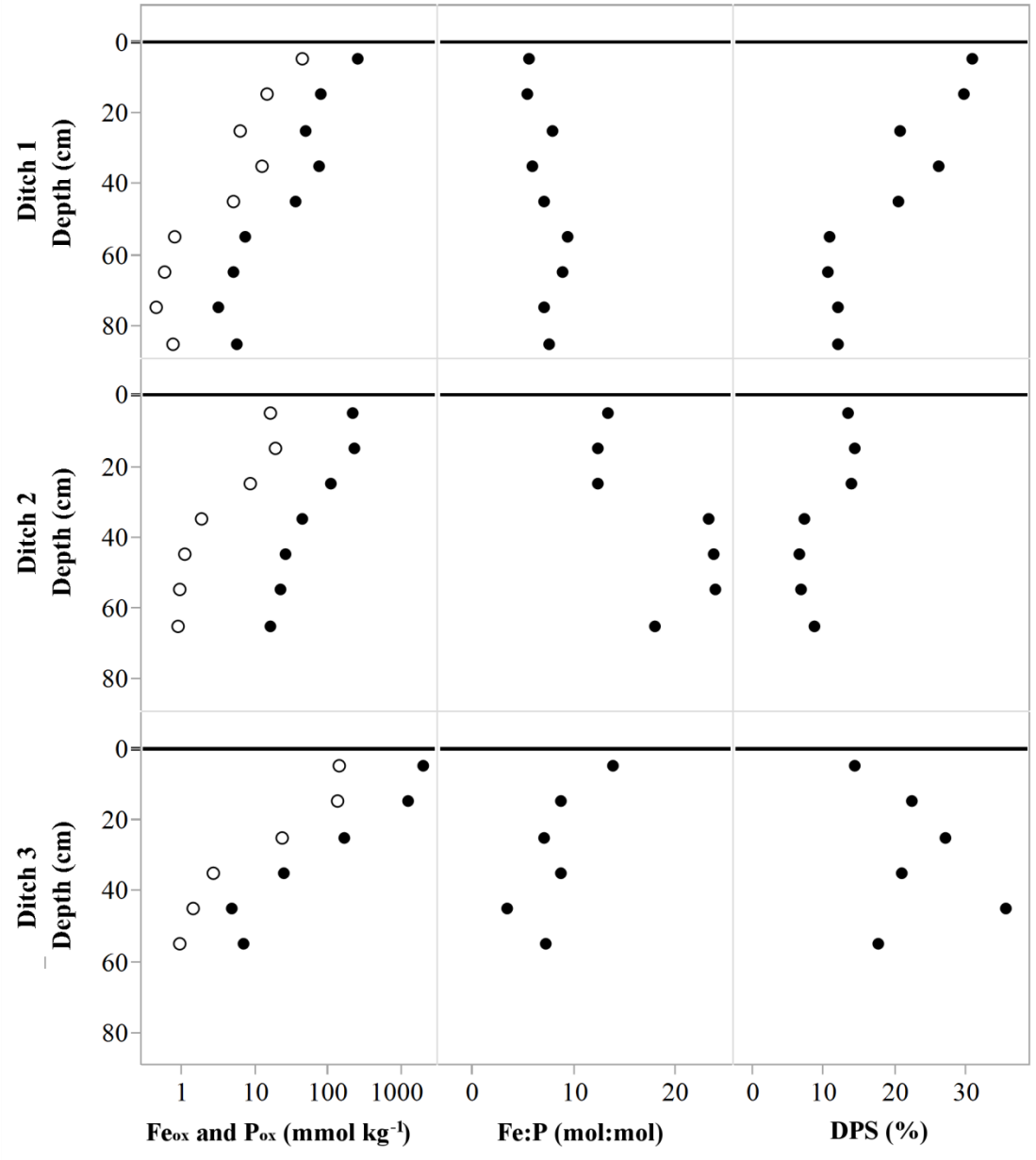

Figure 5.2: Oxalate extractable concentrations of Fe and P (Fe_{ox}: closed symbols; P_{ox}: open symbols), their molar ratios, and the degree of P saturation (DPS) in the ditch sediment and the underlying parent material of the three studied ditches. The depth was measured from the surface of the ditch sediment.

Composition and fluxes of groundwater and ditchwater

The average composition of groundwater and ditchwater is reported separately for each studied ditch (Table 5.1). The groundwater was slightly acidic to neutral (pH between 5.5 and 7.0), moderately hard, and contained dissolved O_2 concentrations below 1 mg L^{-1}. The groundwater contained, on average, 9 mg L^{-1} Fe (near ditch 1) and 7 mg L^{-1} Fe (near ditch 3), with little temporal variation, whereas the groundwater near ditch 2 contained much less Fe (0.2 mg L^{-1}). The average P concentrations in the groundwater near ditches 1 and 3 also exceeded that near ditch 2 by approximately one order of magnitude. The SRP concentrations in selected groundwater samples were almost equal to the P concentrations measured by ICP-MS (data not shown), suggesting that most P in the groundwater is present as inorganic orthophosphate, and that organic P compounds play a minor role [75]. However, we have not monitored organic P concentrations throughout this study, and we were unable to discriminate between different P species in the sediment pore water. Therefore, the contribution of organic P components to the P fluxes remains somewhat uncertain.

The ditchwater was stratified: 10 cm below the surface of the ditchwater, the O_2 concentration was around 1 mg L^{-1}, *i.e.* not much different from that in the groundwater, whereas just below the water surface, the O_2 concentration generally increased to 2–5 mg L^{-1}. Conversely, the Fe concentrations in the ditchwater at 10 cm below the surface exceeded those near the water surface by up to two orders of magnitude. In most samples, the "dissolved" Fe was almost exclusively present as reduced Fe(II). No clear temporal trend was observed in the Fe and P concentrations in ditchwater. The groundwater and ditchwater contained relatively high concentrations of SO_4, and the SO_4 concentrations in the ditchwater are above those in the groundwater. This shows that the ditch was no sink for SO_4, suggesting that no extensive SO_4 reduction occurred in the studied systems.

The average discharge of ditch 1 into the adjacent river was 8.5 m^3 d^{-1}. The ditch can be roughly approximated by a semi-cylinder with length 180 m and radius 40 cm; the total water volume in the ditch is then 45 m^3. The average retention time of the water in the ditch is therefore about 5 days. Ditch 2 is adjacent to the same field and has similar dimensions, and therefore the retention time is likely of the same order of magnitude. No discharge measurements are available for ditch 3.

Table 5.1: The composition (mean ± standard deviation; n = 1–7 for anion and C measurements and 5–12 for other measurements) of drained groundwater (0.45 µm filtered) at different stages along its trajectory from the subsurface to the surface. The groundwater was sampled using monitoring wells, the sediment pore water was sampled with DET probes at 1–10 cm below the sediment-water interface, and the ditchwater was sampled with a syringe either 1 cm or 10 cm below the water surface. The reported values are derived from measurements at two locations along each ditch and on up to 6 occasions between September 2013 and February 2014.

		pH	O_2	Fe	P	Fe:P	Al	Mn	Ca	Cl	SO_4	NO_3	DOC	DIC
			mg L^{-1}	*mg L^{-1}*	*µg L^{-1}*	*mol:mol*	*µg L^{-1}*	*µg L^{-1}*	*mg L^{-1}*	*mg L^{-1}*	*mg L^{-1}*	*mg L^{-1}*	*mg L^{-1}*	*mg L^{-1}*
DITCH 1	ditchwater, 1 cm deep	5.9 ± 0.3	4.5 ± 2.5	3.2 ± 3.6	20 ± 21	136 ± 108	15 ± 9	335 ± 57	29 ± 2	50 *	93 *	11.0 *	7 *	5 *
	ditchwater, 10 cm deep	5.7 ± 0.3	0.7 ± 0.8	25.5 ± 27.9	71 ± 117	335 ± 117	12 ± 6	337 ± 61	26 ± 7	nm	nm	nm	10 ± 4	5 *
	sediment pore water			77.5 ± 21.8	653 ± 430	233 ± 105								
	groundwater	6.0 ± 0.4	0.5 ± 0.1	8.5 ± 3.6	1085 ± 1228	12 ± 9	18 ± 13	289 ± 156	49 ± 21	44 ± 10	60 ± 31	1.2 ± 1.9	22 ± 15	36 ± 4
DITCH 2	ditchwater, 1 cm deep	5.9 ± 0.7	3.9 ± 1.5	11.0 ± 9.0	18 ± 10	393 ± 323	10 ± 7	551 ± 289	48 ± 5	44 ± 9	146 ± 66	0.5 ± 0.4	7 ± 0.4	11 ± 7
	ditchwater, 10 cm deep	5.9 ± 0.3	0.7 ± 0.5	33.8 ± 23.2	19 ± 9	1010 ± 785	12 ± 6	630 ± 240	54 ± 7	51 ± 3	195 ± 14	0.2 ± 0.04	10 ± 3	9 ± 6
	sediment pore water			101.2 ± 57.9	219 ± 157	1006 ± 576								
	groundwater	6.1 ± 0.2	0.6 ± 0.2	0.2 ± 0.3	49 ± 19	2 ± 3	11 ± 7	230 ± 254	72 ± 17	59 ± 6	69 ± 6	84.3 ± 80.5	27 ± 5	53 ± 9
DITCH 3	ditchwater, 1 cm deep	6.7 ± 0.3	3.1 ± 1.7	1.5 ± 2.2	37 ± 32	16 ± 12	5 ± 2	111 ± 87	72 ± 8	20 *	66 *	0.1 *	11 ± 2	49 ± 5
	ditchwater, 10 cm deep	6.8 ± 0.2	1.1 ± 0.4	6.2 ± 10.5	100 ± 154	27 ± 21	5 ± 1	227 ± 211	77 ± 8	16 ± 6	45 ± 28	0.2 *	14 ± 3	50 ± 6
	sediment pore water			47.7 ± 33.7	2743 ± 1903	30 ± 7								
	groundwater	6.4 ± 0.4	0.5 ± 0.2	7.1 ± 1.2	744 ± 525	8 ± 4	4 ± 2	70 ± 47	44 ± 8	10 ± 3	13 ± 6	1.9 ± 2.0	8 ± 1	30 ± 1

DOC: dissolved organic carbon; DIC: dissolved inorganic carbon; nm: not measured; *: single observation, no standard deviation available

Concentration profiles of Fe and P by diffusive equilibration

The Fe and P in synthetic solutions are almost quantitatively recovered from diffusive gels after equilibration, immobilization in 0.01 M NaOH, and re-elution in 1 M HCl (>87%, mean 94% for both elements, Table 5.2). The P measured in the diffusive gels differed from that in solution in only one treatment, which was likely because the P concentration was near the detection limit (100 µg L^{-1}) of this method. Surprisingly, the recovery of P remained unaffected when the molar Fe:P ratio in the synthetic solutions decreased to unity. The above results show that the P is effectively bound to the Fe after immersion in NaOH, likely as coprecipitate with Fe oxyhydroxide or as ferric phosphate. The diffusive gels appear to underestimate the Fe and the P concentrations slightly but systematically by about 6%. This may be caused by minor errors in gel thickness or porosity. Alternatively, upon immersing the gel in NaOH, a small part of the Fe and P may be lost from the gel by diffusion before it is precipitated and immobilized. Despite these minor issues, the experiment overall shows that Fe and P can be quantified at molar Fe:P ratios down to unity by means of diffusive gel equilibration, immobilization in NaOH, and re-elution in HCl

Table 5.2: Fe and P concentrations, their standard errors (n = 4), and their recovery measured in diffusive gels after equilibration with synthetic solutions, fixation with NaOH, and re-elution with HCl.

IN SYNTHETIC SOLUTION			IN DIFFUSIVE GELS				
Fe	**P**	**Fe:P**	**Fe**	**recovery**	**P**	**recovery**	**Fe:P**
mg L^{-1}	**mg L^{-1}**	**mol:mol**	**mg L^{-1}**	**%**	**mg L^{-1}**	**%**	**mol:mol**
10.4	0.14	41	9.3 ± 0.2	90	0.20 ± 0.01	141	26
10.2	0.29	19	9.3 ± 0.1	92	0.31 ± 0.02	105	17
10.0	0.57	10	9.7 ± 0.1	97	0.55 ± 0.04	96	10
10.2	1.18	4.8	9.5 ± 0.04	93	1.04 ± 0.03	88	5.1
10.1	1.50	3.8	9.8 ± 0.1	96	1.31 ± 0.07	87	4.2
10.1	1.95	2.9	10.0 ± 0.2	98	1.91 ± 0.06	98	2.9
10.2	2.94	1.9	9.5 ± 0.1	93	2.70 ± 0.09	92	2.0
10.2	5.93	1.0	9.3 ± 0.2	91	5.60 ± 0.13	94	0.9

Seventeen concentration profiles of Fe and P in the sediment pore water and in the overlying ditchwater were obtained with the DET method. The probes revealed Fe concentrations in the sediment pore water between 10 and 200 mg L^{-1}, which is up to two orders of magnitude above those in groundwater (Table 5.1) In Figure 5.3, selected concentration profiles are shown. In the sediment pore water, the profiles of the Fe concentrations were variable: they decreased, remained more or less constant, or increased with elevation. In the overlying ditchwater, some profiles showed a sharp decrease in Fe concentrations just above the sediment-water interface (e.g. profiles C and D in Figure 5.3), but in other profiles, the Fe concentrations remained more or less equal to those in the sediment pore water (e.g. profiles A and B in Figure 5.3). The spatial heterogeneity was large: probes installed 50 cm apart yielded markedly different concentration profiles. We did not observe any clear temporal trends in sediment pore water concentrations of Fe and P, possibly because such trends are overshadowed by the large spatial heterogeneity. However, in spite of the large variability, the ditchwater samples taken with a syringe at 1 cm and 10 cm below the water surface invariably contained lower Fe concentrations than those measured with DET probes in the water layers close to the sediment-water interface. The average Fe concentrations decreased from 77 mg L^{-1} in the sediment pore water to 5 mg L^{-1} near the water surface. Hence, Fe concentrations in the ditchwater decreased with decreasing depth.

The P concentrations in the sediment pore water varied from below detection limit (<100 µg L^{-1}) to 6000 µg L^{-1}. The P concentrations in the sediment pore water of ditch 1 covered the range of the corresponding groundwater, whereas the P concentrations in the sediment pore water of ditches 2 and 3 exceeded those in the groundwater by a factor of 4. Four out of 17 concentration profiles contained sections in which the P concentrations were below the detection limit of the DET sampling method (100 µg L^{-1}), e.g. profile C in Figure 5.3, and for plotting purposes these data points are shown at an arbitrary value of 50 µg L^{-1}. In the sediment pore water, the P concentrations generally did not vary much with depth below the sediment-water interface. However, most P concentration profiles, including profiles B, C, and D in Figure 5.3, showed a sharp decrease in P concentrations near the sediment-water interface. The P concentrations measured in the ditchwater at 1 cm and 10 cm below the water surface were invariably lower than those in the sediment pore water. The average P concentrations decreased from 890 µg L^{-1} in the sediment pore water to 26 µg L^{-1} near the water surface. No clear temporal trends in P

concentrations in the sediment pore water were observed. In summary, as groundwater flows into the drainage ditches, the P concentrations decrease sharply.

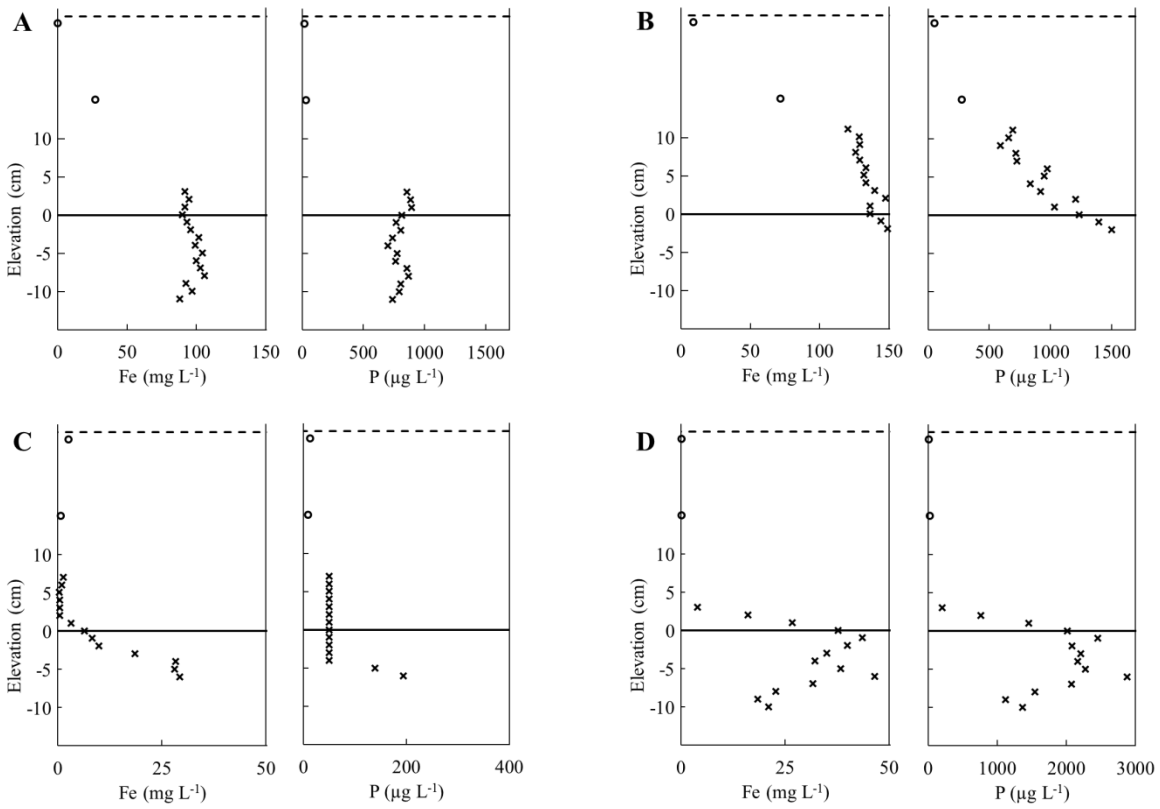

Figure 5.3: Selected concentration profiles of Fe and P, plotted versus the elevation above the sediment-water interface of open drainage ditches. The profiles are labelled (A–D) for easy reference in the text. Open circles refer to water samples taken with a syringe either 1 or 10 cm below the water surface; crosses refer to concentration profiles determined by diffusive equilibration (DET). If P concentrations were below the detection limit of the DET method (100 µg L^{-1}), e.g. as in profile C, they are plotted at 50 µg L^{-1}. The full line is the water-sediment interface, the dashed line is the water surface.

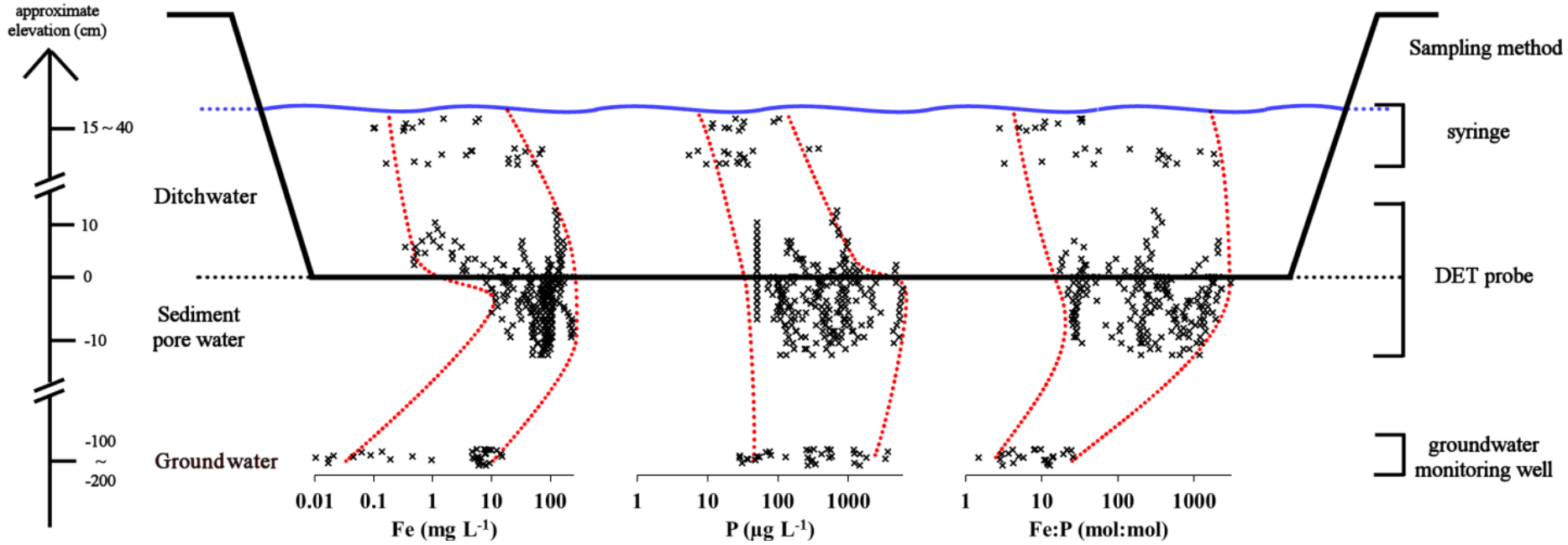

Figure 5.4: Schematic overview of the evolution of "dissolved" (<0.45 µm) Fe and P concentrations (log scale) as groundwater flows through Fe-rich sediments into open drainage ditches. All available data from all three studied ditches are combined. Dotted lines are drawn to guide the eye.

Discussion

Reductive dissolution and oxidative precipitation of Fe

Similar mechanisms appear to govern the behavior of Fe and its interaction with P in the three studied ditches. The concentrations of Fe and P in the groundwater, sediment pore water, and ditchwater of the three ditches are summarized in Figure 5.4. As groundwater flows into the sediment of the drainage ditch, the Fe concentrations strongly increase by up to two orders of magnitude. Reductive dissolution of Fe oxyhydroxides in the sediment likely explains this increase. The oxalate extractions of the sediment cores showed that there is an abundant stock of readily reducible Fe oxyhydroxides available. There is also ample supply of electron donors, *i.e.* readily degradable organic C derived from decaying vegetation which grows lavishly in the ditch in the summer season. The abundant stock of readily reducible Fe oxyhydroxides in the sediment of the studied drainage ditches may be the result of a process similar to the formation of bog iron ore: an accumulation of groundwater-borne Fe over prolonged periods of time in hydromorphic soils. Due to the fluctuating groundwater table, the top sediment layer is oxic in summer, but it is likely gradually more reduced as it becomes submerged in autumn. Previous studies have shown similar or greater increases in Fe concentrations upon waterlogging of soils [14,239], and the reduction of Fe oxyhydroxides may occur at rates well above those needed to explain the observed increase in Fe concentrations from the groundwater to the sediment pore water [27,115]. Possibly, oxidation and reduction reactions occur simultaneously and at approximately the same location in the sediment, which result in strong Fe redox cycling. We were unable to measure the O_2 concentrations in the sediment, and therefore the extent of Fe redox cycling in the sediment of the studied systems remains unknown. Possibly, the ditch sediments exhibit transitions in redox regime as they are submerged for increasingly longer times during the winter. Our data did not show any clear temporal trends in Fe concentrations in the sediment pore water or in the overlying ditchwater, but such temporal trends may be overshadowed by the large variability due to spatial heterogeneity. In addition, we studied the ditches only from September to February, but they are usually submerged until April or May. Any shifts in redox regime during these final months of waterlogging are not reflected in this study.

Based on the results of oxalate extractions and on previous studies [17], we assume that poorly crystalline oxyhydroxides and perhaps amorphous ferric phosphates are the most important reactive Fe phases present in the sediment. We did not study e.g. the conversion of poorly crystalline Fe oxyhydroxides to more crystalline phases. Goethite may occur in systems similar to the ones in this study [240]. However, goethite would not dissolve in oxalate extractions, and its presence would therefore not affect our results [241]. Furthermore, other reactive Fe phases, such as vivianite or Fe sulfides, may be present, even though SO_4 measurements suggest that no extensive sulfate reduction occurred in the studied systems.

In the ditch, *i.e.* above the sediment-water interface, the Fe concentrations decrease with increasing elevation above the interface (Figure 5.4). Oxidation of Fe(II) and subsequent precipitation of Fe oxyhydroxides is the key mechanism by which removal of Fe from the "dissolved" (<0.45 µm) fraction occurs. The oxidation of Fe(II) is kinetically limited; the kinetics of Fe oxidation in drainage systems have been studied in greater detail by Van der Grift et al. [242]. In this study, accurately predicting the reaction rate is difficult due to the highly heterogeneous system and the wide pH range encountered. The chemical rate of Fe(II) oxidation may be predicted assuming pH values between 5.5 and 7.0, dissolved O_2 concentrations of 2–6 mg L^{-1}, and temperatures between 5 and 15°C. These values result in half-lives of Fe(II) between 2 hours and 3 years [179]. In addition, groundwater seeps are typical environments where Fe oxidizing (and reducing) bacteria thrive [27], and therefore it is likely that microbially mediated Fe oxidation outpaces the chemical oxidation reaction.

The vertical concentration profiles of Fe in the ditchwater were highly variable, which may mostly be due to physical processes such as the local flow velocity, turbulence, and mixing, and due to the heterogeneity in factors that determine the Fe(II) oxidation rate (pH and O_2 concentration). Nevertheless, the average Fe concentration near the water surface was only 7% of that in the sediment pore water, showing that most of the Fe produced in the sediment is re-oxidized and precipitated in the ditch before it is drained into the receiving streams. The average retention time of the water in one of the studied ditches was around 5 days. Given that most of the Fe(II) is oxidized before it leaves the ditch, this suggests that the half-life of Fe(II) oxidation in this ditch must be towards the lower end of the range estimated above. In summary, as drainage water flows upward into the ditch, the Fe concentrations decrease due to oxidation of Fe(II).

Release and binding of P

The average P concentrations in the sediment pore water were similar to those in groundwater, or they exceeded those in the groundwater by at most a factor of four (Figure 5.4 and Table 5.1). Surprisingly, this increase (in relative terms) is much less pronounced than that of Fe. Since Fe and P are strongly associated with each other in the sediment, it is expected that reductive dissolution releases Fe and P at a molar ratio equal to that in the sediment. Most likely, the released P is bound again by the residual pool of Fe oxyhydroxides in the sediment. The oxalate extractions showed that Fe is present in excess in the sediments (Fe:P>5 mol Fe (mol P)$^{-1}$ in the top sediment layer). Previous work on Fe-rich submerged soils has also shown that the release of P is less than expected based on the release of Fe and the molar Fe:P ratio in the solid [243]. Alternatively, the P-containing Fe oxyhydroxides may be less available for microbial reductive dissolution than P-free Fe oxyhydroxides, as previously shown by O'Loughlin et al. [244]. Based on our data, we can neither confirm nor rule out that the P concentrations in the sediment pore water vary temporally due to shifts in redox regime as the ditch sediment is inundated for increasingly longer times: we did not observe such temporal trends, but they may be overshadowed by the high spatial variability. Based on the oxalate extractions, it is expected that poorly crystalline Fe oxyhydroxides are primarily responsible for binding and release of P in the sediments. Perhaps also ferric phosphates play a role [113]. Other minerals, such as vivianite [45], may also contribute to binding and release of P, but vivianite formation could not explain the rapid removal of P as the groundwater surfaces and reaches (micro-)oxic environments. In summary, the above shows that reductive dissolution solubilizes P in the sediments of drainage ditches, but due to the abundantly present Fe oxyhydroxides, much of this P is again bound to the residual pool of Fe oxyhydroxides.

The sharp change in P concentrations near the sediment-water interface (Figures 5.3 and 5.4) is most likely caused by oxidation of Fe(II) and binding of P. Despite the variable sediment pore water P concentrations, those in the top ditchwater layer were invariably low (<100 µg L^{-1}), showing that P removal was efficient during the studied period (September-February). The rapid removal of P from oxidizing Fe-containing groundwater samples has previously been noted. Studies in synthetic solutions have shown that, as Fe(II) is oxidized in the presence of phosphate, amorphous ferric phosphate with a molar

Fe:P ratio of 1.8 is formed until P is nearly depleted from solution. Thereafter, during continued oxidation of Fe(II), the ferric phosphate is converted to a P-containing Fe oxyhydroxide [17,123]. Results from a recent field study strongly suggest that these mechanisms also occur in the environment as Fe-containing groundwater is oxidized [242].

Taken together, reductive dissolution of P-containing Fe oxyhydroxides in the sediment preferentially solubilizes Fe, because the released P is bound again by residual Fe oxyhydroxides. Conversely, oxidative precipitation in the overlying water preferentially immobilizes P: since the water contains molar Fe:P ratios far above unity, the formation of ferric phosphate or P-saturated Fe oxyhydroxides causes faster immobilization of P than of Fe. The combination of these processes results in a natural and highly efficient sink for P: the average P concentrations in the groundwater feeding two out of three studied drainage ditches exceeded environmental limits for freshwaters (70 $\mu g\ L^{-1}$, commonly measured as SRP in unfiltered samples [245]) by factors 11 and 16, but after passing through the Fe-rich sediments, the "dissolved" P concentrations in the drainage water were below these limits. This study has some limitations: we did not monitor concentrations of organic P, and the role of such compounds therefore remains unclear. In addition, it is well established that the redox chemistry and the Fe and P concentrations change over time upon inundation of soils and sediments, but we have insufficient data to document such temporal trends. However, despite these limitations, our results confirm that oxidizing Fe in groundwater or drainage water is a highly efficient natural mechanism for immobilization of P.

Implications for P removal technology and watershed management

Interactions between Fe and P have already been utilized in technological applications. For example, Fe-coated sand as a liner in drainage systems reduce the P export [94]. We showed that a similar result is obtained by reaction of P with naturally present Fe. One difference is that, in the present study, the P was removed while oxidation of Fe was ongoing. Previous studies in synthetic solutions have shown that, under such conditions, ferric phosphates are formed [123]. Ferric phosphates may contain up to one mole of P per mole of Fe, which is stoichiometrically the highest possible efficiency for P binding. We speculate that technology for the removal of P from diffuse sources, such as agricultural drainage systems, may be based on the oxidation of reduced Fe. However, key challenges

include the mode of Fe addition to the system, and the retention of the formed Fe oxyhydroxide particles at the outlet.

Since Fe–P interactions can critically affect P fluxes, such processes should be taken into account when assessing the eutrophication risk associated with P losses from agricultural land. A key challenge is to determine the circumstances under which P is retained by Fe in drainage systems. Based on this study, it appears that the P concentrations in drainage water are mostly determined by the composition and reactivity of the sediment of the drainage ditch, and not much by the initial composition of the groundwater. The molar Fe:P ratio has previously been proposed as a useful tool for estimating the mobility of P in lake sediments and rewetted fens [114,231,232,246–248]. This approach may also be applicable to estimate P losses from the sediments of periodically inundated drainage systems. In this study, the Fe:P ratios in oxalate extracts of drainage ditch sediments between 6 and 14, and under these conditions, the P concentrations in drainage water did not exceed environmental limits. These Fe:P ratios are in the same range as the critical limits proposed earlier for lakes and rewetted fens. It is concluded that efforts to reduce P losses from groundwater to surface water in lowlands should focus on systems with limited ability to retain P, *i.e.* on systems with low Fe:P ratio.

We have based our study on measurements of concentrations in the operationally defined "dissolved" (<0.45 µm) fraction, and have so far ignored the transport of P in larger particles. It must be acknowledged that during periods of very high flow, particles >0.45 µm may be mobilized from drainage ditches and exported to the receiving streams. The P associated with Fe oxyhydroxides is less available to biota than free ionic orthophosphate [166], but it may become available e.g. after undergoing reductive dissolution in the streambed sediment further downstream. Therefore, even though losses of "dissolved" P are low in the studied areas, sediment losses from drainage systems may still impair water quality in the receiving streams.

Chapter 6 Phosphorus and arsenic sequestration by oxidizing iron in catchments

This chapter is adapted from Baken et al., *Environ. Sci. Technol.* **2015** *49* 2886–2894 (ref. [165]).

Summary

The fate of iron (Fe) may affect that of phosphorus (P) and arsenic (As) in natural waters. This study addresses the removal of Fe, P, and As from streams in lowland catchments fed by reduced, Fe-rich groundwater (average: 20 mg Fe L^{-1}). The removal of Fe from the "dissolved" fraction (<0.45 µm) of streamwater is governed by chemical reactions and hydrological processes: the oxidation of Fe(II) and the subsequent formation of Fe oxyhydroxide particles proceeds as the water flows through the catchment into increasingly larger streams. The Fe removal exhibits first-order kinetics with a mean half-life of 12 hours, a value in line with predictions by a kinetic model for Fe(II) oxidation. The Fe concentrations in streams vary seasonally: they are higher in winter than in summer, due to shorter hydraulic residence time and lower temperature in winter. The removal of P and As is much faster than that of Fe. The average concentrations of P and As in streams (42 µg P L^{-1} and 1.4 µg As L^{-1}) are one order of magnitude below those in groundwater (393 µg P L^{-1} and 17 µg As L^{-1}). The removal of P and As is attributed to fast sequestration by oxidizing Fe when the water enters oxic zones, possibly by adsorption on Fe oxyhydroxides or by formation of ferric phosphates. The average P and As concentrations in groundwater largely exceed local environmental limits for freshwater (140 µg P L^{-1} and 3 µg As L^{-1}), but in streams, they are below these limits. Naturally occurring Fe in groundwater may alleviate the environmental risk associated with P and As in the receiving streams.

Introduction

Eutrophication adversely affects water quality in many countries worldwide. In most cases, eutrophication of freshwater is related to increased concentrations of phosphorus (P) [13]. In lowland areas with acid sandy soils and shallow groundwater tables, leaching of P to the groundwater is the principal pathway for P transfer from agricultural land to streams. Arsenic (As) is a major source of impaired water quality at various locations worldwide [249,250]. In lowland streams fed by shallow, reduced groundwater, the transfer of P and As from groundwater to streams is not necessarily conservative. Upon exfiltration (seepage) of groundwater, P and As may interact with redox-active elements, most notably iron (Fe) [242,251,252]. The reduced ferrous iron (Fe(II)) is mobile in submerged environments [16], but as reduced Fe(II) is transported from sediments to oxic environments, it is oxidized either abiotically or biotically. Subsequent precipitation yields "particulate" (>0.45 µm) authigenic (or diagenetic) Fe oxyhydroxides which have been characterized as ferrihydrite and lepidocrocite [41]. Such precipitates may bind other elements by adsorption or coprecipitation, including As, Cu, Ni, P, Pb, and Zn [99,253–255].

As Fe(II) enters oxic environments, the rate of its oxidation to Fe(III) can in a first approach be approximated by a simple first order kinetic model [179]. Ligands such as chloride, bicarbonate, and natural organic matter may affect the oxidation rate, mostly at concentrations below 1 mg Fe L^{-1} [211,256]. The biological Fe(II) oxidation may outpace the chemical oxidation under acidic [23] or micro-oxic conditions [24,25]. The oxidation of Fe(II) and the production of Fe oxyhydroxides at circumneutral groundwater seeps has been studied extensively, both from a microbiological [27,222,223] as well as from a chemical perspective [256–258], and a large number of elaborate models for the chemical oxidation of Fe(II) have been developed. The fate of Fe(II) derived from acid mine drainage has also been widely investigated [259,260]. Burns et al. [261] have developed predictive models for the Fe oxidation rate and applied these models to streamwater sampled at various locations of a catchment. Van der Grift et al. [242] have recently studied oxidation rates of naturally occurring Fe and removal of P from drainage water in reservoirs. They found that Fe oxidation is much slower in winter than in summer, but that removal of P by oxidizing Fe(II) was at all times highly efficient. However, the combined effect of Fe(II) oxidation and hydrological processes has rarely been addressed. After exfiltration of groundwater, Fe(II) may persist temporarily if oxidation kinetics are slow, and the oxidation reaction

proceeds as the Fe(II) is transported by the streamwater. The oxidation half-life of Fe(II) is predicted to range between a few hours and a few days under conditions typical for streams fed by circumneutral Fe-rich groundwater [179]. This range is comparable to the hydraulic residence time of water in the headwater streams of lowland river catchments. The above suggests that spatial and seasonal trends in hydrological properties and chemical characteristics might explain the fate of Fe in catchments and, hence, govern the dynamics of other elements such as P and As in these systems.

The goal of this study was to determine the fate of high Fe(II) inputs in catchments, and to address how this affects the fate of P and As. We selected four Belgian catchments, the Kleine Nete catchment and three northern tributaries to the Demer river, as study sites. These lowland catchments are well suited to study such processes due to their hydrogeological setting. They are mainly fed by Fe-rich groundwater from the shallow, permeable, glauconite-containing aquifers of the Central Campine groundwater system [198,199]. Their flat topography limits erosion processes and the contribution of overland runoff to streamflow. Previous work showed that oxidation of Fe(II) in these streams yields authigenic ferrihydrite particles [133,199] (see also chapter 4). A key objective of this follow-up study was to relate spatial and temporal trends in Fe concentrations in the streams of these catchments to chemical (Fe(II) oxidation) and hydrological processes (the travel time or hydraulic residence time of water in the streams). In addition, we determined whether and how fast P and As are removed from the "dissolved" fraction of streamwater through sequestration by the authigenic ferrihydrite particles.

Materials and methods

Field campaign and data acquisition

Two study sites were selected: the Kleine Nete catchment, and the northern part of the Demer catchment. These sites are described in Chapter 4. In a field campaign, 56 sampling locations were selected near the streams of both study areas (Figure 4.1). The locations were chosen in order to reflect the trajectory of the water in the streams from the headwaters to the major rivers, *i.e.* to reflect the gradual increase in contact time with atmospheric oxygen as the water moves downstream. At each location, fully screened groundwater monitoring wells were installed at 3–4 m depth and at close distance (<5 m) to streams. The monitoring wells and the nearby streams were sampled on four occasions

throughout the year (April - June - September - November 2013), hereinafter referred to as "sampling moments". The water temperature, O_2 concentration, electrical conductivity (EC), and pH were measured in the field. Groundwater and streamwater samples were membrane filtered in the field (0.45 µm Chromafil Xtra PET 45/25 filters), and the concentrations of elements including P and Fe (ICP-MS), anions (ion chromatography), dissolved organic carbon (DOC), dissolved inorganic carbon (DIC), and Fe(II) and Fe(III) (colorimetric reaction with ferrozine reagent [136]) were determined. All reported concentrations refer to the "dissolved" (<0.45 µm) fraction, 'Fe(II)' refers to concentrations measured with ferrozine, whereas 'Fe' refers to ICP-MS measurements, which includes both Fe(II) and Fe(III). At selected locations, suspended sediment was sampled and the Fe, P, and As concentrations were determined by ICP-MS after digestion in boiling *aqua regia*.

Additional data were obtained from permanent monitoring programs. The water flow velocity was recorded by flow velocity loggers at selected locations throughout the study area. The O_2 concentration, streamwater temperature, and pH in the Kleine Nete were measured at 5-min intervals by a multiparameter probe (YSI 6600) installed near the outlet of the catchment. The discharge was monitored at the same location. All data are publicly available (http://www.waterinfo.be) and were downloaded for a 3-year period (2011–2014).

Calculations

The hydraulic residence time or travel time of the streamwater in the catchment was calculated for each streamwater sample that was collected, *i.e.* for each of the 56 sampling locations and for each of the four sampling moments. The residence time estimates the average travel time of the water from the moment of its exfiltration (seepage) to the moment it was sampled. Calculations were based on the hydrographic atlas of the Flanders region, which includes GIS information on the location and length of each stream stretch [262]. For each stream stretch, the water flow velocity at each sampling moment was estimated based on data from eight permanent flow velocity loggers installed at selected locations throughout the studied catchments. At each stream node, the relative contribution of each of both tributaries to the total discharge was estimated using the groundwater recharge in the area drained by each tributary. The groundwater recharge was retrieved from the WetSpass model for the Kleine Nete catchment [204,263], and from

the regional MODFLOW model of the central Campine groundwater system for the northern tributaries to the Demer river [196]. Finally, the average hydraulic residence time of each water sample was calculated by integration of all stream stretches upstream of the sampling location. This method for residence time calculation has limitations: it relies on water flow velocity data at selected locations only, and the method is less reliable during dynamic peak flow events. The method was sufficiently detailed for the purpose of this study. More detailed residence time calculations would require a catchment model which includes the smallest headwater streams, and flow velocity measurements at more locations, but such was beyond the scope of this study.

The Fe(II) oxidation rate constants in streams were derived by fitting a first order kinetic model to plots of Fe concentrations in streams versus hydraulic residence time, which is a proxy for the reaction time. When water containing an initial Fe concentration, defined as $Fe(II)_0$, reaches oxic environments, the Fe(II) concentration decreases with time (t) due to chemical oxidation, according to [179]:

$$Fe(II) = Fe(II)_0 \cdot \exp(-k_1 \cdot t) \qquad (Equation\ 6.1)$$

The rate constant of the pseudo first order chemical oxidation (k_1, in units of h^{-1}), which may also be expressed as a half-life ($t_{1/2}$), is given by:

$$k_1 = k \cdot pO_2 \cdot (OH^-)^2 \qquad (Equation\ 6.2)$$

where k is a 'universal' rate constant of approximately $2 \cdot 10^{13}$ M^{-2} atm^{-1} min^{-1} (uncertainty range $1.5–3 \cdot 10^{13}$ M^{-2} atm^{-1} min^{-1}), pO_2 is the O_2 concentration in the water (expressed as a partial pressure in atm), and (OH^-) is hydroxyl activity (in M) [179]. The (OH^-) is calculated from pH and from the temperature-dependent dissociation constant of water [264], and therefore k_1 depends on pH, temperature and the O_2 concentration.

All reported means and standard deviations are based on untransformed data. Regression analyses were performed using untransformed data and a least-squares algorithm. For correlation analyses, variable clustering, comparison of means (Student's t-test), and ANOVA tests, all variables except pH, hydraulic residence time, and temperature were log-transformed. Based on a visual inspection of QQ-plots, the distribution of all variables appeared to be well approximated by a lognormal distribution, and Shapiro-Wilk tests confirmed that lognormal distributions were preferable to normal ones in

nearly all cases. Correlation analyses, ANOVA tests, and nonlinear least-squares fitting were carried out in JMP Pro 11 (SAS Institute, Cary, United States).

Results and discussion

Groundwater: the source of Fe(II)

The characteristics and composition of filtered (0.45 µm) groundwater samples are shown in Table 6.1. The groundwater is generally reduced, as evidenced by low O_2 and NO_3 concentrations and by the pale grey color of the material which was recovered upon installation of the monitoring wells. This may be due to large inputs of DOC, originating from animal manure or from peat accumulated in plaggic soil horizons which are common in the area. The groundwater is strongly enriched in Fe, which is entirely present as reduced Fe(II). The Fe concentrations average 20 mg L^{-1} and range over two orders of magnitude. The P concentrations (average 393 µg L^{-1}) and As concentrations (average 17 µg L^{-1}) range over three orders of magnitude.

The correlation analysis indicate that the concentrations of Fe in groundwater are positively correlated with those of As ($r = 0.48$), P ($r = 0.42$), and Mn ($r = 0.31$). This hints at reductive dissolution of Fe oxyhydroxides which may supply these elements to the groundwater [199,249,250], even though no clear correlation with DOC (a plausible reductant) is observed. The P in groundwater mainly originates from fertilizer leaching from the excessively fertilized acid sandy soils of the region [200], whereas the As likely originates from weathering of As containing glauconite [251]. The large variability in groundwater Fe concentrations is neither explained by pH, EC, water temperature, nor by the concentration of any other measured element. Seasonality does not affect the groundwater Fe concentrations much: at four moments throughout the year, the average Fe concentrations range only between 16 and 24 mg L^{-1}. Analysis of variance confirms that the groundwater Fe concentrations vary spatially, whereas temporal effects are comparably small. The groundwater Fe concentrations likely vary due to the heterogeneity of the greensand parent material [198]. This may be due to local differences in glauconite content of the parent material, in hydraulic conductivity, in glauconite weathering rate, or in the presence of electron donors which reductively dissolve Fe oxyhydroxides.

Table 6.1: Characteristics and composition of filtered (0.45 µm) groundwater and streams, sampled at 56 locations and on 4 occasions throughout the year.

		pH	temp	O_2	EC	Fe	Fe(II)	Na	Al	P	Ca	Mn	Cu	Zn	As	Pb	OC
			°C	*mg L^{-1}*	*µS cm^{-1}*	*mg L^{-1}*	*mg L^{-1}*	*mg L^{-1}*	*µg L^{-1}*	*µg L^{-1}*	*mg L^{-1}*	*µg L^{-1}*	*µg L^{-1}*	*µg L^{-1}*	*µg L^{-1}*	*µg L^{-1}*	*mg L^{-1}*
Groundwater	**Min**	4.8	5.9	0.6	119	0.4	<0.02	3	2	3	5	9	<0.1	2.1	0.3	0.03	1.3
	P_{10}	5.6	7.9	1.0	192	3.9	3.0	5	4	24	11	25	0.1	3.3	1.0	0.05	3.0
	Median	6.3	11.7	1.4	469	13.2	13.9	15	15	203	37	167	0.5	6.4	6.1	0.18	7.8
	P_{90}	6.8	16.2	2.3	799	44.5	45.0	55	124	938	72	773	1.9	24.4	36.0	0.60	18.9
	Max	7.2	20.7	9.6	1780	91.5	97.5	202	1778	2611	131	3346	33.0	253.4	294.3	28.64	42.4
	Mean	6.2	12.0	1.6	491	19.5	20.5	24	77	393	38	295	1.3	12.3	16.5	0.55	10.0
	Stdev	0.5	3.1	0.9	256	17.8	19.4	26	226	528	26	456	3.8	22.0	35.2	2.47	8.4
	N	162	163	163	155	162	136	162	162	160	162	162	162	162	162	162	160
Streams	**Min**	4.3	3.0	1.6	75	0.08	0.02	4	1	2	9	5	0.1	1.7	0.3	0.01	2.3
	P_{10}	6.1	6.6	4.8	264	0.2	0.08	11	5	11	21	31	0.3	7.3	0.6	0.07	4.2
	Median	6.6	12.9	6.8	415	1.0	0.5	23	12	33	34	125	0.9	16.5	1.1	0.19	7.4
	P_{90}	7.0	17.9	9.6	683	6.1	4.4	53	51	79	56	233	2.2	51.7	2.5	0.47	11.8
	Max	8.2	23.9	14.7	1800	70.2	74.6	127	162	374	112	539	6.6	203.3	10.3	2.96	29.7
	Mean	6.6	12.1	6.9	458	3.6	2.9	28	23	42	37	136	1.2	25.0	1.4	0.24	7.8
	Stdev	0.5	4.6	1.9	198	9.2	9.1	19	27	38	15	91	0.9	26.0	1.1	0.27	3.8
	N	194	195	195	189	194	187	196	196	194	196	196	196	196	196	196	194

min: lowest observed value; P_{10}: 10th percentile; P_{90}: 90th percentile; max: highest observed value; stdev: standard deviation; N:number of observations; temp: water temperature; EC: electrical conductivity; OC: organic carbon

Chemical processes occurring after exfiltration of groundwater

The characteristics and composition of filtered (0.45 µm) streamwater samples are shown in Table 6.1. Some samplings occurred during dry spells, whereas others coincided with rainfall events of low or moderate intensity. Separation of the baseflow from the total hydrograph using the WETSPRO numerical filtering procedure [265] shows that, during sampling, baseflow contributed between 67 and 95% to the total stream flow of the Kleine Nete (Figure 6.1). No discharge data are available for the Demer tributaries, but given its nearby location and similar geographic hydrogeological setting, baseflow contributions to stream flow during the sampling moments are likely similar. In addition, the mean and median Ca concentrations and EC in streamwater do not differ much between different sampling moments. This shows that dilution of baseflow by faster, more dilute components of stream flow was likely limited in most samples.

Given the large baseflow contribution, a comparison of the composition of groundwater and streams may yield information about chemical processes occurring at the groundwater-surface water interface (Figure 6.2). Contrary to the Ca concentration and the EC, the concentrations of dissolved O_2, Fe, As, and P differ considerably between groundwater and streams. The O_2 concentration increases strongly from groundwater to streams due to contact with the atmosphere. The concentrations of "dissolved" (<0.45 µm) Fe concomitantly decrease: upon exfiltration (seepage) of Fe(II)-rich groundwater, the Fe(II) is oxidized to Fe oxyhydroxides which are poorly soluble and readily form precipitates (>0.45 µm). The concentrations of many cationic trace metals, including Ni, Cu, Cd, Zn, and Co, increase from the groundwater to the streams. We speculate that this may reflect anthropogenic inputs through wastewater discharge, or it may be the result of oxidation and mobilization of metals sulfides from streambed sediments which contain known legacy contaminations of trace metals, such as Zn and Cd [266]. The concentrations of P and As in streams are almost one order of magnitude lower than those in groundwater. These elements commonly occur as oxyanions and are known for their high affinity for fresh Fe oxyhydroxides [51]. The concentrations of Fe, P, and As in suspended matter are around one order of magnitude above the typical concentration range of these elements in soils in the region [3,4,267]. Taken together, these data strongly suggest that the P and As are sequestered throughout the studied catchments by freshly formed Fe oxyhydroxide precipitates.

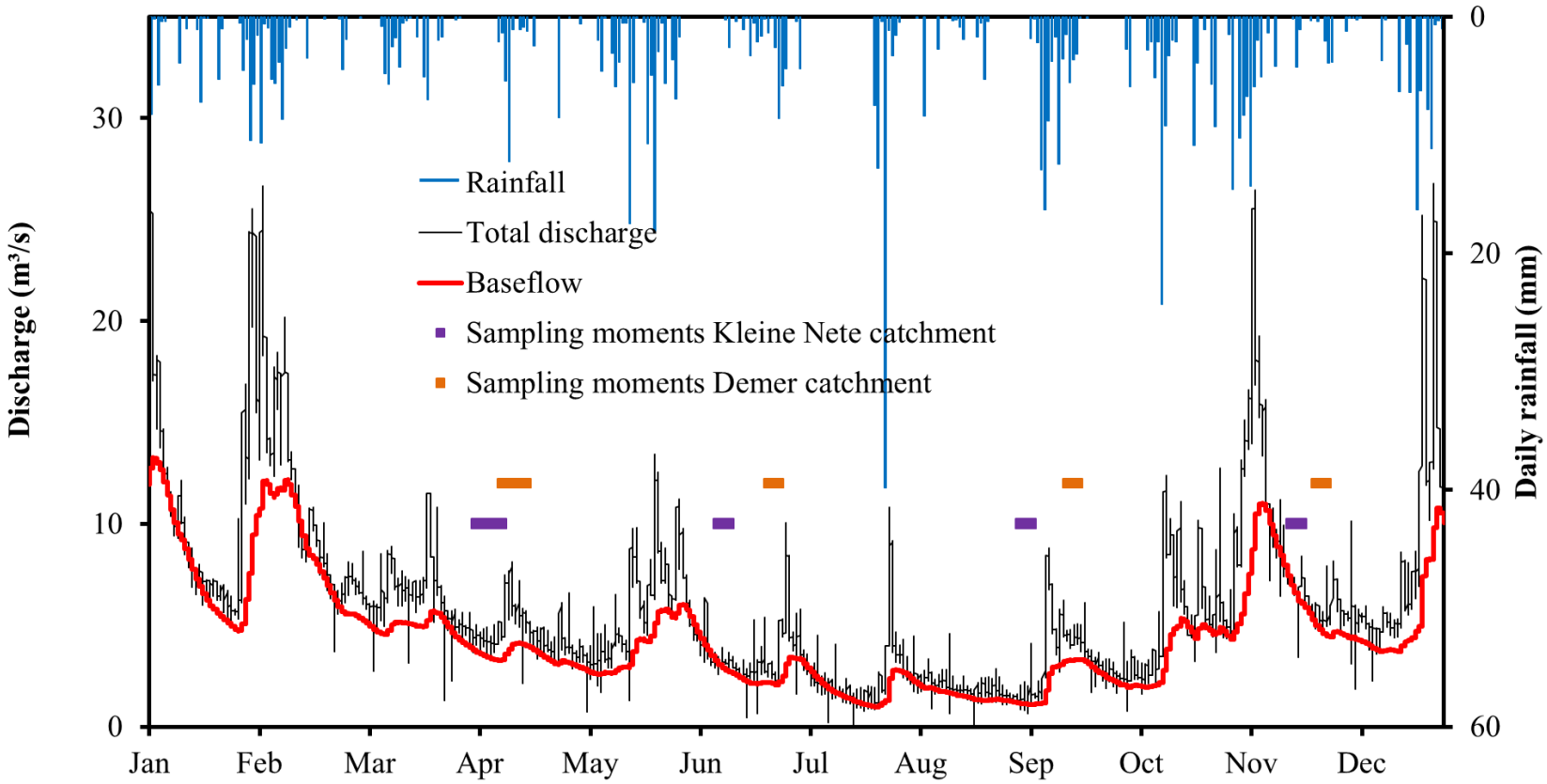

Figure 6.1: Total discharge (black line) and baseflow contribution (red line) during 2013 in the Kleine Nete at the Grobbendonk permanent monitoring station (primary vertical axis). The baseflow contribution was separated from the total hydrograph using WETSPRO[265]. The daily rainfall (secondary vertical axis) and the sampling moments in each study area (orange and purple lines) are also shown.

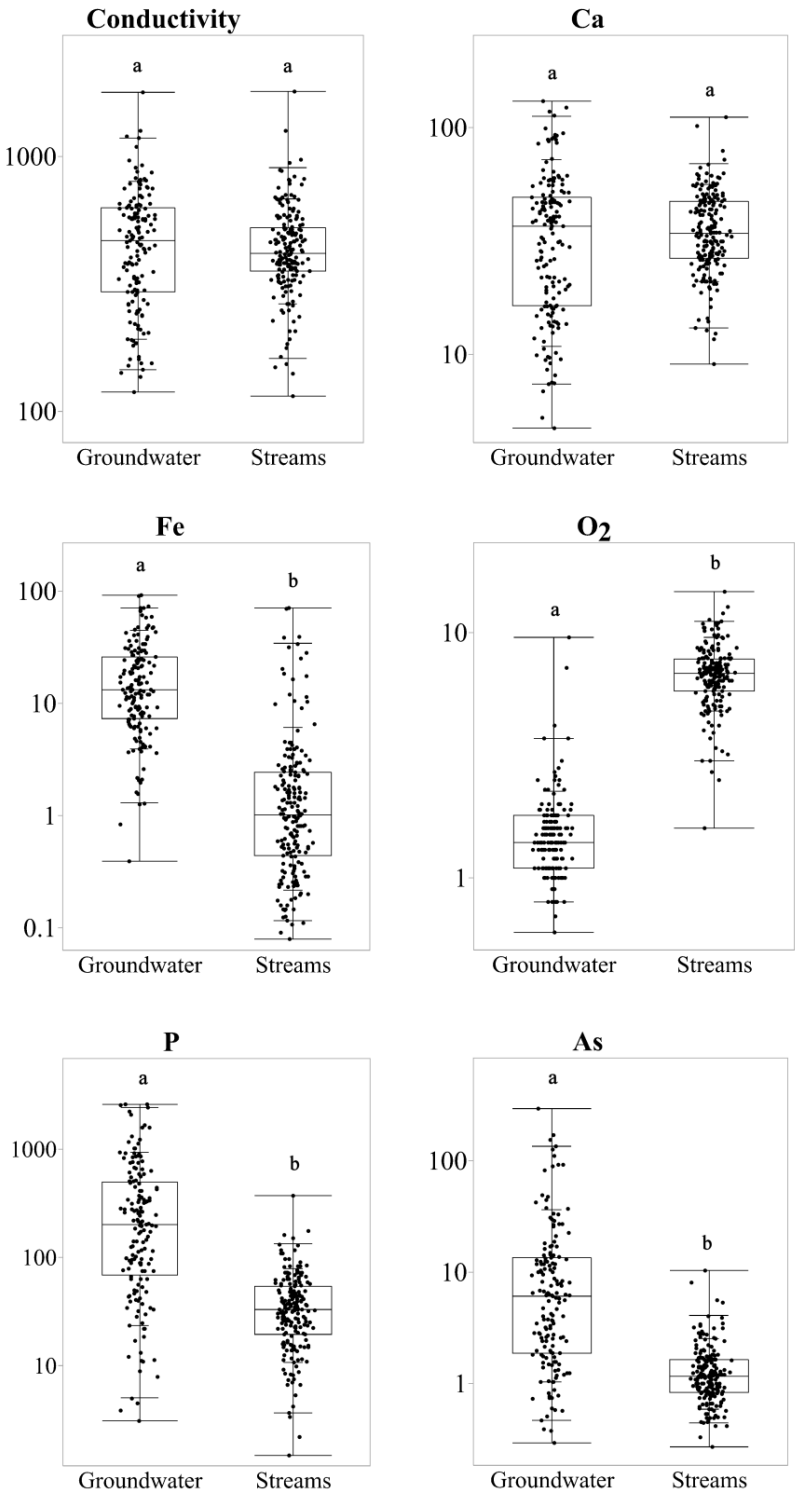

Figure 6.2: A comparison of the composition of groundwater and streams hints at chemical interactions between O_2, Fe, P, and As. Elements were measured after membrane filtration (0.45 µm). Units: µS cm^{-1} (electrical conductivity), mg L^{-1} (Ca, Fe, O_2), µg L^{-1} (P, As). Means followed by different characters are significantly different (Student's t-test performed on log-transformed data; $P < 0.05$).

Oxidation of Fe(II) and removal of Fe from the dissolved (<0.45 µm) fraction

The "dissolved" (<0.45 µm) Fe concentrations in streams range between 0.1 and 70 mg L^{-1}. In streams containing Fe concentrations more than 3 mg Fe L^{-1}, the Fe redox speciation is dominated by Fe(II). Conversely, in streams with lower Fe concentrations, the Fe consists of a mixture of Fe(II) and Fe(III) in varying proportions. The median hydraulic residence time (travel time) of the water in the streams is 27 hours (10^{th}–90^{th} percentile: 7–105 hours). A plot of the Fe concentrations versus stream order (Box 6.1) shows that the small headwater streams (order 1 and 2) may contain up to 70 mg Fe L^{-1}, but this drops to below 3 mg Fe L^{-1} in the streams of order 4 and 5 (Figure 6.4A). If plotted against the hydraulic residence time of the water in the streams, a similar trend (r = –0.54) is observed: the Fe concentrations decrease with increasing residence time, which reflects the exposure time of water to oxic environments (Figure 6.4B). Similar trends emerge if Fe(II) instead of Fe concentrations are plotted. The Fe(II) supplied by the groundwater is increasingly oxidized, precipitated, and removed from the "dissolved" (<0.45 µm) fraction as the water flows through the catchment into increasingly larger streams. This process results in the observed Fe concentration gradient which decreases from the smallest headwaters to the receiving streams.

Box 6.1: Stream orders or Strahler numbers

In hydrology, streams are classified using the concept of stream orders or Strahler numbers. The classification scheme start by assigning stream order 1 to the smallest, unbranched headwater streams. At each confluence of streams with the same order, the stream order increases by 1. As a result, the largest stream of a network is assigned the highest order.

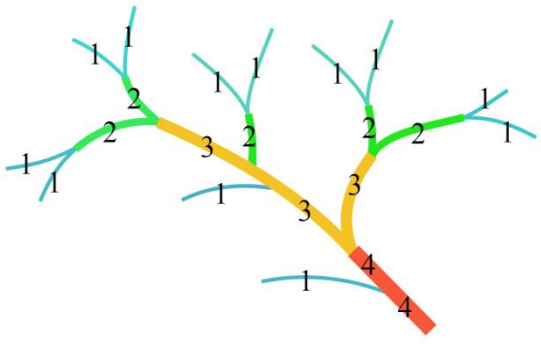

Figure 6.3: Illustration of Strahler numbers.

Adapted from Wikipedia: the free encyclopedia, "Strahler number", retrieved: April 13, 2015.

A catchment-scale Fe(II) oxidation rate is derived based on measured Fe concentrations in streams and on the first order kinetic model (Equation 6.1). Previous laboratory studies have shown that this model is appropriate for oxidation of Fe(II) in the study area [133]. The first order rate constant for oxidation of Fe(II) at the catchment scale is estimated at $k_1 = 0.056 \pm 0.015\ h^{-1}$, corresponding to a half-life of 12 hours, and the initial Fe concentration is 13.7 ± 2.5 mg Fe L^{-1} (error estimates are standard errors). The fitted catchment-scale oxidation rate agrees with theoretical predictions (Equation 6.2): it corresponds to the 42nd and 82nd percentile of the predicted oxidation rates in the samples from the Kleine Nete catchment and Demer tributaries, respectively (Table 6.2). The fitted initial Fe concentration $Fe(II)_0$ is significantly ($P < 0.05$) below the average groundwater Fe concentration (20 mg L^{-1}). This suggests that only part of the Fe(II) supplied by the groundwater is oxidized in the streams, whereas the remainder is oxidized and precipitated before it enters the streams, e.g. in open drainage ditches, drainage tubes, or in the hyporheic zone. This interpretation is further corroborated by the average Fe concentration in streams with low residence times (<10 hours), which is 11 mg L^{-1}. The fitted kinetic model is visualized in Figure 6.4B. The groundwater-derived Fe is largely removed from solution within approximately 50 hours. After that, the "dissolved" Fe concentrations in streams no longer decrease. The remaining Fe in samples with long residence times is a mixture of Fe(II) and Fe(III). In these samples, the Fe(III) likely occurs as complexes with organic matter or as colloidal Fe oxyhydroxides; the residual Fe(II) (around 0.3 mg L^{-1}) may be protected against oxidation through complexation with organic matter [15].

The concentrations of Fe and Fe(II) in streams exhibit pronounced seasonal variability (Figure 6.5A). Due to the meteorological and flow conditions, this variability was even more pronounced in the Kleine Nete catchment than in the Demer tributaries, and therefore the discussion below is focused on the Kleine Nete catchment. During the sampling in late summer (September), the median Fe and Fe(II) concentrations were 5-fold and 7-fold lower than those measured in early spring (April) and late autumn (November). We set out to determine whether the rate of Fe(II) oxidation or the reaction time (hydraulic residence time) can explain this seasonal variability.

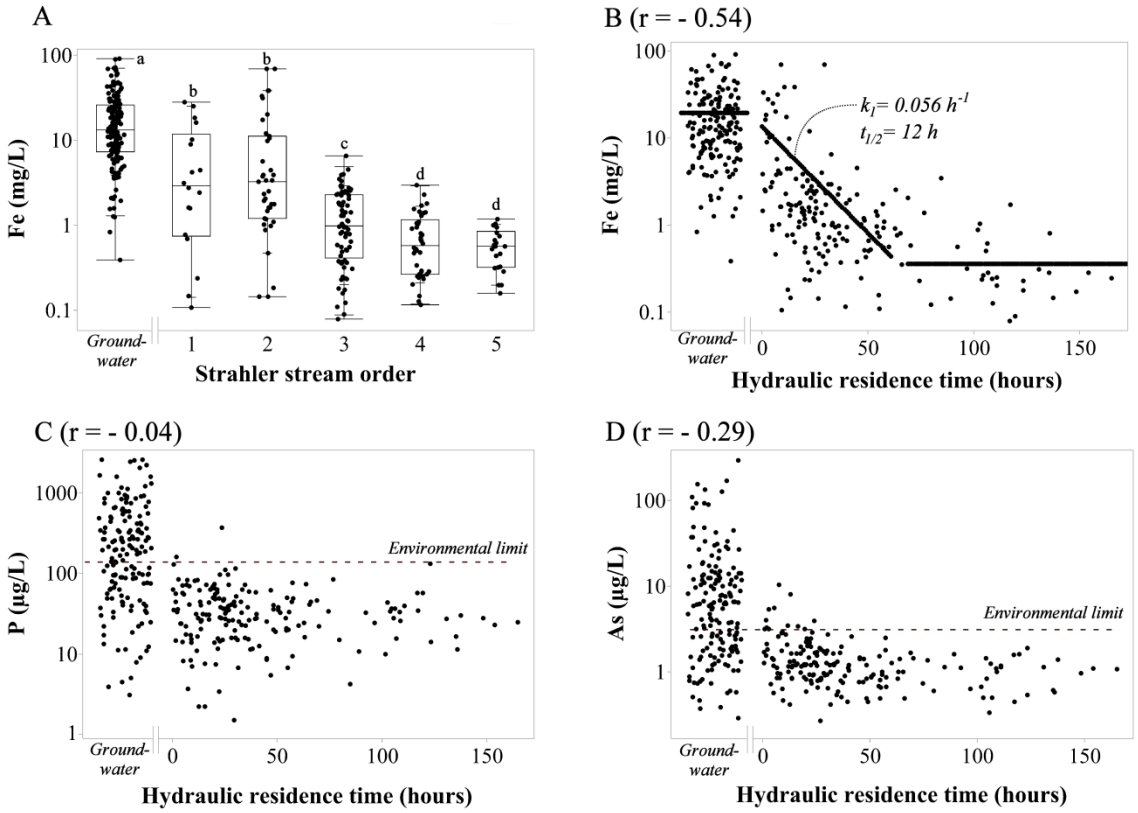

Figure 6.4: The concentrations of "dissolved" (<0.45 µm) Fe, P, and As in streams plotted against the Strahler stream order and against the hydrological residence time of the water in the catchment. The concentrations in groundwater are shown on the left for comparison, but the correlation coefficients refer to streamwater samples only. A: Means followed by different characters are significantly different (Student's t-test performed on log-transformed data; $P < 0.05$). B: The decreasing line is the fitted first order model for catchment-scale Fe(II) oxidation, and the horizontal lines indicate the average Fe concentration in groundwater and the average Fe(III) concentration in streams. C and D: The horizontal lines indicate local environmental limits for freshwater.

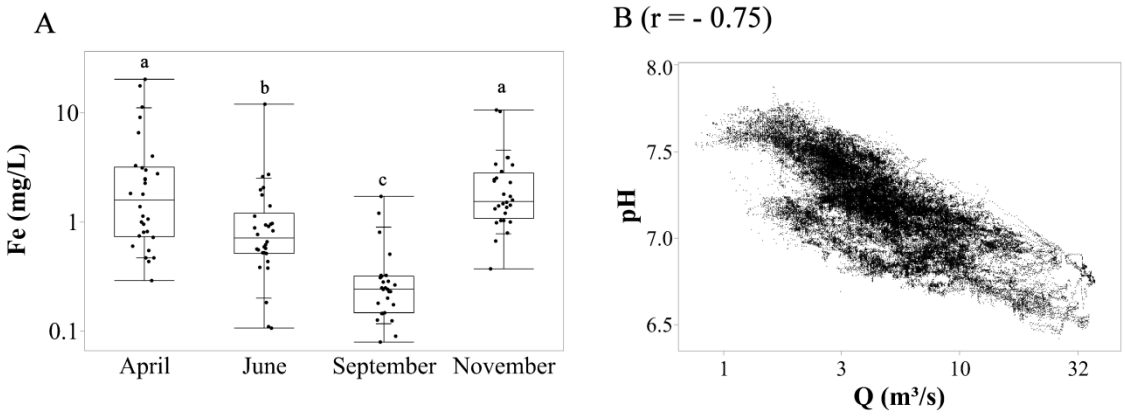

Figure 6.5: A: Seasonal variations of dissolved (<0.45 µm) Fe concentrations in streams of the Kleine Nete catchment. Means followed by different characters are significantly different (Student's t-test performed on log-transformed data; $P < 0.05$). B: Plot of pH versus discharge (Q) near the outlet of the Kleine Nete catchment ($r = –0.75$; $P < 0.001$).

Table 6.2: The abiotic first order rate constant for the oxidation of Fe(II) (predicted using Equation 6.2) and hydraulic residence time of streamwater in the Kleine Nete catchment at four sampling moments throughout the year. Averages, medians and percentiles refer to measurements obtained at 31 sampling locations. The discharge at the catchment outlet at the moment of sampling is also shown.

	first order rate constant for Fe(II) oxidation				**hydraulic residence time**	**discharge**
	P_{10}	*median*	P_{90}	*average*	*average*	
	h^{-1}	h^{-1}	h^{-1}	h^{-1}	*h*	$m^3\ s^{-1}$
April 2013	0.01	0.06	0.40	0.13	26	4.3
June 2013	0.03	0.14	0.84	0.26	49	3.1
September 2013	0.01	0.12	3.18	0.93	106	1.4
November 2013	0.001	0.02	0.54	0.12	20	7.0

P_{10}: 10th percentile; P_{90}: 90th percentile

Based on permanent monitoring data recorded near the outlet of the Kleine Nete, the predicted rate of Fe oxidation varies widely depending on the season (predictions based on Equation 6.2; data not shown). The oxidation rate in summer is up to 50-fold faster than in winter, mainly caused by higher summer pH and temperature. Stream pH strongly and significantly decreases with increasing discharge ($r = 0.75$; Figure 6.5B). Stream pH is governed by degassing of CO_2 which is kinetically limited: lower discharge in summer than in winter causes increased hydraulic residence times, which in turn causes more CO_2 degassing and higher pH. The oxidation rate constants in the streams of the Kleine Nete catchment, predicted with Equation 6.2 using locally measured pH, O_2 concentrations and temperature, exhibit seasonal trends similar to those near the outlet of the catchment (Table 6.2). These theoretical predictions are in line with our measurements: the fitted catchment-scale oxidation rate constant (which does not account for seasonal effects, Figure 6.4B) is close to the median predicted oxidation rate constant in streams throughout the Kleine Nete catchment. Moreover, the predicted slow oxidation rates during the April and November samplings coincide with high measured Fe concentrations in the headwaters. In order to quantitatively relate this predicted seasonal variability to actual measurements of Fe concentrations, oxidation rates in the Kleine Nete catchment were derived separately for each sampling moment using Equation 6.1. For the June and September samplings, the oxidation rate cannot be estimated: all Fe had already been oxidized before it reached the headwaters. For the April and November sampling, the first-order rate constants are estimated at 0.06 ± 0.02 h^{-1}, and 0.06 ± 0.01 h^{-1}, respectively (error estimates are standard errors). Given the uncertainty generally associated with determining the oxidation rate of Fe(II) [179], these fitted rate constants agree relatively well with the median predicted oxidation rate constant (respectively 0.06 and 0.02 h^{-1}; Table 6.2). Therefore, the theoretical predictions and the measured Fe concentrations both illustrate that the Fe oxidation rate varies seasonally. The theoretical predictions do not take into account microbially catalyzed Fe(II) oxidation, which may outpace the chemical oxidation reaction under specific circumstances at circumneutral pH [268]. If the rate of microbial Fe(II) oxidation exceeds that of chemical Fe(II) oxidation, it is expected to do so under conditions where the chemical oxidation reaction is slow, *i.e.* in winter [268]. This process may therefore to some extent counteract the seasonal trends discussed above.

The hydraulic residence times of the field campaign samples from the Kleine Nete catchment are shown in Table 6.2; data represent averages across 31 sampled locations.

The average hydraulic residence time differs seasonally by factors of up to 5, and long residence times are associated with low discharge. The residence times during sampling of the Kleine Nete catchment are a good indication of typical seasonal variability and trends: the flow velocities recorded at the sampling moments cover the 3rd–85th percentile range of the annual flow velocity, and flow velocities were lower in summer than in winter. A numerical example illustrates the effect of hydraulic residence time on the oxidation of Fe(II) and the resulting Fe concentration gradient: if in a hypothetical scenario 50% of the Fe(II) has already been oxidized at a certain location in the catchment, then a 5-fold longer residence time results in 97% oxidized Fe at this location. Clearly, the observed seasonal differences in Fe oxidation gradients can be ascribed to effects of both the oxidation rate and of the hydraulic residence time.

Taken together, our results show that oxidation of groundwater-borne Fe(II) in a catchment creates a Fe concentration gradient which decreases from the headwaters to the major streams. The fate of high Fe(II) inputs in catchments is governed by water temperature, pH, and hydraulic residence time. These findings are in line with previous studies. Spiteri et al. [269] showed that a pH gradient in a subterranean estuary created a Fe concentration gradient through its effect on the Fe oxidation rate. Van der Grift et al. [242] showed that the Fe oxidation rate and residence time in drainage reservoirs exhibit seasonal variations similar to those observed in this study. However, to the best of our knowledge, this study is the first to document the oxidation gradient of naturally occurring Fe in river catchments at circumneutral pH. Some previous studies have addressed the fate of naturally occurring Fe(II)-rich water entering circumneutral streams, but they concluded that most of the Fe(II) is already oxidized and removed from solution before it enters the streams [242,270]. Our observation of continued oxidation of Fe(II) in the receiving streams of a catchment can be ascribed to the combination of two factors. First, in the studied catchments, high concentrations of Fe(II) enter the streams across a geographically large area. Second, stream pH and temperature are such that the half-life of chemical Fe(II) oxidation is in the same range as the hydraulic residence time of the water in the catchment.

Removal of P and As by freshly formed Fe minerals

The measured concentrations of dissolved (<0.45 µm) P and As in streams are, on average, an order of magnitude lower than those in the groundwater that feeds these

streams. If plotted against the hydraulic residence time of the water, the P and As concentrations do not exhibit the same trend as observed for Fe (Figure 6.4C and D). In addition, the P and As concentrations in streams exhibit only minor seasonal variations: their means across different sampling moments differed less than a factor of two. Whereas Fe is gradually oxidized and removed, the removal of P and As occurs much faster after exfiltration of reduced groundwater. The removal of P is complete before the water reaches the smallest headwater streams: the average P concentration in streams with residence times below 10 hours does not exceed the average of all streams. The average As concentration in streams with short residence times (2 μg L^{-1}) is somewhat larger than that in the other streams (1 μg L^{-1}), which may indicate that As removal is to a small extent still going on in the headwater streams. Nevertheless, the removal of P and As from groundwater occurs predominantly before the water reaches the headwater streams, most likely in the hyporheic zone, in small unmapped streams, or in drainage systems. The local environmental limits for freshwaters are 3 μg As L^{-1} (measured in filtered samples), and 140 μg P L^{-1} (measured in unfiltered samples). In this study, the average concentrations of P and As in groundwater exceed these limits by factors of 2.8 for P and 5.5 for As, but in streams, they are more a factor of 2 below these limits. In the absence of high Fe concentrations in groundwater, there may have been a risk for eutrophication or As toxicity in these catchments. Clearly, the observed removal of P and As by oxidizing Fe has implications for surface water quality.

The removal of As upon oxidation of Fe(II) has been widely studied in the context of drinking water production [271]. At the catchment scale, it has been shown that As concentrations in particles are related to the Fe concentrations [272], and that As removal in a catchment may occur through adsorption on suspended Fe oxyhydroxides [252]. A more recent study in a setting similar to this study confirmed that As in such systems may be sequestered by Fe [251]. Based on these previous studies, the observed As removal in this study is likely due to Fe-As interactions, and the As is bound to freshly formed Fe oxyhydroxides.

The fast immobilization of P in the presence of oxidizing Fe(II) has already been observed in synthetic systems [17,100,123,226], in aerated groundwater [273], and in natural waters [98,99,242,274]. It has also been observed in drainage ditches in the same study area [214]. Upon oxidation of Fe(II) in the presence of phosphate, ferric phosphate minerals are formed, with molar Fe:P as low as unity. After time, ferric phosphates may be converted

into Fe oxyhydroxides with surface-adsorbed P [123]. At low Fe:P ratios, this may result in release of P to the solution [100]. However, in the groundwater feeding the studied catchments, Fe is present in large excess: the molar Fe:P ratio in groundwater ranges between 8 and 218 (10^{th} and 90^{th} percentile), and the average molar Fe concentration in groundwater exceeds the average molar P concentration by a factor of 28. At such high Fe:P ratios, binding of P by Fe oxyhydroxides is highly efficient, and no release of P is expected [247].

The fate of "particulate" (>0.45 µm) P-containing Fe oxyhydroxides is governed by the hydrological regime: under low flow conditions, such particles are readily removed from the water column, whereas they may be mobilized and transported downstream during rainstorm events [198]. After settling to the bottom, the fate of such particles is most likely governed by the chemical boundary conditions in the receiving streams. The Kleine Nete and the Demer are ultimately only minor contributors to the suspended sediment load of the major receiving stream, the Scheldt (e.g. 4% for the Kleine Nete catchment) [275]. Due to the high molar Fe:P ratio in the authigenic material [133], it may be able to sequester additional P: it has been shown that ferric phosphates are a major sink for P in the freshwater portion of the Scheldt [113]. If the settled particles reach anoxic sediments, reductive dissolution may release the P. Perhaps this does not increase the eutrophication risk: P and Fe(II) are released simultaneously to the sediment pore water, and if such water reaches oxic environments again, the P may again be sequestered by the oxidizing Fe [114]. The fate of P-containing authigenic material may be of greater environmental concern if it reaches brackish water. The large concentrations of sulfate cause the presence of sulfide in bottom sediments, which promotes conversion of Fe from oxyhydroxides and phosphates to sulfides, causing a release of P [113]. However, the processes governing P binding and release in the bottom sediments of brackish water are poorly understood [58]. Release of P from Fe-containing phases in bottom sediments is likely governed by the availability of electron donors, such as organic matter, and electron acceptors, such as sulfate or Fe. Further research should focus on the fate of Fe–P minerals in receiving streams and estuaries, and on the risk of P-release from the bottom sediments of brackish waters.

General conclusions and future prospects

This work confirms that the fate and effect of P in natural waters is intimately linked to the biogeochemical cycle of Fe and NOM. The conclusions and implications of this work are discussed below, using the initial research objectives and hypotheses (see Chapter 1) as a framework. This work was set up:

To determine the structure, size, and composition of natural iron-rich particles in streams. *It was hypothesized that small Fe-bearing colloids prevail in soft water and at low Fe:NOM ratio, since these factors limit particle aggregation.*

Iron-rich particles in natural waters mostly occur as Fe oxyhydroxides associated with NOM, and possibly also with Al oxyhydroxides and clay minerals. These particles range in size between 1 nm and 100 µm. A conceptual model for Fe–NOM associations in natural waters is shown in Figure 7.1. In this study, few mononuclear complexes (type A in Figure 7.1) and simple hydrolyzed Fe polymers (type B) were identified. The smallest Fe(III) particles identified in this study mostly contain primary Fe oxyhydroxide particles (type C), as evidenced by the shift between the main NOM peak and the main Fe peak in the AF4 fractograms (Chapter 2). The larger particles consist of aggregates of such primary particles (type D). The lack of mononuclear Fe–NOM complexes identified in this study may be because only samples at relatively high pH (>6.3) were included. According to a previous study on Fe(III) binding by NOM, the Fe complexing capacity of NOM greatly increases at low pH (Figure 1.3) [18]. For example, in a moderately hard water (1 mM Ca) at pH 5 and 10 mg DOC L^{-1}, speciation modelling with WHAM7 predicts that the concentration of mononuclear Fe–NOM complexes is 93 µg Fe L^{-1}. This decreases to only 6 µg Fe L^{-1} at pH 7. Spectroscopic studies have confirmed that in more acidic waters, mononuclear Fe–NOM complexes may prevail [40].

The transition from types A to B and C (Figure 7.1) is determined by the Fe complexing capacity of the NOM and by Fe oxyhydroxide formation. In contrast, the transition from type C to D is governed by particle aggregation, which depends on the particle concentration, and the zeta potential of the particles, which is in turn affected by pH, by adsorbed molecules such as NOM and phosphate, and by the concentration of multivalent

cations (e.g. water hardness). Table 7.1 shows the properties of various particles isolated in this study and of the water they were recovered from. Smaller particles (type C) were found in soft waters, whereas larger aggregates (>40 nm, type D) were recovered from moderately hard to hard waters. A spectroscopic (EXAFS) study of streamwater colloids, (see ref. [276]; results not yet published) revealed a similar trend and showed additionally that in colloids from soft waters, hydrolysis of Fe (type B and C colloids in Figure 7.1) increased with increasing Fe:NOM ratio. Determining the factors governing particle aggregation (the transition from type C to type D) is somewhat speculative based on these limited samples. For example, the moderately hard to very hard waters also contain high total Fe concentration or have higher pH than the soft waters. These factors may also contribute to particle aggregation. A systematic and quantitative study is currently lacking on how the particle size of Fe–NOM associations depends on the Fe:NOM ratio, particle concentration, the type of NOM (NOM quality), phosphate concentration, water hardness, and pH. Nevertheless, water hardness is likely a key factor governing the aggregation of nanosized primary Fe oxyhydroxide particles to form larger aggregates.

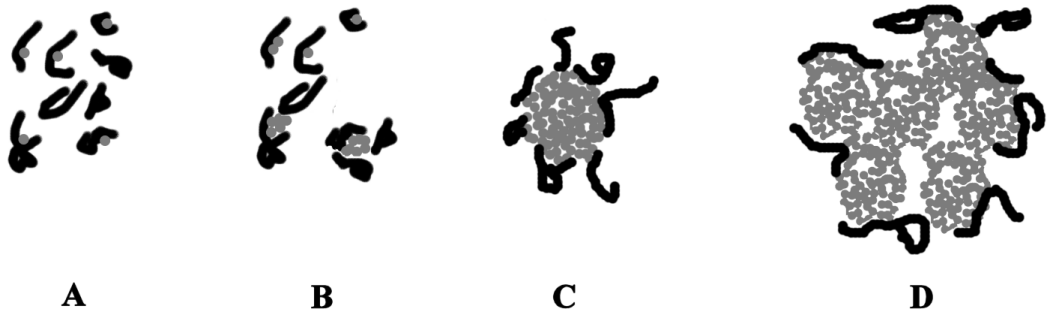

Figure 7.1: Conceptual model for interactions between iron (Fe, gray) and natural organic matter (NOM, black) in particles. The Fe concentration increases from left to right, whereas the NOM concentration remains constant. **A**: Initially, mononuclear Fe–NOM complexes are formed. **B**: As the complexation capacity of NOM is exceeded, small clusters of hydrolyzed and polymerized Fe are formed. **C**: Further increasing the Fe concentration causes crystallization of the hydrolyzed Fe, yielding nanosized primary Fe oxyhydroxide particles (e.g. ferrihydrite) which are protected from aggregation by surface-adsorbed NOM. **D**: Finally, at high Fe concentrations, the primary particles form larger aggregates. Multivalent cations may promote aggregation by reducing the zeta potential and acting as bridging cations between adjacent NOM moieties.

Table 7.1: Iron-rich particles identified in this study. Estimates of Fe–NOM complexes are made with the geochemical speciation model WHAM7.

		PARTICLE PROPERTIES				WATER PROPERTIES (<0.45 µm filtered fraction)						
sample	**chapter**	**size range**	**speciation**	**Fe**	**Fe:P**	**catchment**	**pH**	**hardness**	**Fe**	**Fe(II)**	**Fe:P**	**Fe:C**
		nm		***µM***				***mM***	***µM***	***µM***		
headwaters in groundwater-fed lowland	6	<3	free Fe^{2+} ions (57%); Fe(II)–NOM complexes (43%)	151		groundwater-fed lowland	6.4	1.1	173	151	139	0.278
Schwarzbach	2	1–40	Fe(III) oxyhydroxides (82%); mononuclear Fe(III)–NOM complexes (18%)	1.1	53	upland peat	6.3	0.1	5.5	2.3	57	0.009
Roer	2	1–40	Fe(III) oxyhydroxides (90%); mononuclear Fe(III)–NOM complexes (10%)	2.1	38	upland peat	6.8	0.2	4.9	1.8	26	0.011
Helle	2	1–40	Al and Fe(III) oxyhydroxides (93 and 83%); Al– and Fe–NOM complexes (7 and 17%)	0.34		upland peat	6.9	0.2	2.8	1.0	4	0.005
Maas	2	40–150	Fe oxyhydroxides associated with clay minerals	0.20	2.8	mountain range; sedimentary and metamorphic rock	7.9	1.2	0.72	0.40	0.4	0.002
Dijle	2	40–150 100–1200	unknown Fe oxyhydroxides?	0.05 1.44	0.6 2.4	calcareous loess plateau	7.9	3.1	0.77	0.17	0.2	0.002
Kleine Nete	2	40–150 100–1200	Fe oxyhydroxides Fe oxyhydroxides	3.8 18.3	13 13	groundwater-fed lowland	7.2	1.1	16.2	2.5	9.5	0.022
synthetic colloids	3	2–450	Fe oxyhydroxides (ferrihydrite)	83.6	66[A] 49[A] 30[B] 9[B]	synthetic colloids	7.5	0.01	84.3	7.3	47 24 29 9	0.202
synthetic colloids	3	2–450	Fe oxyhydroxides (ferrihydrite)	7.5	17[B] 13[B] 12[B]	synthetic colloids	7.5	0.01	8.6	2.1	9 7 6	0.021
authigenic particles	4	1000–18000	Fe oxyhydroxides (ferrihydrite)	387	19	oxidized groundwater-streamwater mixture	6.5	1.7	485	479	31	0.434
suspended particles in ground-water-fed lowland streams	4; 6	3000–86000	Fe oxyhydroxides (ferrihydrite)		19	groundwater-fed lowland	6.6	1.2	65	52	48	0.100

A: P binding by adsorption to post-synthesis ferrihydrite; B: P binding by coprecipitation in ferrihydrite during oxidation of Fe(II)

To determine phosphorus binding by natural iron-rich particles, and to relate this to particle properties (size, composition) and to the chemical and physical properties of the streams which carry them. *It was speculated that the Fe:NOM ratio and the Fe:P ratio in particles determine the binding of P. It was anticipated that the phosphate binding strength to Fe-rich particles increases with increasing Fe:NOM ratio, due to reduced competition between phosphate and NOM for sorption on a Fe oxyhydroxide phase. At high Fe:P ratio, P is likely strongly bound by Fe-rich particles. Conversely, at low Fe:P ratio, P binding by particles is ultimately limited to 1–2 mol Fe (mol P)$^{-1}$.*

Table 7.1 shows the various P-binding particles isolated in this study. The Fe:P ratio in these particles ranges widely between 0.6 and 60 mol Fe (mol P)$^{-1}$. The lowest Fe:P ratio observed is less than the lower Fe:P ratio in ferric phosphate ($FePO_4$) which is the theoretical minimum. The identity of these P-bearing particles remains unclear. In the rivers Maas and Dijle which have molar Fe:P ratio in filtered samples below unity, colloids were identified with a Fe:P ratio approaching 2 mol Fe (mol P)$^{-1}$, a value in line with P-saturated Fe-rich particles found in other studies [98,123]. Conversely, in other streams with higher Fe:P ratio in filtered samples, the particles also have higher Fe:P ratio. The Fe:P ratios in the filtered streamwater samples and in the particles are approximately equal, confirming that most of the P is bound by Fe-rich particles. It is concluded that the Fe and P concentrations in particles reflect the general composition of the water. “Low Fe–high P” waters contain P-saturated Fe-particles and have most of the P in true solution, whereas “high Fe–low P” waters contain Fe-particles which bind most of the P. This is shown visually in Figure 7.2.

The C content in the particles was not quantified in this study, and a comparison between different samples is not possible. However, in individual samples, AF4 measurements show that the Fe:NOM ratio in particles increases with increasing particle size, whereas the Fe:P ratio follows the opposite trend. This shows that competition between NOM and phosphate for binding on Fe oxyhydroxides may govern P-binding by particles. The trend of decreasing Fe:P ratio with increasing particle size is not observed in Table 7.1, because the Fe:P ratio also depends on the total P concentration in the water.

Apart from the Fe:C and Fe:P ratios, the P binding by particles additionally depends on the mechanism of particle formation. The P binding to synthetic ferrihydrite colloids is very strong if the P is present during Fe(II) oxidation, due to coprecipitation with Fe

oxyhydroxides. In contrast, P binding is less strong if it binds to existing Fe oxyhydroxides. These hysteresis effects suggest that oxidizing Fe(II) in natural waters is a potent sink for P, but that existing Fe(III) oxyhydroxides are comparably poorly able to mobilize P. This is currently being verified in additional experiments involving P binding by synthetic and natural colloids.

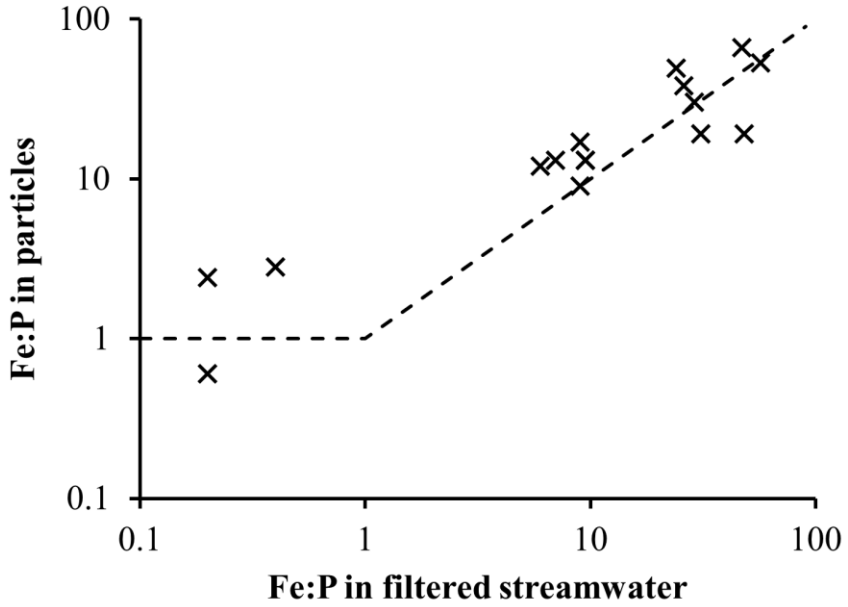

Figure 7.2: The Fe:P ratio (mol Fe (mol P)$^{-1}$) in particles and in filtered (<0.45 µm) stream water. In "low Fe, high P" waters, the particles are saturated with P, and their Fe:P ratio is low. The theoretical minimum Fe:P ratio for a ferric phosphate ($FePO_4$) is unity (horizontal dashed line). In "high Fe, low P" waters, most of the P is bound to Fe-rich particles, and therefore the Fe:P ratio in particles is close to that in filtered streamwater (dashed line with nonzero slope).

To determine how binding to iron-rich particles affects the fate and bioavailability of phosphorus in natural waters. *It was hypothesized that the Fe:NOM ratio and the Fe:P ratio in particles determine the fate of P.*

The binding of P by Fe-rich particles reduces its bioavailability: the particle bound P is not directly available to algal cells. Further experiments have revealed that after up to two weeks, part of the colloidal P may become available through desorption of colloidal P which is kinetically slow [277]. The mechanism of particle formation affects the bioavailability of P: the bioavailable P fraction is smaller if the P is present during

oxidation of Fe(II) than if it is added to existing ferrihydrite colloids. It is concluded that colloidal P in oxic natural waters is less available to biota than free ionic orthophosphate and poses a lower eutrophication risk.

In groundwater-fed catchments, the fate of P is mainly determined by the Fe:P ratio in the groundwater. As reduced Fe-rich groundwater surfaces, the oxidation of Fe in the water proceeds as the water flows through the catchment into increasingly larger streams. Authigenic ferrihydrite is produced which readily forms large aggregates (>0.45 µm). These aggregates are transported downstream as part of the suspended sediment. This study showed that, if Fe is present in large excess of P (average Fe:P ratio in groundwater: 28 mol Fe (mol P)$^{-1}$), the P in the groundwater is quickly bound by oxidizing Fe as the groundwater surfaces and reaches oxic zones, such as drainage ditches. The sequestration of P does not depend on the oxidation rate of Fe. In four studied catchments, this process reduces the P concentrations in streams by approximately one order of magnitude. Studying "high Fe, low P" catchments was useful to unravel these processes, but more work is needed in order to determine the fate of P in catchments with other Fe:P ratios. It is speculated that in catchments with less excess Fe, e.g. as in ref. [94], the situation may be more complex: P binding is expected to be slower, and may still proceed together with the oxidation of Fe in the streams. The P sequestration may under such circumstances depend on the rate of Fe(II) oxidation, which is a function of pH and temperature.

The fate of a P-containing particle is also a function of its size. Since colloids do not settle, they remain in suspension until they form larger aggregates. In contrast, large particles (>1 µm) in streams may settle to the bottom and be resuspended during rainstorms. If the settled particles reach anoxic sediments, reductive dissolution may release the P. Perhaps this does not increase the eutrophication risk: P and Fe(II) are released simultaneously to the sediment pore water, and if such water reaches oxic environments again, the P may again be sequestered by the oxidizing Fe [114]. The fate of P-containing authigenic material may be of greater environmental concern if it reaches brackish water. In estuaries, small particles commonly aggregate to larger sizes due to the increased salinity, which promotes settling of particles to the bottom sediments and which removes much of the Fe and the particle-bound P from the water column [109,110]. In estuaries, the large concentrations of sulfate commonly cause the presence of sulfide in bottom sediments, which promotes conversion of Fe from oxyhydroxides and phosphates

to sulfides, causing a release of P [113]. However, the processes governing P binding and release in the bottom sediments of brackish water are poorly understood [58]. Release of P from Fe-containing phases in bottom sediments is likely governed by the availability of electron donors, such as organic matter, and electron acceptors, such as sulfate or Fe(III). In summary, the fate of large (>1 µm) P-containing Fe oxyhydroxide particles is determined by the geochemical boundary conditions in the sediments where it settles.

Implications for environmental managers

The results of this work have implications for environmental managers. Legislators and agencies involved in water quality monitoring should be aware that a significant fraction of the phosphate in streams is bound to Fe-rich particles. Since this fraction is not directly available to algae, the eutrophication risk associated with it is likely less than that associated with dissolved (free) phosphate. In Flanders, for example, the concentrations of "total phosphorus" and "orthophosphate" are monitored in surface water, the latter of which should presumably reflect the directly bioavailable phosphate fraction. However, a major part of the particle-bound phosphate is included in the colorimetric assay for measurement of "orthophosphate". In addition, filtration procedures for this assay are poorly standardized in the ISO guidelines to determine "orthophosphate", leading to pronounced discrepancies between the results from different laboratories due to the presence of particle-bound phosphorus [278]. In order to better reflect the directly available phosphorus fraction, the filtration guidelines in the "orthophosphate" protocol should be more stringent, and a membrane with small pore size should be used.

Managers of agricultural land should be aware that phosphate does not behave as a conservative solute at the interface between groundwater and streams. This study showed an extreme example: in lowland catchments fed by iron-rich groundwater, the phosphate concentrations in the streams are tenfold below those in the groundwater that feeds the streams. As a consequence, lowland areas with iron-rich groundwater may be able to tolerate more phosphorus applications than comparable areas with iron-poor groundwater, before the P concentrations in the receiving streams reach a critical limit. Nutrient emission models, such as the Flemish ArcNEMO model [279], should ideally take this into account. For example, a continuous production of P-binding Fe oxyhydroxide sediment at the groundwater-surface water interface may be included. This requires data on the Fe

concentrations in groundwater, and a parameterization of P-binding by the Fe oxyhydroxide. In Flanders, Fe concentrations in phreatic groundwater bodies are monitored by the Flemish Environment Agency. The P-binding may be parameterized using a relationship between the initial molar Fe:P ratio of groundwater and the final "dissolved" (<0.45 µm) P concentration after complete oxidation of the Fe(II). However, presently such data are lacking, and oxidation experiments may need to be performed first in order to derive such a relationship.

Suggestions for further research

Our present understanding of P binding to Fe-rich particles is far from complete. We are able to characterize P–Fe–natural organic matter associations quite well. Some studies have modelled the competition between phosphate and humic substances or soil organic matter for binding on Fe oxyhydroxides [120–122]. However, such models appear presently unable to quantitatively predict P–Fe–NOM associations in aquatic systems due to 1) hysteresis effects, *i.e.* P binding to oxidizing Fe is more effective than post-synthesis binding of P to Fe oxyhydroxides, and 2) the complexity and diversity of aquatic natural organic matter. In order to move forward, further research may therefore put specific emphasis on the mechanism of formation of P–Fe–NOM associations (due to hysteresis effects) and on the organic matter quality. In addition, the size of such associations governs their fate since larger particles may settle, but predicting the size of Fe–NOM associations is presently difficult. A systematic and quantitative study is lacking on how the particle size of Fe–NOM associations depends on the Fe:NOM ratio, particle concentration, NOM quality, water hardness, phosphate concentration, and pH. Furthermore, data are presently lacking on the sequestration of P by Fe in catchments at different molar Fe:P ratios. This study shows how Fe affects the fate of P in catchments with a high Fe:P ratio. It may be expected that P sequestration is less efficient as the Fe:P ratio of the groundwater that feeds the streams decreases. However, it has not yet been quantitatively determined how P sequestration by oxidizing Fe is a function of the Fe:P ratio in groundwater across different catchments.

The interaction between P, Fe, and natural organic matter in oxic systems is now relatively well understood compared to other processes governing the effects of P in natural waters. Two major aspects along the pathway of P from its source (e.g.

fertilization of agricultural land, or discharge of sewage) to where it causes environmental effects (its uptake into an algal cell) remain notably unclear. First, the different sources of P in catchments and their relative contributions are poorly known. Decades of excessive fertilization and application of animal manure have caused the buildup of legacy P stocks in agricultural catchments at many locations along the land-water continuum, e.g. in soils, groundwater, riparian strips, wetlands, and bottom sediments [71]. These stocks continuously leak P to the receiving waters and mix there with more recent sources of P, such as sewage discharge. The contribution of different legacy P pools to the P loads of catchments, and how these pools respond to varying conditions and management scenarios, remain unclear [68]. In the absence of such knowledge, environmental managers struggle to find effective management strategies to limit riverine P loads. A feasible approach would be to perform catchment scale studies in a range of catchments with contrasting geomorphology and lithology. Long-term monitoring of P fluxes and stable isotopes may yield insight into how different P sources and pools contribute to P export from catchments under different environmental conditions and management scenarios.

Second, Fe-rich particles are a major vector of P in many aquatic systems, but their fate is poorly understood once they settle and reach the bottom sediments of streams or estuaries. Binding and release of P from sediments not only depends on Fe, but it is coupled to the cycle of other elements, such as S and C. In addition, mineralization of organic P may contribute to P release from sediments. Presently, we are unable to predict the fate of particle-bound P across a wide range of geochemical conditions in the receiving waters, and therefore, the interactions between P and other elements are often ignored when addressing the environmental risk associated with P. Therefore, more research is needed on how the fate of particle-bound P in sediments is a function of the chemistry of the receiving waters. A feasible approach would be to combine long-term incubation experiments, measurements of P speciation in sediments, and *in situ* measurements of the sediment pore water. If such studies are performed under a wide variety of freshwater and brackish water conditions, they may enable us to obtain a better general overview of the fate of Fe-rich particles in contrasting aquatic environments.

Cited references

(1) Van Dale. *Groot Woordenboek van de Nederlandse Taal*; 14th ed.; VBK Media, Utrecht, the Netherlands, 2014.

(2) Daubrée, G.-A. Observations sur le minerai de fer qui se forme journellement dans les marais et dans les lacs. *Bulletin de la Société Géologique de France* **1845**, *12 janvier*.

(3) *Chemistry of Europe's Agricultural Soils, Part A*; Reimann, C.; Birke, M.; Demetriades, A.; Filzmoser, P.; O'Connor, P., Eds.; Schweizerbart Science Publishers: Stuttgart, Germany, 2014.

(4) *Geochemical Atlas of Europe. Part 1: Background Information, Methodology and Maps*; Salminen, R., Ed.; Geological Survey of Finland: Espoo, Finland, 2005.

(5) Briat, J. F.; Curie, C.; Gaymard, F. Iron utilization and metabolism in plants. *Curr. Opin. Plant Biol.* **2007**, *10*, 276–282.

(6) Yunta, F.; Martín, I.; Lucena, J. J.; Gárate, A. Iron chelates supplied foliarly improve the iron translocation rate in Tempranillo grapevine. *Commun. Soil Sci. Plant Anal.* **2013**, *44*, 794–804.

(7) Lucena, J. J. Effects of bicarbonate, nitrate and other environmental factors on iron deficiency chlorosis. A review. *J. Plant Nutr.* **2000**, *23*, 1591–1606.

(8) Stein, R. J.; Lopes, S. I. G.; Fett, J. P. Iron toxicity in field-cultivated rice: Contrasting tolerance mechanisms in distinct cultivars. *Theor. Exp. Plant Physiol.* **2014**, *26*, 135–146.

(9) Sunda, W. G.; Huntsman, S. A. Iron uptake and growth limitation in oceanic and coastal phytoplankton. *Mar. Chem.* **1995**, *50*, 189–206.

(10) Tollefson, J. Ocean-fertilization project off Canada sparks furore. *Nature* **2012**, *490*, 458–459.

(11) Buesseler, K. O.; Doney, S. C.; Karl, D. M.; Boyd, P. W.; Caldeira, K.; Chai, F.; Coale, K. H.; de Baar, H. J. W.; Falkowski, P. G.; Johnson, K. S.; et al. Ocean iron fertilization - Moving forward in a sea of uncertainty. *Science* **2008**, *319*, 162.

(12) Wilhelm, S. W. Ecology of iron-limited cyanobacteria: A review of physiological responses and implications for aquatic systems. *Aquat. Microb. Ecol.* **1995**, *9*, 295–303.

(13) Schindler, D. W. The dilemma of controlling cultural eutrophication of lakes. *Proc. Biol. Sci.* **2012**, *279*, 4322–4333.

(14) Van Laer, L.; Degryse, F.; Leynen, K.; Smolders, E. Mobilization of Zn upon waterlogging riparian Spodosols is related to reductive dissolution of Fe minerals. *Eur. J. Soil Sci.* **2010**, *61*, 1014–1024.

(15) Gaffney, J. W.; White, K. N.; Boult, S. Oxidation state and size of Fe controlled by organic matter in natural waters. *Environ. Sci. Technol.* **2008**, *42*, 3575–3581.

(16) Kirk, G. *The Biogeochemistry of Submerged Soils*; Wiley, Chichester, 2004.

(17) Voegelin, A.; Kaegi, R.; Frommer, J.; Vantelon, D.; Hug, S. J. Effect of phosphate, silicate, and Ca on Fe(III)-precipitates formed in aerated Fe(II)- and As(III)-containing water studied by X-ray absorption spectroscopy. *Geochim. Cosmochim. Acta* **2010**, *74*, 164–186.

(18) Lofts, S.; Tipping, E.; Hamilton-Taylor, J. The chemical speciation of Fe(III) in freshwaters. *Aquat. Geochem.* **2008**, *14*, 337–358.

(19) Michel, F. M.; Ehm, L.; Antao, S. M.; Lee, P. L.; Chupas, P. J.; Liu, G.; Strongin, D. R.; Schoonen, M. A. A.; Phillips, B. L.; Parise, J. B. The structure of ferrihydrite, a nanocrystalline material. *Science* **2007**, *316*, 1726–1729.

(20) *Lecture Notes on the Major Soils of the World*; Driessen, P.; Deckers, J.; Spaargaren, O.; Nachtergaele, F., Eds.; Food and Agricultural Organization (FAO) of the United Nations, Rome, Italy, 2001.

(21) Stumm, W.; Sulzberger, B. The cycling of iron in natural environments: Considerations based on laboratory studies of heterogeneous redox processes. *Geochim. Cosmochim. Acta* **1992**, *56*, 3233–3257.

(22) Bonneville, S.; Van Cappellen, P.; Behrends, T. Microbial reduction of iron(III) oxyhydroxides: Effects of mineral solubility and availability. *Chem. Geol.* **2004**, *212*, 255–268.

(23) Singer, P. C.; Stumm, W. Acidic mine drainage: The rate-determining step. *Science* **1970**, *167*, 1121–1123.

(24) Vollrath, S.; Behrends, T.; Bender Koch, C.; Van Cappellen, P. Effects of temperature on rates and mineral products of microbial Fe(II) oxidation by Leptothrix cholodnii at microaerobic conditions. *Geochim. Cosmochim. Acta* **2013**, *108*, 107–124.

(25) Kasama, T.; Murakami, T. The effect of microorganisms on Fe precipitation rates at neutral pH. *Chem. Geol.* **2001**, *180*, 117–128.

(26) Davison, W. Iron and manganese in lakes. *Earth-Science Rev.* **1993**, *34*, 119–163.

(27) Blöthe, M.; Roden, E. E. Microbial iron redox cycling in a circumneutral-pH groundwater seep. *Appl. Environ. Microbiol.* **2009**, *75*, 468–473.

(28) Gault, A. G.; Ibrahim, A.; Langley, S.; Renaud, R.; Takahashi, Y.; Boothman, C.; Lloyd, J. R.; Clark, I. D.; Ferris, F. G.; Fortin, D. Microbial and geochemical features suggest iron redox cycling within bacteriogenic iron oxide-rich sediments. *Chem. Geol.* **2011**, *281*, 41–51.

(29) Scott, D. T.; Runkel, R. L.; McKnight, D. M.; Voelker, B. M.; Kimball, B. A.; Carraway, E. R. Transport and cycling of iron and hydrogen peroxide in a freshwater stream: Influence of organic acids. *Water Resour. Res.* **2003**, *39*, 1–14.

(30) Deiana, S.; Gessa, C.; Manunza, B.; Rausa, R.; Solinas, V. Iron(III) reduction by natural humic acids: A potentiometric and spectroscopic study. *Eur. J. Soil Sci.* **1995**, *46*, 103–108.

(31) Karlsson, T.; Persson, P. Complexes with aquatic organic matter suppress hydrolysis and precipitation of Fe(III). *Chem. Geol.* **2012**, *322-323*, 19–27.

(32) Carter, H. T.; Tipping, E.; Koprivnjak, J.-F.; Miller, M. P.; Cookson, B.; Hamilton-Taylor, J. Freshwater DOM quantity and quality from a two-component model of UV absorbance. *Water Res.* **2012**, *46*, 4532–4542.

(33) Tipping, E.; Corbishley, H. T.; Koprivnjak, J.-F.; Lapworth, D. J.; Miller, M. P.; Vincent, C. D.; Hamilton-Taylor, J. Quantification of natural DOM from UV absorption at two wavelengths. *Environ. Chem.* **2009**, *6*, 472.

(34) Tipping, E.; Rey-Castro, C.; Bryan, S. E.; Hamilton-Taylor, J. Al(III) and Fe(III) binding by humic substances in freshwaters, and implications for trace metal speciation. *Geochim. Cosmochim. Acta* **2002**, *66*, 3211–3224.

(35) Tipping, E. The adsorption of aquatic humic substances by iron oxides. *Geochim. Cosmochim. Acta* **1981**, *45*, 191–199.

(36) Gustafsson, J. P.; Persson, I.; Kleja, D. B.; Van Schaik, J. W. J. Binding of iron(III) to organic soils: EXAFS spectroscopy and chemical equilibrium modeling. *Environ. Sci. Technol.* **2007**, *41*, 1232–1237.

(37) Karlsson, T.; Persson, P. Coordination chemistry and hydrolysis of Fe(III) in a peat humic acid studied by X-ray absorption spectroscopy. *Geochim. Cosmochim. Acta* **2010**, *74*, 30–40.

(38) Pédrot, M.; Le Boudec, A.; Davranche, M.; Dia, A.; Henin, O. How does organic matter constrain the nature, size and availability of Fe nanoparticles for biological reduction? *J. Colloid Interface Sci.* **2011**, *359*, 75–85.

(39) Perret, D.; Gaillard, J.-F.; Dominik, J.; Atteia, O. The diversity of natural hydrous iron oxides. *Environ. Sci. Technol.* **2000**, *34*, 3540–3546.

(40) Sjöstedt, C.; Persson, I.; Hesterberg, D.; Kleja, D. B.; Borg, H.; Gustafsson, J. P. Iron speciation in soft-water lakes and soils as determined by EXAFS spectroscopy and geochemical modelling. *Geochim. Cosmochim. Acta* **2013**, *105*, 172–186.

(41) Fortin, D.; Leppard, G.; Tessier, A. Characteristics of lacustrine diagenetic iron oxyhydroxides. *Geochim. Cosmochim. Acta* **1993**, *57*, 4391–4404.

(42) Belzile, N.; De Vitre, R. R.; Tessier, A. In situ collection of diagenetic iron and manganese oxyhydroxides from natural sediments. *Nature* **1989**, *340*, 376–377.

(43) Tipping, E.; Thompson, D. W.; Woof, C. Iron oxide particulates formed by the oxygenation of natural and model lakewaters containing Fe(II). *Arch. für Hydrobiol.* **1989**, *115*, 59–70.

(44) Vanlierde, E.; De Schutter, J.; Jacobs, P.; Mostaert, F. Estimating and modeling the annual contribution of authigenic sediment to the total suspended sediment load in the Kleine Nete basin, Belgium. *Sediment. Geol.* **2007**, *202*, 317–332.

(45) Walpersdorf, E.; Bender Koch, C.; Heiberg, L.; O'Connell, D. W.; Kjaergaard, C.; Bruun Hansen, H. C. Does vivianite control phosphate solubility in anoxic meadow soils? *Geoderma* **2013**, *193-194*, 189–199.

(46) Heiberg, L.; Bender Koch, C.; Kjaergaard, C.; Jensen, H. S.; Hansen, H. C. B. Vivianite precipitation and phosphate sorption following iron reduction in anoxic soils. *J. Environ. Qual.* **2012**, *41*, 938–949.

(47) Fuss, C. B.; Driscoll, C. T.; Johnson, C. E.; Petras, R. J.; Fahey, T. J. Dynamics of oxidized and reduced iron in a northern hardwood forest. *Biogeochemistry* **2010**, *104*, 103–119.

(48) Neubauer, E.; von der Kammer, F.; Knorr, K.-H.; Peiffer, S.; Reichert, M.; Hofmann, T. Colloid-associated export of arsenic in stream water during stormflow events. *Chem. Geol.* **2013**, *352*, 81–91.

(49) Sarkkola, S.; Nieminen, M.; Koivusalo, H.; Laurén, A.; Kortelainen, P.; Mattsson, T.; Palviainen, M.; Piirainen, S.; Starr, M.; Finér, L. Iron concentrations are increasing in surface waters from forested headwater catchments in eastern Finland. *Sci. Total Environ.* **2013**, *463-464*, 683–689.

(50) Neal, C.; Lofts, S.; Evans, C. D.; Reynolds, B.; Tipping, E.; Neal, M. Increasing iron concentrations in UK upland waters. *Aquat. Geochem.* **2008**, *14*, 263–288.

(51) Dzombak, D. A.; Morel, F. M. M. *Surface Complexation Modeling: Hydrous Ferric Oxide*; Wiley-Interscience, New York, 1990.

(52) Baalousha, M.; von der Kammer, F.; Motelica-Heino, M.; Baborowski, M.; Hofmeister, C.; Le Coustumer, P. Size-based speciation of natural colloidal particles by flow field flow fractionation, inductively coupled plasma-mass spectroscopy, and transmission electron microscopy/X-ray energy dispersive spectroscopy: Colloids-trace element interaction. *Environ. Sci. Technol.* **2006**, *40*, 2156–2162.

(53) Stolpe, B.; Hassellöv, M.; Andersson, K.; Turner, D. R. High resolution ICPMS as an on-line detector for flow field-flow fractionation; multi-element determination of colloidal size distributions in a natural water sample. *Anal. Chim. Acta* **2005**, *535*, 109–121.

(54) Lyvén, B.; Hassellöv, M.; Turner, D. R.; Haraldsson, C.; Andersson, K. Competition between iron- and carbon-based colloidal carriers for trace metals in a freshwater assessed using flow field-flow fractionation coupled to ICPMS. *Geochim. Cosmochim. Acta* **2003**, *67*, 3791–3802.

(55) Stolpe, B.; Guo, L.; Shiller, A. M.; Aiken, G. R. Abundance, size distributions and trace-element binding of organic and iron-rich nanocolloids in Alaskan rivers, as revealed by field-flow fractionation and ICP-MS. *Geochim. Cosmochim. Acta* **2013**, *105*, 221–239.

(56) Vega, F. A.; Weng, L. Speciation of heavy metals in River Rhine. *Water Res.* **2013**, *47*, 363–372.

(57) Cánovas, C. R.; Olías, M.; Sarmiento, A. M.; Nieto, J. M.; Galván, L. Pollutant transport processes in the Odiel River (SW Spain) during rain events. *Water Resour. Res.* **2012**, *48*, W06508.

(58) Ekholm, P.; Lehtoranta, J. Does control of soil erosion inhibit aquatic eutrophication? *J. Environ. Manage.* **2012**, *93*, 140–146.

(59) Wang, X.; Liu, F.; Tan, W.; Li, W.; Feng, X.; Sparks, D. L. Characteristics of phosphate adsorption-desorption onto ferrihydrite: Comparison with well crystalline Fe (hydr)oxides. *Soil Sci.* **2013**, *178*, 1–11.

(60) Alcacio, T. E.; Hesterberg, D.; Chou, J. W.; Martin, J. D.; Beauchemin, S.; Sayers, D. E. Molecular scale characteristics of Cu(II) bonding in goethite-humate complexes. *Geochim. Cosmochim. Acta* **2001**, *65*, 1355–1366.

(61) Hiemstra, T. Surface and mineral structure of ferrihydrite. *Geochim. Cosmochim. Acta* **2013**, *105*, 316–325.

(62) Cordell, D.; Drangert, J.; White, S. The story of phosphorus: Global food security and food for thought. *Glob. Environ. Chang.* **2009**, *19*, 292–305.

(63) European Commission. *Summary of the responses to the Consultative Communication on the sustainable use of phosphorus [COM(2013) 517]*; Brussels, 2014.

(64) Flemish Environment Agency VMM. *MIRA Indicator Report*; 2012.

(65) Hansen, N.; Daniel, T.; Sharpley, A.; Lemunyon, J. The fate and transport of phosphorus in agricultural systems. *J. Soil Water Conserv.* **2002**, *57*, 408–417.

(66) Sharpley, A. N.; McDowell, R. W.; Kleinman, P. J. A. Phosphorus loss from land to water: Integrating agricultural and environmental management. *Plant Soil* **2001**, *237*, 287–307.

(67) Schoumans, O. F.; Groenendijk, P. Modeling soil phosphorus levels and phosphorus leaching from agricultural land in the Netherlands. *J. Environ. Qual.* **2000**, *29*, 111–116.

(68) Haygarth, P. M.; Jarvie, H. P.; Powers, S. M.; Sharpley, A. N.; Elser, J. J.; Shen, J.; Peterson, H. M.; Chan, N.; Howden, N. J. K.; Burt, T.; et al. Sustainable phosphorus management and the need for a long-term perspective: The legacy hypothesis. *Environ. Sci. Technol.* **2014**, *48*, 8417–8419.

(69) Withers, P.; Neal, C.; Jarvie, H.; Doody, D. Agriculture and eutrophication: Where do we go from here? *Sustainability* **2014**, *6*, 5853–5875.

(70) Jarvie, H. P.; Sharpley, A. N.; Spears, B.; Buda, A. R.; May, L.; Kleinman, P. J. A. Water quality remediation faces unprecedented challenges from "legacy phosphorus." *Environ. Sci. Technol.* **2013**, *47*, 8997–8998.

(71) Sharpley, A.; Jarvie, H. P.; Buda, A.; May, L.; Spears, B.; Kleinman, P. Phosphorus legacy: Overcoming the effects of past management practices to mitigate future water quality impairment. *J. Environ. Qual.* **2013**, *42*, 1308–1326.

(72) Sattari, S. Z.; Bouwman, A. F.; Giller, K. E.; van Ittersum, M. K. Residual soil phosphorus as the missing piece in the global phosphorus crisis puzzle. *Proc. Natl. Acad. Sci.* **2012**, *109*, 6348–6353.

(73) Turner, B. L.; Frossard, E.; Baldwin, D. S. *Organic Phosphorus in the Environment*; CABI Publishing, Wallingford, U.K., 2005.

(74) Ekholm, P. Bioavailability of phosphorus in agriculturally loaded rivers in southern Finland. *Hydrobiologia* **1994**, *287*, 179–194.

(75) Van Moorleghem, C.; Six, L.; Degryse, F.; Smolders, E.; Merckx, R. Effect of organic P forms and P present in inorganic colloids on the determination of dissolved P in environmental samples by the diffusive gradient in thin films technique, ion chromatography, and colorimetry. *Anal. Chem.* **2011**, *83*, 5317–5323.

(76) Mayer, T. D.; Jarrell, W. M. Assessing colloidal forms of phosphorus and iron in the Tualatin River Basin. *J. Environ. Qual.* **1995**, *24*, 1117–1124.

(77) Henderson, R.; Kabengi, N.; Mantripragada, N.; Cabrera, M.; Hassan, S.; Thompson, A. Anoxia-induced release of colloid- and nanoparticle-bound phosphorus in grassland soils. *Environ. Sci. Technol.* **2012**, *46*, 11727–11734.

(78) Regelink, I. C.; Koopmans, G. F.; van der Salm, C.; Weng, L.; van Riemsdijk, W. H. Characterization of colloidal phosphorus species in drainage waters from a clay soil using asymmetric flow field-flow fractionation. *J. Environ. Qual.* **2012**, *42*, 464–473.

(79) Hens, M.; Merckx, R. Functional characterization of colloidal phosphorus species in the soil solution of sandy soils. *Environ. Sci. Technol.* **2001**, *35*, 493–500.

(80) Liu, J.; Yang, J.; Liang, X.; Zhao, Y.; Cade-Menun, B. J.; Hu, Y. Molecular speciation of phosphorus present in readily dispersible colloids from agricultural soils. *Soil Sci. Soc. Am. J.* **2014**, *78*, 47–53.

(81) Cembella, A. D.; Antia, N. J.; Harrison, P. J. The utilization of inorganic and organic phosphorus compounds as nutrients by eukaryotic microalgae: A multidisciplinary perspective. Part 1. *Crit. Rev. Microbiol.* **1984**, *10*, 317–391.

(82) Uusitalo, R.; Turtola, E.; Puustinen, M.; Paasonen-Kivekäs, M.; Uusi-Kämppä, J. Contribution of particulate phosphorus to runoff phosphorus bioavailability. *J. Environ. Qual.* **2003**, *32*, 2007–2016.

(83) Uusitalo, R.; Yli-Halla, M.; Turtola, E. Suspended soil as a source of potentially bioavailable phosphorus in surface runoff waters from clay soils. *Water Res.* **2000**, *34*, 2477–2482.

(84) Sinaj, S.; Mächler, F.; Frossard, E.; Faïsse, C.; Oberson, A.; Morel, C. Interference of colloidal particles in the determination of orthophosphate concentrations in soil water extracts. *Commun. Soil Sci. Plant Anal.* **1998**, *29*, 1091–1105.

(85) Regelink, I. C.; Voegelin, A.; Weng, L.; Koopmans, G. F.; Comans, R. N. J. Characterization of colloidal Fe from soils using field-flow fractionation and Fe K-edge X-ray absorption spectroscopy. *Environ. Sci. Technol.* **2014**, *48*, 4307–4316.

(86) Wang, X.; Li, W.; Harrington, R.; Liu, F.; Parise, J. B.; Feng, X.; Sparks, D. L. Effect of ferrihydrite crystallite size on phosphate adsorption reactivity. *Environ. Sci. Technol.* **2013**, *47*, 10322–10331.

(87) Van der Eijk, D.; Janssen, B. H.; Oenema, O. Initial and residual effects of fertilizer phosphorus on soil phosphorus and maize yields on phosphorus fixing soils. A case study in south-west Kenya. *Agric. Ecosyst. Environ.* **2006**, *116*, 104–120.

(88) Torrent, J.; Schwertmann, U.; Barrón, V. Fast and slow phosphate sorption by goethite-rich natural materials. *Clays Clay Miner.* **1992**, *40*, 14–21.

(89) Lehtoranta, J.; Ekholm, P.; Wahlström, S.; Tallberg, P.; Uusitalo, R. Labile organic carbon regulates phosphorus release from eroded soil transported into anaerobic coastal systems. *Ambio* **2015**, *44*, 263–273.

(90) Van der Zee, S. E. A. T. M.; van Riemsdijk, W. H.; De Haan, F. A. M. *Het protokol fosfaatverzadigde gronden*; Vakgroep Bodemkunde en Plantenvoeding, Agricultural University, Wageningen, the Netherlands, 1990.

(91) Schoumans, O. F.; Chardon, W. J. Phosphate saturation degree and accumulation of phosphate in various soil types in the Netherlands. *Geoderma* **2015**, *237-238*, 325–335.

(92) Hens, M.; Merckx, R. The role of colloidal particles in the speciation and analysis of "dissolved" phosphorus. *Water Res.* **2002**, *36*, 1483–1492.

(93) Ilg, K.; Dominik, P.; Kaupenjohann, M.; Siemens, J. Phosphorus-induced mobilization of colloids: Model systems and soils. *Eur. J. Soil Sci.* **2008**, *59*, 233–246.

(94) Groenenberg, J. E.; Chardon, W. J.; Koopmans, G. F. Reducing phosphorus loading of surface water using iron-coated sand. *J. Environ. Qual.* **2013**, *42*, 250–259.

(95) Stolpe, B.; Guo, L.; Shiller, A. M.; Hassellöv, M. Size and composition of colloidal organic matter and trace elements in the Mississippi River, Pearl River and the northern Gulf of Mexico, as characterized by flow field-flow fractionation. *Mar. Chem.* **2010**, *118*, 119–128.

(96) Gottselig, N.; Bol, R.; Nischwitz, V.; Vereecken, H.; Amelung, W.; Klumpp, E. Distribution of phosphorus-containing fine colloids and nanoparticles in stream water of a forest catchment. *Vadose Zone J.* **2014**, *13*.

(97) Shaw, P. J.; Jones, R. I.; De Haan, H. The influence of humic substances on the molecular weight distributions of phosphate and iron in epilimnetic lake waters. *Freshw. Biol.* **2000**, *45*, 383–393.

(98) Lienemann, C.-P.; Monnerat, M.; Dominik, J.; Perret, D. Identification of stoichiometric iron-phosphorus colloids produced in a eutrophic lake. *Aquat. Sci.* **1999**, *61*, 133.

(99) Gunnars, A.; Blomqvist, S.; Johansson, P.; Andersson, C. Formation of Fe(III) oxyhydroxide colloids in freshwater and brackish seawater, with incorporation of phosphate and calcium. *Geochim. Cosmochim. Acta* **2002**, *66*, 745–758.

(100) Mayer, T. D.; Jarrell, W. M. Phosphorus sorption during iron(II) oxidation in the presence of dissolved silica. *Water Res.* **2000**, *34*, 3949–3956.

(101) Châtellier, X.; West, M. M.; Rose, J.; Fortin, D.; Leppard, G. G.; Ferris, F. G. Characterization of iron oxides formed by oxidation of ferrous ions in the presence of various bacterial species and inorganic ligands. *Geomicrobiol. J.* **2004**, *21*, 99–112.

(102) Châtellier, X.; Grybos, M.; Abdelmoula, M.; Kemner, K. M.; Leppard, G. G.; Mustin, C.; West, M. M.; Paktunc, D. Immobilization of P by oxidation of Fe(II) ions leading to nanoparticle formation and aggregation. *Appl. Geochem.* **2013**, *35*, 325–339.

(103) Buffle, J.; Leppard, G. G. Characterization of aquatic colloids and macromolecules. 1. Structure and behavior of colloidal material. *Environ. Sci. Technol.* **1995**, *29*, 2169–2175.

(104) Haygarth, P. M.; Warwick, M. S.; House, W. A. Size distribution of colloidal molybdate reactive phosphorus in river waters and soil solution. *Water Res.* **1997**, *31*, 439–448.

(105) Filella, M.; Deville, C.; Chanudet, V.; Vignati, D. Variability of the colloidal molybdate reactive phosphorous concentrations in freshwaters. *Water Res.* **2006**, *40*, 3185–3192.

(106) Jarvie, H. P.; Neal, C.; Rowland, A. P.; Neal, M.; Morris, P. N.; Lead, J. R.; Lawlor, A. J.; Woods, C.; Vincent, C.; Guyatt, H.; et al. Role of riverine colloids in macronutrient and metal partitioning and transport, along an upland-lowland land-use continuum, under low-flow conditions. *Sci. Total Environ.* **2012**, *434*, 171–185.

(107) Honeyman, B. D.; Santschi, P. H. A Brownian-pumping model for oceanic trace metal scavenging: Evidence from Th isotopes. *J. Mar. Res.* **1989**, *47*, 951–992.

(108) Honeyman, B. D.; Santschi, P. H. Coupling adsorption and particle aggregation: laboratory studies of “colloidal pumping” using iron-59-labeled hematite. *Environ. Sci. Technol.* **1991**, *25*, 1739–1747.

(109) Boyle, E. A.; Edmond, J. M.; Sholkovitz, E. R. The mechanism of iron removal in estuaries. *Geochim. Cosmochim. Acta* **1977**, *41*, 1313–1324.

(110) Hartzell, J. L.; Jordan, T. E.; Cornwell, J. C. Phosphorus burial in sediments along the salinity gradient of the Patuxent River, a subestuary of the Chesapeake Bay (USA). *Estuaries and Coasts* **2010**, *33*, 92–106.

(111) Machesky, M. L.; Holm, T. R.; Slowikowski, J. A. Phosphorus speciation in stream bed sediments from an agricultural watershed: Solid-phase associations and sorption behavior. *Aquat. Geochem.* **2010**, *16*, 639–662.

(112) Maynard, J. J.; O’Geen, A. T.; Dahlgren, R. A. Sulfide induced mobilization of wetland phosphorus depends strongly on redox and iron geochemistry. *Soil Sci. Soc. Am. J.* **2011**, *75*, 1986.

(113) Hyacinthe, C.; Van Cappellen, P. An authigenic iron phosphate phase in estuarine sediments: Composition, formation and chemical reactivity. *Mar. Chem.* **2004**, *91*, 227–251.

(114) Zak, D.; Wagner, C.; Payer, B.; Augustin, J.; Gelbrecht, J. Phosphorus mobilization in rewetted fens: The effect of altered peat properties and implications for their restoration. *Ecol. Appl.* **2010**, *20*, 1336–1349.

(115) Kleeberg, A.; Herzog, C.; Hupfer, M. Redox sensitivity of iron in phosphorus binding does not impede lake restoration. *Water Res.* **2013**, *47*, 1491–1502.

(116) Liu, Y.-T. Phosphate sorption and reductive dissolution in aluminum/iron-hydroxide coprecipitates, PhD thesis, North Carolina State University, U.S., 2010.

(117) Hupfer, M.; Lewandowski, J. Oxygen Controls the Phosphorus Release from Lake Sediments - a Long-Lasting Paradigm in Limnology. *Int. Rev. Hydrobiol.* **2008**, *93*, 415–432.

(118) Amery, F.; Smolders, E. Unlocking fixed soil phosphorus upon waterlogging can be promoted by increasing soil cation exchange capacity. *Eur. J. Soil Sci.* **2012**, *63*, 831–838.

(119) Sundman, A.; Karlsson, T.; Laudon, H.; Persson, P. XAS study of iron speciation in soils and waters from a boreal catchment. *Chem. Geol.* **2014**, *364*, 93–102.

(120) Antelo, J.; Arce, F.; Avena, M.; Fiol, S.; López, R.; Macías, F. Adsorption of a soil humic acid at the surface of goethite and its competitive interaction with phosphate. *Geoderma* **2007**, *138*, 12–19.

(121) Regelink, I. C. Natural nanoparticles in soils and their role in organic-mineral interactions and colloid-facilitated transport, PhD thesis, Wageningen University, the Netherlands, 2014.

(122) Weng, L.; van Riemsdijk, W. H.; Hiemstra, T. Humic nanoparticles at the oxide-water interface: Interactions with phosphate ion adsorption. *Environ. Sci. Technol.* **2008**, *42*, 8747–8752.

(123) Voegelin, A.; Senn, A.-C.; Kaegi, R.; Hug, S. J.; Mangold, S. Dynamic Fe-precipitate formation induced by Fe(II) oxidation in aerated phosphate-containing water. *Geochim. Cosmochim. Acta* **2013**, *117*, 216–231.

(124) Beckett, R.; Jue, Z.; Giddings, J. C. Determination of molecular weight distributions of fulvic and humic acids using flow field-flow fractionation. *Environ. Sci. Technol.* **1987**, *21*, 289–295.

(125) Manku, G. S. *Theoretical Principles of Inorganic Chemistry*; McGraw-Hill, New Delhi, India, 1980.

(126) Stumm, W.; Morgan, J. J. *Aquatic Chemistry: Chemical Equilibria and Rates in Natural Waters*; 3rd ed.; John Wiley & Sons, New York, U.S., 1996.

(127) Jones, R. I.; Shaw, P. J.; De Haan, H. Effects of dissolved humic substances on the speciation of iron and phosphate at different pH and ionic strength. *Environ. Sci. Technol.* **1993**, *27*, 1052–1059.

(128) Liu, J.; Liang, X.; Yang, J.; Ye, Y.; Su, M.; Nie, Z.; Chen, Y. Size distribution and composition of phosphorus in the East Tiao River, China: The significant role of colloids. *J. Environ. Monit.* **2011**, *13*, 2844–2850.

(129) Buffle, J.; Leppard, G. G. Characterization of aquatic colloids and macromolecules. 2. Key role of physical structures on analytical results. *Environ. Sci. Technol.* **1995**, *29*, 2176–2184.

(130) Hassellöv, M.; Lyvén, B.; Haraldsson, C.; Sirinawin, W. Determination of continuous size and trace element distribution of colloidal material in natural water by on-line coupling of flow field-flow fractionation with ICPMS. *Anal. Chem.* **1999**, *71*, 3497–3502.

(131) Andersson, K.; Dahlqvist, R.; Turner, D.; Stolpe, B.; Larsson, T.; Ingri, J.; Andersson, P. Colloidal rare earth elements in a boreal river: Changing sources and distributions during the spring flood. *Geochim. Cosmochim. Acta* **2006**, *70*, 3261–3274.

(132) Wastiaux, C.; Hallneux, L.; Schumacker, R.; Streel, M.; Jacqmotte, J.-M. Development of the Hautes-Fagnes peat bogs (Belgium): New perspectives using ground-penetrating radar. *Suo* **2000**, *51*, 115–120.

(133) Baken, S.; Sjöstedt, C.; Gustafsson, J. P.; Seuntjens, P.; Desmet, N.; De Schutter, J.; Smolders, E. Characterisation of hydrous ferric oxides derived from iron-rich groundwaters and their contribution to the suspended sediment of streams. *Appl. Geochem.* **2013**, *39*, 59–68.

(134) De Mars, H.; Ransijn, M.; Verbraak, P.; Schuttelaar, M.; Vercoutere, B.; Buskens, R. *Internationale ecologische verkenning Maas - Oriëntatie en projectaanpak (fase 1)*; Report, Rijkswaterstaat directie Limburg, Maastricht, the Netherlands, 2000.

(135) Notebaert, B.; Verstraeten, G.; Rommens, T.; Vanmontfort, B.; Govers, G.; Poesen, J. Establishing a Holocene sediment budget for the river Dijle. *Catena* **2009**, *77*, 150–163.

(136) Viollier, E.; Inglett, P. W.; Hunter, K.; Roychoudhury, A. N.; Van Cappellen, P. The ferrozine method revisited: Fe(II)/Fe(III) determination in natural waters. *Appl. Geochem.* **2000**, *15*, 785–790.

(137) Poulin, B. A.; Ryan, J. N.; Aiken, G. R. Effects of iron on optical properties of dissolved organic matter. *Environ. Sci. Technol.* **2014**, *48*, 10098–10106.

(138) Weishaar, J. L.; Aiken, G. R.; Bergamaschi, B. A.; Fram, M. S.; Fujii, R.; Mopper, K. Evaluation of specific ultraviolet absorbance as an indicator of the chemical composition and reactivity of dissolved organic carbon. *Environ. Sci. Technol.* **2003**, *37*, 4702–4708.

(139) Von der Kammer, F. Characterization of environmental colloids applying field-flow fractionation – multi detection analysis with emphasis on light scattering techniques, 2004.

(140) Von der Kammer, F.; Legros, S.; Hofmann, T.; Larsen, E. H.; Loeschner, K. Separation and characterization of nanoparticles in complex food and environmental samples by field-flow fractionation. *TrAC Trends Anal. Chem.* **2011**, *30*, 425–436.

(141) Baalousha, M.; Stolpe, B.; Lead, J. R. Flow field-flow fractionation for the analysis and characterization of natural colloids and manufactured nanoparticles in environmental systems: A critical review. *J. Chromatogr. A* **2011**, *1218*, 4078–4103.

(142) Giddings, J. C. Field-flow fractionation: Analysis of macromolecular, colloidal, and particulate materials. *Science* **1993**, *260*, 1456–1465.

(143) Giddings, J. C. Field-flow fractionation. *Sep. Sci. Technol.* **1984**, *19*, 831–847.

(144) Regelink, I. C.; Weng, L.; Koopmans, G. F.; van Riemsdijk, W. H. Asymmetric flow field-flow fractionation as a new approach to analyse iron-(hydr)oxide nanoparticles in soil extracts. *Geoderma* **2013**, *202-203*, 134–141.

(145) Erickson, H. P. Size and shape of protein molecules at the nanometer level determined by sedimentation, gel filtration, and electron microscopy. *Biol. Proced. Online* **2009**, *11*, 32–51.

(146) Baalousha, M.; Lead, J. R. Rationalizing nanomaterial sizes measured by atomic force microscopy, flow field-flow fractionation, and dynamic light scattering: Sample preparation, polydispersity, and particle structure. *Environ. Sci. Technol.* **2012**, *46*, 6134–6142.

(147) Neubauer, E.; von der Kammer, F.; Hofmann, T. Influence of carrier solution ionic strength and injected sample load on retention and recovery of natural nanoparticles using flow field-flow fractionation. *J. Chromatogr. A* **2011**, *1218*, 6763–6773.

(148) Hagendorfer, H.; Kaegi, R.; Traber, J.; Mertens, S. F. L.; Scherrers, R.; Ludwig, C.; Ulrich, A. Application of an asymmetric flow field flow fractionation multi-detector approach for metallic engineered nanoparticle characterization - Prospects and limitations demonstrated on Au nanoparticles. *Anal. Chim. Acta* **2011**, *706*, 367–378.

(149) Tipping, E.; Lofts, S.; Sonke, J. E. Humic ion-binding model VII: A revised parameterisation of cation-binding by humic substances. *Environ. Chem.* **2011**, *8*, 225–235.

(150) Hochella, M. F.; Lower, S. K.; Maurice, P. A.; Penn, R. L.; Sahai, N.; Sparks, D. L.; Twining, B. S. Nanominerals, mineral nanoparticles, and Earth systems. *Science* **2008**, *319*, 1631–1635.

(151) Neubauer, E.; Köhler, S.; von der Kammer, F.; Laudon, H.; Hofmann, T. Effect of pH and stream order on iron and arsenic speciation in boreal catchments. *Environ. Sci. Technol.* **2013**, *47*, 7120–7128.

(152) Chanudet, V.; Filella, M. A non-perturbing scheme for the mineralogical characterization and quantification of inorganic colloids in natural waters. *Environ. Sci. Technol.* **2006**, *40*, 5045–5051.

(153) Fontes, M. P. F. Iron oxide-clay mineral association in Brazilian Oxisols: A magnetic separation study. *Clays Clay Miner.* **1992**, *40*, 175–179.

(154) Arias, M.; Teresa Barral, M.; Diaz-Fierros, F. Effects of iron and aluminium oxides on the colloidal and surface properties of kaolin. *Clays Clay Miner.* **1995**, *43*, 406–416.

(155) White, R. E. *Principles and Practice of Soil Science*; 4th ed.; Blackwell Publishing, Carlton, Australia, 2006.

(156) Dietzel, M. Dissolution of silicates and the stability of polysilicic acid. *Geochim. Cosmochim. Acta* **2000**, *64*, 3275–3281.

(157) Suzumura, M.; Ishikawa, K.; Ogawa, H. Characterization of dissolved organic phosphorus in coastal seawater using ultrafiltration and phosphohydrolytic enzymes. *Limnol. Oceanogr.* **1998**, *43*, 1553–1564.

(158) Wällstedt, T.; Björkvald, L.; Gustafsson, J. P. Increasing concentrations of arsenic and vanadium in (southern) Swedish streams. *Appl. Geochem.* **2010**, *25*, 1162–1175.

(159) Eusterhues, K.; Wagner, F. E.; Häusler, W.; Hanzlik, M.; Knicker, H.; Totsche, K. U.; Kögel-Knabner, I.; Schwertmann, U. Characterization of ferrihydrite-soil organic matter coprecipitates by X-ray diffraction and Mössbauer spectroscopy. *Environ. Sci. Technol.* **2008**, *42*, 7891–7897.

(160) Schwertmann, U.; Wagner, F.; Knicker, H. Ferrihydrite–humic associations: Magnetic hyperfine interactions. *Soil Sci. Soc. Am. J.* **2005**, *69*, 1009–1015.

(161) Mikutta, R.; Lorenz, D.; Guggenberger, G.; Haumaier, L.; Freund, A. Properties and reactivity of Fe-organic matter associations formed by coprecipitation versus adsorption: Clues from arsenate batch adsorption. *Geochim. Cosmochim. Acta* **2014**, *144*, 258–276.

(162) Mikutta, C.; Frommer, J.; Voegelin, A.; Kaegi, R.; Kretzschmar, R. Effect of citrate on the local Fe coordination in ferrihydrite, arsenate binding, and ternary arsenate complex formation. *Geochim. Cosmochim. Acta* **2010**, *74*, 5574–5592.

(163) Sahai, N.; Lee, Y. J.; Xu, H.; Ciardelli, M.; Gaillard, J. F. Role of Fe(II) and phosphate in arsenic uptake by coprecipitation. *Geochim. Cosmochim. Acta* **2007**, *71*, 3193–3210.

(164) Pokrovsky, O. S.; Dupré, B.; Schott, J. Fe-Al-organic colloids control of trace elements in peat soil solutions: Results of ultrafiltration and dialysis. *Aquat. Geochem.* **2005**, *11*, 241–278.

(165) Baken, S.; Salaets, P.; Desmet, N.; Seuntjens, P.; Vanlierde, E.; Smolders, E. Oxidation of iron causes removal of phosphorus and arsenic from streamwater in groundwater-fed lowland catchments. *Environ. Sci. Technol.* **2015**, *49*, 2886–2894.

(166) Baken, S.; Nawara, S.; Van Moorleghem, C.; Smolders, E. Iron colloids reduce the bioavailability of phosphorus to the green alga Raphidocelis subcapitata. *Water Res.* **2014**, *59*, 198–206.

(167) Boström, B.; Persson, G.; Broberg, B. Bioavailability of different phosphorus forms in freshwater systems. *Hydrobiologia* **1988**, *170*, 133–155.

(168) Ekholm, P.; Krogerus, K. Determining algal-available phosphorus of differing origin: Routine phosphorus analyses versus algal assays. *Hydrobiologia* **2003**, *492*, 29–42.

(169) Björkman, K.; Karl, D. Bioavailability of inorganic and organic phosphorus compounds to natural assemblages of microorganisms in Hawaiian coastal waters. *Mar. Ecol. Prog. Ser.* **1994**, *111*, 265–273.

(170) Cotner, J. B.; Wetzel, R. G. Uptake of dissolved inorganic and organic phosphorus compounds by phytoplankton and bacterioplankton. *Limnol. Oceanogr.* **1992**, *37*, 232–243.

(171) Van Moorleghem, C. Detection of bioavailable phosphorus forms for the alga Pseudokirchneriella subcapitata, PhD thesis, KU Leuven, Belgium, 2013.

(172) Santner, J.; Smolders, E.; Wenzel, W. W.; Degryse, F. First observation of diffusion-limited plant root phosphorus uptake from nutrient solution. *Plant. Cell Environ.* **2012**, *35*, 1558–1566.

(173) Paerl, H. W.; Downes, M. T. Biological availability of low versus high molecular weight reactive phosphorus. *J. Fish. Res. Board Canada* **1978**, *35*, 1639–1643.

(174) White, E.; Payne, G. Distribution and biological availability of reactive high molecular weight phosphorus in natural waters in New Zealand. *Can. J. Fish. Aquat. Sci.* **1980**, *37*, 664–669.

(175) Van Moorleghem, C.; Schutter, N.; Smolders, E.; Merckx, R. The bioavailability of colloidal and dissolved organic phosphorus to the alga Pseudokirchneriella subcapitata in relation to analytical phosphorus measurements. *Hydrobiologia* **2013**, *709*, 41–53.

(176) Round, F. E. *The Ecology of Algae*; Cambridge University Press, U.K., 1981.

(177) Carr, O. J.; Goulder, R. Fish-farm effluents in rivers-II. Effects on inorganic nutrients, algae and the macrophyte Ranunculus penicillatus. *Water Res.* **1990**, *24*, 639–647.

(178) Ekholm, P.; Rita, H.; Pitkänen, H.; Rantanen, P.; Pekkarinen, J.; Münster, U. Algal-available phosphorus entering the Gulf of Finland as estimated by algal assays and chemical analyses. *J. Environ. Qual.* **2003**, *38*, 2322–2333.

(179) Davison, W.; Seed, G. The kinetics of the oxidation of ferrous iron in synthetic and natural waters. *Geochim. Cosmochim. Acta* **1983**, *47*, 67–79.

(180) Schlosser, C.; Streu, P.; Croot, P. L. Vivaspin ultrafiltration: A new approach for high resolution measurements of colloidal and soluble iron species. *Limnol. Oceanogr. Methods* **2013**, *11*, 187–201.

(181) Van Schaik, J. W. J.; Persson, I.; Kleja, D. B.; Gustafsson, J. P. EXAFS study on the reactions between iron and fulvic acid in acid aqueous solutions. *Environ. Sci. Technol.* **2008**, *42*, 2367–2373.

(182) Kleja, D. B.; van Schaik, J. W. J.; Persson, I.; Gustafsson, J. P. Characterization of iron in floating surface films of some natural waters using EXAFS. *Chem. Geol.* **2012**, *326-327*, 19–26.

(183) Karlsson, T.; Persson, P.; Skyllberg, U.; Mörth, C.-M.; Giesler, R. Characterization of iron(III) in organic soils using extended X-ray absorption fine structure spectroscopy. *Environ. Sci. Technol.* **2008**, *42*, 5449–5454.

(184) Funke, H.; Scheinost, A.; Chukalina, M. Wavelet analysis of extended x-ray absorption fine structure data. *Phys. Rev. B* **2005**, *71*, 1–7.

(185) Van Moorleghem, C.; De Schutter, N.; Smolders, E.; Merckx, R. Bioavailability of organic phosphorus to Pseudokirchneriella subcapitata as affected by phosphorus starvation: an isotope dilution study. *Water Res.* **2013**, *47*, 3047–3056.

(186) Weiner, J. A.; DeLorenzo, M. E.; Fulton, M. H. Relationship between uptake capacity and differential toxicity of the herbicide atrazine in selected microalgal species. *Aquat. Toxicol.* **2004**, *68*, 121–128.

(187) Manceau, A.; Drits, V. A. Local structure of ferrihydrite and feroxyhite by EXAFS spectroscopy. *Clay Miner.* **1993**, *28*, 165–184.

(188) Cismasu, A. C.; Michel, F. M.; Tcaciuc, A. P.; Tyliszczak, T.; Brown, G. E. Composition and structural aspects of naturally occurring ferrihydrite. *Comptes Rendus Geosci.* **2011**, *343*, 210–218.

(189) Yao, B.; Xi, B.; Hu, C.; Huo, S.; Su, J.; Liu, H. A model and experimental study of phosphate uptake kinetics in algae: Considering surface adsorption and P-stress. *J. Environ. Sci.* **2011**, *23*, 189–198.

(190) Schulz, H. N.; Jørgensen, B. B. Big bacteria. *Annu. Rev. Microbiol.* **2001**, *55*, 105–137.

(191) Vandamme, E. Phosphorus-efficient soybean germplasm as an entry point to integrated soil fertility management in Western Kenya, PhD thesis, KU Leuven, Belgium, 2013.

(192) European Environment Agency EEA. Waterbase (online database), date accessed: November 19, 2013 http://www.eea.europa.eu/data-and-maps/data/waterbase-rivers-9.

(193) Rhoton, F. E.; Bigham, J. M.; Lindbo, D. L. Properties of iron oxides in streams draining the Loess Uplands of Mississippi. *Appl. Geochem.* **2002**, *17*, 409–419.

(194) Huser, B. J.; Köhler, S. J.; Wilander, A.; Johansson, K.; Fölster, J. Temporal and spatial trends for trace metals in streams and rivers across Sweden (1996–2009). *Biogeosciences* **2011**, *8*, 1813–1823.

(195) Dondeyne, S.; Vanierschot, L.; Langohr, R.; Van Ranst, E.; Deckers, S. *The soil map of the Flemish region converted to the third edition of the World Reference Base for soil resources*; Report to the Flemish Government, Department of Environment, Nature, and Energy, 2014.

(196) Meyus, Y.; Severyns, J.; Batelaan, O.; De Smedt, F. *Ontwikkeling van regionale modellen ten behoeve van het Vlaams Grondwater Model in GMS/MODFLOW. Perceel 1: Het Centraal*

Kempisch model. Deelrapport 1: Basisgegevens en conceptueel model; Report to the Flemish Government, Department of Environment and Infrastructure, 2004.

(197) Flemish Environment Agency VMM. *Grondwater in Vlaanderen: het Centraal Kempisch Systeem*; Aalst, Belgium, 2008.

(198) Vanlierde, E. Sediment concentrations, fluxes and source apportionment: Methodology assessment and application in Nete and Demer, PhD thesis, Flanders Hydraulics Research, Antwerp, Belgium, 2013.

(199) Dekov, V. M.; Vanlierde, E.; Billström, K.; Garbe-Schönberg, C.-D.; Weiss, D. J.; Gatto Rotondo, G.; Van Meel, K.; Kuzmann, E.; Fortin, D.; Darchuk, L.; et al. Ferrihydrite precipitation in groundwater-fed river systems (Nete and Demer river basins, Belgium): Insights from a combined Fe-Zn-Sr-Nd-Pb-isotope study. *Chem. Geol.* **2014**, *386*, 1–15.

(200) Lookman, R.; Vandeweert, N.; Merckx, R.; Vlassak, K. Geostatistical assessment of the regional distribution of phosphate sorption capacity parameters (FeOX and AlOX) in northern Belgium. *Geoderma* **1995**, *66*, 285–296.

(201) Batelaan, O. Phreatology - Characterizing groundwater recharge and discharge using remote sensing, GIS, ecology, hydrochemistry and groundwater modelling, PhD thesis, Vrije Universiteit Brussel, 2006.

(202) Van Der Beken, A.; Huybrechts, W. De waterbalans van het Vlaams gewest, een rationeel waterbeheer via kennis van de waterbalans. *Water* **1990**, *50*, 88–92.

(203) De Geyter, G.; Vandenberghe, R. E.; Verdonck, L.; Stoops, G. Mineralogy of holocene bog-iron ore in northern Belgium. *Neues Jahrb. für Mineral. - Abhandlungen* **1985**, *153*, 1–17.

(204) Batelaan, O.; De Smedt, F. GIS-based recharge estimation by coupling surface–subsurface water balances. *J. Hydrol.* **2007**, *337*, 337–355.

(205) Kelly, S.; Hesterberg, D.; Ravel, B. Analysis of soils and minerals using X-ray absorption spectroscopy. In *Methods of Soil Analysis. Part 5: Mineralogical Methods*; Soil Science Society of America, 2008; pp. 387–464.

(206) Jalilehvand, F. Structure of hydrated ions and cyanide complexes by X-ray absorption spectroscopy, PhD thesis, KTH-Royal Institute of Technology, Stockholm, Sweden, 2000.

(207) Carlson, S.; Clausén, M.; Gridneva, L.; Sommarin, B.; Svensson, C. XAFS experiments at beamline I811, MAX-lab synchrotron source, Sweden. *J. Synchrotron Radiat.* **2006**, *13*, 359–364.

(208) Ravel, B.; Newville, M. ATHENA, ARTEMIS, HEPHAESTUS: Data analysis for X-ray absorption spectroscopy using IFEFFIT. *J. Synchrotron Radiat.* **2005**, *12*, 537–541.

(209) Toner, B. M.; Santelli, C. M.; Marcus, M. A.; Wirth, R.; Chan, C. S.; McCollom, T.; Bach, W.; Edwards, K. J. Biogenic iron oxyhydroxide formation at mid-ocean ridge hydrothermal vents: Juan de Fuca Ridge. *Geochim. Cosmochim. Acta* **2009**, *73*, 388–403.

(210) Mikutta, C. X-ray absorption spectroscopy study on the effect of hydroxybenzoic acids on the formation and structure of ferrihydrite. *Geochim. Cosmochim. Acta* **2011**, *75*, 5122–5139.

(211) Rose, A. L.; Waite, T. D. Kinetic model for Fe(II) oxidation in seawater in the absence and presence of natural organic matter. *Environ. Sci. Technol.* **2002**, *36*, 433–444.

(212) Craig, P. S.; Shaw, T. J.; Miller, P. L.; Pellechia, P. J.; Ferry, J. L. Use of multiparametric techniques to quantify the effects of naturally occurring ligands on the kinetics of Fe(II) oxidation. *Environ. Sci. Technol.* **2009**, *43*, 337–342.

(213) Prietzel, J.; Thieme, J.; Eusterhues, K.; Eichert, D. Iron speciation in soils and soil aggregates by synchrotron-based X-ray microspectroscopy (XANES, μ-XANES). *Eur. J. Soil Sci.* **2007**, *58*, 1027–1041.

(214) Baken, S.; Verbeeck, M.; Verheyen, D.; Diels, J.; Smolders, E. Phosphorus losses from agricultural land to natural waters are reduced by immobilization in iron-rich sediments of drainage ditches. *Water Res.* **2015**, *71*, 160–170.

(215) Correll, D. L. Phosphorus: A rate limiting nutrient in surface waters. *Poult. Sci.* **1999**, *78*, 674–682.

(216) Smith, V. H. Eutrophication of freshwater and coastal marine ecosystems: A global problem. *Environ. Sci. Pollut. Res. Int.* **2003**, *10*, 126–139.

(217) Van der Zee, S. E. A. T. M. Transport of reactive contaminants in heterogeneous soil systems, PhD thesis, Agricultural University, Wageningen, the Netherlands, 1988.

(218) Del Campillo, M. C.; van der Zee, S. E. A. T. M.; Torrent, J. Modelling long-term phosphorus leaching and changes in phosphorus fertility in excessively fertilized acid sandy soils. *Eur. J. Soil Sci.* **1999**, *50*, 391–399.

(219) Van der Salm, C.; Dupas, R.; Grant, R.; Heckrath, G.; Lversen, B. V; Kronvang, B.; Levi, C.; Rubaek, G.; Schoumans, O. F. Predicting phosphorus losses with the PLEASE model on a local scale in Denmark and the Netherlands. *J. Environ. Qual.* **2011**, *40*, 1617–1626.

(220) Schoumans, O. F.; Van der Salm, C.; Groenendijk, P. PLEASE: A simple model to determine P losses by leaching. *Soil Use Manag.* **2013**, *29*, 138–146.

(221) Lovley, D. R. Microbial Fe(III) reduction in subsurface environments. *FEMS Microbiol. Rev.* **1997**, *20*, 305–313.

(222) Druschel, G. K.; Emerson, D.; Sutka, R.; Suchecki, P.; Luther, G. W. Low-oxygen and chemical kinetic constraints on the geochemical niche of neutrophilic iron(II) oxidizing microorganisms. *Geochim. Cosmochim. Acta* **2008**, *72*, 3358–3370.

(223) Duckworth, O. W.; Holmström, S. J. M.; Peña, J.; Sposito, G. Biogeochemistry of iron oxidation in a circumneutral freshwater habitat. *Chem. Geol.* **2009**, *260*, 149–158.

(224) Zak, D.; Gelbrecht, J. The mobilisation of phosphorus, organic carbon and ammonium in the initial stage of fen rewetting (a case study from NE Germany). *Biogeochemistry* **2007**, *85*, 141–151.

(225) Heiberg, L.; Pedersen, T. V.; Jensen, H. S.; Kjaergaard, C.; Hansen, H. C. B. A comparative study of phosphate sorption in lowland soils under oxic and anoxic conditions. *J. Environ. Qual.* **2008**, *39*, 734–743.

(226) Kaegi, R.; Voegelin, A.; Folini, D.; Hug, S. J. Effect of phosphate, silicate, and Ca on the morphology, structure and elemental composition of Fe(III)-precipitates formed in aerated Fe(II) and As(III) containing water. *Geochim. Cosmochim. Acta* **2010**, *74*, 5798–5816.

(227) Cesbron, F.; Metzger, E.; Launeau, P.; Deflandre, B.; Delgard, M.; Thibault de Chanvalon, A.; Geslin, E.; Anschutz, P.; Jézéquel, D. Simultaneous 2D imaging of dissolved iron and reactive phosphorus in sediment porewaters by thin-film and hyperspectral methods. *Environ. Sci. Technol.* **2014**, *48*, 2816–2826.

(228) Xu, D.; Chen, Y.; Ding, S.; Sun, Q.; Wang, Y.; Zhang, C. Diffusive gradients in thin films technique equipped with a mixed binding gel for simultaneous measurements of dissolved reactive phosphorus and dissolved iron. *Environ. Sci. Technol.* **2013**, *47*, 10477–10484.

(229) Kjaergaard, C.; Heiberg, L.; Jensen, H. S.; Hansen, H. C. B. Phosphorus mobilization in rewetted peat and sand at variable flow rate and redox regimes. *Geoderma* **2012**, *173-174*, 311–321.

(230) Zak, D.; Gelbrecht, J.; Steinberg, C. E. W. Phosphorus retention at the redox interface of peatlands adjacent to surface waters in Northeast Germany. *Biogeochemistry* **2004**, *70*, 357–368.

(231) Maassen, S.; Uhlmann, D.; Röske, I. Sediment and pore water composition as a basis for the trophic evaluation of standing waters. *Hydrobiologia* **2005**, *543*, 55–70.

(232) Ramm, K.; Scheps, V. Phosphorus balance of a polytrophic shallow lake with the consideration of phosphorus release. *Hydrobiologia* **1997**, *342-343*, 43–53.

(233) Brand-Klibanski, S.; Litaor, M. I.; Shenker, M. Overestimation of phosphorus adsorption capacity in reduced soils: An artifact of typical batch adsorption experiments. *Soil Sci. Soc. Am. J.* **2007**, *71*, 1128.

(234) Schwertmann, U. Differenzierung der Eisenoxide des Bodens durch Extraktion mit Ammmoniumoxalat-Lösung (The differentiation of iron oxides in soils by extraction with ammonium oxalate solution). *Z. Pflanz. Bodenk.* **1964**, *105*, 194–202.

(235) Murphy, J.; Riley, J. A modified single solution method for the determination of phosphate in natural waters. *Anal. Chim. Acta* **1962**, *27*, 31–36.

(236) Davison, W.; Grime, G. W.; Morgan, J. A. W.; Clarke, K. Distribution of dissolved iron in sediment pore waters at submillimetre resolution. *Nature* **1991**, *352*, 323–325.

(237) Davison, W.; Zhang, H.; Grime, G. Performance characteristics of gel probes used for measuring the chemistry of pore waters. *Environ. Sci. Technol.* **1994**, *28*, 1623–1632.

(238) Davison, W.; Zhang, H.; Grime, G. W. Performance characteristics of gel probes used for measuring the chemistry of pore waters. *Environ. Model. Softw.* **1994**, *28*, 1623–1632.

(239) Hofacker, A. F.; Voegelin, A.; Kaegi, R.; Weber, F.-A.; Kretzschmar, R. Temperature-dependent formation of metallic copper and metal sulfide nanoparticles during flooding of a contaminated soil. *Geochim. Cosmochim. Acta* **2013**, *103*, 316–332.

(240) Mansfeldt, T.; Schuth, S.; Häusler, W.; Wagner, F. E.; Kaufhold, S.; Overesch, M. Iron oxide mineralogy and stable iron isotope composition in a Gleysol with petrogleyic properties. *J. Soils Sediments* **2012**, *12*, 97–114.

(241) Schwertmann, U. Use of oxalate for Fe extraction from soils. *Can. J. Soil Sci.* **1973**, *53*, 244–246.

(242) Van der Grift, B.; Rozemeijer, J. C.; Griffioen, J.; van der Velde, Y. Iron oxidation kinetics and phosphate immobilization along the flow-path from groundwater into surface water. *Hydrol. Earth Syst. Sci.* **2014**, *18*, 4687–4702.

(243) Rakotoson, T.; Amery, F.; Rabeharisoa, L.; Smolders, E. Soil flooding and rice straw addition can increase isotopic exchangeable phosphorus in P-deficient tropical soils. *Soil Use Manag.* **2014**, *30*, 189–197.

(244) O'Loughlin, E. J.; Boyanov, M. I.; Flynn, T. M.; Gorski, C. A.; Hofmann, S. M.; McCormick, M. L.; Scherer, M. M.; Kemner, K. M. Effects of bound phosphate on the bioreduction of lepidocrocite

(γ-FeOOH) and maghemite (γ-Fe2O3) and formation of secondary minerals. *Environ. Sci. Technol.* **2013**, *47*, 9157–9166.

(245) Flemish Government. Besluit van de Vlaamse regering van 1 juni 1995 houdende algemene en sectorale bepalingen inzake milieuhygiëne - Bijlage 2.3.1. Basismilieukwaliteitsnormen voor oppervlaktewater, 1995.

(246) Loeb, R.; Lamers, L. P. M.; Roelofs, J. G. M. Prediction of phosphorus mobilisation in inundated floodplain soils. *Environ. Pollut.* **2008**, *156*, 325–331.

(247) Geurts, J. J. M.; Smolders, A. J. P.; Verhoeven, J. T. A.; Roelofs, J. G. M.; Lamers, L. P. M. Sediment Fe:PO4 ratio as a diagnostic and prognostic tool for the restoration of macrophyte biodiversity in fen waters. *Freshw. Biol.* **2008**, *53*, 2101–2116.

(248) Jensen, H. S.; Kristensen, P.; Jeppesen, E.; Skytthe, A. Iron:phosphorus ratio in surface sediment as an indicator of phosphate release from aerobic sediments in shallow lakes. *Hydrobiologia* **1992**, *235-236*, 731–743.

(249) Rotiroti, M.; Sacchi, E.; Fumagalli, L.; Bonomi, T. Origin of arsenic in groundwater from the multilayer aquifer in Cremona (northern Italy). *Environ. Sci. Technol.* **2014**, *48*, 5395–5403.

(250) McArthur, J. M.; Banerjee, D. M.; Hudson-Edwards, K. A.; Mishra, R.; Purohit, R.; Ravenscroft, P.; Cronin, A.; Howarth, R. J.; Chatterjee, A.; Talukder, T.; et al. Natural organic matter in sedimentary basins and its relation to arsenic in anoxic ground water: The example of West Bengal and its worldwide implications. *Appl. Geochem.* **2004**, *19*, 1255–1293.

(251) Barringer, J. L.; Reilly, P. A.; Eberl, D. D.; Blum, A. E.; Bonin, J. L.; Rosman, R.; Hirst, B.; Alebus, M.; Cenno, K.; Gorska, M. Arsenic in sediments, groundwater, and streamwater of a glauconitic Coastal Plain terrain, New Jersey, USA-Chemical "fingerprints" for geogenic and anthropogenic sources. *Appl. Geochem.* **2011**, *26*, 763–776.

(252) Webster-Brown, J. G.; Lane, V. Modeling seasonal arsenic behavior in the Waikato river, New Zealand. In *Advances in Arsenic Research*; O'Day, P. A.; Vlassopoulos, D.; Meng, X.; Benning, L. G., Eds.; ACS Symposium Series; American Chemical Society: Washington, DC, 2005; Vol. 915, pp. 253–266.

(253) Tessier, A.; Fortin, D.; Belzile, N.; DeVitre, R. R.; Leppard, G. G. Metal sorption to diagenetic iron and manganese oxyhydroxides and associated organic matter: Narrowing the gap between field and laboratory measurements. *Geochim. Cosmochim. Acta* **1996**, *60*, 387–404.

(254) De Vitre, R.; Belzile, N.; Tessier, A. Speciation and adsorption of arsenic on diagenetic iron oxyhydroxides. *Limnol. Oceanogr.* **1991**, *36*, 1480–1485.

(255) Frierdich, A. J.; Hasenmueller, E. A.; Catalano, J. G. Composition and structure of nanocrystalline Fe and Mn oxide cave deposits: Implications for trace element mobility in karst systems. *Chem. Geol.* **2011**, *284*, 82–96.

(256) King, D. W. Role of carbonate speciation on the oxidation rate of Fe(II) in aquatic systems. *Environ. Sci. Technol.* **1998**, *32*, 2997–3003.

(257) Millero, F. J.; Sotolongo, S.; Izaguirre, M. The oxidation kinetics of Fe(II) in seawater. *Geochim. Cosmochim. Acta* **1987**, *51*, 793–801.

(258) Pham, A. N.; Waite, T. D. Oxygenation of Fe(II) in natural waters revisited: Kinetic modeling approaches, rate constant estimation and the importance of various reaction pathways. *Geochim. Cosmochim. Acta* **2008**, *72*, 3616–3630.

(259) Larson, L. N.; Sánchez-España, J.; Kaley, B.; Sheng, Y.; Bibby, K.; Burgos, W. D. Thermodynamic controls on the kinetics of microbial low-pH Fe(II) oxidation. *Environ. Sci. Technol.* **2014**, *48*, 9246–9254.

(260) Geroni, J. N.; Sapsford, D. J. Kinetics of iron (II) oxidation determined in the field. *Appl. Geochem.* **2011**, *26*, 1452–1457.

(261) Burns, J. M.; Craig, P. S.; Shaw, T. J.; Ferry, J. L. Combinatorial parameter space as an empirical tool for predicting water chemistry: Fe(II) oxidation across a watershed. *Environ. Sci. Technol.* **2011**, *45*, 4023–4029.

(262) AGIV - Agentschap voor Geografische Informatie Vlaanderen. *Vlaamse Hydrografische Atlas*; accessible at http://www.geopunt.be; Ghent, Belgium, 2014.

(263) Batelaan, O.; De Smedt, F. WetSpass: A flexible, GIS based, distributed recharge methodology for regional groundwater modelling. In *Impact of Human Activity on Groundwater Dynamics*; Gehrels, H.; Peter, S. N.; Hoehn, E.; Jensen, K.; Leidundgut, C.; Griffioen, J.; Webb, B.; Zaadnoordijk, W. J., Eds.; International Association of Hydrological Sciences: Wallingford, U.K., 2001; pp. 11–17.

(264) Millero, F. J. Thermodynamics of the carbon dioxide system in the oceans. *Geochim. Cosmochim. Acta* **1995**, *59*, 661–677.

(265) Willems, P. A time series tool to support the multi-criteria performance evaluation of rainfall-runoff models. *Environ. Model. Softw.* **2009**, *24*, 311–321.

(266) Van Laer, L.; Smolders, E. Does soil water saturation mobilize metals from riparian soils to adjacent surface water? A field monitoring study in a metal contaminated region. *Environ. Sci. Process. Impacts* **2013**, *15*, 1181–1190.

(267) Tarvainen, T.; Albanese, S.; Birke, M.; Poňavič, M.; Reimann, C. Arsenic in agricultural and grazing land soils of Europe. *Appl. Geochem.* **2013**, *28*, 2–10.

(268) De Vet, W. W. J. M.; Dinkla, I. J. T.; Rietveld, L. C.; van Loosdrecht, M. C. M. Biological iron oxidation by Gallionella spp. in drinking water production under fully aerated conditions. *Water Res.* **2011**, *45*, 5389–5398.

(269) Spiteri, C.; Regnier, P.; Slomp, C. P.; Charette, M. A. pH-Dependent iron oxide precipitation in a subterranean estuary. *J. Geochemical Explor.* **2006**, *88*, 399–403.

(270) Hart, B. T.; Hines, T.; Coller, B. A. W. Geochemistry of Cu, Zn and Fe in the Tambo River, Australia II. Field investigation under low-flow conditions. *Mar. Freshw. Res.* **2008**, *59*, 80–88.

(271) Roberts, L. C.; Hug, S. J.; Ruettimann, T.; Billah, M. M.; Khan, A. W.; Rahman, M. T. Arsenic removal with iron(II) and iron(III) in waters with high silicate and phosphate concentrations. *Environ. Sci. Technol.* **2004**, *38*, 307–315.

(272) Buzek, F.; Cejkova, B.; Dousova, B.; Jackova, I.; Kadlecova, R.; Lnenickova, Z. Mobilization of arsenic from acid deposition – The Elbe River catchment, Czech Republic. *Appl. Geochem.* **2013**, *33*, 281–293.

(273) Griffioen, J. Extent of immobilisation of phosphate during aeration of nutrient-rich, anoxic groundwater. *J. Hydrol.* **2006**, *320*, 359–369.

(274) Gunnars, A.; Blomqvist, S. Phosphate exchange across the sediment-water interface when shifting from anoxic to oxic conditions – An experimental comparison of freshwater and brackish-marine systems. *Biogeochemistry* **1997**, *37*, 203–226.

(275) Van Hoestenberghe, T.; Ferket, B.; De Boeck, K.; Vanlierde, E.; Vanlede, J.; Verwaest, T.; Mostaert, F. *Slibbalans Zeeschelde. Deelrapport 2: Sediment load for the river Scheldt and its main tributaries (1972-2009)*; Flanders Hydraulics Research, Antwerp, Belgium, 2009.

(276) Baken, S.; Gustafsson, J. P.; Smolders, E. The association between iron and carbon in freshwater colloids. *Mineral. Mag.* **2013**, *77*, 643.

(277) Baken, S.; Nawara, S.; Van Acker, E.; Smolders, E. *The bioavailability of colloidal P to freshwater algae*; presented at the Phosphorus in Soils and Plants (PSP) 5 conference, Montpellier, France, August 26-29, 2014.

(278) Nawara, S.; Baken, S.; Smolders, E. *Freshwater phosphate limits are based on a poorly standardized molybdate reactive P method*; presented at the Phosphorus in Soils and Plants (PSP) 5 conference, Montpellier, France, 26–29 August 2014.

(279) Van Opstal, M.; Tits, M.; Beckers, V.; Batelaan, O.; Van Orshoven, J.; Elsen, A.; Diels, J.; D'heygere, T.; Van Hoof, K. ArcNEMO, a spatially distributed nutrient emission model developed in Python to quantify losses of nitrogen and phosphorus from agriculture to surface waters. *Geophys. Res. Abstr.* **2014**, *16*, 11652.

Curriculum vitae

Name:	Stijn BAKEN
Address:	Rue du Cellier 15, 4000 Liège, Belgium
Date of birth:	23 / 01 / 1987
Place of birth:	Oss (NL)
Mobile phone:	+32 499 612 007
E-mail:	stijn.baken (at) gmail.com

Work experience

2011-present Fellow of the FWO-Research Foundation Flanders, and PhD researcher at Dept. of Earth and Environmental Sciences, KU Leuven, Belgium. *PhD title*: The effect of iron-rich particles on the fate and bioavailability of phosphorus in streams. *Supervisor*: prof. Erik Smolders.

- Research visit at KTH – Royal Institute of Technology, Stockholm, Sweden (2 months in 2012).
- Research visit at Wageningen UR, the Netherlands (1 week in 2014).

2010-2011 Researcher at the Department of Earth and Environmental Sciences, KU Leuven. *Project title*: Toxicity of vanadium to micro-organisms and higher plants in soil. Funding by the vanadium industry federation.

Education

2011-present PhD in Bioscience Engineering, KU Leuven.

2008-2010 Master in Environmental Science and Technology, option bioscience engineering, KU Leuven. Graduated *maxima cum laude* in July 2010.

2005-2008 Bachelor in Bioscience Engineering, KU Leuven. Graduated *maxima cum laude* in July 2008.

2004-2005 Intercultural exchange by AFS as exchange student at the senior high school of Ilmajoki, Finland (1 year). Stay with a host family.

1998-2004 High school at Don Bosco Instituut Haacht (ASO). Graduated in 2004.

Languages

Dutch	Mother tongue
English	Excellent reading, writing and speaking skills
Finnish	Excellent colloquial speaking skills, good reading and writing skills
French	Good reading, writing and speaking skills
German	Good reading skills, moderate speaking skills
Swedish	Good reading and speaking skills

Voluntary work

2014-present	Member of GRACQ, the French-speaking Belgian cyclist federation. We are a forum where cyclists meet and interact, and we defend the interest of cyclists in meetings with politicians, policy makers, and urban planners.
2011-2014	Member of Bouworde, a non-profit offering volunteer vacations for youths. I contributed by running workshops on construction site safety and on intercultural awareness for outgoing volunteers.
2006-2010	Student representative at the Faculty of Bioscience Engineering, KU Leuven. In 2007-2008, I was elected by the student union (LBK) as the main coordinator of student representation at the faculty (which counts 1000 students). I formulated and defended a student opinion in several commissions and boards, and I was a key communication link between academic staff and students.
2008-2009	International coordinator of the union of students in bioscience engineering (LBK). I organized union activities for incoming international students and stimulated interaction with local students.

List of publications

Baken, S.; Salaets, P.; Desmet, N.; Seuntjens, P.; Vanlierde, E.; Smolders, E. Oxidation of iron causes removal of phosphorus and arsenic from streamwater in groundwater-fed lowland catchments. *Environmental Science & Technology* **2015**, *49*, 2886–2894.

Baken, S.; Verbeeck, M.; Verheyen, D.; Diels, J.; Smolders, E. Phosphorus losses from agricultural land to natural waters are reduced by immobilization in iron-rich sediments of drainage ditches. *Water Research* **2015**, *71*, 160–170.

Baken, S.; Nawara, S.; Van Moorleghem, C.; Smolders, E. Iron colloids reduce the bioavailability of phosphorus to the green alga Raphidocelis subcapitata. *Water Research* **2014**, *59*, 198–206.

Baken, S.; Sjöstedt, C.; Gustafsson, J. P.; Seuntjens, P.; Desmet, N.; De Schutter, J.; Smolders, E. Characterisation of hydrous ferric oxides derived from iron-rich groundwaters and their contribution to the suspended sediment of streams. *Applied Geochemistry* **2013**, *39*, 59–68.

Larsson, M.; Baken, S.; Gustafsson, J. P.; Hadialhejazi, G.; Smolders, E. Vanadium bioavailability and toxicity to soil microorganisms and plants. *Environmental Toxicology and Chemistry* **2013**, *32*, 2266–2273.

Baken, S.; Larsson, M.; Gustafsson, J. P.; Cubadda, F.; Smolders, E. Ageing of vanadium in soils and consequences for bioavailability. *European Journal of Soil Science* **2012**, *63*, 839–847.

Baken, S.; Degryse, F.; Verheyen, L.; Merckx, R.; Smolders, E. Metal complexation properties of freshwater dissolved organic matter are explained by its aromaticity and by anthropogenic ligands. *Environmental Science & Technology* **2011**, *45*, 2584–2590.